TRANSCRIPTOME-NEUROIMAGING ASSOCIATION: BRIDGING THE GAP BETWEEN MICROSCALE GENETIC EXPRESSION AND MACROSCALE BRAIN ORGANIZATION

EDITED BY: Jiajia Zhu, Junping Wang and Liang Zhan
PUBLISHED IN: Frontiers in Neuroscience

frontiers Research Topics

frontiers

ISSN 1664-8714
ISBN 978-2-83250-097-2
DOI 10.3389/978-2-83250-097-2

About Frontiers

Frontiers is more than just an open-access publisher of scholarly articles: it is a pioneering approach to the world of academia, radically improving the way scholarly research is managed. The grand vision of Frontiers is a world where all people have an equal opportunity to seek, share and generate knowledge. Frontiers provides immediate and permanent online open access to all its publications, but this alone is not enough to realize our grand goals.

Frontiers Journal Series

The Frontiers Journal Series is a multi-tier and interdisciplinary set of open-access, online journals, promising a paradigm shift from the current review, selection and dissemination processes in academic publishing. All Frontiers journals are driven by researchers for researchers; therefore, they constitute a service to the scholarly community. At the same time, the Frontiers Journal Series operates on a revolutionary invention, the tiered publishing system, initially addressing specific communities of scholars, and gradually climbing up to broader public understanding, thus serving the interests of the lay society, too.

Dedication to Quality

Each Frontiers article is a landmark of the highest quality, thanks to genuinely collaborative interactions between authors and review editors, who include some of the world's best academicians. Research must be certified by peers before entering a stream of knowledge that may eventually reach the public - and shape society; therefore, Frontiers only applies the most rigorous and unbiased reviews.
Frontiers revolutionizes research publishing by freely delivering the most outstanding research, evaluated with no bias from both the academic and social point of view. By applying the most advanced information technologies, Frontiers is catapulting scholarly publishing into a new generation.

What are Frontiers Research Topics?

Frontiers Research Topics are very popular trademarks of the Frontiers Journals Series: they are collections of at least ten articles, all centered on a particular subject. With their unique mix of varied contributions from Original Research to Review Articles, Frontiers Research Topics unify the most influential researchers, the latest key findings and historical advances in a hot research area! Find out more on how to host your own Frontiers Research Topic or contribute to one as an author by contacting the Frontiers Editorial Office: frontiersin.org/about/contact

TRANSCRIPTOME-NEUROIMAGING ASSOCIATION: BRIDGING THE GAP BETWEEN MICROSCALE GENETIC EXPRESSION AND MACROSCALE BRAIN ORGANIZATION

Topic Editors:
Jiajia Zhu, First Affiliated Hospital of Anhui Medical University, China
Junping Wang, Tianjin Medical University General Hospital, China
Liang Zhan, University of Pittsburgh, United States

Citation: Zhu, J., Wang, J., Zhan, L., eds. (2022). Transcriptome-Neuroimaging Association: Bridging the gap Between Microscale Genetic Expression and Macroscale Brain Organization. Lausanne: Frontiers Media SA.
doi: 10.3389/978-2-83250-097-2

Table of Contents

frontiers in Neuroscience

ORIGINAL RESEARCH
published: 07 September 2021
doi: 10.3389/fnins.2021.733316

The Vital Role of Central Executive Network in Brain Age: Evidence From Machine Learning and Transcriptional Signatures

*Keke Fang[1], Shaoqiang Han[2], Yuming Li[3], Jing Ding[1], Jilian Wu[1] and Wenzhou Zhang[1]**

[1] Department of Pharmacy, Affiliated Cancer Hospital of Zhengzhou University, Henan Cancer Hospital, Zhengzhou, China,
[2] Department of Magnetic Resonance Imaging, The First Affiliated Hospital of Zhengzhou University, Zhengzhou, China,
[3] Department of Radiotherapy, Affiliated Cancer Hospital of Zhengzhou University, Henan Cancer Hospital, Zhengzhou, China

Recent studies combining neuroimaging with machine learning methods successfully infer an individual's brain age, and its discrepancy with the chronological age is used to identify age-related diseases. However, which brain networks play decisive roles in brain age prediction and the underlying biological basis of brain age remain unknown. To answer these questions, we estimated an individual's brain age in the Southwest University Adult Lifespan Dataset (N = 492) from the gray matter volumes (GMV) derived from T1-weighted MRI scans by means of Gaussian process regression. Computational lesion analysis was performed to determine the importance of each brain network in brain age prediction. Then, we identified brain age-related genes by using prior brain-wide gene expression data, followed by gene enrichment analysis using Metascape. As a result, the prediction model successfully inferred an individual's brain age and the computational lesion prediction results identified the central executive network as a vital network in brain age prediction (Steiger's Z = 2.114, p = 0.035). In addition, the brain age-related genes were enriched in Gene Ontology (GO) processes/Kyoto Encyclopedia of Genes and Genomes (KEGG) pathways grouped into numbers of clusters, such as regulation of iron transmembrane transport, synaptic signaling, synapse organization, retrograde endocannabinoid signaling (e.g., dopaminergic synapse), behavior (e.g., memory and associative learning), neurotransmitter secretion, and dendrite development. In all, these results reveal that the GMV of the central executive network played a vital role in predicting brain age and bridged the gap between transcriptome and neuroimaging promoting an integrative understanding of the pathophysiology of brain age.

Keywords: brain age, Allen Human Brain Atlas, structural brain imaging, machine learning, gene

OPEN ACCESS

Edited by:
Jiajia Zhu,
First Affiliated Hospital of Anhui Medical University, China

Reviewed by:
Changchun He,
University of Electronic Science and Technology of China, China
Chao Li,
The First Affiliated Hospital of China Medical University, China

****Correspondence:***
Wenzhou Zhang
hnzzzwz@hotmail.com

Specialty section:
This article was submitted to Brain Imaging Methods, a section of the journal Frontiers in Neuroscience

Received: *30 June 2021*
Accepted: *06 August 2021*
Published: *07 September 2021*

Citation:
Fang K, Han S, Li Y, Ding J, Wu J and Zhang W (2021) The Vital Role of Central Executive Network in Brain Age: Evidence From Machine Learning and Transcriptional Signatures. Front. Neurosci. 15:733316. doi: 10.3389/fnins.2021.733316

INTRODUCTION

Normal brain aging is accompanied by a decline of brain region volumes (Anderton, 2002) and cognition such as conceptual reasoning, executive function, and memory (Harada et al., 2013; Kirova et al., 2015). As the brain ages, many age-related diseases emerge, such as Alzheimer's disease (AD) (Amaducci and Tesco, 1994; Ferri et al., 2005). As the fifth leading cause of death in people

over the age of 65 years (Kirova et al., 2015), AD burdens the society heavily. The risk of developing AD increases exponentially with age (Plassman et al., 2007). Thus, revealing the mechanism of the normal brain age is the key to understanding age-related diseases (Raji et al., 2009). Recent studies combining neuroimaging and machine learning methods predict brain age successfully and found that the chronological age is not exactly equal to brain age in both normal and pathological subjects such as patients with schizophrenia, mild cognitive impairments, and depression (Gaser et al., 2013; Habes and Janowitz, 2016; Hajek et al., 2019; Han et al., 2021; He et al., 2020). This discordance between brain age and chronological age helps explain individual differences in brain aging (Jylhävä et al., 2017). However, the underlying biological basis of brain age is not well elaborated.

Extensive efforts have been made to identify reliable indictors of biological age (Wagner et al., 2016). In recent years, the brain age method identifying normal aging pattern has turned out to be an informative biomarker of healthy brain aging at the individual level (Cole and Franke, 2017; Franke et al., 2010). For example, Vishnu et al. accurately predicted MRI-derived brain age, helping to identify various brain diseases (Bashyam et al., 2020). Using this framework, studies have uncovered accelerated brain aging in several neurological diseases using the brain-predicted age difference (brain-PAD) scores, defined as the discordance between the predicted brain age and the chronological age (Gaser et al., 2013; Habes and Janowitz, 2016; Hajek et al., 2019; Han et al., 2021; He et al., 2020). The brain age method outperforms other state-of-the-art biomarkers, with accuracy rates reaching 81% in identifying mild cognitive impairments (Gaser et al., 2013). Despite these remarkable findings, these studies have failed to elucidate the underlying biological basis of brain age, limiting our understanding of the biological mechanism of brain age and its application.

It is widely accepted that genetic factors play important roles in normal brain aging (Lin et al., 2020). For example, the expressions of genes playing roles in synaptic functional and neuronal plasticity in the frontal cortex are reduced with aging (Sikora et al., 2021). However, the relation between genetic factors and brain age derived from neuroimaging remains unknown. Advances in comprehensive brain-wide gene expression atlases make possible linking the spatial variations in gene expressions to macroscopic neuroimaging phenotypes (Fornito et al., 2019; Zhu et al., 2021). For example, Reardon et al. found that the genetic spatial expression is tied with cortical scaling gradients (Reardon and Seidlitz, 2018). Resting-state intrinsic brain synchronization is also supported by related gene expression (Richiardi et al., 2015). Combing neuroimaging and gene transcripts provides insights into how disease-related aberrance at the microscale architecture drives macroscale brain abnormalities in mental disorders such as depression and schizophrenia (Romero-Garcia et al., 2020; Li and Seidlitz, 2021). The details of the underlying transcriptional mechanisms of brain age remain unknown.

The aims of the current study were twofold. Firstly, we investigated the importance of brain networks in brain age prediction. The Southwest University Adult Lifespan Dataset ($N = 492$) was used in the current study. For each subject, the gray matter volumes (GMV) quantified by voxel-based morphometry (VBM) of brain regions were treated as features to predict an individual's brain age. In the prediction model, Gaussian process regression (GPR) was chosen for its superior performance compared to existing methods (Han et al., 2021). The importance of a distinct brain network was determined by computational lesion analysis (Feng et al., 2018). Secondly, genetic annotation of the brain networks playing decisive roles in brain age prediction was generated by employing the Brain Annotation Toolbox (BAT) (Liu et al., 2019) followed by functional enrichment analysis to infer the ontological pathways of the brain age-related genes.

MATERIALS AND METHODS

Sample

The dataset used in the current study come from the Southwest University Adult Lifespan Dataset (SALD). This dataset was obtained from healthy participants ($N = 492$, 308 females and 187 males; age range, 19–80 years). The exclusion criteria included MRI-related exclusion criteria, current psychiatric/neurological disorders, and use of psychiatric drugs in the past 3 months prior to scanning, among others. More description on the subjects and data acquisition parameters can be found in Wei et al. (2018). The data are available for research purposes through the International Neuroimaging Data-Sharing Initiative.[1]

Data Acquisition

High-resolution T1-weighted anatomical images of the participants were acquired using a magnetization-prepared rapid gradient echo (MPRAGE) sequence (repetition time = 1,900 ms, echo time = 2.52 ms, inversion time = 900 ms, flip angle = 90°, resolution matrix = 256 × 256, slices = 176, thickness = 1.0 mm, and voxel size = 1 mm^3 × 1 mm^3 × 1 mm^3).

Voxel-Based Morphometry Analysis

We followed the standard pipeline of the CAT12 toolbox[2] to calculate the VBM. The main steps included bias field correction, segmentation [gray and white matter and cerebrospinal fluid, adjustment for partial volume effects, normalization into the Montreal Neurological Institute (MNI) space, resampled to 1.5 mm × 1.5 mm × 1.5 mm], and non-linear modulation (Ashburner, 2009). Finally, the gray matter (GM) maps were smoothed using 6 mm full width at half maximum (FWHM) Gaussian kernel. The total intracranial volume (TIV) of each participant was also calculated to explore its association with brain age.

Prediction Model

GPR was used to infer an individual's brain age from the mean GMV of 246 brain regions (Fan et al., 2016) due to its superior performance (Han et al., 2021). The GPR method used in this study was implemented in the Gaussian Processes for

[1] http://fcon_1000.projects.nitrc.org/indi/retro/sald.html

[2] http://dbm.neuro.uni-jena.de/cat12/

Machine Learning (GPML) toolbox.[3] As done in previous study (Marquand et al., 2016; Rasmussen and Williams, 2005), the parameters were optimized using a conjugate gradient optimizer (included in the GPML toolbox).

Model Validation

A 10-fold cross-validation was used to evaluate the performance of the prediction model (Sone et al., 2019; Ziegel, 2010). This procedure was repeated 100 times to obtain more stable results. To evaluate the performance of the prediction model, we calculated (1) the mean absolute error (MAE) between the estimated brain age (output of the prediction model) and the chronological age and (2) the correlation between the chronological age and the estimated brain age across 100 repetitions. The mean brain-PAD score of each subject was calculated (brain-PAD score: predicted age - the chronological age).

To explore whether there was gender difference in the brain-PAD score, the brain-PAD scores of male subjects were compared with those of female subjects using a two-sample *t*-test controlling for age and age^2. The correlation between the TIV and brain-PAD was also calculated to investigate its effect on brain age.

Computational Lesion Prediction

As done in a previous study, lesion prediction analysis was performed to examine the importance of the brain networks defined in the 17 networks of Yeo et al. (2011). Specifically, the regions belonging to one specific network were excluded and the GMV of the rest of the networks were treated as features to predict brain age (Feng et al., 2018). Afterward, the importance of an individual network was determined by comparing the performance of a "lesioned" model with that of a model with all regions using Steiger's *Z* (Feng et al., 2018; Ren et al., 2021). Here, we used the opposite value of the *Z* value. A higher *Z* meant a lower of performance of the "lesioned" model, thus declaring the more important role of the "lesioned" network in brain age prediction. The correlation between the chronological age and the mean GMV of each network was also calculated.

Genetic Annotation Using BAT

Then, we performed a genetic annotation analysis for the brain age-related networks to identify the gene expression profile for this network using BAT[4] (Hawrylycz et al., 2012). The gene profiles used in BAT (see text footnote 4) come from the Allen Human Brain Atlas (AHBA)[5] obtained from six adult human brains (Hawrylycz et al., 2012). The number of anatomic samples obtained for each brain varied from 363 to 946. Details on the processing expression data were included in Liu et al. (2019). Here, we just provide a brief description. Processing the raw expression data followed the pipeline provided by the AHBA. The probe with the highest average expression was picked to represent that gene. In sum, 3,695 unique anatomic samples with 20,738 gene expression profiles were obtained. Expressions were normalized by extracting the median of the gene's expression across all samples of the individual, then divided by the median. For each AHBA tissue sample, a 6-mm sphere region of interest (ROI) in the MNI volume space centered on its MNI centroid coordinate. Finally, 3,695 ROIs with their corresponding normalized gene expression profiles were used in the following analysis (Hawrylycz et al., 2012).

For each background AHBA sample, that with more than 50% of voxels that were also present in the given background mask was mapped to one of the given clusters. The gene expression profile of each cluster was defined as the average gene expression of all the samples mapped to the given cluster. Permutation analysis was adopted to identify the differentially expressed genes in the given cluster. Lastly, for each gene, the name and the corresponding *p*-value were obtained. In the current study, brain age-related genes were identified if their $p < 0.05$ [family-wise error (FWE) corrected] (Hawrylycz et al., 2012).

Enrichment Pathways Associated With Brain Age-Related Genes

Thereafter, we aligned the Gene Ontology (GO) and Kyoto Encyclopedia of Genes and Genomes (KEGG) pathways with the genes obtained in the previous step using Metascape. Metascape provided automated meta-analysis tools to understand either common or unique pathways in 40 independent knowledge bases (Zhou et al., 2019). The gene list was input into the Metascape website and the results corrected by the false discovery rate (FDR; $p < 0.05$).

RESULTS

Demographic Information

Demographic information of the dataset used in the current study is included in **Table 1**.

Performance of the Prediction Model

The correlation between the chronological age and the estimated brain age reached $R = 0.889$ (**Figure 1**). Consistent with the findings of a previous study, the performance of the prediction model was better that that in Han et al. (2021) because the sample size used in the current study was larger (Franke et al., 2010). There was no significant difference between male and female subjects ($p > 0.05$). The correlation between TIV and brain-PAD was also not significant ($p > 0.05$).

TABLE 1 | Demographic information of the dataset.

	Subjects
Age (years), mean ± SD, (range), y	45.10 ± 17.43, (19–80)
Gender, male: female	186: 306

[3] www.gaussianprocess.org/gpml/code/

[4] http://123.56.224.61/softwares

[5] http://human.brain-map.org/

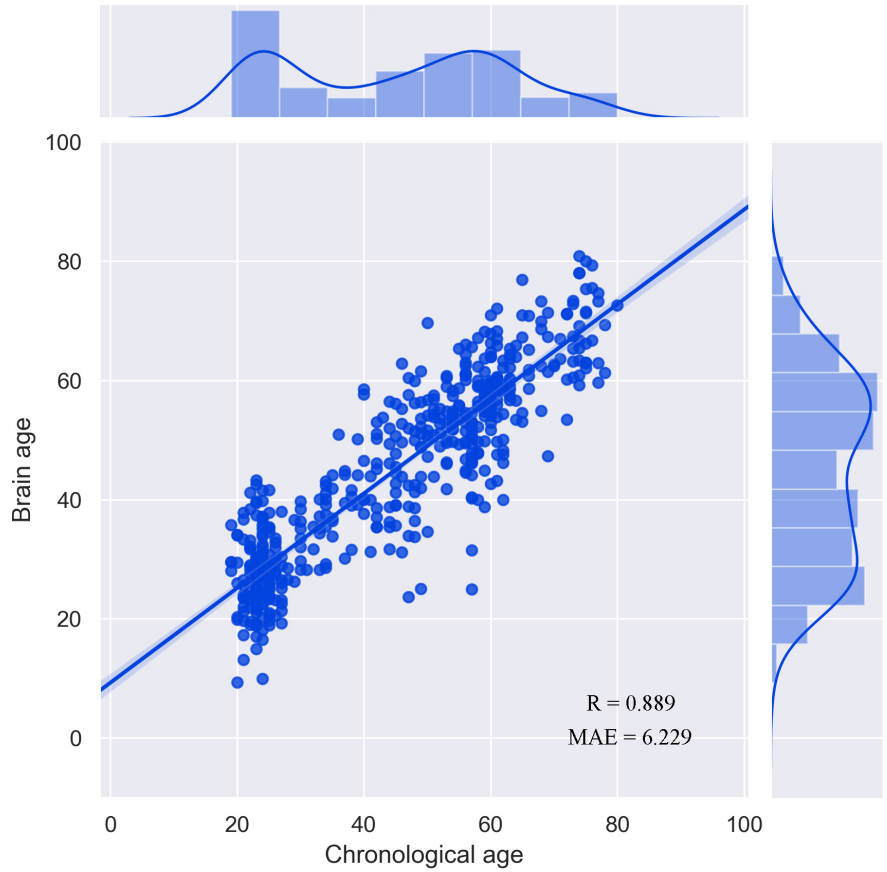

FIGURE 1 | Performance of the prediction model.

Computational Lesion Prediction

The results of computational lesion prediction revealed that the performance of the prediction model significantly degraded (Steiger's $Z = 2.114$, $p = 0.035$) only if the central executive network, including the bilateral middle temporal gyrus, right middle frontal gyrus, the bilateral dorsolateral frontal gyrus, and the right inferior parietal lobule, was excluded (**Supplementary Figure 1**). The mean GMV of the 17 networks were all negatively correlated with the chronological age, suggesting that the GMV decreases in normal aging (**Supplementary Figure 2**).

Enrichment Pathways

BAT identified 2,927 genes associated with brain age-related networks. Then, we aligned the GO biological processes and KEGG pathways using Metascape. The results reported in this study were corrected for FDR ($p < 0.05$) and discrete enrichment clusters were discarded. The GO processes and KEGG pathways were clustered into a number of groups such as regulation of iron transmembrane transport, synaptic signaling, synapse organization, retrograde endocannabinoid signaling (e.g., dopaminergic synapse), behavior (e.g., memory and associative learning), neurotransmitter secretion, and dendrite development. The top 20 enrichment terms were included in **Figure 2** and the enrichment networks were drawn in **Figure 3**.

DISCUSSION

In this study, we investigated the importance of brain networks contributing to brain age prediction and the underlying molecular mechanisms of brain age. As a result, the central executive network turned out to be a vital network in predicting brain age due to the performance of the prediction model being significantly degraded (Steiger's $Z = 2.114$, $p = 0.035$) when it was excluded from the model. The genes associated with the central executive network were ontologically enriched in clusters such as regulation of ion transmembrane transport, synaptic signaling, synapse organization, retrograde endocannabinoid signaling (e.g., dopaminergic synapse), behavior (e.g., memory and associative learning), and so on. In all, these results reveal that the GMV of the central executive network played a vital role in predicting brain age and bridged the gap between transcriptome and neuroimaging promoting an integrative understanding of the pathophysiology of brain age.

Our results hinted that the GMV of the central executive network is a potential biomarker of brain age. Normal brain

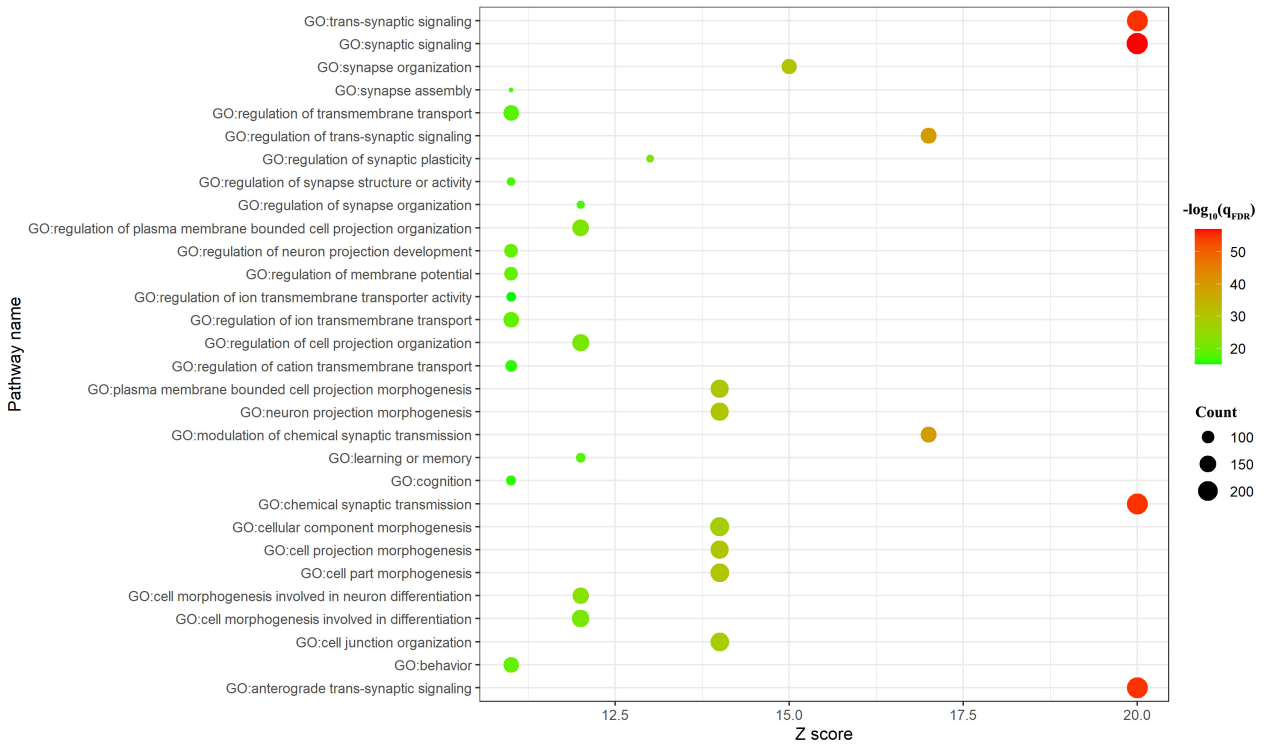

FIGURE 2 | Top 20 significant Gene Ontology (GO) biological processes/Kyoto Encyclopedia of Genes and Genomes (KEGG) pathways. The count meant the number of genes involved in the given term.

aging is associated with GM volume loss (Allen et al., 2005; Walhovd et al., 2005), including in the parietal lobe, temporal cortex, and especially in the frontal lobe (Matsuda, 2013; Van Petten et al., 2004). Along with losses of GMV, normal aging is characterized by a gradual decline in cognitive processes such as executive function, episodic memory, working memory, and processing speed (Lee et al., 2016). Consistent with these studies, our results presented that the GMV of all networks correlated with brain age significantly. In addition, we found that only when the central executive network was excluded did the performance of the prediction model significantly degrade (Steiger's $Z = 2.114$, $p = 0.035$). These results hinted that the central executive network could be a potential biomarker of brain age. The reason might be that the effect of brain aging on the central executive network was more consistent across different populations than regions like the amygdala, hippocampus, and thalamus (Matsuda, 2013). Individuals exhibiting age-related decline tended to show impairments of executive functions first, suggesting that this network might be particularly vulnerable during normal aging (Sorel and Pennequin, 2008). In addition, a linear volume reduction of the central executive network with increasing age even occurred during the earlier stages of adulthood (Terribilli et al., 2011). As a supplement to these studies, our results revealed that the GMV of the central executive network played a decisive role in predicting brain age.

We further investigated the transcriptional signatures of the brain age-related networks. Although brain age was employed in abnormal aging trajectories in various diseases (Gaser et al., 2013; Habes and Janowitz, 2016; Hajek et al., 2019; Han et al., 2021; He et al., 2020), studies investigating the underlying biological foundation of brain age are scarce. To the best of our knowledge, only one study linked polygenic risk score and accelerated brain aging in AD (Habes and Janowitz, 2016). For the first time, we found that brain age-related genes were enriched in GO processes/KEGG pathways clustered into a number of groups such as regulation of iron/calcium transmembrane transport, synaptic signaling, synapse organization, retrograde endocannabinoid signaling (e.g., dopaminergic synapse), behavior (e.g., memory and associative learning), neurotransmitter secretion, and dendrite development. Calcium-dependent signals were key triggers of the molecular mechanisms underlying learning and memory; dysregulation of its homeostasis in the aging brain was hypothesized to underlie aging-related cognitive decline (Oliveira and Bading, 2011). In the brain, iron was involved in many fundamental biological processes, including neurotransmitter synthesis and metabolism; its homoeostasis played an important role in maintaining normal function (Ward et al., 2014). Normal brain aging is accompanied by selective accumulation of iron. Greater accumulation of iron was observed in neurodegenerative diseases associated with oxidative stress and cellular damage (Zecca et al., 2004). In addition, both the density and morphology of dendritic trees mainly possessed by pyramidal neurons underwent progressive regression in the neocortex

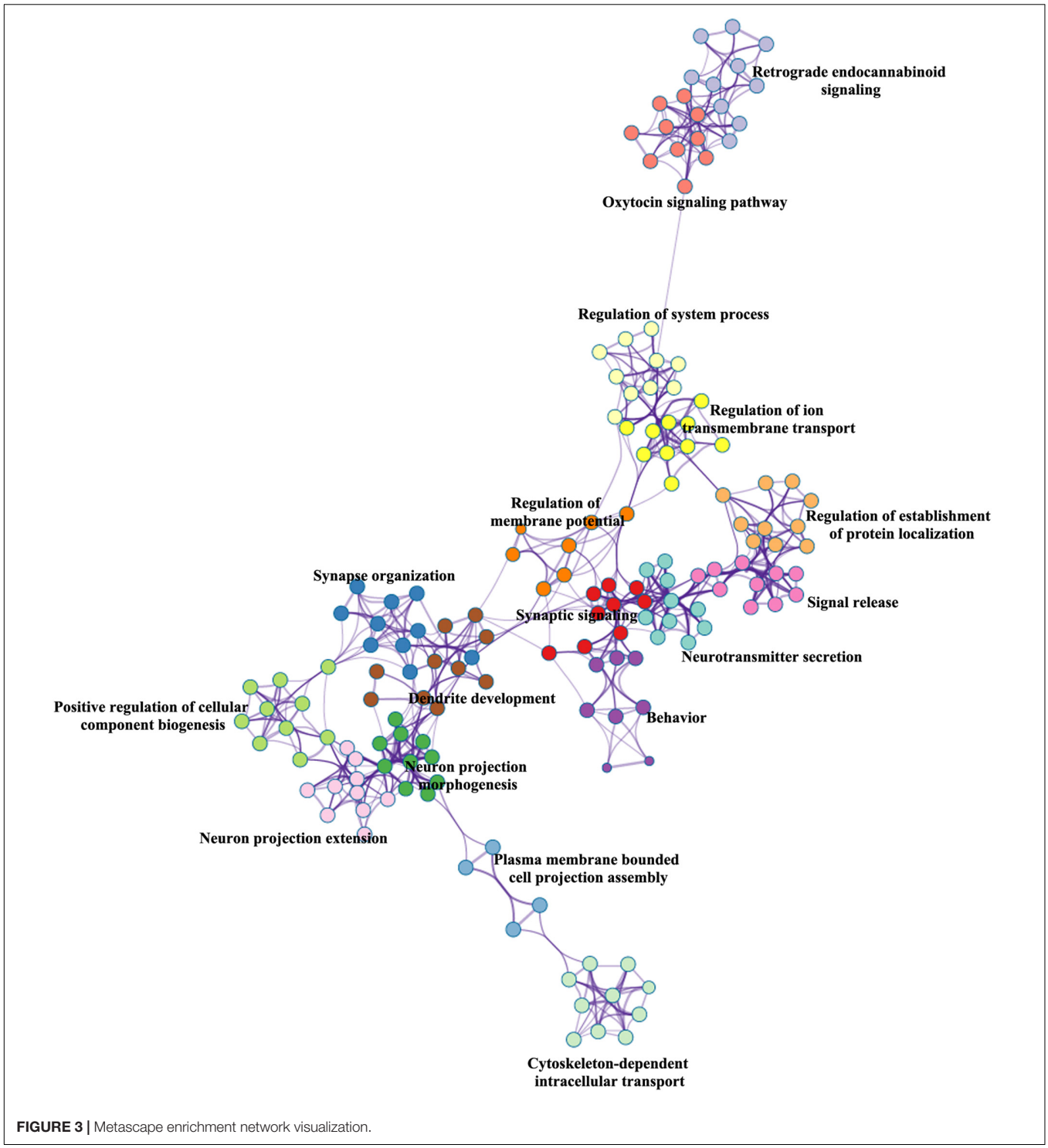

FIGURE 3 | Metascape enrichment network visualization.

(Dickstein et al., 2013) without neuronal death (Morrison and Hof, 1997). Consistent with the notion that no single mechanism explains the aging process (Kyng et al., 2003), we identified a number of GO processes/KEGG pathways underlying brain age.

Several limitations should be considered when understanding our results. Firstly, factors such as educational level could also affect the GMV. For example, greater GMV in the superior temporal gyrus, insula, and anterior cingulate cortex were found in more educated individuals (Arenaza-Urquijo et al., 2013). As this information was not included in the dataset used in the current study, future studies might explore its effect on brain age. Secondly, the gene expression data and neuroimaging

data did not come from the same subjects. Considering the high degree of conservation in overall gene expression across human populations (Stranger et al., 2007; Zhu et al., 2021), the expressions of brain age-related genes could be believable.

CONCLUSION

As a supplement to previous studies exploring brain age, our results reveal a decisive role of the GMV of the central executive network in brain age prediction. In addition, the present study investigated the underlying transcriptional profiling of the central executive network. As a result, we found that brain age-related genes were enriched in GO processes/KEGG pathways clustered into a number of aging-related mechanisms such as regulation of iron/calcium transmembrane transport and dendrite development. In all, these results reveal that the GMV of the central executive network played a vital role in predicting brain age and bridged the gap between transcriptome and neuroimaging promoting an integrative understanding of the pathophysiology of brain age.

DATA AVAILABILITY STATEMENT

The original contributions presented in the study are included in the article/**Supplementary Material**, further inquiries can be directed to the corresponding author/s.

ETHICS STATEMENT

The studies involving human participants were reviewed and approved by the Research Ethics Committee of the Brain Imaging Center of Southwest University, in accordance with the Declaration of Helsinki. The patients/participants provided their written informed consent to participate in this study.

AUTHOR CONTRIBUTIONS

KF analyzed the data and wrote the manuscript. SH designed the research, analyzed the data, and wrote the manuscript. YL and JD searched the literature. JW modified the language. WZ directed the research program and provided guidance and suggestions for the study. All authors read and approved the final manuscript.

FUNDING

This research study was supported by the Soft Science Project of Medical Science and Technology of Henan Province (RKX202002011).

ACKNOWLEDGMENTS

The authors thank all subjects who participated in this study.

SUPPLEMENTARY MATERIAL

The Supplementary Material for this article can be found online at: https://www.frontiersin.org/articles/10.3389/fnins.2021.733316/full#supplementary-material

REFERENCES

Allen, J. S., Bruss, J., Brown, C. K., and Damasio, H. (2005). Normal neuroanatomical variation due to age: the major lobes and a parcellation of the temporal region. *Neurobiol. Aging* 26, 1245–1260. doi: 10.1016/j.neurobiolaging.2005.05.023

Amaducci, L., and Tesco, G. (1994). Aging as a major risk for degenerative diseases of the central nervous system. *Curr. Opin. Neurol.* 7, 283–286.

Anderton, B. H. (2002). Ageing of the brain. *Mech. Ageing Dev.* 123, 811–817.

Arenaza-Urquijo, E. M., Landeau, B., La Joie, R., Mevel, K., Mézenge, F., Perrotin, A., et al. (2013). Relationships between years of education and gray matter volume, metabolism and functional connectivity in healthy elders. *Neuroimage* 83, 450–457. doi: 10.1016/j.neuroimage.2013.06.053

Ashburner, J. (2009). Computational anatomy with the SPM software. *Magn. Reson. Imaging* 27, 1163–1174.

Bashyam, V. M., Erus, G., Doshi, J., Habes, M., Nasrallah, I., Truelove-Hill, M., et al. (2020). MRI signatures of brain age and disease over the lifespan based on a deep brain network and 14 468 individuals worldwide. *Brain* 143, 2312–2324.

Cole, J. H., and Franke, K. (2017). Predicting age using neuroimaging: innovative brain ageing biomarkers. *Trends Neurosci.* 40, 681–690.

Dickstein, D. L., Weaver, C. M., Luebke, J. I., and Hof, P. R. (2013). Dendritic spine changes associated with normal aging. *Neuroscience* 251, 21–32.

Fan, L., Li, H., Zhuo, J., Zhang, Y., Wang, J., Chen, L., et al. (2016). The human brainnetome atlas: a new brain atlas based on connectional architecture. *Cereb. Cortex* 26, 3508–3526. doi: 10.1093/cercor/bhw157

Feng, C., Yuan, J., Geng, H., Gu, R., Zhou, H., Wu, X., et al. (2018). Individualized prediction of trait narcissism from whole-brain resting-state functional connectivity. *Hum. Brain Mapp.* 39, 3701–3712. doi: 10.1002/hbm.24205

Ferri, C. P., Prince, M., Brayne, C., Brodaty, H., Fratiglioni, L., Ganguli, M., et al. (2005). Global prevalence of dementia: a Delphi consensus study. *Lancet* 366, 2112–2117.

Fornito, A., Arnatkevièiûtë, A., and Fulcher, B. D. (2019). Bridging the gap between connectome and transcriptome. *Trends Cogn. Sci.* 23, 34–50.

Franke, K., Ziegler, G., Klöppel, S., and Gaser, C. (2010). Estimating the age of healthy subjects from T1-weighted MRI scans using kernel methods: exploring the influence of various parameters. *Neuroimage* 50, 883–892. doi: 10.1016/j.neuroimage.2010.01.005

Gaser, C., Franke, K., Klöppel, S., Koutsouleris, N., and Sauer, H. (2013). BrainAGE in mild cognitive impaired patients: predicting the conversion to Alzheimer's disease. *PLoS One* 8:e67346. doi: 10.1371/journal.pone.0067346

Habes, M., and Janowitz, D. (2016). Advanced brain aging: relationship with epidemiologic and genetic risk factors, and overlap with Alzheimer disease atrophy patterns. *Transl. Psychiatry* 6:e775. doi: 10.1038/tp.2016.39

Hajek, T., Franke, K., Kolenic, M., Capkova, J., Matejka, M., Propper, L., et al. (2019). Brain age in early stages of bipolar disorders or schizophrenia. *Schizophr. Bull.* 45, 190–198.

Han, S., Chen, Y., Zheng, R., Li, S., Jiang, Y., Wang, C., et al. (2021). The stage-specifically accelerated brain aging in never-treated first-episode patients with depression. *Hum. Brain Mapp.* 42, 3656–3666. doi: 10.1002/hbm.25460

Harada, C. N., Natelson Love, M. C., and Triebel, K. L. (2013). Normal cognitive aging. *Clin. Geriatr. Med.* 29, 737–752.

Hawrylycz, M. J., Lein, E. S., Guillozet-Bongaarts, A. L., Shen, E. H., Ng, L., Miller, J. A., et al. (2012). An anatomically comprehensive atlas of the adult human brain transcriptome. *Nature* 489, 391–399.

He, C., Chen, H., Uddin, L. Q., Erramuzpe, A., Bonifazi, P., Guo, X., et al. (2020). Structure-function connectomics reveals aberrant developmental trajectory occurring at preadolescence in the autistic brain. *Cereb. Cortex* 30, 5028–5037. doi: 10.1093/cercor/bhaa098

Jylhävä, J., Pedersen, N. L., and Hägg, S. (2017). Biological age predictors. *EBioMedicine* 21, 29–36.

Kirova, A. M., Bays, R. B., and Lagalwar, S. (2015). Working memory and executive function decline across normal aging, mild cognitive impairment, and Alzheimer's disease. *Biomed. Res. Int.* 2015:748212.

Kyng, K. J., May, A., Kølvraa, S., and Bohr, V. A. (2003). Gene expression profiling in Werner syndrome closely resembles that of normal aging. *Proc. Natl. Acad. Sci. U.S.A.* 100, 12259–12264. doi: 10.1073/pnas.2130723100

Lee, A., Tan, M., and Qiu, A. (2016). Distinct aging effects on functional networks in good and poor cognitive performers. *Front. Aging Neurosci.* 8:215. doi: 10.3389/fnagi.2016.00215

Li, J., and Seidlitz, J. (2021). Cortical structural differences in major depressive disorder correlate with cell type-specific transcriptional signatures. *Nat. Commun.* 12:1647. doi: 10.1038/s41467-021-21943-5

Lin, C. W., Chang, L. C., Ma, T., Oh, H., and French, B. (2020). Older molecular brain age in severe mental illness. *Mol. Psychiatry* doi: 10.1038/s41380-020-0834-1 [Epub ahead of print].

Liu, Z., Rolls, E. T., Liu, Z., Zhang, K., Yang, M., Du, J., et al. (2019). Brain annotation toolbox: exploring the functional and genetic associations of neuroimaging results. *Bioinformatics* 35, 3771–3778. doi: 10.1093/bioinformatics/btz128

Marquand, A. F., Rezek, I., Buitelaar, J., and Beckmann, C. F. (2016). Understanding heterogeneity in clinical cohorts using normative models: beyond case-control studies. *Biol. Psychiatry* 80, 552–561.

Matsuda, H. (2013). Voxel-based morphometry of brain mri in normal aging and Alzheimer's disease. *Aging Dis.* 4, 29–37.

Morrison, J. H., and Hof, P. R. (1997). Life and death of neurons in the aging brain. *Science* 278, 412–419.

Oliveira, A. M., and Bading, H. (2011). Calcium signaling in cognition and aging-dependent cognitive decline. *Biofactors* 37, 168–174.

Plassman, B. L., Langa, K. M., Fisher, G. G., Heeringa, S. G., Weir, D. R., Ofstedal, M. B., et al. (2007). Prevalence of dementia in the United States: the aging, demographics, and memory study. *Neuroepidemiology* 29, 125–132.

Raji, C. A., Lopez, O. L., Kuller, L. H., Carmichael, O. T., and Becker, J. T. (2009). Age, Alzheimer disease, and brain structure. *Neurology* 73, 1899–1905.

Rasmussen, C. E., and Williams, C. K. I. (2005). *Gaussian Processes for Machine Learning*. Cambridge, MA: MIT Press.

Reardon, P. K., and Seidlitz, J. (2018). Normative brain size variation and brain shape diversity in humans. *Science* 360, 1222–1227. doi: 10.1126/science.aar2578

Ren, Z., Daker, R. J., Shi, L., Sun, J., Beaty, R. E., Wu, X., et al. (2021). Connectome-based predictive modeling of creativity anxiety. *Neuroimage* 225:117469. doi: 10.1016/j.neuroimage.2020.117469

Richiardi, J., Altmann, A., Milazzo, A. C., Chang, C., Chakravarty, M. M., Banaschewski, T., et al. (2015). Brain networks. Correlated gene expression supports synchronous activity in brain networks. *Science* 348, 1241–1244.

Romero-Garcia, R., Seidlitz, J., Whitaker, K. J., Morgan, S. E., Fonagy, P., Dolan, R. J., et al. (2020). Schizotypy-related magnetization of cortex in healthy adolescence is colocated with expression of schizophrenia-related genes. *Biol. Psychiatry* 88, 248–259. doi: 10.1016/j.biopsych.2019.12.005

Sikora, E., Bielak-Zmijewska, A., Dudkowska, M., Krzystyniak, A., Mosieniak, G., Wesierska, M., et al. (2021). Cellular senescence in brain aging. *Front. Aging Neurosci.* 13:646924. doi: 10.1172/JCI95145

Sone, D., Beheshti, I., Maikusa, N., Ota, M., Kimura, Y., Sato, N., et al. (2019). Neuroimaging-based brain-age prediction in diverse forms of epilepsy: a signature of psychosis and beyond. *Mol. Psychiatry* 26, 825–834. doi: 10.1038/s41380-019-0446-9

Sorel, O., and Pennequin, V. (2008). Aging of the planning process: the role of executive functioning. *Brain Cogn.* 66, 196–201.

Stranger, B. E., Nica, A. C., Forrest, M. S., Dimas, A., Bird, C. P., Beazley, C., et al. (2007). Population genomics of human gene expression. *Nat. Genet.* 39, 1217–1224.

Terribilli, D., Schaufelberger, M. S., Duran, F. L., Zanetti, M. V., Curiati, P. K., Menezes, P. R., et al. (2011). Age-related gray matter volume changes in the brain during non-elderly adulthood. *Neurobiol. Aging* 32, 354–368.

Van Petten, C., Plante, E., Davidson, P. S., Kuo, T. Y., Bajuscak, L., and Glisky, E. L. (2004). Memory and executive function in older adults: relationships with temporal and prefrontal gray matter volumes and white matter hyperintensities. *Neuropsychologia* 42, 1313–1335. doi: 10.1016/j.neuropsychologia.2004.02.009

Wagner, K. H., Cameron-Smith, D., Wessner, B., and Franzke, B. (2016). Biomarkers of aging: from function to molecular biology. *Nutrients* 8:338.

Walhovd, K. B., Fjell, A. M., Reinvang, I., Lundervold, A., Dale, A. M., Eilertsen, D. E., et al. (2005). Effects of age on volumes of cortex, white matter and subcortical structures. *Neurobiol. Aging* 26, 1261–1270.

Ward, R. J., Zucca, F. A., Duyn, J. H., Crichton, R. R., and Zecca, L. (2014). The role of iron in brain ageing and neurodegenerative disorders. *Lancet Neurol.* 13, 1045–1060.

Wei, D., Zhuang, K., Ai, L., Chen, Q., Yang, W., Liu, W., et al. (2018). Structural and functional brain scans from the cross-sectional Southwest University adult lifespan dataset. *Sci. Data* 5:180134. doi: 10.1038/sdata.2018.134

Yeo, B. T., Krienen, F. M., Sepulcre, J., Sabuncu, M. R., Lashkari, D., Hollinshead, M., et al. (2011). The organization of the human cerebral cortex estimated by intrinsic functional connectivity. *J. Neurophysiol.* 106, 1125–1165.

Zecca, L., Stroppolo, A., Gatti, A., Tampellini, D., Toscani, M., Gallorini, M., et al. (2004). The role of iron and copper molecules in the neuronal vulnerability of locus coeruleus and substantia nigra during aging. *Proc. Natl. Acad. Sci. U.S.A.* 101, 9843–9848. doi: 10.1073/pnas.0403495101

Zhou, Y., Zhou, B., Pache, L., and Chang, M. (2019). Metascape provides a biologist-oriented resource for the analysis of systems-level datasets. *Nat. Commun.* 10:1523. doi: 10.1038/s41467-019-09234-6

Zhu, D., Yuan, T., Gao, J., Xu, Q., Xue, K., Zhu, W., et al. (2021). Correlation between cortical gene expression and resting-state functional network centrality in healthy young adults. *Hum. Brain Mapp.* 42, 2236–2249. doi: 10.1002/hbm.25362

Ziegel, E. R. (2010). The elements of statistical learning. *Technometrics* 45, 267–268.

Conflict of Interest: The authors declare that the research was conducted in the absence of any commercial or financial relationships that could be construed as a potential conflict of interest.

Publisher's Note: All claims expressed in this article are solely those of the authors and do not necessarily represent those of their affiliated organizations, or those of the publisher, the editors and the reviewers. Any product that may be evaluated in this article, or claim that may be made by its manufacturer, is not guaranteed or endorsed by the publisher.

frontiers in Neuroscience

ORIGINAL RESEARCH
published: 29 September 2021
doi: 10.3389/fnins.2021.731292

Bridging the Gap Between Morphometric Similarity Mapping and Gene Transcription in Alzheimer's Disease

*Yang Zhang[1], Min Ma[1], Zhonghua Xie[2], Heng Wu[3], Nan Zhang[4] and Junlin Shen[1]**

[1] Department of Medical Imaging and Tianjin Key Laboratory of Functional Imaging, Tianjin Medical University General Hospital, Tianjin, China, [2] Department of Mathematics, School of Science, Tianjin University of Science and Technology, Tianjin, China, [3] Tianjin Key Laboratory of Lung Cancer Metastasis and Tumor Microenvironment, Tianjin Lung Cancer Institute, Tianjin Medical University General Hospital, Tianjin, China, [4] Department of Neurology, Tianjin Medical University General Hospital, Tianjin, China

Disruptions in brain connectivity have been widely reported in Alzheimer's disease (AD). Morphometric similarity (MS) mapping provides a new way of estimating structural connectivity by interregional correlation of T1WI- and DTI-derived parameters within individual brains. Here, we aimed to identify AD-related MS changing patterns and genes related to the changes and further explored the molecular and cellular mechanism underlying MS changes in AD. Both 3D-T1WI and DTI data of 106 AD patients and 106 well-matched healthy elderly individuals from the ADNI database were included in our study. Cortical regions with significantly decreased MS were found in the temporal and parietal cortex, increased MS was found in the frontal cortex and variant changes were found in the occipital cortex in AD patients. Mean MS in regions with significantly changed MS was positively or negatively associated with memory function. Negative MS-related genes were significantly downregulated in AD, specifically enriched in neurons, and participated in biological processes, with the most significant term being synaptic transmission. This study revealed AD-related cortical MS changes associated with memory function. Linking gene expression to cortical MS changes may provide a possible molecular and cellular substrate for MS abnormality and cognitive decline in AD.

Keywords: Alzheimer's disease, morphometric similarity, Allen Human Brain Atlas, gene transcription, sMRI = structural MRI

OPEN ACCESS

Edited by:
Liang Zhan,
University of Pittsburgh, United States

Reviewed by:
Zhigang Qi,
Capital Medical University, China
Shaoqiang Han,
First Affiliated Hospital of Zhengzhou University, China

****Correspondence:***
Junlin Shen
shenjunlin8390@163.com

Specialty section:
This article was submitted to Brain Imaging Methods, a section of the journal Frontiers in Neuroscience

Received: *26 June 2021*
Accepted: *03 September 2021*
Published: *29 September 2021*

Citation:
Zhang Y, Ma M, Xie Z, Wu H, Zhang N and Shen J (2021) Bridging the Gap Between Morphometric Similarity Mapping and Gene Transcription in Alzheimer's Disease. Front. Neurosci. 15:731292. doi: 10.3389/fnins.2021.731292

INTRODUCTION

Alzheimer's disease (AD) is a neurodegenerative disease marked by progressive neuron loss, manifested by short-term memory and other cognitive impairment symptoms (Wang et al., 2020). AD-related neurodegeneration involves several brain regions, in which the entorhinal, hippocampal and temporal cortices are the most reported (Lerch et al., 2005; Im et al., 2008; Morra et al., 2008; Seong et al., 2010; Li et al., 2014; Femminella et al., 2018). Structural indicators of these regions, including gray matter density (Frisoni et al., 2002), volume (Busatto et al., 2003), cortical thickness (Pettigrew et al., 2017), and curvature (Im et al., 2008; Seong et al., 2010), have been found to be decreased in AD patients. White matter studies based on diffusion tensor imaging (DTI) have also demonstrated reduced integrity in the temporal lobe as well as white matter tracts connecting

frontal and temporal regions in AD (Naggara et al., 2006; Kantarci et al., 2017). In recent years, AD has been widely regarded as a disconnected syndrome whereby a large-scale brain network is progressively disrupted by neuropathological processes. MR topological studies constructed whole-brain structural networks and demonstrated abnormal topological properties in multiple brain regions, including the hippocampal, frontal, temporal, parietal and occipital regions, verifying brain network disruption and disconnection between anatomically connected brain regions in AD patients (Lo et al., 2010; Yao et al., 2010).

All the above-mentioned multiregional changes in either gray matter (from 3D T1WI) or white matter (from DTI) may be attributed to dysconnectivity of large-scale brain structural networks in AD. However, a structural covariance network using T1WI could not be applied to single-subject level analysis, and precisely estimating long-distance connections still constrains DTI-based tractography. Here, we adopted a different parameter from the past—"morphometric similarity (MS)"—which is estimated as the inter-regional correlation of multiple macro- and micro-structural multimodal MRI variables, based on both structural T1WI and DTI (Stam et al., 2007). It reflects the anatomical connections of different brain areas from histological similarity and axonal connectivity within an individual human brain (Seidlitz et al., 2018). Given that AD has been considered a disconnection syndrome due to regional vulnerability to cellular neurodegeneration and disconnection of distant cortical regions (Gonzalez-Escamilla et al., 2020), it is suitable to evaluate brain anatomical connectivity in AD patients using MS as a neuroimaging indicator.

AD is a highly heritable disease (Bellenguez et al., 2020). Investigating the link between related gene expression and internal brain structure helps to understand the pathophysiological processes of the disease. The Allen Human Brain Atlas (AHBA) can present gene transcription information in the same standard space as neuroimaging data, providing a new approach for linking gene expression to neuroimaging phenotypes. With this approach, only a few reports combine gene transcription data with gray matter volumes in AD. However, it is unclear which genes related to AD-specific MS changes are specific to which neurological functions and how the expression of these genes affects MS changes. In the current study, we investigated the MS changing pattern map in AD and spatially associated the MS changing pattern map with anatomically patterned gene expression using data from the AHBA. We aimed to identify AD-related MS changing patterns and genes closely related to the changes and further explore the cellular and molecular mechanism underlying MS changes in AD.

MATERIALS AND METHODS

Participates

A total of 113 AD patients with their initial 3T MRI scans, including both 3D T1WI and DTI data, were obtained from ADNI database[1] which followed the standard ADNI-GO and ADNI-2 protocols (Jack et al., 2010; Weiner et al., 2017). The main inclusion criteria were as follows: (1). subjective memory concern as reported by subject, study partner or clinician; (2). abnormal memory function documented by scoring within the education adjusted ranges on the Logical Memory II subscale from the Wechsler Memory Scale-Revised; (3). Mini-Mental State Exam (MMSE) score between 20 and 26; (4). Clinical Dementia Rating 0.5 or 1.0; and 5. NINCDS/ADRDA criteria for probable AD. All images were visually inspected by two radiologists, and seven patients with poor image quality (2 patients' 3D T1WI and five patients' DTI) were excluded. Finally, 106 AD patients with qualified image data were included (63 males and 43 females; mean age 75, ranging from 55 to 90 years). For comparison, an equal number of age- and gender-matched healthy elders with qualified 3D-T1WI and DTI were selected from the ADNI database (63 males and 43 females; mean age 75, ranging from 55 to 90 years). The detailed scan parameters are provided in **Supplementary Table 1**. General cognitive function was assessed by the MMSE and the Clinical Dementia Rating. Memory function was evaluated by a memory composite score obtained for the majority of participants (94 subjects with AD and 99 subjects with healthy elderly individuals) (Crane et al., 2012).

Morphometric Similarity Estimation

Surface-based morphology parameter estimation from high-resolution T1WI was performed using FreeSurfer v6.0.0.[2] The DTI data were preprocessed according to the pipeline of FMRIB's Diffusion Toolbox implemented in FSL 5.0.10.[3] The detailed preprocessing procedures for T1WI and DTI data are provided in **Supplementary Material**.

The DTI parameters of fractional anisotropy and mean diffusion were defined as myelination metrics. Among the surface-based morphology parameters, the gray matter, surface area and cortical thickness were defined as gray matter metrics, and the intrinsic/Gaussian curvature and mean curvature were the curvature metrics.

To adjust the variation from multiple sites and scanners, the ComBat harmonization of surface-based morphology and diffusion parameters across scanners and sites was performed before the downstream morphometric similarity estimation (Fortin et al., 2017, 2018). Then, these metrics were Z-score transformed to improve normality.

The Pearson correlation of gray matter, curvature and myelination metrics between each pair of cortical regions was performed to generate 308 × 308 MS matrices for each subject. Then, the 308 × 308 MS matrices were averaged across the 308 cortical regions to calculate the regional MS for every 308 cortical regions. From the brain connectome perspective, the regional MS represents the weighted degree of each cortical node, which was connected by signed and

[1] http://adni.loni.ucla.edu

[2] http://surfer.nmr.mgh.harvard.edu/

[3] http://www.fmrib.ox.ac.uk

weighted edges of pairwise similarity to all other cortical nodes in the whole brain.

Transcription-Imaging Association

A compiled transcription matrix of six postmortem adult brains from the AHBA[4] was acquired from the data directory for Neuroscience in Psychiatry Network manuscript,[5] which provided expression values for each of 20,737 genes estimated in 151 cortical regions of the left hemisphere. PLS regression was used to identify genes whose transcriptional profiles were significantly associated with regional MS differences. In this study, the independent variable was the compiled AHBA transcription matrix (151 regions × 20,737 genes), and the dependent variables were the vector of regional MS case-control *T*-values from the left hemisphere (151 regions). The first PLS component (PLS1) weight of each gene was assigned in terms of its contribution to the overall model. Then, the ratio of each gene's PLS1 weight to its bootstrapped standard error (1,000 resamplings with replacement of the 151 cortical regions) was calculated as a *Z* score. Here, genes with | *Z* score | > 4.72 (Bonferroni correction of $P < 0.05$) denoted the PLS1 gene set. Details about the transcription-imaging association are provided in **Supplementary Material**.

Disease Enrichment Analyses

Disease enrichment analyses were used to explore whether the PLS1 gene set was enriched in AD-related differentially expressed genes (DEGs). The expression dataset with series accession number GSE5281 from the Gene Expression Omnibus database[6] was acquired to screen the AD-related DEGs. The LIMMA package (version 3.42.2) of R software was used to analyze the DEGs between AD and normal elderly individuals. $P < 0.01$ and | $\log_2$ (fold change) | > 1 were defined as the thresholds for screening AD-related DESs. Fisher's exact test was used to evaluate the significance of the overlap between PLS1 gene sets and AD-related DEGs. The Bonferroni method was used to correct for multiple comparisons (both up- and downregulated DEGs) ($Pc < 0.05$, an uncorrected $P < 0.05/2 = 0.025$). Details about the disease enrichment analyses are provided in **Supplementary Material**.

Cell-Type-Specific Analysis

The RNAseq dataset with series accession number GSE73721 from the Gene Expression Omnibus database was acquired to perform cell-type-specific analysis. pSI v1.1[7] was used to determine the specific neocortical cell type for which the PLS1-genes were enriched. A pSI threshold of 0.05 was used to generate the cell-type-enriched gene lists for each type of cortical cell. Fisher's exact test was used to evaluate the significance of the overlap between PLS1 gene sets and cell-type-specific genes for each type of cortical cell. The Bonferroni method was used to correct for multiple comparisons (5 cell types) ($Pc < 0.05$, an uncorrected $P < 0.05/4 = 0.01$). Details about the cell type-specific analysis are provided in **Supplementary Material**.

Gene Ontology Analysis

The clusterProfiler package (v3.14.3) of R software was used to perform the gene ontology (GO) analysis. Our study only focused on the biological process of GO terms in which the PLS1 gene sets were enriched. A Bonferroni adjusted *P*-value < 0.05 was considered significant.

Statistical Analysis

The statistical analyses for demographic and cognitive data were performed using the Statistical Package for the Social Sciences (SPSS version 18.0). Comparisons between AD patients and healthy elderly individuals were performed using a two-sample *T*-test for continuous variables with a normal distribution and

TABLE 1 | Demographics and cognition.

	AD (n = 106)	NC (n = 106)	T/χ^2	*P*-value
Age, years	74.94 ± 8.02	74.92 ± 7.84	0.026	0.979
Education, years	15.59 ± 2.60	16.27 ± 2.50	−1.92	0.06
Gender, male/female	63/43	63/43	0	1
MMSE	22.92 ± 3.13	28.57 ± 1.73	−16.26	0.0001
CDR	0.81 ± 0.27	0.04 ± 0.13	26.13	0.0001
Memory composite score*	−0.85 ± 0.50	0.79 ± 0.54	−22.01	0.0001

*The data are shown as means (SD). The symbol * indicates that the composite memory score was available from 94 of the 106 AD and 99 of the 106 NC. AD, Alzheimer's disease; CDR, Clinical Dementia Rating; MMSE, Mini-Mental State Examination; NC, normal control subject.*

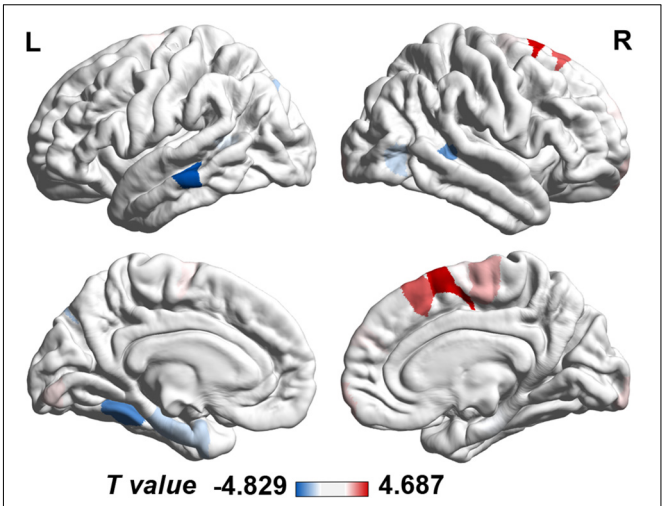

FIGURE 1 | Case-control differences in regional morphometric similarity ($P < 0.05$, FDR corrected). Regions in blue indicate significantly decreased morphometric similarity in AD, whereas regions in red indicate significantly increased morphometric similarity in AD. FDR, false discovery rate; L, left; R, right.

[4]http://human.brain-map.org/

[5]https://doi.org/10.6084/m9.figshare.2057796.v1

[6]https://www.ncbi.nlm.nih.gov/geo/

[7]http://genetics.wustl.edu/jdlab/psi_package/

TABLE 2 | Cortical regions of case-control differences in regional morphometric similarity.

Cortical regions	Coordinates (MNI)			*T* value	*P*-value	FDR
	x	y	z			
L_middletemporal_part5	−60.019	−27.635	−13.299	−4.8294	2.66E-06	7.74E-04
L_fusiform_part1	−30.238	−46.494	−17.452	−4.2592	3.11E-05	3.196E-04
R_bankssts_part1	53.969	−39.123	1.4973	−4.1341	5.18E-05	3.986E-03
L_superiorparietal_part8	−23.65	−73.056	29.861	−3.5866	4.18E-04	0.021429
L_parahippocampal_part1	−25.991	−25.187	−25.332	−3.5065	5.57E-04	0.021429
R_lateraloccipital_part2	44.513	−70.022	−2.0359	−3.4184	7.59E-04	0.024105
L_entorhinal_part1	−24.011	−5.8614	−32.827	−3.4094	7.83E-04	0.024105
L_bankssts_part2	−53.141	−49.843	8.2646	−3.2373	0.001405	0.035229
R_parahippocampal_part2	27.448	−24.861	−24.205	−3.0702	0.002426	0.04151
L_supramarginal_part7	−49.357	−38.912	32.554	−3.0206	0.00284	0.046042
R_superiorfrontal_part7	9.6868	8.2947	60.026	4.6868	5.03E-06	7.74E-04
R_superiorfrontal_part11	9.2005	24.389	53.686	4.0632	6.87E-05	4.232E-03
R_paracentral_part2	5.3566	−16.772	61.135	3.5071	5.56E-04	0.021429
R_frontalpole_part1	9.8338	62.819	−10.737	3.285	0.0011976	0.033534
R_lateraloccipital_part1	18.646	−99.162	−7.394	3.2203	0.001487	0.035229
L_lingual_part2	−6.5596	−88.407	−8.0452	3.1896	0.001646	0.036218
L_superiorfrontal_part2	−11.687	−8.4248	64.785	3.1488	0.001882	0.038635
R_superiorfrontal_part6	10.21	54.909	26.16	3.1191	0.002073	0.039895
R_superiorfrontal_part3	12.367	−3.2651	65.643	3.0906	0.002272	0.041168

The cortical regions above the middle line of the table are regions with significantly decreased morphometric similarity in AD, whereas the cortical regions under the middle line of the table are regions with significantly increased morphometric similarity in AD. FDR, the corrected P-value with the false discovery rate method.

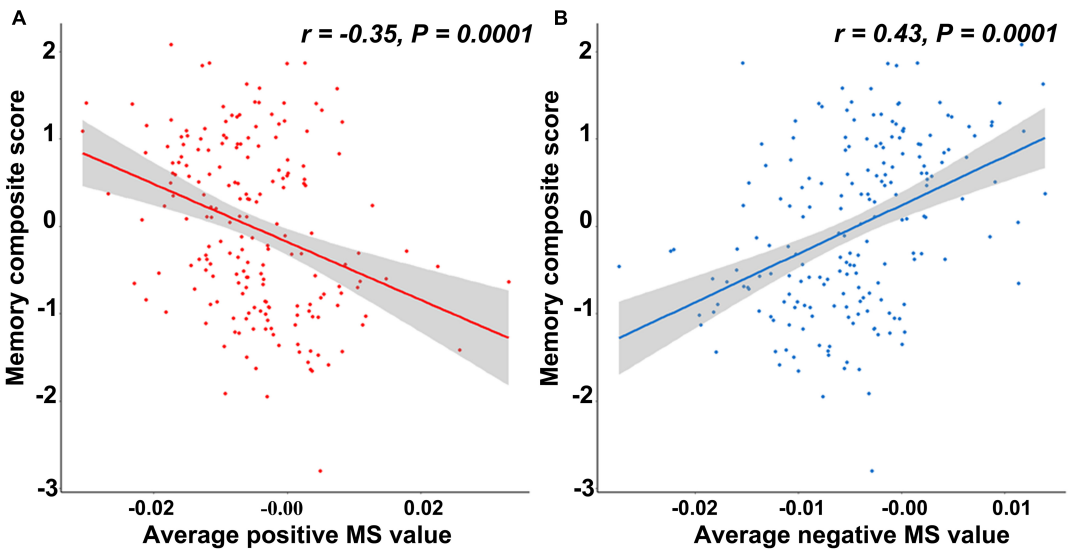

FIGURE 2 | The relationship between the memory composite score and regional morphometric similarity. **(A)** The average morphometric similarity in regions with significantly increased morphometric similarity in AD is significantly negatively correlated with the memory composite score. **(B)** The average morphometric similarity in regions with significantly decreased morphometric similarity in AD is significantly positively correlated with the memory composite score.

a chi-squared test for categorical variables. To test whether the MS of brain regions with significant case-control differences were associated with memory function, partial correlation analysis was conducted with age, gender, and years of education as nuisance covariates. The Pearson correlation analysis was used to test the association between the *Z* scored expression values of PLS1 gene sets and the *T* statistics of case-control differences in MS. The resulting *P*-values above were Bonferroni corrected for multiple comparisons. The case-control difference in regional MS was estimated by fitting linear models with age, gender and education as covariates, and the resulting *P*-values for each region were false discovery rate (FDR) corrected for multiple comparisons.

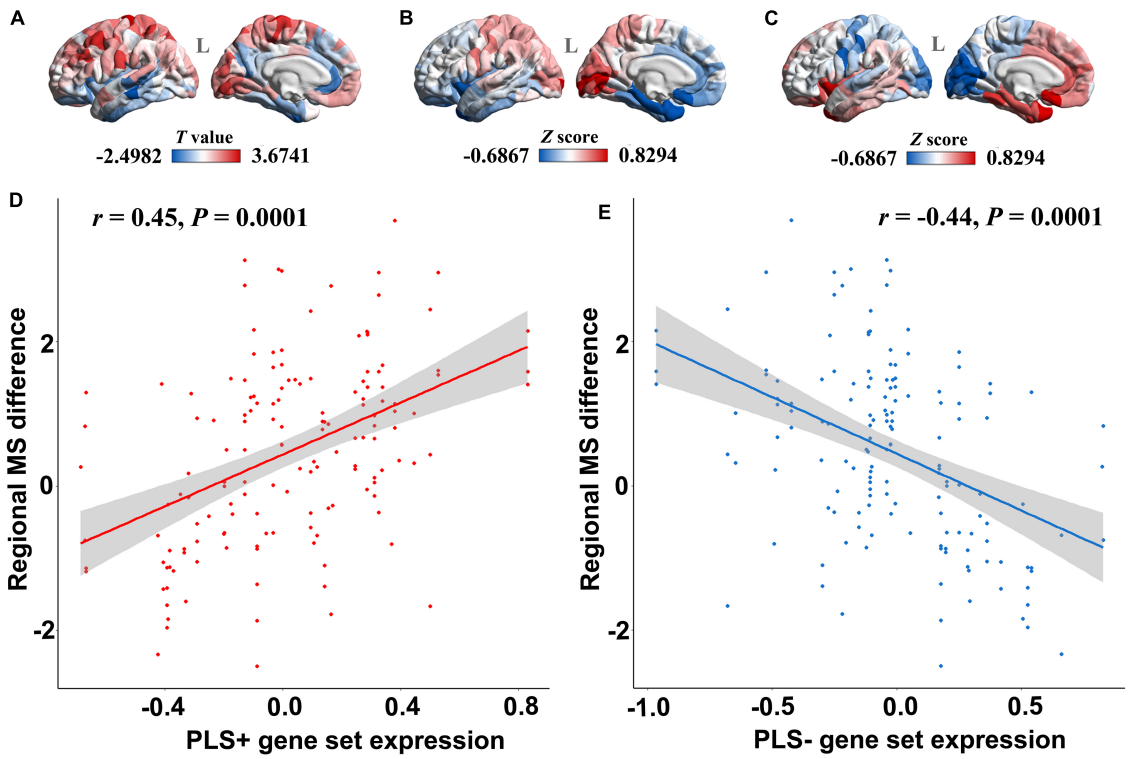

FIGURE 3 | The relationship between PLS1 gene set expression and regional morphometric similarity differences. **(A)** The regional morphometric similarity case-control *T* map in the left hemisphere. The regions in red indicate increased morphometric similarity in AD, whereas the blue color indicates decreased morphometric similarity in AD. **(B)** The PLS1 + gene set expression map illustrates that regions in red have increased expression of the PLS1 + gene set, whereas regions in blue have decreased expression of the PLS1 + gene set. **(C)** The PLS1- gene set expression map illustrates that regions in red have increased expression of the PLS1- gene set, whereas regions in blue have decreased expression of the PLS1- gene set. **(D)** The point plot in red shows that the expression of the PLS1 + gene set is significantly positively correlated with the regional morphometric similarity difference between AD patients and healthy elderly individuals. **(E)** The blue point plot shows that the expression of the PLS1- gene set is significantly negatively correlated with regional morphometric similarity differences between AD patients and healthy elderly individuals.

RESULTS

Demographics and Cognition

A total of 106 AD patients and the same number of age- and gender-matched healthy elderly individuals with qualified image data were ultimately included in the present study. The demographic and cognitive data of these subjects are shown in **Table 1**. Significant differences were found in terms of MMSE ($P = 0.0001$), Clinical Dementia Rating ($P = 0.0001$), and memory composite scores ($P = 0.0001$). No significant differences were observed in terms of age ($P = 0.98$), gender ($P = 1$), or years of education ($P = 0.06$).

Morphometric Similarity Differences Between Alzheimer's Disease and Healthy Elders

The cortical map in **Figure 1** demonstrated the significant differences in regional MS at each cortical area between AD and healthy elderly individuals. Cortical regions with significantly decreased MS were observed in the left middle temporal lobe, left fusiform gyrus, bilateral banks of superior temporal sulci, bilateral parahippocampal lobes, left entorhinal cortex, left superior parietal lobe, left supramarginal gyrus and right lateral occipital lobe (**Table 2**). Cortical regions with significantly increased MS were found in the bilateral superior frontal lobes, right paracentral lobe, right frontal pole cortex, left lingual gyrus and right lateral occipital lobe (**Table 2**). The partial correlation analysis showed that the mean MS average across the 10 regions with decreased MS was significantly positively associated with the memory composite score ($r = 0.43$, $P = 0.0001$), and the mean MS average across the nine regions with increased MS was significantly negatively associated with the memory composite score ($r = -0.35$, $P = 0.0001$) (**Figure 2**).

Gene-Morphometric Similarity Spatial Correlations and Characters

First PLS Component Gene Expression Associated With Morphometric Similarity Difference

The PLS regression analysis revealed 1,932 genes with normalized PLS1 weights *Z* score < -4.72 (Bonferroni correction of $P < 0.05$), which were defined as the PLS1- genes, and 2,139 genes with normalized PLS1 weights *Z* score > 4.72 (Bonferroni

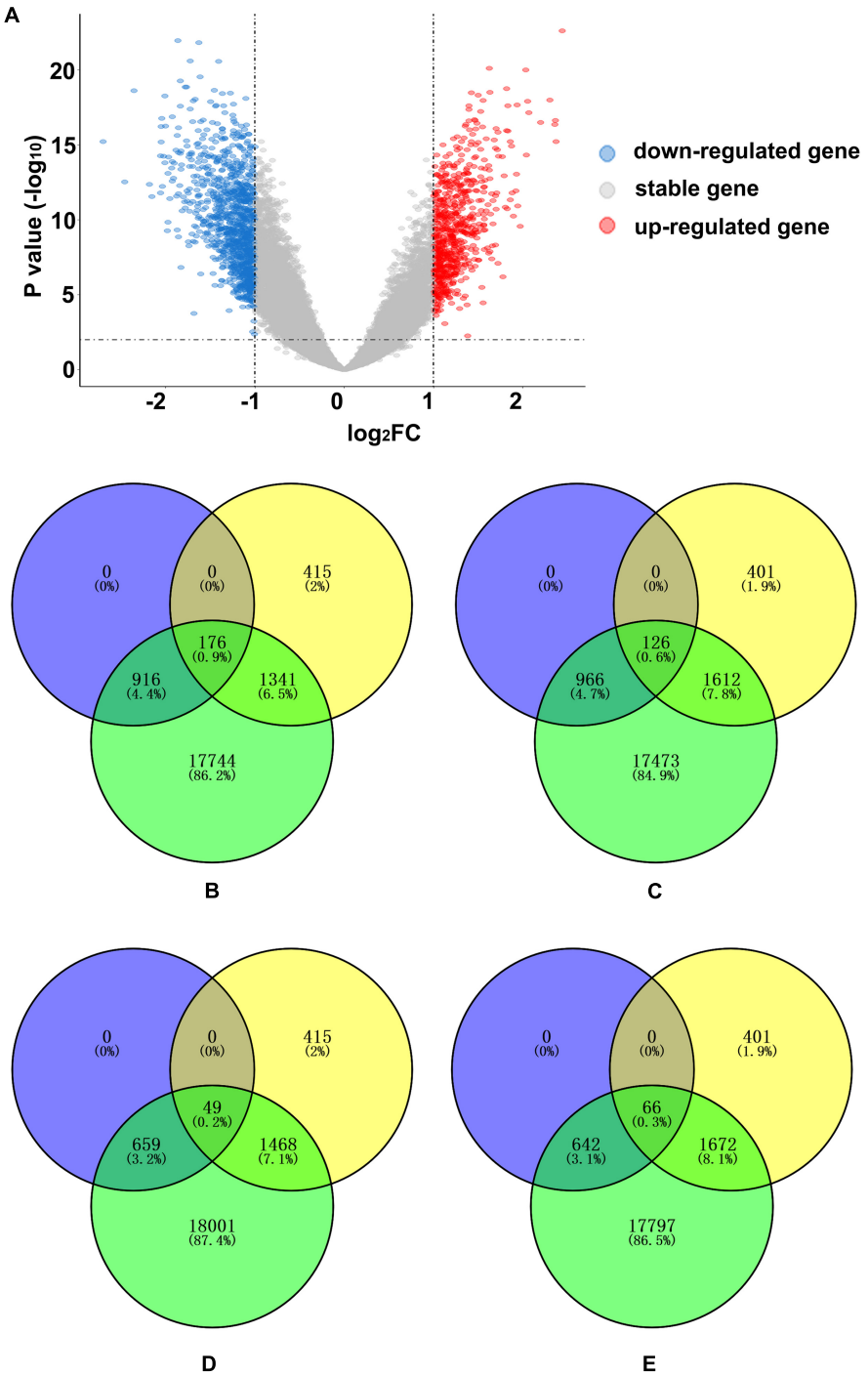

FIGURE 4 | AD-related DEG enrichment analyses for PLS1 gene sets. **(A)** The volcano plot shows 708 upregulated genes in red on the right and 1,092 downregulated genes in blue on the left. **(B)** The PLS1- genes significantly overlapped with downregulated genes. The number of overlapping genes was 176, accounting for 0.9% of the total genes. The purple circle indicates 1,092 downregulated genes, the yellow circle indicates 1,932 PLS1- genes and the green circle indicates 20,177 background genes. **(C)** The PLS1 + genes did not significantly overlap with downregulated genes. The number of overlapping genes was 126, accounting for 0.6% of the total genes. The purple circle indicates 1,092 downregulated genes, the yellow circle indicates 2,139 PLS1 + genes and the green circle indicates 20,177 background genes. **(D)** The PLS1- genes did not significantly overlap with the upregulated genes. The number of overlapping genes was 49, accounting for 0.2% of the total genes. The purple circle indicates 708 up-regulated genes, the yellow circle indicates 1,932 PLS1- genes, and the green circle indicates 20,177 background genes. **(E)** The PLS1 + genes did not significantly overlap with upregulated genes. The number of overlapping genes was 66, accounting for 0.3% of the total genes. The purple circle indicates 708 upregulated genes, the yellow circle indicates 2,139 PLS1 + genes and the green circle indicates 20,177 background genes. DEGs, differentially expressed genes; FC, fold change; PLS, partial least squares regression.

TABLE 3 | The significance of the overlap between PLS1- genes and cell-type-specific genes.

	Astrocytes	Neurons	Oligodendrocytes	Microglia
Overlapped genes	139	195	33	71
Cell-type-specific genes	1,160	1,770	684	746
Gene ratio	0.12	0.11	0.048	0.095
Pc values	1.83×10^{-5}	1.74×10^{-5}	1	0.57

PLS1, the first component of partial least squares regression; Overlapped genes, the number of overlapping genes between PLS1- genes and cell-type-specific genes; Gene ratio, gene ratio between the number of overlapping genes and the number of cell-type-specific genes; Pc values, the Bonferroni corrected P-values.

correction of $P < 0.05$), which were defined as the PLS1 + genes (**Supplementary Table 2**). The majority of cortical regions on the PLS1 + gene expression map were in accordance with those on the case-control T map of regional MS (**Figures 3A,B**), whereas the majority of cortical regions on the PLS1- gene expression map were in contrast with those on the case-control T map of regional MS (**Figures 3A–C**). Pearson correlation analysis revealed that the expression of PLS1 + genes was significantly positively correlated with regional MS differences ($r = 0.45$, $P = 0.0001$) (**Figure 3D**), whereas the expression of PLS1- genes was significantly negatively correlated with regional MS differences ($r = -0.44$, $P = 0.0001$) (**Figure 3E**).

Alzheimer's Disease -Related Differentially Expressed Genes Enrichment for First PLS Component- Genes

A total of 1,800 significant DEGs between AD and normal elderly individuals were identified from the GSE5281 series, with 708 upregulated and 1,092 downregulated genes (**Figure 4A** and **Supplementary Table 3**). Both upregulated and downregulated genes were defined as AD-related DEGs. The enrichment analysis revealed that PLS1- genes were significantly enriched in downregulated DEGs ($Pc = 5.43 \times 10^{-12}$) but not in upregulated DEGs ($Pc = 1$) (**Figures 4B–D**). In addition, PLS1 + genes were not significantly enriched in upregulated DEGs ($Pc = 1$) or in downregulated DEGs ($Pc = 1$) (**Figures 4C–E**).

Cell-Type Specificity of First PLS Component- Genes

The cell-type-enriched gene lists for each type of cortical cell are provided in **Supplementary Table 4**. The PLS1- genes showed significant specific expression in neurons ($Pc = 1.83 \times 10^{-5}$) and astrocytes ($Pc = 1.74 \times 10^{-5}$) but not in oligodendrocytes ($Pc = 1$) or microglia ($Pc = 0.57$) (**Table 3** and **Figure 5A**). The PLS1 + genes were not significantly enriched in any type of neocortical cell ($Pc = 1$ for all) (**Table 4** and **Figure 5B**).

Gene Ontology Enrichment for First PLS Component-Gene Sets

The GO analysis revealed that significant biological processes of the PLS1- genes were mainly enriched in neuron-specific terms, including synaptic signaling, neurotransmitter release, axonogenesis, and cognition (**Figure 6A** and **Supplementary Table 5**). However, the PLS1 + genes were involved in non-neuron-specific biological processes, including potassium ion transport and protein localization (**Figure 6B** and **Supplementary Table 5**).

DISCUSSION

Morphometric Similarity Changing Patterns and Associated Memory Function in Alzheimer's Disease

The MS quantifies the similarity in terms of multiple MRI parameters measured in each area. Compared with traditional measurements based on a single MRI sequence, MS considering multiple MRI morphometric indices (based on both structural T1WI and DTI) could reflect the anatomical connections of different brain areas based on histological similarity and axonal connectivity within an individual human brain.

This study showed that AD patients had decreased regional MS in multiple AD-susceptible regions in the temporal and parietal cortex. Additionally, increased regional MS in several frontal areas and variable changing MS in parts of the occipital cortex were also detected in AD patients compared with healthy elderly individuals. The mean MS average across those regions with decreased regional MS was positively associated with memory function. In contrast, the mean MS average across those regions with increased regional MS was negatively associated with memory function.

Our findings were consistent with a large number of studies reporting decreased gray matter volume and cortical thickness (Lerch et al., 2005; Femminella et al., 2018), lower average mean curvature (Im et al., 2008; Morra et al., 2008) and shallower sulcal depth (Im et al., 2008) in the hippocampus, temporal lobe, fusiform gyrus, and entorhinal cortex in AD, with the left hemisphere being dominant. DTI studies revealed disruptions of white matter integrity in the early stage of AD in limbic fiber tracks with direct connections to medial temporal lobe structures (Kalus et al., 2006; Zhang et al., 2007; Sexton et al., 2010). Moreover, decreased connectivity of multiple brain regions, including the temporal lobe, hippocampus, fusiform gyrus and parietal lobe, has also been documented as the cause of cognitive decline in AD patients (Bokde et al., 2006; Stam et al., 2007; He et al., 2008). Decreased MS in multiple brain regions, including the temporal, parietal and part of the occipital cortical regions in AD, reflected the weakening of the abovementioned brain regions' anatomical connections from the histological and cellular architecture level and implied increased architectonic differentiation and decreased axonal connectivity between these cortical regions. We further found a correlation between the weakening of this anatomical connection and the impairment of memory function, suggesting that the anatomical disconnection caused by the reduction of the similarity of histology and cellular architecture may be the neural basis for the impairment of memory function in AD patients.

Our result of elevated MS in the prefrontal areas and the left lingual gyrus in AD patients suggested increased architectonic similarity and enhanced axonal connectivity in these regions in AD patients. These findings were consistent with enhanced

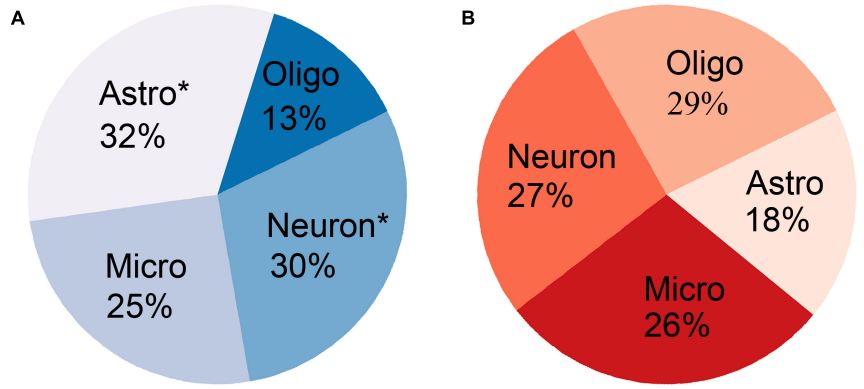

FIGURE 5 | The percentage of gene ratio between overlapping genes and cell-type-specific genes for each type of neocortical cell. **(A)** The PLS1- genes significantly overlapped with cell-type-specific genes in neurons and astrocytes (asterisk) but not in oligodendrocytes and microglia. **(B)** The PLS1 + genes did not significantly overlap with cell-type-specific genes in any type of neocortical cell.

functional activation and connectivity within frontal regions in the early stage of AD (Grady et al., 2003; Aganj et al., 2020). In addition, at the local network level, changes in connectivity of the left lingual gyrus were also reported to be significantly negatively correlated with behavioral performance in AD patients (Chang et al., 2020). We tended to interpret the increased prefrontal and lingual MS in AD as a structural compensatory reallocation of cognitive resources. This explanation was further supported by the negative correlation between the average MS value of the brain areas and increased MS and memory function in AD patients. The more structural compensatory the increase in MS is, the worse the performance of the memory function is. As the disease becomes severe, the structural compensatory increase may disappear, but this needs to be confirmed by future longitudinal studies. Regarding the occipital areas, most AD studies have reported atrophy, hypometabolism (Ten Kate et al., 2018; Das et al., 2021) and connection changes (Huang et al., 2020) in this area in AD patients. Studies have also found an up-regulated signaling pathway located in the occipital area in AD patients, which suggests that an enhancement in dying or surviving neurons plays a protective role by compensating for decreased neurotransmission during the progression of AD (Jacobs et al., 2006). The inconsistent MS change patterns in the occipital areas in AD patients in the current study may be related to different functional areas with distinct changing patterns in the occipital lobe, which was supported by the evidence of the dissociation between impaired explicit memory encoding in secondary visual areas and intact implicit encoding in the primary visual cortex in AD.

TABLE 4 | The significance of the overlap between PLS1 + genes and cell-type-specific genes.

	Astrocytes	Neurons	Oligodendrocytes	Microglia
Overlapped genes	67	153	62	61
Cell-type-specific genes	1,160	1,770	684	746
Gene ratio	0.058	0.086	0.091	0.082
Pc values	1	1	1	1

PLS1, the first component of partial least squares regression; Overlapped genes, the number of overlapping genes between PLS1 + genes and cell-type-specific genes; Gene ratio, ratio between the number of overlapping genes and the number of cell-type-specific genes; Pc values, the Bonferroni corrected P-values.

Linking Gene Expression to Morphometric Similarity Difference Map and Functional Annotation

PLS analysis showed that the PLS1 + gene was positively correlated with the AD-related MS difference map, and the PLS1- gene was negatively correlated with the AD-related MS difference map. However, only PLS1- genes were significantly enriched in downregulated AD-related DEGs. GO analysis and cell-type-specific analysis showed that the PLS- genes were cytologically enriched in neurons and astrocytes and functionally involved in neuron-specific biological processes, including synaptic signaling, neurotransmitter release, axonogenesis, and cognition. Because PLS1 + genes were not enriched in AD differential genes and implicated in non-neuron-specific functions, the following discussion mainly focuses on the PLS1- genes.

The circuitry of the human brain is formed by neuronal networks in which astrocytes embed. Synaptic signaling, neurotransmitter release and axonogenesis are fundamental to highly efficient neuronal networks, which maintain normal cognition in humans (Verkhratsky et al., 2010). The loss of neurons and synapses and axon destruction are common findings in AD neuropathology and are related to cognitive decline in AD patients. Exposure of astrocytes to Aβ may induce astrocyte activation (Diniz et al., 2017) and release proinflammatory cytokines, contributing to neuronal death (Wood et al., 2015). As PLS1- genes were significantly enriched in downregulated AD-related DEGs, it can be presumed that the reduced expression of PLS1- genes may lead to neuron death, axon deterioration and synapse loss, causing histological similarity and anatomical connectivity destruction and, thus, abnormal MS changes in AD.

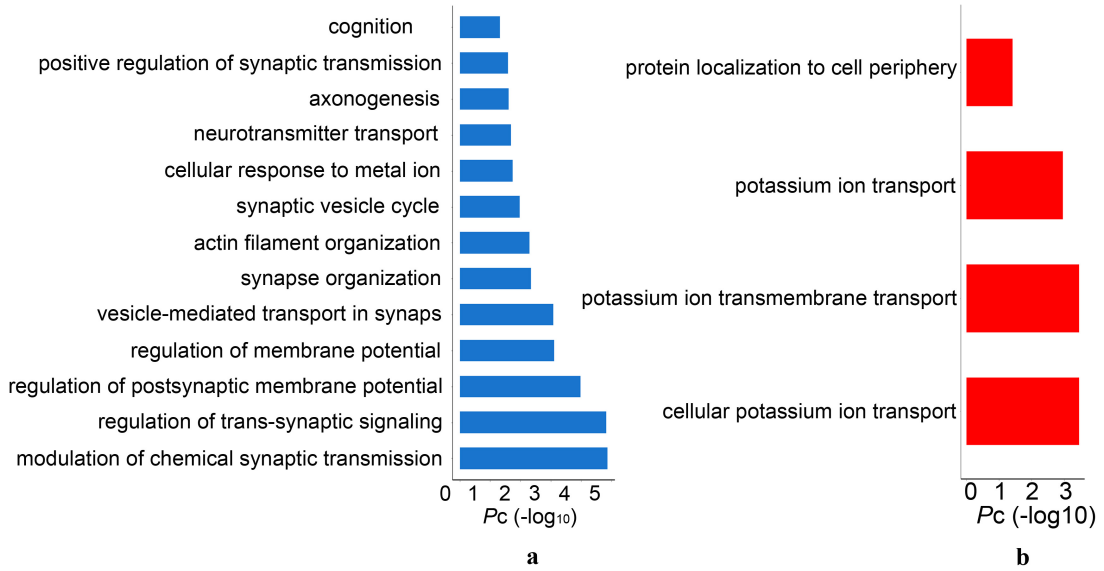

FIGURE 6 | The significant gene ontology terms of biological process for PLS1 gene sets. **(A)** The PLS1- genes were significantly enriched in synaptic signaling, neurotransmitter release, axonogenesis and cognition. **(B)** The PLS1 + genes were significantly enriched in potassium ion transport and protein localization. *Pc*, the Bonferroni corrected *P*-values.

The PLS1- genes acted as a whole gene set in the enrichment analysis for AD-related DEGs, cortical cell types and GO terms. We cannot ensure that every single gene in the PLS1- gene set was enriched in AD-related DEGs, cortical cell types and GO terms simultaneously. The significance of the enrichment analysis did not represent for the true biological connection. Further *in vitro* and *in vivo* experiments are warranted to validate our hypothesis. Although variation from multiple sites and scanners could be moderately adjusted using ComBat harmonization, different scan protocols still affected the results. More robust methods are needed in the future to properly control the batch effect from multiple sites and scanners.

In summary, this study revealed AD-related cortical MS changes associated with memory function. Linking gene expression to cortical MS changes, the negative MS-related genes were found to be enriched explicitly in neurons and astrocytes, participate in neuron-specific biological processes and be significantly downregulated in AD. These findings may provide a possible molecular and cellular substrate for MS abnormalities and cognitive decline in AD.

DATA AVAILABILITY STATEMENT

The original contributions presented in the study are included in the article/**Supplementary Material**, further inquiries can be directed to the corresponding author/s.

ETHICS STATEMENT

The Data used in this study were obtained from the Alzheimer's Disease Neuroimaging Initiative (ADNI) (http://adni.loni.usc.edu/). The ADNI data were previously collected across 50 research sites. Study subjects gave written informed consent at the time of enrollment for imaging and genetic sample collection and completed questionnaires approved by each participating sites' Institutional Review Board (IRB). The list of all sites can be found in **Supplementary Material**, **Data Sheet 2**. All procedures performed in studies involving human participants were in accordance with the ethical standards of the institutional and/or national research committee and with the 1964 Helsinki declaration and its later amendments or comparable ethical standards. The patients/participants provided their written informed consent to participate in this study.

AUTHOR CONTRIBUTIONS

JS and YZ conceived the idea. MM and ZX analyzed the MRI data. HW analyzed the transcription data. NZ analyzed the behavioral data. YZ wrote the initial draft. All authors agreed with the final version of the manuscript.

FUNDING

This work was supported by the National Natural Science Foundation of China (81601476 and 81870831).

SUPPLEMENTARY MATERIAL

The Supplementary Material for this article can be found online at: https://www.frontiersin.org/articles/10.3389/fnins.2021.731292/full#supplementary-material

REFERENCES

Aganj, I., Frau-Pascual, A., Iglesias, J. E., Yendiki, A., Augustinack, J. C., Salat, D. H., et al. (2020). Compensatory brain connection discovery in Alzheimer's disease. *Proc. IEEE Int. Symp. Biomed. Imaging* 2020, 283–287. doi: 10.1109/ISBI45749.2020.9098440

Bellenguez, C., Grenier-Boley, B., and Lambert, J. C. (2020). Genetics of Alzheimer's disease: where we are, and where we are going. *Curr. Opin. Neurobiol.* 61, 40–48. doi: 10.1016/j.conb.2019.11.024

Bokde, A. L., Lopez-Bayo, P., Meindl, T., Pechler, S., Born, C., Faltraco, F., et al. (2006). Functional connectivity of the fusiform gyrus during a face-matching task in subjects with mild cognitive impairment. *Brain* 129, 1113–1124. doi: 10.1093/brain/awl051

Busatto, G. F., Garrido, G. E., Almeida, O. P., Castro, C. C., Camargo, C. H., Cid, C. G., et al. (2003). A voxel-based morphometry study of temporal lobe gray matter reductions in Alzheimer's disease. *Neurobiol. Aging* 24, 221–231. doi: 10.1016/S0197-4580(02)00084-2

Chang, Y. T., Hsu, J. L., Huang, S. H., Hsu, S. W., Lee, C. C., and Chang, C. C. (2020). Functional connectome and neuropsychiatric symptom clusters of Alzheimer's disease. *J. Affect. Disord.* 273, 48–54. doi: 10.1016/j.jad.2020.04.054

Crane, P. K., Carle, A., Gibbons, L. E., Insel, P., Mackin, R. S., Gross, A., et al. (2012). Development and assessment of a composite score for memory in the Alzheimer's Disease Neuroimaging Initiative (ADNI). *Brain Imaging Behav.* 6, 502–516. doi: 10.1007/s11682-012-9186-z

Das, G., Dubey, S., Sinharoy, U., Mukherjee, A., Banerjee, S., Lahiri, D., et al. (2021). Clinical and radiological profile of posterior cortical atrophy and comparison with a group of typical Alzheimer disease and amnestic mild cognitive impairment. *Acta Neurol. Belg.* 121, 1009–1018. doi: 10.1007/s13760-020-01547-4

Diniz, L. P., Tortelli, V., Matias, I., Morgado, J., Bérgamo Araujo, A. P., Melo, H. M., et al. (2017). Astrocyte transforming growth factor beta 1 protects synapses against Aβ oligomers in Alzheimer's disease model. *J Neurosci* 37, 6797–6809. doi: 10.1523/JNEUROSCI.3351-16.2017

Femminella, G. D., Thayanandan, T., Calsolaro, V., Komici, K., Rengo, G., Corbi, G., et al. (2018). Imaging and molecular mechanisms of alzheimer's disease: a review. *Int. J. Mol. Sci.* 19:3702. doi: 10.3390/ijms19123702

Fortin, J. P., Cullen, N., Sheline, Y. I., Taylor, W. D., Aselcioglu, I., Cook, P. A., et al. (2018). Harmonization of cortical thickness measurements across scanners and sites. *Neuroimage* 167, 104–120. doi: 10.1016/j.neuroimage.2017.11.024

Fortin, J. P., Parker, D., Tunç, B., Watanabe, T., Elliott, M. A., Ruparel, K., et al. (2017). Harmonization of multi-site diffusion tensor imaging data. *Neuroimage* 161, 149–170. doi: 10.1016/j.neuroimage.2017.08.047

Frisoni, G. B., Testa, C., Zorzan, A., Sabattoli, F., Beltramello, A., Soininen, H., et al. (2002). Detection of grey matter loss in mild Alzheimer's disease with voxel based morphometry. *J. Neurol. Neurosurg. Psychiatry* 73, 657–664. doi: 10.1136/jnnp.73.6.657

Gonzalez-Escamilla, G., Miederer, I., Grothe, M. J., Schreckenberger, M., Muthuraman, M., and Groppa, S. (2020). Metabolic and amyloid PET network reorganization in Alzheimer's disease: differential patterns and partial volume effects. *Brain Imaging Behav.* 15, 190–204. doi: 10.1007/s11682-019-00247-9

Grady, C. L., McIntosh, A. R., Beig, S., Keightley, M. L., Burian, H., and Black, S. E. (2003). Evidence from functional neuroimaging of a compensatory prefrontal network in Alzheimer's disease. *J. Neurosci.* 23, 986–993. doi: 10.1523/JNEUROSCI.23-03-00986.2003

He, Y., Chen, Z., and Evans, A. (2008). Structural insights into aberrant topological patterns of large-scale cortical networks in Alzheimer's disease. *J. Neurosci.* 28, 4756–4766. doi: 10.1523/JNEUROSCI.0141-08.2008

Huang, S. Y., Hsu, J. L., Lin, K. J., and Hsiao, I. T. (2020). A novel individual metabolic brain network for 18F-FDG PET imaging. *Front. Neurosci.* 14:344. doi: 10.3389/fnins.2020.00344

Im, K., Lee, J. M., Seo, S. W., Hyung Kim, S., Kim, S. I., and Na, D. L. (2008). Sulcal morphology changes and their relationship with cortical thickness and gyral white matter volume in mild cognitive impairment and Alzheimer's disease. *Neuroimage* 43, 103–113. doi: 10.1016/j.neuroimage.2008.07.016

Jack, C. R. Jr., Bernstein, M. A., Borowski, B. J., Gunter, J. L., Fox, N. C., Thompson, P. M., et al. (2010). Update on the magnetic resonance imaging core of the Alzheimer's disease neuroimaging initiative. *Alzheimers Dement.* 6, 212–220. doi: 10.1016/j.jalz.2010.03.004

Jacobs, E. H., Williams, R. J., and Francis, P. T. (2006). Cyclin-dependent kinase 5, Munc18a and Munc18-interacting protein 1/X11alpha protein up-regulation in Alzheimer's disease. *Neuroscience* 138, 511–522. doi: 10.1016/j.neuroscience.2005.11.017

Kalus, P., Slotboom, J., Gallinat, J., Mahlberg, R., Cattapan-Ludewig, K., Wiest, R., et al. (2006). Examining the gateway to the limbic system with diffusion tensor imaging: the perforant pathway in dementia. *Neuroimage* 30, 713–720. doi: 10.1016/j.neuroimage.2005.10.035

Kantarci, K., Murray, M. E., Schwarz, C. G., Reid, R. I., Przybelski, S. A., Lesnick, T., et al. (2017). White-matter integrity on DTI and the pathologic staging of Alzheimer's disease. *Neurobiol. Aging* 56, 172–179. doi: 10.1016/j.neurobiolaging.2017.04.024

Lerch, J. P., Pruessner, J. C., Zijdenbos, A., Hampel, H., Teipel, S. J., and Evans, A. C. (2005). Focal decline of cortical thickness in Alzheimer's disease identified by computational neuroanatomy. *Cereb. Cortex* 15, 995–1001. doi: 10.1093/cercor/bhh200

Li, S., Yuan, X., Pu, F., Li, D., Fan, Y., Wu, L., et al. (2014). Abnormal changes of multidimensional surface features using multivariate pattern classification in amnestic mild cognitive impairment patients. *J. Neurosci.* 34, 10541–10553. doi: 10.1523/JNEUROSCI.4356-13.2014

Lo, C. Y., Wang, P. N., Chou, K. H., Wang, J., He, Y., and Lin, C. P. (2010). Diffusion tensor tractography reveals abnormal topological organization in structural cortical networks in Alzheimer's disease. *J. Neurosci.* 30, 16876–16885. doi: 10.1523/JNEUROSCI.4136-10.2010

Morra, J. H., Tu, Z., Apostolova, L. G., Green, A. E., Avedissian, C., Madsen, S. K., et al. (2008). Validation of a fully automated 3D hippocampal segmentation method using subjects with Alzheimer's disease mild cognitive impairment, and elderly controls. *Neuroimage* 43, 59–68. doi: 10.1016/j.neuroimage.2008.07.003

Naggara, O., Oppenheim, C., Rieu, D., Raoux, N., Rodrigo, S., Dalla Barba, G., et al. (2006). Diffusion tensor imaging in early Alzheimer's disease. *Psychiatry Res.* 146, 243–249. doi: 10.1016/j.pscychresns.2006.01.005

Pettigrew, C., Soldan, A., Zhu, Y., Wang, M. C., Brown, T., Miller, M., et al. (2017). Cognitive reserve and cortical thickness in preclinical Alzheimer's disease. *Brain Imaging Behav.* 11, 357–367. doi:10.1007/s11682-016-9581-y

Seidlitz, J., Vasa, F., Shinn, M., Romero-Garcia, R., Whitaker, K. J., Vertes, P. E., et al. (2018). Morphometric similarity networks detect microscale cortical organization and predict inter-individual cognitive variation. *Neuron* 97, 231.e7–247.e7. doi: 10.1016/j.neuron.2017.11.039

Seong, J. K., Im, K., Yoo, S. W., Seo, S. W., Na, D. L., and Lee, J. M. (2010). Automatic extraction of sulcal lines on cortical surfaces based on anisotropic geodesic distance. *Neuroimage* 49, 293–302. doi: 10.1016/j.neuroimage.2009.08.013

Sexton, C. E., Mackay, C. E., Lonie, J. A., Bastin, M. E., Terrière, E., O'Carroll, R. E., et al. (2010). MRI correlates of episodic memory in Alzheimer's disease, mild cognitive impairment, and healthy aging. *Psychiatry Res.* 184, 57–62. doi: 10.1016/j.pscychresns.2010.07.005

Stam, C. J., Jones, B. F., Nolte, G., Breakspear, M., and Scheltens, P. (2007). Small-world networks and functional connectivity in Alzheimer's disease. *Cereb. Cortex* 17, 92–99. doi: 10.1093/cercor/bhj127

Ten Kate, M., Dicks, E., Visser, P. J., van der Flier, W. M., Teunissen, C. E., Barkhof, F., et al. (2018). Atrophy subtypes in prodromal Alzheimer's disease are associated with cognitive decline. *Brain* 141, 3443–3456. doi: 10.1093/brain/awy264

Verkhratsky, A., Olabarria, M., Noristani, H. N., Yeh, C. Y., and Rodriguez, J. J. (2010). Astrocytes in Alzheimer's disease. *Neurotherapeutics* 7, 399–412. doi: 10.1016/j.nurt.2010.05.017

Wang, Y., Yang, D., Li, Q., Kaufer, D., Styner, M., and Wu, G. (2020). Characterizing the propagation pattern of neurodegeneration in Alzheimer's disease by longitudinal network analysis. *Proc. IEEE Int. Symp. Biomed. Imaging* 2020, 292–295. doi: 10.1109/ISBI45749.2020.9098513

Weiner, M. W., Veitch, D. P., Aisen, P. S., Beckett, L. A., Cairns, N. J., Green, R. C., et al. (2017). The Alzheimer's disease neuroimaging initiative 3: continued innovation for clinical trial improvement. *Alzheimers Dement.* 13, 561–571. doi: 10.1016/j.jalz.2016.10.006

Wood, L. B., Winslow, A. R., Proctor, E. A., McGuone, D., Mordes, D. A., Frosch, M. P., et al. (2015). Identification of neurotoxic cytokines by profiling Alzheimer's disease tissues and neuron culture viability screening. *Sci. Rep.* 5:16622. doi: 10.1038/srep16622

Yao, Z., Zhang, Y., Lin, L., Zhou, Y., Xu, C., Jiang, T., et al. (2010). Abnormal cortical networks in mild cognitive impairment and Alzheimer's disease. *PLoS Comput. Biol.* 6:e1001006. doi: 10.1371/journal.pcbi.1001006

Zhang, Y., Schuff, N., Jahng, G. H., Bayne, W., Mori, S., Schad, L., et al. (2007). Diffusion tensor imaging of cingulum fibers in mild cognitive impairment and Alzheimer disease. *Neurology* 68, 13–19. doi: 10.1212/01.wnl.0000250326.77323.01

Conflict of Interest: The authors declare that the research was conducted in the absence of any commercial or financial relationships that could be construed as a potential conflict of interest.

frontiers in Neuroscience

ORIGINAL RESEARCH
published: 01 October 2021
doi: 10.3389/fnins.2021.733501

Transcriptomic Signatures Associated With Regional Cortical Thickness Changes in Parkinson's Disease

Arlin Keo[1,2], Oleh Dzyubachyk[3], Jeroen van der Grond[3], Jacobus J. van Hilten[4], Marcel J. T. Reinders[1,2,5†] and Ahmed Mahfouz[1,2,5*†]*

[1] Leiden Computational Biology Center, Leiden University Medical Center, Leiden, Netherlands, [2] Delft Bioinformatics Lab, Delft University of Technology, Delft, Netherlands, [3] Department of Radiology, Leiden University Medical Center, Leiden, Netherlands, [4] Department of Neurology, Leiden University Medical Center, Leiden, Netherlands, [5] Department of Human Genetics, Leiden University Medical Center, Leiden, Netherlands

OPEN ACCESS

Edited by:
Jiajia Zhu,
First Affiliated Hospital of Anhui Medical University, China

Reviewed by:
Jolanta Dorszewska,
Poznan University of Medical Sciences, Poland
Huaigui Liu,
Tianjin Medical University General Hospital, China
Roger Jacob Mullins,
National Institutes of Health (NIH), United States

***Correspondence:**
Marcel J. T. Reinders
m.j.t.reinders@tudelft.nl
Ahmed Mahfouz
a.mahfouz@lumc.nl

[†] These authors have contributed equally to this work and share last authorship

Specialty section:
This article was submitted to Brain Imaging Methods, a section of the journal Frontiers in Neuroscience

Received: 30 June 2021
Accepted: 08 September 2021
Published: 01 October 2021

Citation:
Keo A, Dzyubachyk O, van der Grond J, van Hilten JJ, Reinders MJT and Mahfouz A (2021) Transcriptomic Signatures Associated With Regional Cortical Thickness Changes in Parkinson's Disease. Front. Neurosci. 15:733501. doi: 10.3389/fnins.2021.733501

Cortical atrophy is a common manifestation in Parkinson's disease (PD), particularly in advanced stages of the disease. To elucidate the molecular underpinnings of cortical thickness changes in PD, we performed an integrated analysis of brain-wide healthy transcriptomic data from the Allen Human Brain Atlas and patterns of cortical thickness based on T1-weighted anatomical MRI data of 149 PD patients and 369 controls. For this purpose, we used partial least squares regression to identify gene expression patterns correlated with cortical thickness changes. In addition, we identified gene expression patterns underlying the relationship between cortical thickness and clinical domains of PD. Our results show that genes whose expression in the healthy brain is associated with cortical thickness changes in PD are enriched in biological pathways related to sumoylation, regulation of mitotic cell cycle, mitochondrial translation, DNA damage responses, and ER-Golgi traffic. The associated pathways were highly related to each other and all belong to cellular maintenance mechanisms. The expression of genes within most pathways was negatively correlated with cortical thickness changes, showing higher expression in regions associated with decreased cortical thickness (atrophy). On the other hand, sumoylation pathways were positively correlated with cortical thickness changes, showing higher expression in regions with increased cortical thickness (hypertrophy). Our findings suggest that alterations in the balanced interplay of these mechanisms play a role in changes of cortical thickness in PD and possibly influence motor and cognitive functions.

Keywords: cortical thickness, neurodegenerative diseases, neuroimaging data, imaging-genetics, gene expression analysis

INTRODUCTION

Parkinson's disease (PD) is a neurodegenerative disorder characterized by a progressive loss of dopaminergic and non-dopaminergic neurons in the brain and peripheral and autonomic nervous system (Hirsch et al., 2012). Cortical atrophy occurs during the later disease stages and has been associated with cognitive decline, including executive, attentional, memory, and visuospatial deficits (Aarsland et al., 2017; Wilson et al., 2019). Although MRI studies of patient brains have tried to link regional cortical atrophy to clinical features of the disease (Rosenberg-Katz et al., 2016;

Wang et al., 2016; Chen et al., 2017; Li et al., 2018; Zheng et al., 2019), little is known about the pathobiology that underlies the selective cortical vulnerability in PD.

Analyzing the transcriptome in vulnerable cortical regions may aid in better understanding the underlying molecular mechanisms of atrophy in PD. Although gene expression data of human post-mortem PD brains is available, most findings relate to studies that focused only on one or few coarse brain regions (Oerton and Bender, 2017). To perform whole brain analysis of both gene expression and imaging data, studies turn to the Allen Human Brain Atlas (AHBA), a high resolution gene expression atlas covering the entire brain of six adult donors without any history of neurological disorders (Hawrylycz et al., 2015; Arnatkevičiūtė et al., 2019). The AHBA has been combined with functional MRI data of PD patients and revealed that the regional expression of *MAPT*, but not *SNCA*, correlated with the loss of regional connectivity (Rittman et al., 2016). Using a similar approach, correlations were identified between a cortical atrophy pattern and the regional expression of 17 genes implicated in PD (Freeze et al., 2018). Although both studies used spatial transcriptomics to explore gene expression across the whole brain, they only analyzed the expression of a limited set of genes that are of interest to PD, e.g., those that are known as genetic risk factors.

To investigate the relationship between high dimensional genome-wide expression patterns and imaging data, multivariate analysis methods are required. Partial least squares (PLS) regression has been used to perform simultaneous analysis of brain-wide gene expression from the AHBA and neuroimaging data of adolescents, healthy adults, and Huntington's disease patients (Vértes et al., 2016; Whitaker et al., 2016a; McColgan et al., 2018). The PLS approach allows the linking of multiple predictor variables (genes) and multiple response variables (imaging features) and deals with multicollinearity by projecting variables to a smaller set of components that are maximally correlated between both datasets. Thus, PLS is an attractive model to identify gene expression patterns associated with imaging features.

Here, we exploited PLS regression to find transcriptomic signatures that are related to changes in cortical thickness (CT) in PD. MRI data was obtained from patients and age-matched controls to find CT changes across all cortical regions. Gene expression samples from healthy donors in the AHBA were anatomically mapped to the cortical regions to find brain-wide gene expression patterns predictive of the CT changes observed in PD patients. In addition, we assessed the relationships between CT and clinical scores in PD patients and used a second PLS model to find expression patterns associated with these relationships across all cortical regions. With these models we address three research questions: (1) Which cortical regions show CT changes in PD, (2) Which genes and biological pathways show expression patterns associated with these regional changes, and (3) Which molecular mechanisms underlie the relationships between CT and clinical scores in PD. To answer these questions, we explored the whole transcriptome in cortical regions of the healthy brain to find expression signatures predictive of imaging features in PD.

MATERIALS AND METHODS

MRI Data Acquisition

MRI images of 149 PD patients (mean age = 64.8 years; 65.7% male) were obtained from a cross-sectional cohort study and is part of the "PROfiling PARKinson's disease" (PROPARK) study (de Schipper et al., 2017; **Supplementary Table 1**). PD patients were recruited from the outpatient clinic for Movement Disorders of the Department of Neurology of the Leiden University Medical Center and nearby university and regional hospitals. All participants fulfilled the United Kingdom Parkinson's Disease Society Brain Bank criteria for idiopathic PD (Gibb and Lees, 1988); written consent was obtained from all participants. The Medical Ethics Committee of the LUMC approved the study. Three-dimensional T1-weighted anatomical images were acquired on a 3 Tesla MRI scanner (Philips Achieva, Best, Netherlands) using a standard 32-channel whole-head coil. Acquisition parameters were: repetition time = 9.8 ms, echo time = 4.6 ms, flip angle = 8°, field of view 220 × 174 × 156 mm, 130 slices with a slice thickness of 1.2 mm with no gap between slices, resulting in a voxel size of 1.15 mm × 1.15 mm × 1.20 mm.

Three−dimensional T1−weighted images from 369 controls (mean age = 65.7 years; 48.1% male) were acquired in a different cohort (Altmann-schneider et al., 2012), where all imaging was performed on a whole body 3 Tesla MRI scanner (Philips Medical Systems, Best, Netherlands), using the following imaging parameters: TR = 9.7 ms, TE = 4.6 ms, FA = 8°, FOV = 224 × 177 × 168 mm. The anatomical images covered the entire brain with no gap between slices resulting in a nominal voxel size of 1.17 × 1.17 × 1.4 mm. Acquisition time was approximately 5 min.

Cortical Thickness Changes in Segmented Cortical Regions

Cortical thickness in cortical regions of PD patients and controls was determined using cortical parcellation implemented in FreeSurfer version 5.3.0 (Fischl and Dale, 2000). The FreeSurfer algorithm automatically parcellates the cortex and assigns a neuroanatomical label to each location on a cortical surface model based on probabilistic information. The parcellation scheme of the Desikan–Killiany atlas was used to divide the cortex into 34 regions per hemisphere (Desikan et al., 2006).

To assess CT changes between patients (149) and controls (369), a two-tailed *t*-test assuming unequal variances was applied in SPSS Statistics version 23. *P*-values were corrected for multiple testing across 68 cortical regions using the Benjamini-Hochberg (BH) method. A two-tailed *t*-test was also used to assess CT differences between the left and right hemisphere for each one of the 34 cortical regions, with *P*-values being BH-corrected across the 34 cortical regions.

Clinical Scores

All patients underwent standardized assessments, and an evaluation of demographic and clinical characteristics (de Schipper et al., 2017). MDS-UPDRS is a clinical rating scale consisting of four parts: (I) Non-motor Experiences of

Daily Living; (II) Motor Experiences of Daily Living; (III) Motor Examination; and (IV) Motor Complications (Goetz et al., 2008). UPDRSTOTSCR is the total score of all four parts. The SENS-PD scale is a composite score of non-dopaminergic symptoms (van der Heeden et al., 2016), LED is the levodopa equivalent dose (Tomlinson et al., 2010), and MMSE is the mini-mental state examination (Folstein et al., 1975).

Relationship Between Cortical Thickness and Clinical Scores

We used CT data and clinical scores from 149 PD patients to determine the relationships between CT and clinical domains. We selected nine clinical features with numeric (non-nominal) values for which scores were available for 82–123 patients: AGEONSET, SENSPDSC, MDS_UPDRS_3, MMSE, LED, MDS_UPDRS_1, MDS_UPDRS_2, MDS_UPDRS_4, and UPDRSTOTSCR (**Supplementary Figure 1**).

The correlation between CT and the scores of each clinical feature individually was determined across patients by applying linear regression. To obtain maximum correlation, separate linear regression models were used for each combination of a region and clinical feature:

$$CT_i = \alpha + \beta_1 K_j + \beta_2 Age + \varepsilon \quad (1)$$

where CT_i is the CT of one region i across patients, K_j is the score of one clinical feature j across patients. *Age* is taken into account to correct for the age of patients. α is the background term, β_1 is the regression coefficient for K_j, β_2 is the regression coefficients for *Age*, and ε is the residual. The regression coefficient β_1 was used to determine the relationship between CT and clinical domain scores, and assessed for statistical significance where *P*-values were BH-corrected for 34 regions and nine clinical features (t-test, H_0: $\beta_1 = 0$, $P < 0.05$).

Mapping Transcriptomic Data to Cortical Regions

We downloaded normalized gene expression data from the Allen Human Brain Atlas (AHBA[1]), a microarray data set of 3,702 anatomical brain regions from six non-neurological individuals [5 males and 1 female, mean age 42, range 24–57 years (Hawrylycz et al., 2015)]. Preprocessing steps are described in **Supplementary Methods**. To analyze the transcriptome in the cortical regions, we used the mapping of AHBA samples to cortical regions in neuroimaging data proposed in Arnatkevičiūtė et al. (2019), where they applied Freesurfer on T1 MRIs of the six donors in the AHBA to segment the cortical regions according to the Desikan-Killiany atlas. AHBA samples were mapped to 34 cortical regions from the left hemisphere, since for only two out of six brains samples were collected from both hemispheres and for four brains they only sampled from the left hemisphere. By only analyzing the left hemisphere, we assumed that there are small to no differences in gene expression between the left and right hemisphere (Hawrylycz et al., 2015). Samples were assigned to a segmented cortical region when their MNI coordinates corresponds to a voxel within a parcel, including samples that are up to 2 mm away from any voxel in the parcel. In total 1,284 samples from the AHBA were assigned to the 34 cortical regions.

[1]http://human.brain-map.org/

Partial Least Squares (PLS) Model-1 and Model-2

We used PLS regression (R-package *pls* 2.7) to find gene expression patterns across the 34 cortical regions that are predictive of gray matter atrophy and possibly their relationship to scores of nine clinical domains (**Supplementary Methods**). PLS regression and principal component analysis regression are both methods where the original measurements are projected to latent variables to study the data in reduced dimensions (**Figure 1A**). PLS, however, projects variables from each dataset to latent variables such that they are maximally correlated between two datasets X and Y (**Figure 1B**). In this study, the predictor X is a gene expression matrix of 34 regions (n) in the left hemisphere and all 20,017 genes (m) and is used to predict imaging variables (p) in the same set of 34 cortical regions. For each cortical region and each gene, expression levels were averaged across samples that fall within that cortical region and then averaged across the six donors from the AHBA, such that the input matrix of predictor variables contains one expression value for every gene per cortical region. We implemented two PLS models (**Figure 1C**): one single-response PLS model, *model-1*, to predict CT changes, measured as the t-statistics of ΔCT between PD patients and controls, and one multi-response PLS model, *model-2*, to predict the correlation between CT and clinical scores in PD patients, measured as the t-statistics of the coefficients β_1 in Eq. 1.

Pathway Enrichment

Pathway enrichment analysis was done using gene set enrichment analysis (GSEA) and 2,225 pathways from the Reactome database in ReactomePA R-package version 1.28. Genes were ranked based on their weights to each PLS component; R in Eqs. 5 and 6 in **Supplementary Methods**. Pathways were significant when the FDR-adjusted $P < 0.05$.

Data and Code Availability

Transcriptomic data from the AHBA is available at http://human.brain-map.org/. All scripts were run in R version 4 and can be found online at https://github.com/arlinkeo/pd_pls.

RESULTS

Cortical Thickness Changes Between Parkinson's Disease Patients and Controls

We analyzed CT changes between PD patients and healthy controls (ΔCT) as a measure for gray matter loss (**Figure 1C**). Each of the 68 cortical regions from both hemispheres was assessed, for which ΔCT was statistically significant in 10 cortical regions (t-test, BH-corrected $P < 0.05$; **Figure 2A** and **Supplementary Table 2**). The lateral occipital cortex showed

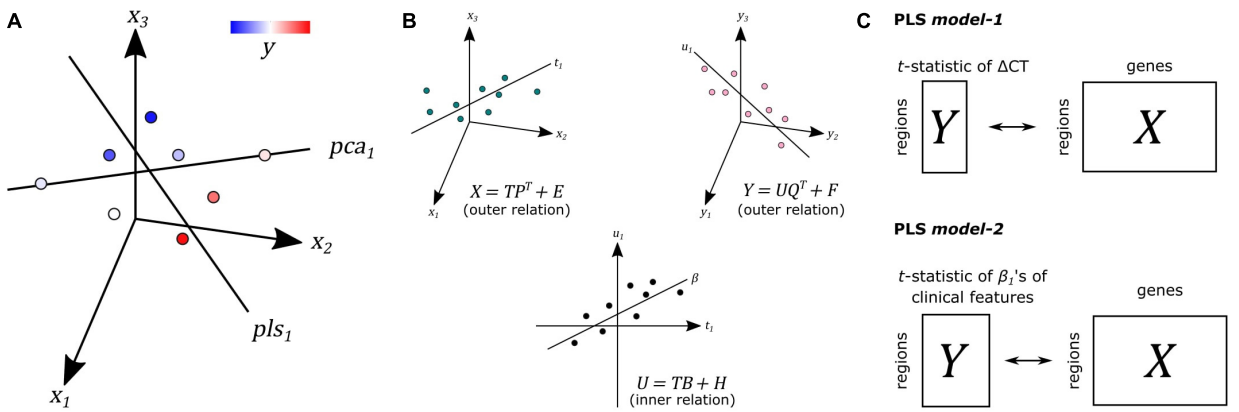

FIGURE 1 | Principal of partial least squares regression (PLS). **(A)** Principal component analysis (PCA) and PLS project measurements to a new latent space. Unlike PCA, PLS tries to find a latent space that is maximally correlated with another measurement ***y*** from dataset ***Y*** on the same samples. **(B)** The first latent component $\boldsymbol{t_1}$ of dataset ***X*** is maximally correlated with the first latent factor $\boldsymbol{u_1}$ of dataset ***Y***. ***T*** and ***U*** scores determine the outer relations of individual datasets in the model. The coefficient **β** determines the inner relation between both datasets X and Y in the model (more details in **Supplementary Methods**). **(C)** In PLS *model-1*, we used regional gene expression as input to predict the regional *t*-statistics of ΔCT. Given the PLS model, ***R*** in Eqs. 5 and 6 in **Supplementary Methods** is used as gene weights. In PLS *model-2*, we used the same input to predict the *t*-statistics of correlation coefficients $\boldsymbol{\beta_1}$ of clinical features from Eq. 1.

decreased CT in patients compared to controls in both the left hemisphere and right hemisphere. The left caudal anterior cingulate, right isthmus cingulate, and right pericalcarine also showed decreased CT in patients. Cortical regions with increased CT in patients included the pars opercularis from both the left hemisphere and right hemisphere, the right rostral middle frontal cortex, right temporal pole, and right superior temporal cortex. In general, we observed more decreased CT (atrophy) in caudal regions of the cortex compared to rostral regions that showed increased CT (hypertrophy).

Cortical Thickness Changes Between Hemispheres in Parkinson's Disease

Clinical symptoms appear asymmetrical at disease onset with the left hemisphere being more susceptible to degeneration than the right (Claassen et al., 2016). To assess whether this asymmetry is reflected also in the observed atrophy patterns, we compared the CT between the left and right hemisphere for each of the 34 cortical regions in PD patients. We found six cortical regions that showed significant hemispheric differences (BH-corrected $P < 0.05$; **Figure 2B** and **Supplementary Table 3**). For five out of six significant regions, CT was indeed smaller in the left hemisphere compared to the right: banks of superior temporal sulcus, entorhinal cortex, temporal pole, medial orbitofrontal cortex, and lateral occipital cortex. For the lateral orbitofrontal cortex, the CT was larger in the left hemisphere compared to the right.

Gene Expression Patterns Predictive of Cortical Thickness Changes in Parkinson's Disease Patients

To identify the molecular mechanisms underlying CT changes in PD, we integrated the imaging features with brain-wide gene expression profiles from the AHBA (**Figure 1C**). Using PLS *model-1* (see section "Materials and Methods"), the expression of all 20,017 genes in 34 brain regions from the left hemisphere was used as predictor variables and we used the *t*-statistics of ΔCT between PD patients and controls in the 34 regions (**Supplementary Table 2**) as a single response variable. The number of AHBA samples varied between 0 and 92 for each one of the six brain donors and 34 cortical regions (**Supplementary Table 4**).

The PLS components that explain maximum covariance between the input space and the response variable are derived from successively deflated predictor and response matrices. Hence, the first component of the predictor matrix, *component-1*, has maximum covariance with the first component of the response matrix, and the second component of the predictor matrix, *component-2*, has maximum covariance with the second component of the response matrix, etc. Since PLS *model-1* has a single response variable, *component-1* of the response matrix is equal to a scaled version of the single response variable. As such, we only examined PLS *component-1* of the predictor matrix (additional checking with leave-one-out cross-validation showed that the optimal number of components is indeed one, **Supplementary Figure 2**).

The scores of PLS *component-1* of the predictor variables (genes) showed a caudal-to-rostral expression pattern (**Figure 3A**) that was correlated with CT changes in PD brains (**Figure 3B**), i.e., gene expression of PLS *component-1* was high in caudal regions associated with atrophy and low in regions associated with hypertrophy. The Pearson correlation between the PLS *component-1* scores of the predictor variables (gene expression) and the response variable (*t*-statistics of ΔCT) was 0.58, and explained 20.5% of the variance in gene expression and 34.2% of the variance in CT changes. Cortical atrophy was highest in the lateral occipital cortex and related to high PLS *component-1* scores. The pericalcarine showed the highest PLS *component-1* score. These results showed that the expression

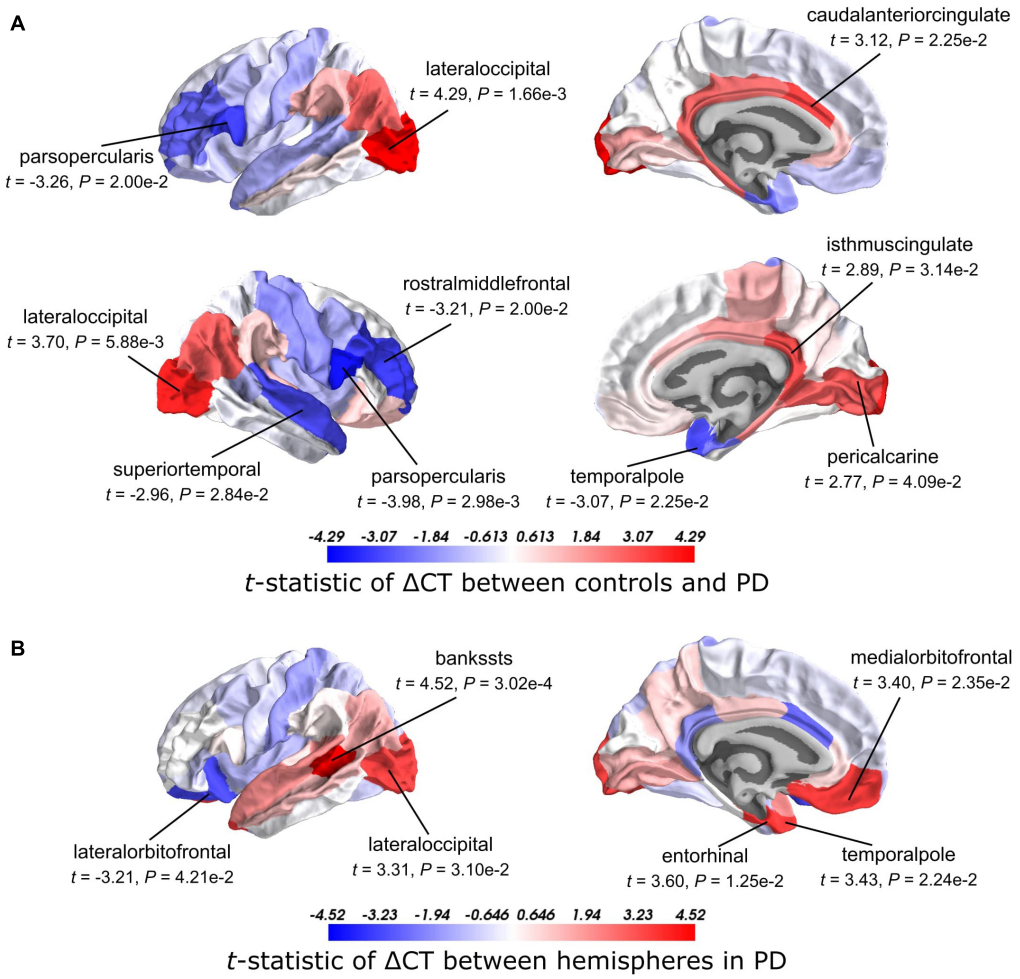

FIGURE 2 | *t*-Statistics of cortical thickness changes (ΔCT) across cortical regions. **(A)** CT was assessed between PD patients and healthy controls. Higher *t*-statistics (red) indicate a larger CT in controls compared to the CT in patients and thus corresponds to cortical atrophy. **(B)** CT in the left hemisphere compared to the right hemisphere in PD patients. Higher *t*-statistics (red) indicate a larger CT in the right hemisphere compared to the left hemisphere and thus corresponds to cortical atrophy in the left hemisphere. *P*-values are BH-corrected and significant regions ($P < 0.05$) are labeled.

profiles of a weighted combination of genes can be predictive of CT changes in PD.

Functionality of Genes Predictive of Cortical Thickness Changes

A PLS component of the predictor variables is a linear combination of weighted gene expression. We used the gene weights of PLS *component*-1 to perform GSEA analysis and revealed significant enrichment of 90 pathways, which were among others involved in DNA damage checkpoints, stabilization of p53, regulation of apoptosis, mitochondrial translation, and SUMOylation of chromatin organization proteins (**Supplementary Table 5**). High overlap of genes between the enriched pathways suggested that these functional processes are highly related to each other (**Supplementary Figure 3**).

Significant pathways are either positively or negatively correlated with CT changes based on the median weight of genes within pathways. Out of the 90 pathways that were significantly enriched, three pathways were positively correlated with the *t*-statistic of ΔCT. These included SUMOylation of chromatin organization proteins, signaling by cytosolic FGFR1 fusion mutants, and class C/3 (Metabotropic glutamate/pheromone receptors). Higher mean expression of genes within these three pathways is related to cortical atrophy (higher *t*-statistics of ΔCT); as apparent in the lateral occipital cortex (**Figure 3C** and **Supplementary Figure 4**). The positive correlation also indicates that a lower expression of these pathways is related to cortical hypertrophy (lower *t*-statistics of ΔCT). We found 87 negatively correlated pathways (median gene weight < 0). These pathways seem to play a role in the mitochondrial regulation of mitosis as we found pathways for mitochondrial translation, the regulation of mitotic cell cycle, p53-(in)dependent DNA damage checkpoints, and the degradation of mitotic proteins, such as cyclins A, and D. In general, the mean expression of genes in the negatively correlated pathways was high in cortical regions

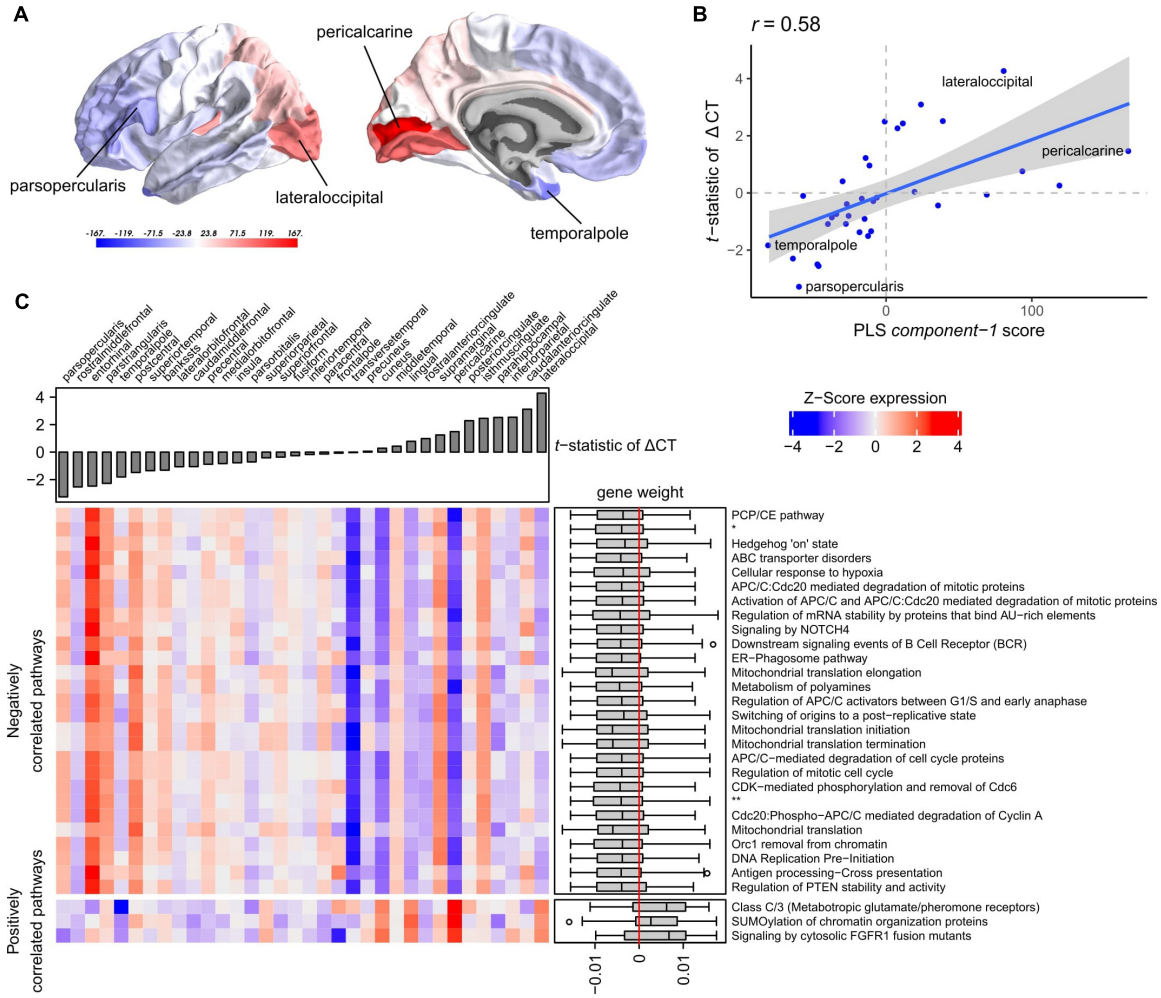

FIGURE 3 | Transcriptional signatures to predict *t*-statistics of ΔCT between PD patients and controls in PLS *model-1*. **(A)** PLS *component-1* scores of predictor variables (gene expression) visualized in cortical regions (lateral and medial view of the left hemisphere). **(B)** Regression fit of the latent predictor variable, PLS *component-1* scores, with the single response variable, CT changes in PD measured as the *t*-statistics of ΔCT between PD patients (149) and controls (369) across the 34 cortical regions. **(C)** Mean expression of genes in the top 30 significant pathways (rows) across cortical regions (columns). A complete heatmap with all significant pathways is given in **Supplementary Figure 4**. The correlation between transcriptomic signatures and CT changes in PD across cortical regions is predicted by the gene weights for PLS *component-1* shown in boxplots for each pathway where the median weight is either negative or positive. Negatively correlated pathways show high gene expression in regions with low *t*-statistics of ΔCT and gene expression decreases in regions with higher *t*-statistics of ΔCT. In our analysis, negative *t*-statistics correspond to increased CT (cortical hypertrophy) and positive *t*-statistics of ΔCT correspond to decreased CT (cortical atrophy). Positively correlated pathways show low expression in regions with low *t*-statistics of ΔCT and expression increases in regions with higher *t*-statistics of ΔCT. * = APC:Cdc20 mediated degradation of cell cycle proteins prior to satisfaction of the cell cycle checkpoint. ** = APC/C:Cdh1 mediated degradation of Cdc20 and other APC/C:Cdh1 targeted proteins in late mitosis/early G1.

that showed hypertrophy, such as the pars opercularis or the entorhinal cortex.

Relationships Between Clinical Scores and Cortical Thickness

Next, we set to understand the relationship between CT in 34 cortical regions and clinical scores of PD patients. Linear regression was used to predict clinical scores from CT across patients and obtain regression coefficients, β_1, for each cortical region and clinical domain (Eq. 1). We assessed the *t*-statistics of the regression coefficients instead of the coefficients β_1 themselves (H_0: $\beta_1 = 0$) (**Figure 4**). Negative *t*-statistics showed that most combinations of cortical regions and clinical features are negatively correlated. For all clinical features, higher scores also indicate more severe symptoms, except for MMSE scores where lower scores indicate more severe symptoms, and thus showed positive relationships with CT. In most regions, age at onset (AGEONSET) also showed positive relationships with CT, indicating that age at onset has an effect on the loss of CT. While

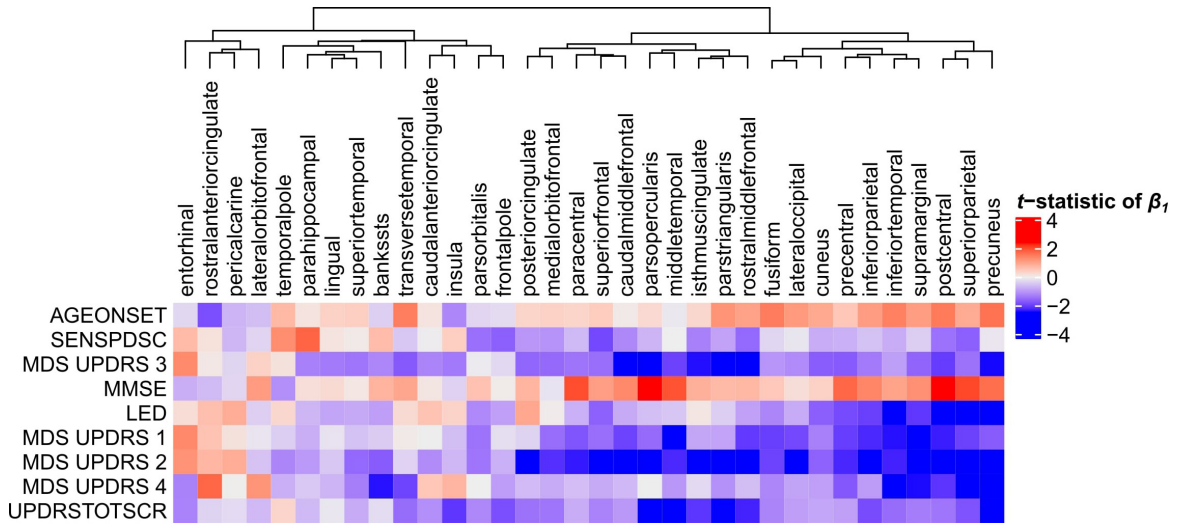

FIGURE 4 | Relationship between clinical scores and CT across PD patients. Linear regression was used to predict clinical scores from CT across at most 123 PD patients (**Supplementary Figure 1**). Separate models were used for each clinical feature (row) and cortical region (column) to obtain regression coefficients, see Eq. 1. The heatmap shows the two-sided *t*-statistics of the regression coefficient when tested for H_0: $\boldsymbol{\beta_1} = 0$. Regions (columns) are clustered based on complete linkage of the Euclidean distance of the *t*-statistics of $\boldsymbol{\beta_1}$.

these general interpretations apply to most cortical regions, some regions showed different relationships with CT. For example, CT in the rostral anterior cingulate is negatively related to age at onset, and positively related to MDS-UPDRS 4 scores.

Genes Predictive of Relationships Between Clinical Scores and Cortical Thickness

With PLS *model-2*, we examined gene expression patterns that are predictive of the relationship between CT and clinical scores measured as *t*-statistics of the correlation coefficients β_1 in Eq. 1 (**Figure 1C**). We selected the first two PLS components for further analysis, which explained 36% of the variance of the predictor variables and 37% of the variance of the response variables (**Supplementary Figure 5**). PLS *component-1* scores of the predictor variables showed a ventral-to-dorsal gene expression pattern (**Figure 5A**) that is correlated with the PLS *component-1* scores of the response variables (Pearson $r = 0.76$, **Figure 5B**). The dorsal regions include the postcentral gyrus which is part of the primary somatosensory cortex. PLS *component-2* scores of the predictor variables showed a caudal-to-rostral gene expression pattern (Pearson $r = 0.56$, **Figure 6A**) that is correlated with the PLS *component-2* scores of the response variables (**Figure 6B**). Moreover, we assessed PLS *component-3* (Pearson $r = 0.76$ between the predictors and response variables), which additionally explained 9% variance of the predictor variables and 11% variance of the response variables. However, further analysis revealed there were no enriched pathways for *component-3* limiting the functional interpretation of this component.

Partial least squares *component-1* and *component-2* of the predictor variables showed 144 and 230 significantly enriched pathways, respectively, with 54 overlapping pathways between the two components (**Supplementary Tables 6, 7**). Both components showed a cluster of related pathways involved in anterograde and retrograde transport between Golgi and endoplasmic reticulum (ER), and asparagine N-linked glycosylation (**Supplementary Figures 6, 7**). Other pathways that overlapped between the two components included macroautophagy, mitochondrial translation, mitochondrial biogenesis, mitochondrial protein import, DNA damage/telomere stress induced senescence, oxidative stress induced senescence, and protein localization.

Furthermore, PLS *component-1* showed enrichment of pathways involved in tRNA and rRNA processing in the nucleus and mitochondrion, voltage-gated potassium channels, uptake and actions of bacterial toxins, and interleukin signaling. PLS *component-2* showed strong enrichment of neutrophil degranulation, DNA replication, p53-(in)dependent DNA damage response, and chaperonin-mediated protein folding, and tubulin folding. Notably, the gene expression pattern of PLS *component-2* was also associated with several sumoylation pathways and pathways involved in mitotic cell cycles and the degradation of mitotic proteins (**Supplementary Table 7**).

The enriched pathways for PLS *component-1 and component-2* either showed negative or positive median gene weights that inform about the sign of the correlation between genes within a pathway and the PLS component score of the response variables (**Figures 5C**, **6C** and **Supplementary Figures 8, 9**). For example, the expression of genes within pathways relating to mitochondrial processes increases for higher PLS *component-1* scores of the response variables. We further assessed PLS *component-1 and component-2* scores of the predictor variables and their correlation with each individual response variable, which are the clinical features and their relationship with CT in

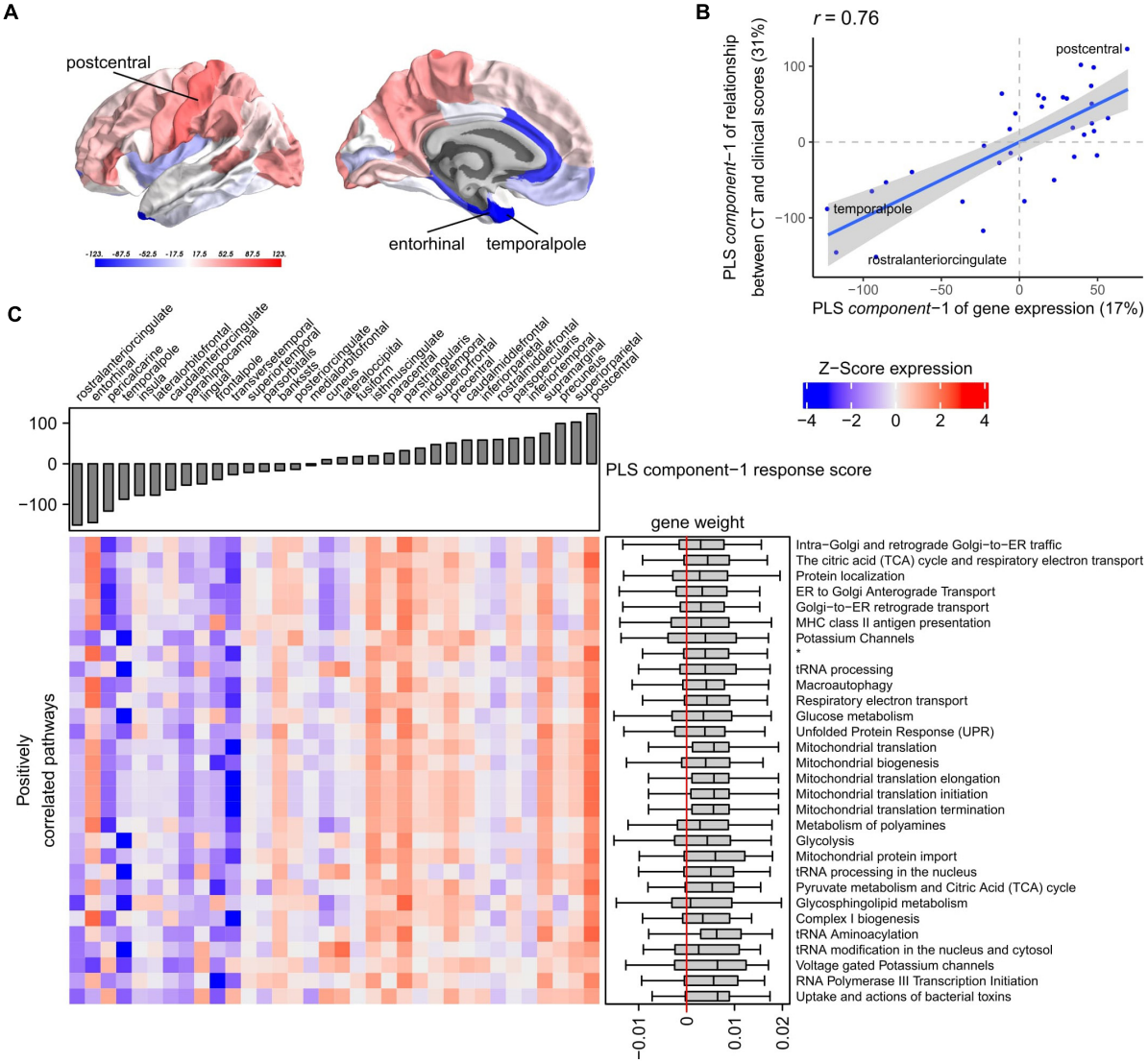

FIGURE 5 | Transcriptional signatures of PLS *component-1* in PLS *model-2* predictive of the relationship between cortical thickness (CT) and clinical scores. **(A)** PLS scores for PLS *component-1* of the predictor variables (gene expression) and **(B)** its correlation with PLS *component-1* of the response variables (*t*-statistic of β_1 in Eq. 1). Axes show the percentage of explained variance for each component; *r* indicates the Pearson correlation. **(C)** Mean expression across cortical regions (columns) of genes in the top 30 significant pathways (rows). A complete heatmap with all significant pathways is given in **Supplementary Figure 8**. * = Respiratory electron transport, ATP synthesis by chemiosmotic coupling, and heat production by uncoupling proteins.

PD patients (**Figure 7**). The rostral-to-dorsal expression pattern of PLS *component-1* is highly predictive of the relationship between CT and MMSE score in patients (Pearson's $r = 0.71$). Thus, pathways associated with PLS *component-1* may play an important role in cognitive circuits, which seems to be apparent based on their expression in the postcentral gyrus, but also the entorhinal cortex. PLS *component-2* scores showed low correlations with the clinical features and their relation with CT across cortical regions, and suggests weak associations between the expression patterns of PLS *component-2* and the response variables.

DISCUSSION

To examine the selective vulnerability of brain regions to PD, we explored PLS regression to find correlations between gene expression signatures across the healthy brain and cortical thinning patterns in PD brains. PLS regression is a suited method to identify relationships between gene expression and neuroimaging data, especially when the number of predictor variables (genes) are highly interdependent or multi-collinear, which is the case for gene expression data. This was shown before by earlier studies (Vértes et al., 2016; Whitaker et al., 2016b;

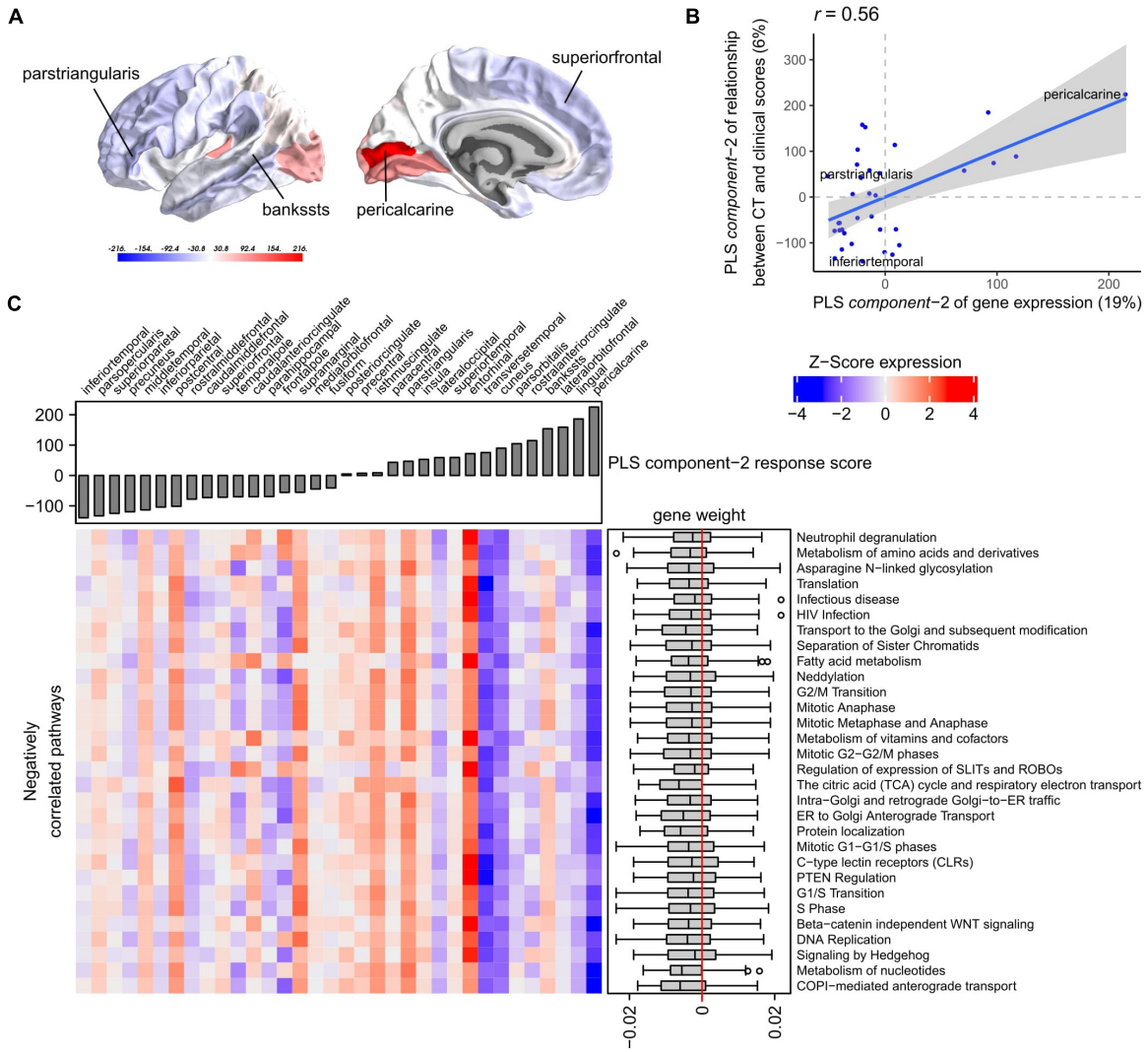

FIGURE 6 | Transcriptional signatures of PLS *component-2* in PLS *model-2* predictive of the relationship between cortical thickness (CT) and clinical scores. **(A)** PLS scores for PLS *component-2* of the predictor variables (gene expression) and **(B)** its correlation with PLS *component-1* of the response variables (*t*-statistic of β_1 in Eq. 1). Axes show the percentage of explained variance for each component; *r* indicates the Pearson correlation. **(C)** Mean expression across cortical regions (columns) of genes in the top 30 significant pathways (rows). A complete heatmap with all significant pathways is given in **Supplementary Figure 9**.

McColgan et al., 2018) and we show here that PLS can also be used to identify molecular signatures that are relevant to PD, namely, we found genes that participate in different pathways involved in cellular maintenance mechanisms. By mapping genes to latent components, genes with similar expression patterns are grouped and can be explored to better understand their collective behavior and their relationship with structural changes in the PD brain. In our study, we found a caudal-to-rostral gene expression pattern that was correlated with CT changes in PD (PLS *model-1*); cortical atrophy was found in caudal regions while rostral regions showed cortical hypertrophy. This transcriptional signature was highly enriched for genes in biological pathways associated with mitochondrial translation and mitotic cell cycle regulation. We also found a ventral-to-dorsal and caudal-to-rostral gene expression pattern that was correlated with the relationship between CT and clinical domains of PD (PLS *model-2*). Both transcriptional signatures were associated with similar pathways, including macroautophagy and Golgi-ER trafficking, and may be involved in the effect of CT on clinical scores, namely MMSE scores for cognitive assessment.

The CT analyses between disease conditions and hemispheres in patients revealed cortical regions that are susceptible to atrophy. Cortical atrophy in PD commonly occurs asymmetrical, with a preference for the left hemisphere, particularly in the early disease stages (Brück et al., 2004; Mak et al., 2014; Pereira et al., 2014; Claassen et al., 2016). Here, we showed

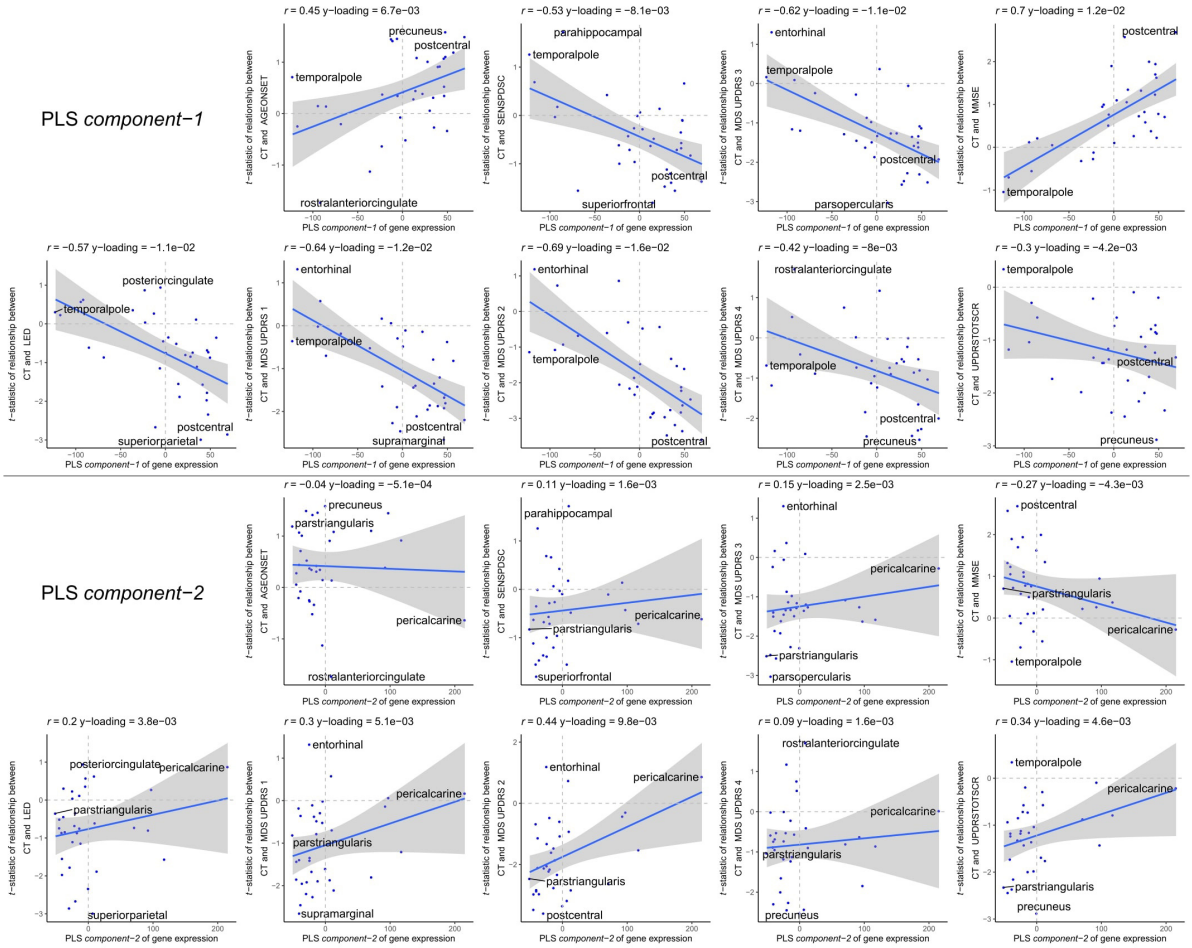

FIGURE 7 | Correlations between PLS *model-2 component-1 and component-2* scores of the predictor variables and individual response variables. Each plot shows the correlation between the predictor variables of gene expression (*x*-axis) and the response variables which are the relationships between CT and scores of a clinical feature across cortical regions (*y*-axis). On top of each plot, the Pearson correlation and the Y-loadings (Q in Eqs. 4 and 8) are shown; both values tell something about the sign (−/+) and magnitude (high/low) of the correlation. Each point or sample is one of the 34 cortical regions. Regions are labeled for those with minimum or maximum value along one of the axes.

that five out of six regions with significant CT changes between hemispheres, indeed revealed more atrophy in the left hemisphere. Two cortical regions that showed significant changes between patients and controls, also showed changes between the left and right hemisphere. Our findings are in line with those of a previous study showing that cortical atrophy in PD most prominently affects the lateral occipital cortex, particularly in the left hemisphere (Freeze et al., 2018). The temporal pole showed hypertrophy in patients compared to controls, which was only significant in the right hemisphere. However, our analysis between hemispheres of PD brains suggests that the left temporal pole is more susceptible to CT loss than the right hemisphere. The remaining regions that were susceptible to CT changes showed atrophy in either the left or right hemisphere; however, differences between hemispheres in patients could not be confirmed. All 10 regions that were different between patients and controls, except the pericalcarine, were earlier identified as part of two structural covariance networks that were related to gray matter atrophy in the same PD dataset as in this study (de Schipper et al., 2017). Overall, we observed atrophy in caudal regions, which earlier has been associated with late stage PD (Claassen et al., 2016).

With our findings of the PLS models we interpret gene expression patterns of the healthy brain in relation to imaging features observed in PD. The six adult donors of the AHBA had no known neuropsychiatric or neuropathological history (Hawrylycz et al., 2012), however, it is unknown whether these individuals could have developed neurodegenerative diseases later in life. The observed spatial gene expression patterns reflect the physiological conditions in the adult healthy brain and are informative of important molecular mechanisms that are vulnerable in PD. The biological pathways found for PLS *model-1* were closely related as they shared many similar genes. These interrelated pathways suggest a strong functional relationship between molecular processes involving mitotic cell cycle, mitochondrial translation, transport between ER and Golgi,

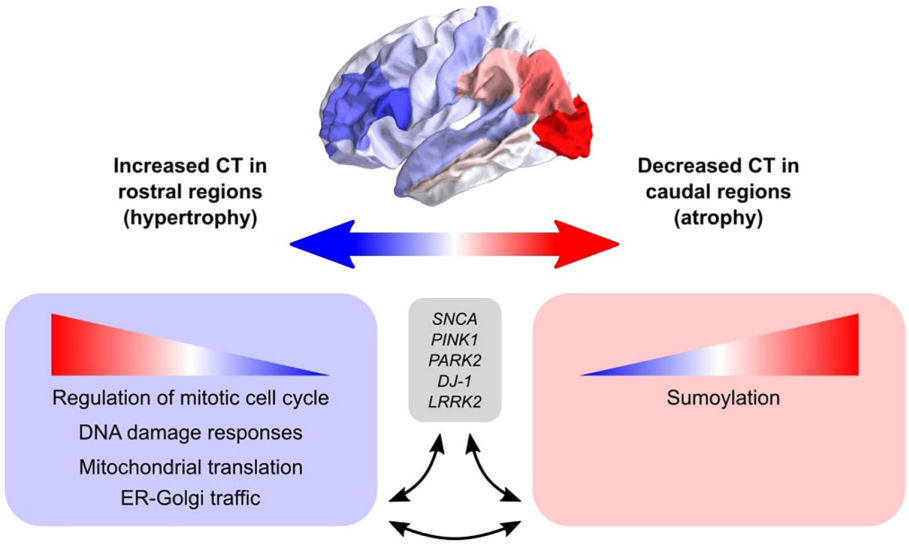

FIGURE 8 | Schematic overview of the balance between biological pathways and their influence on CT across cortical brain regions. The big arrow indicates the caudal-to-rostral (red-to-blue) or rostral-to-caudal (blue-to-red) change in CT across cortical brain regions of PD patients with red indicating decreased CT (atrophy) in caudal regions and blue indicating increased CT (hypertrophy) in rostral regions. Genes within pathways associated with sumoylation showed that the expression of these genes within the pathways increases from rostral to caudal regions. Other biological pathways that were correlated with CT changes in PD included regulation of mitotic cell cycle, mitochondrial translation, DNA damage responses, and ER-Golgi traffic, and the involved genes showed decreasing expression patterns from rostral to caudal regions (or increasing from caudal to rostral regions). All enriched pathways shared many common genes and were generally associated with cellular maintenance mechanisms. Literature studies suggest that these biological pathways may be involved in the pathobiology of PD through their interaction with genetic risk variants.

DNA damage checkpoints, and sumoylation. We found that differential regulation of these molecular processes across the brain was associated with CT changes observed in PD. Similar pathways were found in PLS *model-2* with multiple response variables corresponding to the relationships between CT and nine clinical domain scores in PD.

There is evidence that impaired cell cycle control plays a role in the pathogenesis of neurodegenerative diseases. In healthy conditions, differentiated neuronal cells become quiescent cells that cannot re-enter the cell cycle, however, in neurodegenerative diseases they are reactivated which is associated with increased cell death (Bonda et al., 2018). Cell cycle checkpoints are controlled by cyclins that guide the cell from one phase to the next phase and its expression can induce cell cycle re-initiation (Walton et al., 2019). Here, we found that regional expression of pathways associated with the degradation of cell cycle proteins in healthy conditions were negatively correlated with CT changes in PD, i.e., higher expression was associated with cortical hypertrophy in rostral regions such as the pars opercularis and temporal pole. Reversely, we observed low expression of protein degradation pathways in caudal regions that were associated with atrophy, and therefore suggests that regions with low expression are more vulnerable to improper degradation of cell cycle proteins leading to cell cycle initiation. This indicates that regions with low expression of such essential pathways are predisposed to neurodegeneration.

We found that the expression of several pathways associated with DNA replication and p53-(in)dependent DNA damage responses and checkpoints were correlated with CT changes. DNA replication during the S-phase may control the survival of post-mitotic cells by DNA repair mechanisms or apoptosis followed by DNA damage, which seems to be the case in neurodegenerative diseases (Tokarz et al., 2016). Furthermore, DNA damage response signaling can be modulated by tumor suppressor p53 and may also contribute to apoptosis in aging and age-related neurodegenerative disorders (Mohammadzadeh et al., 2019). These pathways showed similar expression patterns as those associated with the mitotic cell cycle, and therefore a lower expression of these DNA damage response pathways in caudal regions is related to cortical atrophy in PD.

Similar caudal-to-rostral expression patterns were found for pathways associated with mitochondrial translation. Increased risk for PD has been associated with mutations in *SNCA*, *PARK2* (parkin), *PINK1*, *DJ-1*, and *LRRK2* which have been linked to mitochondrial function and oxidative stress (Yan et al., 2013). *PINK1* and parkin mediates clearance of damaged mitochondria by mitophagy and may therefore influence mitotic cell cycle progression (Sarraf et al., 2019). *PINK1* also regulates both retrograde and anterograde axonal transport of mitochondria via axonal microtubules (Liu et al., 2012). The interaction between *PINK1* and parkin is likely involved in mitochondrial quality control mechanisms, where anterograde transport of damaged mitochondria is reduced and retrograde transport is enhanced for elimination by mitophagy in the neuronal cell body (Lionaki et al., 2015).

A cluster of pathways involved in ER-Golgi traffic were found enriched for PLS *model-2 component-1 and component-2*, and involved both ER-to-Golgi anterograde and Golgi-to-ER

retrograde transport. *Component-1* showed a ventral-to dorsal gene expression pattern that was associated with higher correlations between CT and clinical scores, namely, the mental state of PD patients and the performance of motor functions. The pathways involved in ER-Golgi traffic were notably high expressed in the postcentral gyrus which contains the somatosensory cortex that is known for its role in processing sensory information and the regulation of emotion (Kropf et al., 2019). Our results suggest that genes in ER-Golgi traffic pathways are important for cognitive functions controlled by the postcentral gyrus. Genes involved in ER-Golgi vesicle trafficking have the ability to modify α-synuclein toxicity in yeast (Cooper et al., 2006). Moreover, fragmentation to the Golgi apparatus has been associated with the accumulation of aberrant proteins in neurodegenerative diseases, including α-synuclein (Fan et al., 2008). A study in yeast models has showed that α-synuclein expression modulates ER stress signaling response and inhibits viral infections and viral replication (Beatman et al., 2016). We found several pathways associated to HIV and influenza infections that were correlated to the relationship between CT and clinical scores. Another pathway that shared overlapping genes with those involved in ER-Golgi traffic was asparagine N-linked glycosylation, which is a biochemical linkage important for the structure and function of proteins. The *N*-glycosylated proteins are synthesized essentially in the ER and Golgi through sequential reactions and aberrant glycolysation of proteins may lead to inflammation and mitochondrial dysfunction in PD and consequently to a cellular overload of dysfunctional proteins (Videira and Castro-Caldas, 2018).

We found that the expression of genes involved in sumoylation of chromatin organization proteins was correlated with CT changes, i.e., higher expression within caudal brain regions, such as the pericalcarine and the lateral occipital cortex, was associated with greater atrophy in PD. Therefore, higher activity of sumoylation events may play a role in the regional vulnerability to neurodegeneration observed in PD. On the other hand, lower expression of these pathways, such as in the pars opercularis, was associated with hypertrophy in rostral regions, suggesting that lower expression of sumoylation pathways has a protective effect. Additionally, the higher expression of sumoylation pathways was associated with higher correlations between CT and clinical scores as projected by PLS *component-2* in *model-2*. Sumoylation involves small ubiquitin-like modifier (SUMO) proteins that increase in response to cellular stress, such as DNA damage and oxidative stress, and can promote α-synuclein aggregation and Lewy body formation (Bologna and Ferrari, 2013; Eckermann, 2013; Rott et al., 2017). Several proteins associated with inherited forms of PD are targets modified by SUMO regulating mitochondrial processes, these include α-synuclein, DJ-1, and parkin (Guerra de Souza et al., 2016). Sumoylation has been associated with several diseases, including cancers, cardiac diseases, and neurodegenerative diseases (Yang et al., 2017). In cancer, sumoylation mediates cell cycle progression and plays an essential role during mitosis (Eifler and Vertegaal, 2015). SUMO seems to promote cell death mediated by the p53 tumor suppressor protein, which may be responsible for the cell death of dopaminergic neurons in PD (Eckermann, 2013). Our findings are in support of these hypotheses, and further suggest that sumoylation is important in specific cortical regions that are atrophic in PD, such as the lateral occipital cortex.

Spatial gene expression data from PD brains are limited in the number of brain donors and brain regions, which is mainly due to the limited availability of well-defined post-mortem PD patients. Therefore, we used healthy gene expression from the AHBA to perform unbiased whole brain and whole transcriptome analysis. Gene expression for all the six healthy adult donors in AHBA was only available for the left hemisphere. Therefore, this study was restricted to the analysis of the left hemisphere when combining gene expression with MRI data. Furthermore, it is generally assumed that gene expression changes with age, however, due to the limited number of brain donors in the AHBA, age-related differences in gene expression were not taken into account. In addition, MRI data from the patient and control groups were collected from different studies in separate cohorts and were age-matched, but the difference in the percentage of men in was not taken into account. In addition, the different scanner parameter settings were used in both studies. However, both datasets were processed with FreeSurfer which is a widely used tool to reliably measure thickness of gray matter in the cerebral cortex and was shown to be robust to variations in scanner platforms, sequence parameters, scan sessions, scanner manufacturer, and field strength (Fischl, 2012). Brain volumetric measurements by FreeSurfer have also been shown to be reproducible between different scanners in multiple sclerosis (Guo et al., 2019) and *in vivo* assessments of cortical thickness from MRI are similar to histological examinations of cortical thickness (Scholtens et al., 2015). Furthermore, an Alzheimer's disease study showed that FreeSurfer competed with manual measurements and encourages the use of FreeSurfer in clinical practice (Clerx et al., 2015). Finally, to determine whether genes and pathways truly have predictive power of imaging features, both PLS models need to be validated with an independent imaging cohort of PD patients.

Imaging cohorts of PD patients are generally quite heterogeneous because PD is a complex disorder with a wide spectrum of symptoms that vary substantially across patients. To better understand the different forms of PD, previous neuroimaging-genetics studies have grouped PD patients based on the presence of a genetic mutation associated with PD, e.g., *LRRK2* and *GBA* (van der Vegt et al., 2009; Weingarten et al., 2015), however, PD diagnosis cannot be confirmed based on genetic mutations. It is nowadays based on clinical observations, but true diagnosis can only be confirmed by pathological examination when patients are diseased. Therefore, it should be noted that patients with different forms of PD cannot be clearly distinguished based on clinical manifestations, genetic overlap or neuroimaging findings.

The 34 brain regions defined by the Desikan-Killiany atlas consist of different volumes and also differ in the number of gene expression samples that fall within a brain region. Since PLS requires the same number of samples for the predictor and response datasets, the transcriptomic and neuroimaging data was processed such that both datasets had an equal number of samples, which are the 34 brain regions. For the transcriptomic

data this meant that the expression for one brain region was based on the average expression of all samples that fall within the brain region. For the neuroimaging data, the CT reported by FreeSurfer is the average CT for a brain region given its volume. Because volume and sample size can affect these estimates, the average gene expression and average CT, the sample size can also affect the correlations predicted by the PLS model. Finally, our PLS models also do not account for the number of subjects used in this study. Future studies may improve in applying machine learning models that are better fitted to the data to find statistical associations that are more relevant to the disease being studied.

CONCLUSION

We set out to find biological explanations for the selective regional vulnerability in PD. For this purpose, we applied PLS to assess the healthy transcriptome across the whole brain and find correlations with cortical thickness changes in PD, which can be observed as atrophy and hypertrophy patterns in neuroimaging data. Previous PD studies analyzed gene expression in only few brain regions due to the limited availability of PD donors, however, we made use of the AHBA to study the healthy transcriptome across the whole brain at a high resolution. We found genes that point toward pathways involved in cellular maintenance mechanisms that are well known in PD and other neurodegenerative diseases, but here we show that these pathways are differently regulated across brain regions. More specifically, sumoylation pathways showed opposite expression patterns across the brain compared to pathways associated with the regulation of mitotic cell cycle, p53-(in)dependent DNA damage response, mitochondrial translation, and ER-Golgi trafficking (**Figure 8**). In addition, multiple genes and biological pathways identified in this study have been associated to PD before, however, their relationship with cortical thickness and clinical features was previously not known. Also, similar pathways were identified that were associated with the severity of clinical symptoms in PD, which could be a consequence of cortical atrophy or hypertrophy. All identified pathways were highly interconnected as shown by the number of shared genes and suggest a balanced interplay between sumoylation events and the other molecular mechanisms that seem to be important in controlling CT in different cortical regions. We believe that these particular pathways are interesting for further research to better understand the shared molecular mechanisms between the multiple pathways that are involved in PD progression. With our multivariate PLS approach we were able to combine multiple data modalities to provide meaningful new insights into the selective vulnerability of brain regions to PD.

DATA AVAILABILITY STATEMENT

Publicly available datasets were analyzed in this study. This data can be found here: http://human.brain-map.org.

ETHICS STATEMENT

The studies involving human participants were reviewed and approved by the Medical Ethics Committee of Leiden University Medical Center. The patients/participants provided their written informed consent to participate in this study.

AUTHOR CONTRIBUTIONS

AK, MR, and AM designed the study. JG provided the neuroimaging data. OD processed the images. AK performed the data analysis. AK, JH, MR, and AM interpreted the data and wrote the manuscript with input from all authors. AM and MR supervised the overall project. All authors read and approved final manuscript.

FUNDING

This research received funding from the Netherlands Technology Foundation (STW), as part of the STW Project 12721 (Genes in Space). OD received funding from The Dutch Research Council (NWO) project 17126 (3DOmics). JH received grants from Alkemade-Keuls Foundation; Stichting Parkinson Fonds (Optimist Study); The Netherlands Organisation for Health Research and Development (#40-46000-98-101); The Netherlands Organisation for Scientific Research (#628.004.001); Hersenstichting; AbbVie; Hoffmann-La-Roche; Lundbeck; and Centre for Human Drug Research outside the submitted work.

ACKNOWLEDGMENTS

We would like to thank Laura J. de Schipper for discussions on atrophy patterns in PD.

SUPPLEMENTARY MATERIAL

The Supplementary Material for this article can be found online at: https://www.frontiersin.org/articles/10.3389/fnins.2021.733501/full#supplementary-material

REFERENCES

Aarsland, D., Creese, B., Politis, M., Chaudhuri, K. R., Ffytche, D. H., Weintraub, D., et al. (2017). Cognitive decline in Parkinson disease. *Nat. Rev. Neurol.* 13, 217–231. doi: 10.1038/nrneurol.2017.27

Altmann-schneider, I., de Craen, A. J. M., Slagboom, P. E., Westendorp, R. G. J., van Buchem, A., Maier, A. B., et al. (2012). Brain tissue volumes in familial longevity: the Leiden longevity study. *Aging Cell* 11, 933–939. doi: 10.1111/j.1474-9726.2012.00868.x

Arnatkevičiūtė, A., Fulcher, B. D., and Fornito, A. (2019). A practical guide to linking brain-wide gene expression and neuroimaging data. *Neuroimage* 189, 353–367. doi: 10.1016/j.neuroimage.2019.01.011

Beatman, E. L., Massey, A., Shives, K. D., Burrack, K. S., Chamanian, M., and Morrison, T. E. (2016). Alpha-synuclein expression restricts RNA viral

infections in the brain. *J. Virol.* 90, 2767–2782. doi: 10.1128/JVI.02949-15. Editor

Bologna, S., and Ferrari, S. (2013). It takes two to tango: ubiquitin and SUMO in the DNA damage response. *Front. Genet.* 4:106. doi: 10.3389/fgene.2013.00106

Bonda, D. J., Casadesus, G., Zhu, X., and Smith, M. A. (2018). Review: cell cycle aberrations and neurodegeneration. *Neuropathol. Appl. Neurobiol.* 36, 157–163. doi: 10.1111/j.1365-2990.2010.01064.x.Review

Brück, A., Kurki, T., Kaasinen, V., Vahlberg, T., and Rinne, J. O. (2004). Hippocampal and prefrontal atrophy in patients with early non-demented Parkinson's disease is related to cognitive impairment. *J. Neurol. Neurosurg. Psychiatry* 75, 1467–1469. doi: 10.1136/jnnp.2003.031237

Chen, B., Wang, S., Sun, W., Shang, X., Liu, H., Liu, G., et al. (2017). Functional and structural changes in gray matter of Parkinson's disease patients with mild cognitive impairment. *Eur. J. Radiol.* 93, 16–23. doi: 10.1016/j.ejrad.2017.05.018

Claassen, D. O., McDonell, K. E., Donahue, M., Rawal, S., Wylie, S. A., Neimat, J. S., et al. (2016). Cortical asymmetry in Parkinson's disease: early susceptibility of the left hemisphere. *Brain Behav.* 6:e00573. doi: 10.1002/brb3.573

Clerx, L., Gronenschild, E. H. B. M., Echavarri, C., Verhey, F., Aalten, P., and Jacobs, H. I. L. (2015). Can FreeSurfer compete with manual volumetric measurements in Alzheimer's disease? *Curr. Alzheimer Res.* 12, 358–367. doi: 10.2174/1567205012666150324174813

Cooper, A. A., Gitler, A. D., Cashikar, A., Haynes, C. M., Hill, K. J., Bhullar, B., et al. (2006). a-synuclein blocks ER-Golgi traffic and Rab1 rescues neuron loss in Parkinson's models. *Science* 313, 324–328. doi: 10.1126/science.1129462

de Schipper, L. J., van der Grond, J., Marinus, J., Henselmans, J. M. L., and van Hilten, J. J. (2017). Loss of integrity and atrophy in cingulate structural covariance networks in Parkinson's disease. *Neuroimage Clin.* 15, 587–593. doi: 10.1016/j.nicl.2017.05.012

Desikan, R. S., Ségonne, F., Fischl, B., Quinn, B. T., Dickerson, B. C., Blacker, D., et al. (2006). An automated labeling system for subdividing the human cerebral cortex on MRI scans into gyral based regions of interest. *Neuroimage* 31, 968–980. doi: 10.1016/j.neuroimage.2006.01.021

Eckermann, K. (2013). SUMO and Parkinson's disease. *Neuromol. Med.* 15, 737–759. doi: 10.1007/s12017-013-8259-5

Eifler, K., and Vertegaal, A. C. O. (2015). SUMOylation-mediated regulation of cell cycle progression and cancer SUMO: a ubiquitin-like modifier that regulates nuclear processes. *Trends Biochem. Sci.* 40, 779–793. doi: 10.1016/j.tibs.2015.09.006

Fan, J., Hu, Z., Zeng, L., Lu, W., Tang, X., Zhang, J., et al. (2008). Golgi apparatus and neurodegenerative diseases. *Int. J. Dev. Neurosci.* 26, 523–534. doi: 10.1016/j.ijdevneu.2008.05.006

Fischl, B. (2012). FreeSurfer. *Neuroimage* 62, 774–781. doi: 10.1016/j.neuroimage.2012.01.021

Fischl, B., and Dale, A. M. (2000). Measuring the thickness of the human cerebral cortex from magnetic resonance images. *Proc. Natl. Acad. Sci. U.S.A.* 97, 11050–11055. doi: 10.1073/pnas.200033797

Folstein, M. F., Folstein, S. E., and McHugh, P. R. (1975). "Mini-mental state" a practical method for grading the cognitive stte of patients for the clinician. *J. Psychiatr. Res.* 12, 189–198. doi: 10.1016/0022-3956(75)90026-6

Freeze, B. S., Acosta, D., Pandya, S., Zhao, Y., and Raj, A. (2018). Regional expression of genes mediating trans-synaptic alpha-synuclein transfer predicts regional atrophy in Parkinson disease. *Neuroimage Clin.* 18, 456–466. doi: 10.1016/j.nicl.2018.01.009

Gibb, W. R., and Lees, A. J. (1988). The relevance of the Lewy body to the pathogenesis of idiopathic Parkinson's disease. *J. Neurol. Neurosurg. Psychiatry* 51, 745–752.

Goetz, C. G., Tilley, B. C., Shaftman, S. R., Stebbins, G. T., Fahn, S., Martinez-Martin, P., et al. (2008). Movement disorder society-sponsored revision of the unified Parkinson's disease rating scale (MDS-UPDRS): scale presentation and clinimetric testing results. *Mov. Disord.* 23, 2129–2170. doi: 10.1002/mds.22340

Guerra de Souza, A. C., Prediger, R. D., and Cimarosti, H. (2016). SUMO-regulated mitochondrial function in Parkinson's disease. *J. Neurochem.* 137, 673–686. doi: 10.1111/jnc.13599

Guo, C., Ferreira, D., Fink, K., Westman, E., and Granberg, T. (2019). Repeatability and reproducibility of FreeSurfer, FSL-SIENAX and SPM brain volumetric measurements and the effect of lesion filling in multiple sclerosis. *Eur. Radiol.* 29, 1355–1364. doi: 10.1007/s00330-018-5710-x

Hawrylycz, M., Miller, J. A., Menon, V., Feng, D., Dolbeare, T., Guillozet-Bongaarts, A. L., et al. (2015). Canonical genetic signatures of the adult human brain. *Nat. Neurosci.* 18, 1832–1844. doi: 10.1038/nn.4171

Hawrylycz, M. J., Lein, E. S., Guillozet-bongaarts, A. L., Shen, E. H., Ng, L., Miller, J. A., et al. (2012). An anatomically comprehensive atlas of the adult human brain transcriptome. *Nature* 489, 391–399. doi: 10.1038/nature11405

Hirsch, E. C., Vyas, S., and Hunot, S. (2012). Neuroinflammation in Parkinson's disease. *Park. Relat. Disord.* 18, S210–S212. doi: 10.1016/s1353-8020(11)70065-7

Kropf, E., Syan, S. K., Minuzzi, L., and Frey, B. N. (2019). From anatomy to function: the role of the somatosensory cortex in emotional regulation. *Braz. J. Psychiatry* 41, 261–269. doi: 10.1590/1516-4446-2018-0183

Li, X., Xing, Y., Martin-Bastida, A., Piccini, P., and Auer, D. P. (2018). Patterns of grey matter loss associated with motor subscores in early Parkinson's disease. *Neuroimage Clin.* 17, 498–504. doi: 10.1016/j.nicl.2017.11.009

Lionaki, E., Markaki, M., Palikaras, K., and Tavernarakis, N. (2015). Mitochondria, autophagy and age-associated neurodegenerative diseases: new insights into a complex interplay. *Biochim. Biophys. Acta* 1847, 1412–1423. doi: 10.1016/j.bbabio.2015.04.010

Liu, S., Sawada, T., Lee, S., Yu, W., Silverio, G., Alapatt, P., et al. (2012). Parkinson's disease-associated kinase PINK1 regulates miro protein level and axonal transport of mitochondria. *PLoS Genet.* 8:e1002537. doi: 10.1371/journal.pgen.1002537

Mak, E., Zhou, J., Tan, L. C. S., Au, W. L., Sitoh, Y. Y., and Kandiah, N. (2014). Cognitive deficits in mild Parkinson's disease are associated with distinct areas of grey matter atrophy. *J. Neurol. Neurosurg. Psychiatry* 85, 576–580. doi: 10.1136/jnnp-2013-305805

McColgan, P., Gregory, S., Seunarine, K. K., Razi, A., Papoutsi, M., Johnson, E., et al. (2018). Brain regions showing white matter loss in Huntington's disease are enriched for synaptic and metabolic genes. *Biol. Psychiatry* 83, 456–465. doi: 10.1016/j.biopsych.2017.10.019

Mohammadzadeh, A., Mirza-aghazadeh-attari, M., Hallaj, S., and Majidinia, M. (2019). Crosstalk between P53 and DNA damage response in ageing. *DNA Repair* 80, 8–15. doi: 10.1016/j.dnarep.2019.05.004

Oerton, E., and Bender, A. (2017). Concordance analysis of microarray studies identifies representative gene expression changes in Parkinson's disease: a comparison of 33 human and animal studies. *BMC Neurol.* 17:58. doi: 10.1186/s12883-017-0838-x

Pereira, J. B., Svenningsson, P., Weintraub, D., Brønnick, K., Lebedev, A., Westman, E., et al. (2014). Initial cognitive decline is associated with cortical thinning in early Parkinson disease. *Neurology* 82, 2017–2025. doi: 10.1212/WNL.0000000000000483

Rittman, T., Rubinov, M., Vértes, P. E., Patel, A. X., Ginestet, C. E., Ghosh, B. C. P., et al. (2016). Regional expression of the *MAPT* gene is associated with loss of hubs in brain networks and cognitive impairment in Parkinson disease and progressive supranuclear palsy. *Neurobiol. Aging* 48, 153–160. doi: 10.1016/j.neurobiolaging.2016.09.001

Rosenberg-Katz, K., Herman, T., Jacob, Y., Kliper, E., Giladi, N., and Hausdorff, J. M. (2016). Subcortical volumes differ in Parkinson's disease motor subtypes: new insights into the pathophysiology of disparate symptoms. *Front. Hum. Neurosci.* 10:356. doi: 10.3389/fnhum.2016.00356

Rott, R., Szargel, R., Shani, V., Hamza, H., Savyon, M., Abd, F., et al. (2017). SUMOylation and ubiquitination reciprocally regulate α-synuclein degradation and pathological aggregation. *Proc. Natl. Acad. Sci. U.S.A.* 114, 13176–13181. doi: 10.1073/pnas.1704351114

Sarraf, S. A., Sideris, D. P., Giagtzoglou, N., Ni, L., Kankel, M. W., Sen, A., et al. (2019). PINK1/Parkin influences cell cycle by sequestering TBK1 at damaged mitochondria, inhibiting mitosis. *Cell Rep.* 29, 225–235. doi: 10.1016/j.celrep.2019.08.085

Scholtens, L. H., de Reus, M. A., and van den Heuvel, M. P. (2015). Linking contemporary high resolution magnetic resonance imaging to the von economo legacy: a study on the comparison of MRI cortical thickness and histological measurements of cortical structure. *Hum. Brain Mapp.* 36, 3038–3046. doi: 10.1002/hbm.22826

Tokarz, P., Kaarniranta, K., and Blasiak, J. (2016). Role of the cell cycle re-initiation in DNA damage response of post-mitotic cells and its implication in the pathogenesis of neurodegenerative diseases. *Aging Dis.* 19, 131–140. doi: 10.1089/rej.2015.1717

Tomlinson, C. L., Stowe, R., Patel, S., Rick, C., Gray, R., and Clarke, C. E. (2010). Systematic review of levodopa dose equivalency reporting in Parkinson's disease. *Mov. Disord.* 25, 2649–2653. doi: 10.1002/mds.23429

van der Heeden, J. F., Marinus, J., Martinez-Martin, P., and van Hilten, J. J. (2016). Evaluation of severity of predominantly non-dopaminergic symptoms in Parkinson's disease: the SENS-PD scale. *Park. Relat. Disord.* 25, 39–44. doi: 10.1016/j.parkreldis.2016.02.016

van der Vegt, J. P. M., Van Nuenen, B. F. L., Bloem, B. R., Klein, C., and Siebner, H. R. (2009). Imaging the impact of genes on Parkinson's disease. *Neuroscience* 164, 191–204. doi: 10.1016/j.neuroscience.2009.01.055

Vértes, P. E., Rittman, T., Whitaker, K. J., Romero-Garcia, R., Váša, F., Kitzbichler, M. G., et al. (2016). Gene transcription profiles associated with inter-modular hubs and connection distance in human functional magnetic resonance imaging networks. *Philos. Trans. R. Soc. B Biol. Sci.* 371:20150362. doi: 10.1098/rstb.2015.0362

Videira, P. A. Q., and Castro-Caldas, M. (2018). Linking glycation and glycosylation with inflammation and mitochondrial dysfunction in Parkinson's disease. *Front. Neurosci.* 12:381. doi: 10.3389/fnins.2018.00381

Walton, C. C., Zhang, W., Patiño-parrado, I., Barrio-alonso, E., Garrido, J., and Frade, J. M. (2019). Primary neurons can enter M-phase. *Sci. Rep.* 9:4594. doi: 10.1038/s41598-019-40462-4

Wang, M., Jiang, S., Yuan, Y., Zhang, L., Ding, J., Wang, J., et al. (2016). Alterations of functional and structural connectivity of freezing of gait in Parkinson's disease. *J. Neurol.* 263, 1583–1592. doi: 10.1007/s00415-016-8174-4

Weingarten, C. P., Sundman, M. H., Hickey, P., and Chen, N. K. (2015). Neuroimaging of Parkinson's disease: expanding views. *Neurosci. Biobehav. Rev.* 59, 16–52. doi: 10.1016/j.neubiorev.2015.09.007

Whitaker, K. J., Vértes, P. E., Romero-garcia, R., Moutoussis, M., and Prabhu, G. (2016a). Adolescence is associated with genomically patterned consolidation of the hubs of the human brain connectome. *Proc. Natl. Acad. Sci. U.S.A.* 113, 9105–9110. doi: 10.1073/pnas.1601745113

Whitaker, K. J., Vértes, P. E., Romero-Garcia, R., Váša, F., Moutoussis, M., Prabhu, G., et al. (2016b). Adolescence is associated with genomically patterned consolidation of the hubs of the human brain connectome. *Proc. Natl. Acad. Sci. U.S.A.* 113, 9105–9110.

Wilson, H., Niccolini, F., Pellicano, C., and Politis, M. (2019). Cortical thinning across Parkinson's disease stages and clinical correlates. *J. Neurol. Sci.* 398, 31–38. doi: 10.1016/j.jns.2019.01.020

Yan, M. H., Wang, X., and Zhu, X. (2013). Mitochondrial defects and oxidative stress in Alzheimer disease and Parkinson disease. *Free Radic. Biol. Med.* 62, 90–101. doi: 10.1016/j.freeradbiomed.2012.11.014

Yang, Y., He, Y., Wang, X., He, G., Zhang, P., Zhu, H., et al. (2017). Protein SUMOylation modification and its associations with disease. *Open Biol.* 7:170167.

Zheng, D., Chen, C., Song, W. C., Yi, Z. Q., Zhao, P. W., Zhong, J. G., et al. (2019). Regional gray matter reductions associated with mild cognitive impairment in Parkinson's disease: a meta-analysis of voxel-based morphometry studies. *Behav. Brain Res.* 371:111973. doi: 10.1016/j.bbr.2019.111973

Conflict of Interest: The authors declare that this study received funding from AbbVie, Hoffmann-La-Roche, and Lundbeck. The funders were not involved in the study design, collection, analysis, interpretation of data, the writing of this article or the decision to submit it for publication.

frontiers in Neuroscience

REVIEW
published: 11 November 2021
doi: 10.3389/fnins.2021.755870

The Etiology of Auditory Hallucinations in Schizophrenia: From Multidimensional Levels

Xu Shao[1], Yanhui Liao[1], Lin Gu[2,3], Wei Chen[1] and Jinsong Tang[1]**

[1] Department of Psychiatry, Sir Run Run Shaw Hospital, Zhejiang University School of Medicine, Hangzhou, China, [2] RIKEN AIP, Tokyo, Japan, [3] Research Center for Advanced Science and Technology, The University of Tokyo, Tokyo, Japan

Enormous efforts have been made to unveil the etiology of auditory hallucinations (AHs), and multiple genetic and neural factors have already been shown to have their own roles. Previous studies have shown that AHs in schizophrenia vary from those in other disorders, suggesting that they have unique features and possibly distinguishable mechanisms worthy of further investigation. In this review, we intend to offer a comprehensive summary of current findings related to AHs in schizophrenia from aspects of genetics and transcriptome, neurophysiology (neurometabolic and electroencephalogram studies), and neuroimaging (structural and functional magnetic resonance imaging studies and transcriptome–neuroimaging association study). Main findings include gene polymorphisms, glutamate level change, electroencephalographic alterations, and abnormalities of white matter fasciculi, cortical structure, and cerebral activities, especially in multiple regions, including auditory and language networks. More solid and comparable research is needed to replicate and integrate ongoing findings from multidimensional levels.

Keywords: auditory hallucination, DTI, EEG, fMRI, genetics, schizophrenia

OPEN ACCESS

Edited by:
Jiajia Zhu,
First Affiliated Hospital of Anhui Medical University, China

Reviewed by:
Chuanjun Zhuo,
Tianjin Anding Hospital, China
Xiaoxia Du,
Shanghai University of Sport, China

***Correspondence:**
Wei Chen
srrcw@zju.edu.cn
Jinsong Tang
tangjinsong@zju.edu.cn

Specialty section:
This article was submitted to Brain Imaging Methods, a section of the journal Frontiers in Neuroscience

Received: *09 August 2021*
Accepted: *14 October 2021*
Published: *11 November 2021*

Citation:
Shao X, Liao Y, Gu L, Chen W and Tang J (2021) The Etiology of Auditory Hallucinations in Schizophrenia: From Multidimensional Levels. Front. Neurosci. 15:755870. doi: 10.3389/fnins.2021.755870

INTRODUCTION

Auditory hallucinations (AHs) are defined as experiences that without an external stimulus, individuals perceive voices as distinct from their own thoughts, whether the voices are familiar or not (American Psychiatric Association, 2013). With nearly 10% of lifetime prevalence rate among the general population (Maijer et al., 2018), this debilitating symptom occurs among healthy population, as well as people with various clinical conditions such as psychiatric diseases (including schizophrenia, mood disorders, dissociative disorders, etc.), neurological diseases, and hearing impairment (Laroi et al., 2012). AHs are most commonly found in major psychotic disorders, with the lifetime prevalence rate of 60-80% in schizophrenia spectrum disorders (Lim et al., 2016), and 1-year prevalence rate of 50-70% in schizophrenia specifically (Bauer et al., 2011; Waters et al., 2014). AHs are a main positive symptom of schizophrenia (American Psychiatric Association, 2013) and can bring severe damage to one's mental health, for instance, increasing depressive symptoms (Chiang et al., 2018) and leading to suicidal ideation or attempt (Koyanagi et al., 2015).

As to the etiology, the past decades have witnessed a rapid growth in clinical studies investigating the genetic and neural substrates for AHs generally and the verbal type specifically [auditory verbal hallucinations (AVHs)] in schizophrenia. Notwithstanding, the possible mechanism remains

unclear, and the existing findings are divergent to some extent. A comprehensive analysis of the ongoing studies will help depict a clearer picture of what current science knows about AHs in schizophrenia. Thus, in this review, we summarize the results from previous research, especially in the field of genetics, neurobiology, and neuroimaging. And we mainly focus on "trait" studies conducted in schizophrenia, that is, schizophrenia with auditory (verbal) hallucinations were compared to patients without the symptom instead of healthy controls. Another type of research, "state" studies that compare on-the-state period to off-the-state period within the same patient group, is also included in the respective sections. At the end of this review, we further discuss the limitations of previous studies and propose several suggestions for ways forward.

GENETIC RESEARCH

Genetic Factor

It is well-known that gene and its interaction with environment play an important role in the development of psychiatric symptoms or disorders. And researchers have been investigating how genetic and environmental factors are linked to AHs.

Most studies were conducted among schizophrenia patients, considering the frequent occurrence of AHs in this population. Abundant studies showed that DNA variations in the *cholecystokinin A receptor* (*CCK-AR*) gene contributed to the formation of schizophrenia and AHs (Wei and Hemmings, 1999; Tachikawa et al., 2001; Sanjuan et al., 2004; Toirac et al., 2007). Schizophrenia carrying *glutathione S-transferase* (*GST*) *A1*B* allele had more severe AHs than non-B carriers (Spalletta et al., 2012). Rajasekaran et al. (2016) found an association between (*human leukocyte antigen-G*) *HLA-G* 14-bp Ins/Ins genotype and lifetime presence of third person AHs, and this association was more significant in males with schizophrenia. The genotype frequency of *matrix metalloproteinase 1* (*MMP1*) single-nucleotide polymorphism (SNP) rs470558 was reported to be associated with AHs, and its A allele frequency was higher in schizophrenia with AHs (SZ-AH) than schizophrenia without AHs (SZ-non-AH) (Kim et al., 2012). *Dystrobrevin binding protein 1* (*DTNBP1*) gene was involved with neurotransmission regulation and neurodevelopment in schizophrenia, and its SNP rs4236167 was found to be associated with AHs generally and third-person and abusive form ones specifically (Cheah et al., 2015). One linkage and association analyses found that D8S1769, located 350 kb upstream of the 5′ end of the first exon of *neuregulin 1* (*NRG1*) gene, had significant linkage signal for SZ-AH, and the frequency of the G allele of SNP8NRG241930 was significantly higher in SZ-AH compared to healthy controls (Kim et al., 2006). Previous research on the association between *serotonin transporter* (*5-HTT*) gene and AHs has been controversial. *5-HTT* gene-linked polymorphic region (5-HTTLPR) is generated by a 44-bp deletion in the promoter site with two principal alleles, short (*s*) and long (*l*), respectively (Heils et al., 1996). At first, *l* allele was found to be associated with the frequency or the severity of hallucinations in schizophrenia (Malhotra et al., 1998). However, Sanjuan et al. (2006a) found that *s* allele was related to emotional response to AHs in schizophrenia, but not to the AH frequency. In another study, 5-HTTLPR polymorphism was also associated with the emotional response to AHs, specifically the distress caused by the symptom, but only with marginal statistical significance (Rivero et al., 2010).

Genetic × Environmental Factor

Some other genes have been reported to predispose to AHs through the interaction with environmental factors. For instance, *forkhead box P2 gene* (*FOXP2*) was involved in the development of the neural systems mediating speech and language (Liegeois et al., 2003). Patients with abnormal *FOXP2* function showed significant underactivation in Broca's area and other language-related cortical regions (Liegeois et al., 2003). And investigators found that *FOXP2* SNPs were associated with SZ-AH (Sanjuan et al., 2006b), but not directly with the symptom of AHs (Tolosa et al., 2010). Further study showed that SNP rs1456031 interacted with childhood parental emotional abuse to predict AVHs (McCarthy-Jones et al., 2014a). Putting these evidences together, *FOXP2* mutation might cause the symptom only in the presence of the environmental factor.

Based on previous findings, multiple genes, along with the influences of psychosocial factors, play their own part in the occurrence of AHs. But it is still unclear whether these genes function independently or they interact with each other, and how much percentage each gene makes up to the pathogenesis of AHs. Among them, *DTNBP1* seems to be the most potential gene candidate for AHs. It is a schizophrenia susceptibility gene related to regulation of glutamate level (Tang T. T.-T. et al., 2009), and its mRNA expression is lower in AH-related regions including superior temporal gyrus, hippocampus, and dorsolateral prefrontal cortex (Talbot et al., 2004; Weickert et al., 2004; Tang J. et al., 2009).

Although great joint efforts have been made to analyze data of large-scale genome-wide association studies in the population of schizophrenia to search for regulatory genes, such efforts are not yet made to investigate the genetic connection with AHs. Moreover, previous results are mainly derived according to bioinformatics methodologies, and it remains to be solved from molecular biological level how much influence individuals might receive from these genetic mutations.

Transcriptional Factor

How gene is expressed in the cerebral area offers a clearer picture of genetic function on human brain. And an increasing amount of studies has investigated differentiated gene expression in specific brain areas using postmortem or database of schizophrenia. ATPase type 13A4 (ATP13A4) gene (verbal and social interaction skills) expression was up-regulated in Broca's area of schizophrenia (Gibbons et al., 2020). Expressions of genes related to cell–cell adhesion, synaptic transmission, and neural excitability were enriched in the prefrontal cortex (Pergola et al., 2019). In dorsolateral prefrontal cortex, to be further, expressions of genes related to regulation of cell survival and growth as well as response to external stimuli (Petralia et al., 2020), related to learning and memory processes (Ohayon et al., 2020),

and related to immune-related functions (Enwright and Lewis, 2021) were up-regulated, whereas expressions of genes related to mitochondrial function (Enwright and Lewis, 2021); related to neurotransmitter release modulation (Tao et al., 2020); related to cell proliferation, differentiation, and transformation (Huang et al., 2019); and related to neuronal homeostasis and intracellular signaling (Petralia et al., 2020) were down-regulated. Oxytocin receptor (social cognition) mRNA was down-regulated in the temporal cortex (Uhrig et al., 2016), and sodium-dependent MI transporter-1 (SLC5A3) gene (metabolic precursor regulation) expression was up-regulated in the superior temporal cortex (Vawter et al., 2019).

There are scattered reports about gene transcription concerning AHs only using peripheral blood samples. The mRNA level of *mitochondrial complex I gene* (NDUFV2) was found to be positively correlated with both overall and positive symptoms in the first-episode schizophrenia patients (Akarsu et al., 2014). Complement 4A (C4A) mRNA expression was found to be positively correlated with positive symptoms in schizophrenia, specifically the presence and severity of delusions (Melbourne et al., 2018). Using gene expression profiling from schizophrenia and related disorders, four genes were found to decrease in high hallucinatory state (Fn1, Rhobtb3, Aldh1l1, Mpp3), and three genes were found to increase (Arhgef9, Phlda1, S100a6) (Kurian et al., 2011). Only one study used gene expression profiling of postmortem brain samples from prefrontal cortex and found that plexin B1 (PLXNB1) expression was decreased in SZ-AH compared to SZ-non-AH (Gilabert-Juan et al., 2015). The different expression of PLXNB1 might be a signature of the hallucinatory endophenotype in schizophrenia.

Therefore, cerebral transcriptomic study of AHs in schizophrenia is scarce. As the importance is increasingly attached to transcriptomics, this research field leaves much to be exploited.

NEUROPHYSIOLOGICAL RESEARCH

Neurometabolic Study

Magnetic resonance spectroscopy (MRS) has been an effective tool to measure cerebral metabolic level of targeted substance and has been used to investigate how certain neurochemicals might affect the occurrence of AHs. For example, as to the measurement of Glx level (composite of glutamate and glutamine), schizophrenia with AVHs (SZ-AVH) had higher Glx level than schizophrenia without AVHs (SZ-non-AVH) in the left lateral prefrontal region (Curcic-Blake et al., 2017), although schizophrenia group generally had lower Glx level than the control group in the temporal and frontal areas (Hugdahl et al., 2015; Curcic-Blake et al., 2017). Besides, AH severity was reported to positively correlate with Glx level both in the frontal and temporal regions (Hugdahl et al., 2015). Glutamate excitatory function is usually balanced by γ-aminobutyric acid (GABA) inhibitory function (Carlsson et al., 2001). Therefore, the glutamate-GABA excitatory–inhibitory imbalance could lead to the development of AHs (Hugdahl and Sommer, 2018). Further, Hjelmervik et al. (2019) found in a larger sample that Glx level was positively correlated with AVH in the left superior temporal gyrus and negatively in the anterior cingulate cortex, but they failed to find any significant result for GABA level. Consequently, they proposed that compared to Glu–GABA imbalance within regions, Glu–Glu imbalance between regions was more plausible especially in the frontal and temporal regions. Therefore, studies above have shown that glutamatergic metabolites serve as a mediating factor in AHs.

Other neurochemical studies remain scarce. N-acetyl-aspartate/choline (NAA/Cho) ratio in the right thalamus was lower in SZ-AH, relative to SZ-non-AH or healthy controls (Martinez-Granados et al., 2008). Besides, NAA level was decreased in the hippocampus in schizophrenia during the episode of AHs (Heckers, 2001) and was also reported to be negatively correlated with the duration of positive symptoms (Theberge et al., 2003). Moreover, phospholipids (phosphomonoesters and phosphodiesters) and energy metabolism (adenosine triphosphate, inorganic phosphate, and phosphocreatine) in left superior temporal gyrus were both positively correlated with AH severity in SZ-AH (Nenadic et al., 2014).

Based on existing findings, the association between glutamate level and AHs is relatively solid, but whether GABA level has a role remains inconclusive. Interregional Glu–Glu imbalance rather than intraregional Glu–GABA imbalance is more suitable at present. Findings of other neurochemical and neurometabolic studies remain scarce. It is worthwhile to finding out in future investigations how chemical substance in the brain and their metabolism influence hallucinatory activities of schizophrenia.

Electroencephalogram Study

The forward model has been illustrated in many studies and can be applied in the auditory system (Wolpert and Miall, 1996; Heinks-Maldonado et al., 2007). When a sound initiates, the auditory feedback can be predicted by the efference copy of the motor command. This corollary discharge is compared with the actual auditory feedback. If the sound is self-generated, the predicted auditory feedback often matches the actual one; the sensory input is suppressed, leading to a dampened auditory experience. If the sound is externally produced, the predicted auditory feedback often contradicts with the actual one, leading to no suppression of the auditory response. During self-generated vocalizations, neural discharges in a majority of auditory cortical neurons are suppressed, and the suppression precedes the onset of vocalizations (Eliades and Wang, 2003), and this suppression helps distinguish between internally and externally initiated sensations. Event-related potential (ERP) results revealed that in healthy controls, N1 to self-voice feedback was dampened compared to alien voice (Heinks-Maldonado et al., 2007). Phase coherence of prespeech electroencephalogram (EEG) was found to be related to reduced speech-onset N1 potentials, showing prespeech neural synchrony suppressed subsequent responsiveness to self-spoken sound (Ford et al., 2007). However, hallucination predisposition in healthy controls might affect voice discrimination and recognition (Pinheiro et al., 2019). These evidences indicate that people with AHs could not

recognize self-generated voice correctly, and they displayed improperly high response to it, as the result of which the forward model was damaged.

Schizophrenia is characterized by the disturbance of sensory gating mechanism that filters out extraneous stimuli from meaningful sensory inputs to focus attention (Freedman et al., 1987). And auditory sensory gating is one way of directly measuring auditory perceptual abnormality, and it assesses modulation of incoming auditory information 50 ms into cortical processing (Thoma et al., 2017). At 50 ms comes a positive wave, P50 potential, as the largest initial cerebral response to an auditory stimulus (Javitt and Freedman, 2015). Sensory gating deficit has been frequently found in schizophrenia (Potter et al., 2006), but limited studies have explored the relationship between sensory gating deficit and AHs. Smith et al. (2013) demonstrated that AVH severity was positively associated with the extent of P50 sensory gating deficit. Faugere et al. (2016) found that schizophrenia with P50 sensory gating impairment had more severe AVH than without that impairment. For the P50, N100, and P200 components, gating ratios were higher in schizophrenia on the state of AVH than those off the state (Thoma et al., 2017). In one magnetoencephalographic study, gating ratio of the magnetic analog of P50 (P50m) in the left hemisphere was positively associated with AHs in schizophrenia (Hirano et al., 2010). These evidences suggest that sensory gating deficit directly contributed to the formation of AHs as well.

Mismatch negativity (MMN) is another EEG-derived ERP, which functions as a neurophysiological index signaling auditory processing (Naatanen et al., 2007) and reflects detection of the change of stimulus in the environment (Salisbury, 2012). Compared to SZ-non-AH, SZ-AH possessed smaller MMNs to duration deviants (Fisher et al., 2008). In SZ-AH, MMN amplitude to gap deviants was negatively correlated with the duration, loudness, and clarity of AHs (Fisher et al., 2012). Furthermore, reduced MMN amplitude was found to be directly correlated with AHs in schizophrenia with early psychosis (Rudolph et al., 2015). Considering previous studies already reported the association between reduced MMN amplitude and general hallucinatory trait in schizophrenia (Youn et al., 2003; Fisher et al., 2011, 2014; Perrin et al., 2018), it is plausible that deficits of auditory processing and external stimulus detection, indicated by MMN alterations, could contribute to the development of AHs.

Studies have found dysfunctional γ frequency (30–100 Hz) oscillations in AHs. γ-Band oscillations play a role in selecting neurons, which communicate about sensory inputs, and higher cognitive functions including perceptual organization and language processing (Uhlhaas et al., 2008). The auditory steady-state response (ASSR), as one kind of ERPs that is elicited by temporally modulated auditory stimulation, has been used to study neural synchrony in schizophrenia (O'Donnell et al., 2013). Phase locking factor of the left hemisphere source was correlated with AHs in schizophrenia during ASSR to 40-Hz γ frequency stimulation (Spencer et al., 2009). In another study, 40-Hz ASSR was found to be diminished in schizophrenia, and phase synchronization between the primary auditory cortices was positively correlated with AHs (Mulert et al., 2011). In SZ-AVH, 40-Hz EEG activity decreased left-laterally, and global measure of phase locking decreased with stimulation (Koenig et al., 2012). Induced 40-Hz γ power in the left hemisphere was correlated with AHs in schizophrenia (Hirano et al., 2015). In another, 80-Hz ASSR-BOLD (blood oxygen–level dependent) signal was positively associated with AHs in acute episode schizophrenia (Kuga et al., 2016). Interestingly, when 40-Hz ASSR was divided as early-latency and late-latency γ response, researchers did not find group differences of early or late γ activity signatures between SZ-AH and SZ-non-AH (Griskova-Bulanova et al., 2016). Apart from ASSR-related results, correlation dimension in the γ-band in the right prefrontal cortex was more chaotic in schizophrenia with treatment-refractory AHs than counterparts without (Lee et al., 2008). Therefore, despite that participants recruited and measures reflecting γ-band oscillations differ in previous studies, results could still suggest that deficit of γ oscillations in schizophrenia was related to AHs.

Alterations of other frequency spectrums and prominent spectral interactions are also reported to be associated with AHs. Compared to SZ-non-AH, SZ-AH had increased α-band coherence between the left and right superior temporal cortices (Sritharan et al., 2005). Schizophrenia with AHs also had increased α-band phase-coupling intrahemispherically and interhemispherically and increased α-band synchrony (Angelopoulos et al., 2011). Correlation dimension in the β-band in the left parietal cortex was more coherent in schizophrenia with treatment-refractory AHs than counterparts without (Lee et al., 2008). Phase coupling between theta and γ rhythms was increased in the left frontotemporal cortices during AVH (Koutsoukos et al., 2013). β1 and β2 frequency amplitude were higher in SZ-AH than SZ-non-AH (Lee et al., 2006). Also, γ frequency was correlated with β (2 and 3) frequencies in SZ-AH, and β (1 and 2) activity was enhanced in the left inferior parietal lobule and the left medial frontal gyrus in SZ-AH relative to SZ-non-AH (Lee et al., 2006).

Combining these evidences together, SZ-AH are deficient in auditory processing, including suppressing inner speech, filtering out meaningless auditory stimuli, detecting stimulus change in the environment, and proper cerebral circuitry function (especially in the primary auditory cortex).

NEUROIMAGING RESEARCH

Structural Magnetic Resonance Imaging Study

Diffusion Tensor Imaging Study

Compared to SZ-non-AH, SZ-AH had lower fractional anisotropy (FA) in bilateral superior longitudinal fasciculi and arcuate fasciculi (Chawla et al., 2019). Compared to schizophrenia with audiovisual hallucinations, SZ-AH showed lower white matter connectivity in the pathways connecting the hippocampal complex with visual areas including the forceps major and the inferior fronto-occipital fasciculus (Amad et al., 2014). Different correlational studies reported that FAs in bilateral arcuate fasciculus (Rotarska-Jagiela et al., 2009), bilateral

superior longitudinal fasciculi (Seok et al., 2007; Shergill et al., 2007), and left anterior cingulum (Shergill et al., 2007) were positively associated with AHs in schizophrenia. Meanwhile, mean diffusivity in left superior temporal gyrus white matter was associated with AHs specifically in male schizophrenia (Lee et al., 2009).

Previous studies focusing on verbal type of AHs have yielded inconsistent results. Relative to SZ-non-AVH, SZ-AVH had higher FA in the lateral parts of the temporoparietal section of the arcuate fasciculus (Hubl et al., 2004), in the left arcuate fasciculus (Psomiades et al., 2016), and in parts of the anterior corpus callosum (Hubl et al., 2004). Paradoxically, other studies showed that SZ-AVH had lower FA in the left frontal–temporal regions involved in language networks (including left inferior fronto-occipital fasciculus and left arcuate fasciculus segments) (Curcic-Blake et al., 2015; McCarthy-Jones et al., 2015; Oestreich et al., 2016) and in tracts involved in interhemispheric language connections (including bilateral anterior corona radiata and posterior parts of the corpus callosum) (Curcic-Blake et al., 2015). Mulert et al. (2012) reported higher but Wigand et al. (2015) reported lower FA in the interhemispheric auditory fibers in SZ-AVH. In correlational analysis, Psomiades et al. (2016) found AVH positively correlated with FA in the left arcuate fasciculus, but Curcic-Blake et al. (2015) found AVH negatively correlated with FA in the left frontal–temporal regions including arcuate fasciculus segments. In addition, some studies did not find the difference of structural integrity of internal capsule (Xi et al., 2016), anterior corona radiata (Xi et al., 2016), the language pathways (Catani et al., 2011; Leroux et al., 2017; Xie et al., 2019), and the interhemispheric auditory pathways (Leroux et al., 2017) between SZ-AVH and SZ-non-AVH, although white matter integrity in SZ-AVH or SZ-non-AVH, respectively, differed from that in healthy controls.

The debate on the involvement of the intrahemispheric and interhemispheric fasciculi in the etiology of AHs thus remains open. And the verbal type might have unique abnormalities of white matter fasciculi relative to the general hallucination. Diffusion tensor imaging (DTI) studies in the past decades are relatively inadequate, and findings of previous studies have been incongruent and contradictory. Still, it can be implied that pathological fasciculus alterations in the language pathways and interhemispheric auditory pathways lead to the emergence of AHs.

Morphological Thickness

Structural correlates of AHs have been frequently reported in schizophrenia. Compared to SZ-non-AVH, SZ-AVH showed reduced thickness in the right Heschl gyrus (Chen et al., 2015), in the language and primary auditory areas including the Broca's area, the Heschl gyrus, and Wernicke's area of the left hemisphere (van Swam et al., 2012), in the bilateral postcentral gyrus (van Swam et al., 2012), and in the left middle temporal gyrus (Cui et al., 2018). Promisingly, the abnormality of the left Heschl gyrus was replicated in schizophrenia spectrum patients with AHs (Morch-Johnsen et al., 2017), and the abnormality of the left middle temporal gyrus was confirmed by the negative correlation between its cortical thickness and AH severity (Cui et al., 2018). On the other hand, SZ-AVH showed increased thickness in the frontal cortex (left insular cortex, and bilaterally anterior/posterior cingulate, and dorsal middle frontal gyrus) and parietal lobe (van Swam et al., 2012). Among all, the left middle temporal gyrus is most related to AHs and deserves closer investigation in the future, as it is a vital part of language pathways connected to other areas (Xu et al., 2015) and related to self-monitoring dysfunction (Shergill et al., 2000).

Morphological Volume

Comparatively, more studies have been conducted concerning structural volume. SZ-AH showed larger volumes of temporal white matter, frontal gray matter, and temporal gray matter when compared to SZ-non-AH (Shin et al., 2005), but Kubera et al. (2014) yielded contrary results when comparing SZ-AVH to schizophrenia without or in remission with AVH. Compared to schizophrenia with audiovisual hallucinations, SZ-AH showed smaller hippocampal complex (Amad et al., 2014). Compared to SZ-non-AVH, SZ-AVH showed increased volume of the right Heschl gyrus (Hubl et al., 2010), but reduced volume of the left insula (Shapleske et al., 2002). Apart from cerebral pathological changes, Cierpka et al. (2017) found that SZ-AVH had lower gray matter volume in lobule VIIIa than SZ-non-AVH, suggesting the possible involvement of cerebellum in the pathophysiology of AVH.

There have been studies investigating the direct relationship between the hallucinatory symptom and morphological volume. In a dichotic listening task, AH severity was negatively correlated with the volume of left anterior superior temporal gyrus in SZ-AH (Levitan et al., 1999). In resting state among schizophrenia, AH severity was reported to be negatively correlated with the volume of the left superior temporal gyrus (Barta et al., 1990), corpus callosum (Knochel et al., 2012), the left Heschl gyrus, left inferior supramarginal gyrus, right middle/inferior prefrontal gyri (Gaser et al., 2004), the right superior temporal gyrus, right fusiform gyrus, and left inferior temporal gyrus (O'Daly et al., 2007), as well as left inferior frontal gyrus and right postcentral gyrus (Garcia-Marti et al., 2008). On the contrary, other studies found positive correlations between AH severity and the volume of left inferior frontal gyrus (Modinos et al., 2009), bilateral superior temporal cortex (including Heschl gyrus), left supramarginal/angular gyrus, left postcentral gyrus, and left posterior cingulate cortex (Nenadic et al., 2010). Voxel-based meta-analysis found a negative correlation between AH severity and gray matter volume in the left insula or right superior temporal gyrus (Palaniyappan et al., 2012). Another meta-analysis found the severity of AVH was correlated with volume reductions in the left and marginally the right superior temporal gyri (including Heschl gyri), implicating the bilateral structural pathology of this region (Modinos et al., 2013). But Modinos et al. (2013) failed to find group difference between SZ-AVH and SZ-non-AVH. Therefore, correlational findings very much contradict with each other.

Previous structural magnetic resonance imaging (sMRI) studies were mainly conducted in participants' resting state. Evidences have demonstrated morphological changes in certain cerebral regions among schizophrenia, and the majority shows

the shrinkage rather than the enlargement of the cerebral regions including auditory and language areas. Among all, reduced volume of temporal gyri, including Heschl gyrus, is most frequently replicated in recent research. According to studies of morphological thickness and volume, it is obvious that temporal region plays the most crucial part in the pathogenesis of AHs. However, current MRI results are heterogeneous to a certain extent and are in lack of replicability, which therefore calls for further confirmation of these results in the future.

Functional Magnetic Resonance Imaging Study

Cerebral Blood Flow Study

Studies across decades have shown that cerebral blood flow (CBF) contributes to the neural underpinning of AHs. "State" study showed that schizophrenia had higher blood flow in Broca's area in auditory hallucinating state than in their resolved state (McGuire et al., 1993). Compared to SZ-non-AVH, SZ-AVH displayed increased CBF in the right superior temporal gyrus and caudate nucleus (Zhuo et al., 2017), in the left superior temporal gyrus and right supramarginal gyrus (Wolf et al., 2012). SZ-AVH also had decreased CBF in the bilateral occipital and left parietal cortices (Zhuo et al., 2017), and in the bilateral superior and middle frontal gyri and postcentral gyri, and right supplementary motor area (Cui et al., 2017a). There were also studies focusing on CBF during task mode. When generating and monitoring inner speech, SZ-AH had reduced CBF in the left middle temporal gyrus and the rostral supplementary motor area compared to SZ-non-AH (McGuire et al., 1995). During verbal memory activation, SZ-AH had increased CBF in the left basal ganglia (Busatto et al., 1995). To sum up, CBF studies have implicated increased brain activities among auditory- and language-related regions, which accords with findings in functional MRI (fMRI) studies talked about later. Still, some results are rather sporadic, thus calling for further replications.

Resting-State Functional MRI

The past decades have witnessed fMRI findings emerging one after another concerning the brain activities during AHs. In order to achieve definite conclusions, meta-analysis has become a powerful systematic tool. Across populations of schizophrenia-spectrum disorder, psychotic disorder, and healthy controls, meta-analyses of trait studies revealed that AVHs were frequently related to activations in the left middle and superior temporal gyrus, left postcentral and precentral gyrus, left insula, left hippocampus/parahippocampal region, right inferior frontal gyrus, and so on (Jardri et al., 2011; Kompus et al., 2011; Kühn and Gallinat, 2012; van Lutterveld et al., 2013; Zmigrod et al., 2016). The inferior parietal lobule was also frequently reported in these analyses, but the lateralization was inconsistent. Other less frequent reported regions include anterior cingulate cortex and thalamus. Generally speaking, the cerebral activations in trait studies reflect lateralization in the left hemisphere, and related regions extensively cover the language/speech, auditory, and limbic networks. On the other hand, meta-analysis of state studies revealed that AVHs were associated with activation in bilateral inferior frontal gyrus, bilateral postcentral gyrus, and left parietal operculum (Kühn and Gallinat, 2012).

Functional connectivity is used to detect the temporal correlation of the low-frequency fluctuation in the BOLD signal between regions (Fox and Raichle, 2007), and the abnormalities of interregional resting-state functional connectivity were found among different brain areas including those reported above. Compared to patients without the symptom, schizophrenia spectrum patients with AHs had higher functional connectivity of left Heschl gyrus (belonging to the primary auditory cortex) with left frontoparietal regions and lower one with right hippocampal formation and mediodorsal thalamus, and functional connectivity of the left Heschl gyrus was correlated with AH severity in regions related to language, memory, and self-monitoring (Shinn et al., 2013). SZ-AH, compared to patients with audiovisual hallucinations, had lower functional connectivity of the bilateral hippocampal complex with the medial prefrontal cortex and the caudate nuclei and had a higher one with the thalamus (Amad et al., 2014), and dysconnectivity of hippocampal subregions was also reported in SZ-AVH (Liu et al., 2019). SZ-AH, compared to SZ-non-AH, displayed enhanced functional connectivity of the bilateral nucleus accumbens with the left superior temporal gyrus, the cingulate gyri, and the ventral tegmental area, indicating that the increased activity of the mesolimbic pathway might underlie the occurrence of AHs (Rolland et al., 2015), while in terms of AVH, SZ-AVH showed higher functional connectivity in a neural circuit involving the anterior cingulate cortex, insula, and language-related areas including superior temporal gyrus and inferior parietal lobule, compared to SZ-non-AVH (Chang et al., 2017). SZ-AVH also showed thalamic–auditory cortical hyperconnectivity and auditory cortical–hippocampal hypoconnectivity, and AVH severity was positively correlated with the connectivity from Broca's area to the auditory cortex (Li et al., 2017). Direct correlational analyses among SZ-AVH showed that AVH severity was negatively correlated with functional connectivity in the left anterior cingulate cortex, positively correlated with the left superior temporal gyrus and right lateral prefrontal cortex (Wolf et al., 2011), and negatively correlated with neural coupling between left temporoparietal junction, bilateral anterior cingulate, and bilateral amygdala (Vercammen et al., 2010).

Within the auditory network, SZ-AH had lower interhemispheric connectivity in both primary and secondary auditory cortices when compared to SZ-non-AH (Gavrilescu et al., 2010). In another study, SZ-AH was reported to have decreased functional connectivity between two regions inside the auditory network, right Heschl gyrus, and right posterior superior temporal gyrus, compared to SZ-non-AH (Guo et al., 2020). Within the language network, SZ-AVH had higher functional connectivity of bilateral Wernicke's area with the left inferior frontal gyrus (Hoffman et al., 2011) and reduced causal interactions from the left inferior frontal gyrus to left middle temporal gyrus (Zhang et al., 2017). In addition, the auditory cortex–posterior language network involving auditory cortex and posterior language regions was more active during AVH-on periods in schizophrenia spectrum disorders, whereas occipital–temporal and medial prefrontal networks were more

active during AVH-off periods (Thoma et al., 2016). Within the default mode network (DMN), SZ-AVH had lower effective connectivity from anteromedial prefrontal cortex to left inferior temporal gyrus and from posterior cingulate cortex to left cerebellum posterior lobe, inferior temporal gyrus, and right middle frontal gyrus than SZ-non-AVH (Zhao et al., 2018). Although Guo et al. (2020) did not find dysconnectivity in the DMN, they reported that SZ-AH had reduced functional connectivity of overall parietal memory network adjacent to the DMN and also reduced functional connectivity between core regions, and the latter negatively correlated with AH severity.

Interactions between multiple networks have also been reported. With independent component analysis and dual regression, Cui et al. (2017b) demonstrated AVH-related coactivation within the auditory, default mode, executive, motor, and frontoparietal networks, which were involved in auditory processing, language production and monitoring, and sensory information filtering. Alonso-Solis et al. (2015) found alterations of resting-state functional connectivity of DMN subsystems with hubs of the salience network, suggesting cross-network abnormalities related to AVH. Further, stochastic dynamic causal modeling analysis captured the link between general ongoing hallucinatory state in schizophrenia with memory-based sensory input from the hippocampus to the salience network (Lefebvre et al., 2016). In another study, Scheinost et al. (2019) put forward a potential AVH network overlying the default mode and language processing networks.

Task-State Functional MRI

Studies of task-state fMRI related to AHs in schizophrenia are in lack so far. During a voice recognition task, SZ-AVH had reduced functional connectivity of right superior temporal gyrus with right superior frontal gyrus (Mou et al., 2013). Within the inner speech processing network, loudness of AVH in SZ-AVH was correlated with reduced activity in bilateral angular gyrus, bilateral anterior cingulate gyrus, left inferior frontal gyrus, left insula, and left middle temporal gyrus, during a metrical stress evaluation task activating inner speech production and perception (Vercammen et al., 2011). During verbal speech perception, SZ-AVH displayed hypercoupling in auditory–motor, language processing, and DMNs compared to SZ-non-AVH (Lavigne and Woodward, 2018), and SZ-AH comorbid with other hallucinatory types displayed a hypercoupling left-dominant temporal–frontal network involving speech-related auditory and motor regions (Lavigne et al., 2015).

Currently, neuroimaging results are still insufficient to draw any decisive conclusions. That being said, fMRI has been an effective tool to offer abundant evidences, implying that neural mechanisms underlying AHs involve abnormal activation among multiple cerebral regions related to speech/language processing, auditory perception, and so on, and disordered brain connections can be found at interregional, intranetwork, and internetwork level. Matching sMRI results and abnormal activation of superior and middle temporal gyrus are replicated constantly in fMRI studies, suggesting these regions have both structural and functional abnormalities related to AHs. As to the interregional connection, functional connectivity of Heschl gyrus, superior temporal gyrus, and hippocampus region is most noteworthy. As to intranetwork and internetwork connection, deficits of the auditory network and language network are most prominent, followed by DMN.

Transcriptome–Neuroimaging Study

Transcriptional and neuroimaging combined studies have received huge popularity in recent years, but few has been conducted related to schizophrenia, let alone AHs. Using postmortem prefrontal cortex samples of male schizophrenia and controls and high-resolution anatomical MRI with optimized voxel-based morphometry, Sanjuán et al. (2021) found low *FOXP2* (language mediation) mRNA level was associated with reduced gray matter density, and SNP rs2396753 played a part in this association. One posttranscriptional study using PET imaging to measure the α5 subtype of the GABA receptor (α5-$GABA_A$Rs) availability found that α5-$GABA_A$Rs protein level was reduced in the hippocampus of antipsychotic-free schizophrenia and correlated positively with total symptom score (Marques et al., 2020), which extended previous results of lower mRNA and protein levels of α5-$GABA_A$Rs in schizophrenia (Duncan et al., 2010; Beneyto et al., 2011). These evidences provided moderate support for central GABA hypofunction underlying the pathophysiology of clinical symptoms, albeit no direct connection with AHs. Only two studies in latest years did belong to transcriptome–neuroimaging association study of AHs. Using high-throughput RNA sequencing and resting-state fMRI data, expression of an lncRNA-mRNA network centered by lncRNA MSTRG.96171.1 was upregulated in SZ-AVH relative to SZ-non-AVH, and functional connectivity of DMN regions was positively correlated with AVH severity and MSTRG.96171.1 expression, respectively (Zhu et al., 2019). Furthermore, Yu et al. (2020) replicated the upregulated expression of this interactive network, and the positive correlation between functional connectivity of similar DMN regions and this lncRNA expression. These two pilot studies offered a clue for coexisting transcriptional and neuroimaging alterations related to AVH.

Up to present, seldom has focused on "trait" studies of SZ-AH measuring the direct relation between cerebral expression of AH-related genes and neuroimaging features. Transcriptome–neuroimaging association studies are urgently required in the future to hopefully better the understanding of endophenotypes of AHs from both molecular and imaging angles.

NEUROCOGNITIVE MODEL

Various models of AHs have been put forward combining evidence of all levels. Generally, there are two main models of the hallucinatory pathogenesis concerning perceptual beliefs and inner speech.

According to the computational model of perception (Fletcher and Frith, 2009; Powers et al., 2017), perceptual beliefs, originating from prior experiences, influence one's sensation together with the actual sensory input, and hallucinations occur when the beliefs cause a percept without actual stimuli. Usually, perceptual beliefs are updated when prediction error

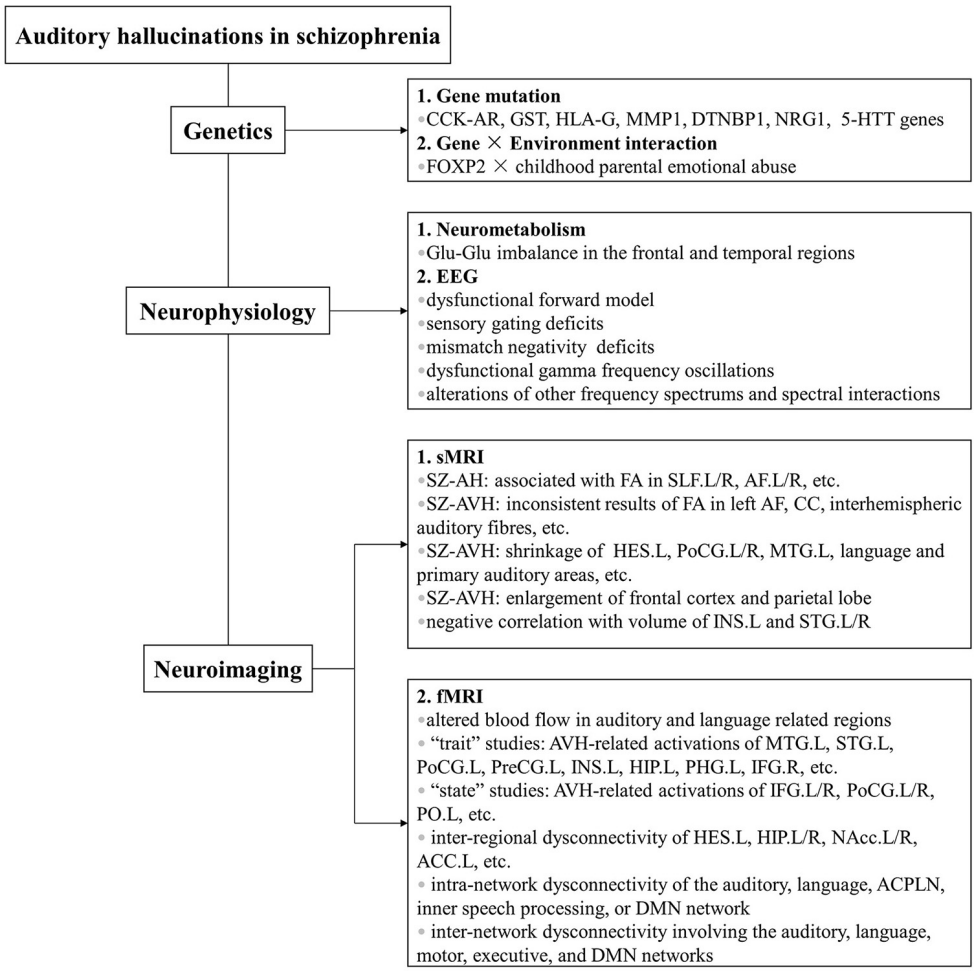

FIGURE 1 | Etiology of auditory hallucinations in schizophrenia from multidimensional levels. Previous work has utilized methods of various kinds, including genetic, neurophysiological, and neuroimaging studies. Main findings are summarized in the figure. Abbreviations: CCK-AR, cholecystokinin A receptor; GST, glutathione S-transferase; HLA-G, human leukocyte antigen-G; MMP1, matrix metalloproteinase 1; DTNBP1, dystrobrevin binding protein 1; NRG1, neuregulin 1; 5-HTT, serotonin transporter; FOXP2, forkhead box P2; EEG, electroencephalogram; sMRI, structural magnetic resonance imaging; SZ-AH, schizophrenia with auditory hallucinations; FA, fractional anisotropy; L, left; R, right; L/R, bilateral; SLF, bilateral superior longitudinal fasciculi; AF, arcuate fasciculi; SZ-AVH, schizophrenia with auditory verbal hallucinations; CC, corpus callosum; HES, Heschl's gyrus; PoCG, postcentral gyrus; MTG, middle temporal gyrus; INS, insula; STG, superior temporal gyrus; fMRI, functional magnetic resonance imaging; PreCG, precentral gyrus; HIP, hippocampus; PHG, parahippocampal gyrus; IFG, inferior frontal gyrus; PO, parietal operculum; NAcc, nucleus accumbens; ACC, anterior cingulate cortex; ACPLN, auditory cortex-posterior language network; DMN, default mode network.

occurs, which is the discrepancy between what is expected and what happens. Nevertheless, this mechanism has been demonstrated abnormal in schizophrenia (Corlett et al., 2007). In addition, hallucinating psychosis, regardless of the diagnosis, is less sensitive to the changes in contingency so as to have rigid perceptual beliefs and weighs more on perceptual beliefs than on actual sensory input, compared to non-hallucinating counterparts (Powers et al., 2017). Therefore, pathological perceptual beliefs may result in sensory perception even without objective stimuli, which further contributes to the formation of AHs among schizophrenia.

Another well-known model is inner speech model, which suggests that AHs arise on condition that inner speech (thinking in words) is perceived as someone else's, and this condition results from the deficits of self-monitoring (Frith and Done, 1988). Self-monitoring refers to one's ability to distinguish sensations evoked by one's own actions from those by external factors (Allen et al., 2007). This process is achieved, as what is mentioned earlier about the forward model, by the comparison between the corollary discharge and the actual auditory outcome to induce different neural responses to internally or externally generated motor action. Abnormal cerebral connectivity impairs the transmission of the corollary discharge in the forward model, resulting in the deficits of self-monitoring among schizophrenia (Stephan et al., 2009; Nazimek et al., 2012). Inner speech, in this case, could also be viewed as a motor action and is accompanied by a corollary discharge (Jack et al., 2019). Thus, failure to executive the function of self-monitoring leads

to the misinterpretation of inner speech as if evoked by external source.

There have been other less popular models. The aberrant memory model postulates that failure to inhibit recalling and unintendedly activation of the memory system brings past traumatic memories to consciousness and generated unexpected intrusive thoughts. Early time trauma is closely connected to later life AVH. Consequently, memories that appear out of context contribute to the sensation of "otherness" and authorship from external side and then cause AVH (Tracy and Shergill, 2013). According to the spontaneous neural activity model (also called resting-state hypothesis), the occurrence of AVH is due to enhanced resting-state activity in the auditory cortex, aberrant modulation of the auditory cortex by anterior cortical midline regions (part of the DMN), and neural confusion between auditory cortical resting-state changes and stimulus-induced activity (Northoff and Qin, 2011). According to the expectation–perception model (related to the self-monitoring mechanism), prefrontal regions are normally responsible for prediction and expectation of sensory input. As AHs happen, anatomical abnormalities in neurons, imbalance of neurotransmitter, and dysfunction of auditory cortex contribute to the deficient processing of prediction error, as a result of which the prediction from prefrontal regions becomes so unconstrained and vague that random fluctuations in spontaneous activity enhance the signal input and becomes a conscious percept in auditory cortex in the absence of external input (Nazimek et al., 2012).

CONCLUSION

Findings From Multidimensional Levels

With advances in our understanding of AHs, there lies an intricate fact that no single explanation so far has simply served for the full mechanism underlying these symptoms. Fruitful findings in the past decades have shown that the pathogenesis of AHs in schizophrenia has independent genetic basis and neural substrates revealed by multidimensional levels. Based on what is summarized in this review, AHs are influenced by multiple gene and gene × environment interactions from genetic level, by glutamate level imbalance from neurometabolic level, by dysfunctional forward model, sensory gating deficits, MMN deficits, dysfunctional γ frequency oscillations, and alterations of other frequency spectrums and spectral interactions from EEG level, by fasciculus alterations of white matter and morphological changes from sMRI level, and by altered cerebral blood flow, abnormal cerebral activations, and dysfunctional brain connectivity of interregion, intranetwork, and internetwork from fMRI level (summarized in **Figure 1**).

However, there are several aspects worthy of discussion in order to improve current research. First, small sample size, heterogeneous patients' condition, and diversified methodologies and study designs make current evidences less easy to be replicated. One priority of future studies is to enlarge sample size and devise comparable design to allow confirmation of existing findings. Second, other types of AHs apart from the verbal type warrant more attention in the future as they are seldom studied up to present. And multimodal studies are also welcomed to combine evidences from different aspects. Third, a body of previous studies was conducted in schizophrenia with auditory (verbal) hallucinations and healthy individuals, which makes it difficult to tell whether the group differences result from the hallucinatory experience or the disease itself. As a result, "trait" study that directly compares SZ-AH and SZ-non-AH or compares SZ-AVH and SZ-non-AVH is more preferred to rule out the possible influence of the clinical state. Fourthly, "state" study that compares hallucinatory with non-hallucinatory period using self-control is tremendously scarce, probably because the ongoing hallucinatory state is relatively tricky to fully capture, and fMRI and EEG are ones of the few tools capable of distinguishing "trait" and "state" studies. Therefore, study of this kind is also wanted in the future. Last but not least, current scanty of transcriptional–neuroimaging studies of AHs calls for more endeavor in this field.

Hypothesis 1. Schizophrenia: Auditory Hallucinations vs. Auditory Verbal Hallucinations

Although plenty of studies focus on AHs in general, there is still an abundant load of work specifically on the verbal type, AVH, probably due to the verbal type as a core positive symptom of schizophrenia. And previous research of the general and the verbal type has yielded inconsistent results.

In genetic research, gene candidates and transcriptomic studies are solely found in SZ-AH, whereas gene × environment interaction is solely found in SZ-AVH. In neurometabolic research, interregional Glu–Glu imbalance was concluded from combined evidence of both general AHs and the verbal type, and other neurometabolic studies have been mainly conducted in SZ-AH. In EEG research, sensory gating deficits are solely found in SZ-AVH, whereas other results are mainly found in SZ-AH. In sMRI research, although cerebral alterations are found from combined evidence of both SZ-AH and SZ-AVH, two groups have yielded inconsistent results. For example, regarding DTI study, "trait" studies showed SZ-AH lower FA in bilateral superior longitudinal fasciculi and arcuate fasciculi. Differently in SZ-AVH, although FA changes in other fasciculi were reported, those in superior longitudinal fasciculi were not, and results concerning arcuate fasciculi were inconclusive. For another example, regarding morphological study, scanty "trait" study in SZ-AH showed larger volumes of temporal white matter, frontal gray matter, and temporal gray matter, which did not accord with findings in SZ-AVH. In fMRI research, SZ-AVH had specific regional activation replicated by meta-analyses. While SZ-AH had enhanced functional connectivity of regions related to mesolimbic pathway, SZ-AVH of regions related to language and auditory system. While SZ-AH had dysconnectivity within the auditory network, SZ-AVH had dysconnectivity not only within the language, the inner speech processing, and the DMNs, but also between cerebral networks.

Therefore, our first hypothesis is that AVH may have independent mechanism from other types of AHs. In fact, one reason for poor replicability of current studies could be

that AHs of different subtypes are treated as a whole group during research. Currently, comparative studies among subtypes of AHs in schizophrenia, although scarce, have shown that different subtypes may have distinct phenomenological features and functional brain patterns. McCarthy-Jones et al. (2014b) classified AHs into constant commanding and commenting AVH, replay AVH, own though AVH, and non-verbal AHs. One study found schizophrenia with non-verbal AHs showed higher global functional connectivity density in bilateral superior temporal gyri and lower global functional connectivity density (gFCD) in bilateral prefrontal cortex, inferior frontal lobe, and occipital lobe (Zhuo et al., 2020). These preliminary evidences have supported our hypothesis. We suggest future research should separate AHs into different groups to make subtype comparisons.

Hypothesis 2. Auditory Hallucinations: From Genotype to Phenotype

Our second hypothesis is that AHs are heterogeneous symptoms rooted deeply in genetic background. Mediating genes cause neurophysiological alterations and structural and functional cerebral changes, which further cause distinct clinical features of AHs in schizophrenia. Based on existing genetic research, *DTNBP1* is a promising gene candidate for AHs. Its function is related to regulation of glutamate level, which is consistent with neurometabolic findings of interregional Glu–Glu imbalance (especially in the frontal and temporal regions). Its mRNA expression is lower in superior temporal gyrus and hippocampus. Regarding superior temporal gyrus, correlation between glutamate level and AHs based on neurometabolic study was found in this area. Morphological volume changes based on sMRI study and aberrant activation and functional connectivity changes based on fMRI study were also found in this area. Regarding hippocampus, structural and functional changes were also found based on sMRI and fMRI study. We hypothesized that reduced cerebral *DTNBP1* expression leads to glutamate level changes and structural and functional changes of superior temporal gyrus and hippocampus. Our hypothesis is according to current multidimensional research, but these evidences are not collected from the same patients. Research to date often utilizes a single scale, resulting in incoherent understanding of the etiology. We suggest future research use a multimode framework that uses multiscale data, from genomics, transcriptomic, neurophysiology, to neuroimaging (i.e., from genotype to phenotype). Therefore, multidimensional research conducted on one batch of patients is strongly preferred to confirm the effect of genetic variants on brain structures that contribute to AHs.

Investigations on pathogenesis of mental disorders and related phenomenology have always been a challenge hard to conquer, and AHs in schizophrenia are no exception. Although great advancement has been accomplished in the past decades, much more endeavor still needs to be made in the future. Hopefully, discovery of mechanisms underlying AHs will contribute to a deeper understanding of the essence of this symptom and will have substantial implications for clinical practice.

AUTHOR CONTRIBUTIONS

XS and JT conceived the study. XS completed the first draft. All authors contributed to the literature research and analyses and approved the final manuscript.

FUNDING

This research was supported by the National Natural Science Foundation of China (grant numbers 81871057 and 8217050237, JT) and in part by the Japan Science and Technology Agency under grant ACT-X (grant number JPMJAX190D and Moonshot R&D grant number JPMJMS2011, LG). The funder had no role in study design, data collection and analysis, decision to publish, or preparation of the manuscript.

REFERENCES

Akarsu, S., Torun, D., Bolu, A., Erdem, M., Kozan, S., Ak, M., et al. (2014). Mitochondrial complex I and III gene mRNA levels in schizophrenia, and their relationship with clinical features. *J. Mol. Psychiatry* 2:6. doi: 10.1186/s40303-014-0006-9

Allen, P., Aleman, A., and McGuire, P. K. (2007). Inner speech models of auditory verbal hallucinations: evidence from behavioural and neuroimaging studies. *Int. Rev. Psychiatry* 19, 407–415. doi: 10.1080/09540260701486498

Alonso-Solis, A., Vives-Gilabert, Y., Grasa, E., Portella, M. J., Rabella, M., Sauras, R. B., et al. (2015). Resting-state functional connectivity alterations in the default network of schizophrenia patients with persistent auditory verbal hallucinations. *Schizophr. Res.* 161, 261–268. doi: 10.1016/j.schres.2014.10.047

Amad, A., Cachia, A., Gorwood, P., Pins, D., Delmaire, C., Rolland, B., et al. (2014). The multimodal connectivity of the hippocampal complex in auditory and visual hallucinations. *Mol. Psychiatry* 19, 184–191. doi: 10.1038/mp.2012.181

American Psychiatric Association (2013). *Diagnostic and Statistical Manual of Mental Disorders*, Fifth Edn. Arlington, TX: American Psychiatric Association.

Angelopoulos, E., Koutsoukos, E., Maillis, A., Papadimitriou, G. N., and Stefanis, C. (2011). Cortical interactions during the experience of auditory verbal hallucinations. *J. Neuropsychiatry Clin. Neurosci.* 23, 287–293. doi: 10.1176/appi.neuropsych.23.3.287

Barta, P. E., Pearlson, G. D., Powers, R. E., Richards, S. S., and Tune, L. E. (1990). Auditory hallucinations and smaller superior temporal gyral volume in schizophrenia. *Am. J. Psychiatry* 147, 1457–1462. doi: 10.1176/ajp.147.11.1457

Bauer, S. M., Schanda, H., Karakula, H., Olajossy-Hilkesberger, L., Rudaleviciene, P., Okribelashvili, N., et al. (2011). Culture and the prevalence of hallucinations in schizophrenia. *Compr. Psychiatry* 52, 319–325.

Beneyto, M., Abbott, A., Hashimoto, T., and Lewis, D. A. (2011). Lamina-specific alterations in cortical GABA(A) receptor subunit expression in schizophrenia. *Cereb. Cortex* 21, 999–1011. doi: 10.1093/cercor/bhq169

Busatto, G. F., David, A. S., Costa, D. C., Ell, P. J., Pilowsky, L. S., Lucey, J. V., et al. (1995). Schizophrenic auditory hallucinations are associated with increased regional cerebral blood flow during verbal memory activation in a study using single photon emission computed tomography. *Psychiatry Res.* 61, 255–264. doi: 10.1016/0925-4927(95)02750-r

Carlsson, A., Waters, N., Holm-Waters, S., Tedroff, J., Nilsson, M., and Carlsson, M. L. (2001). Interactions between monoamines, glutamate, and GABA in schizophrenia: new evidence. *Annu. Rev. Pharmacol. Toxicol.* 41, 237–260. doi: 10.1146/annurev.pharmtox.41.1.237

Catani, M., Craig, M. C., Forkel, S. J., Kanaan, R., Picchioni, M., Toulopoulou, T., et al. (2011). Altered integrity of perisylvian language pathways in

schizophrenia: relationship to auditory hallucinations. *Biol. Psychiatry* 70, 1143–1150. doi: 10.1016/j.biopsych.2011.06.013

Chang, X., Collin, G., Xi, Y., Cui, L., Scholtens, L. H., Sommer, I. E., et al. (2017). Resting-state functional connectivity in medication-naive schizophrenia patients with and without auditory verbal hallucinations: a preliminary report. *Schizophr. Res.* 188, 75–81. doi: 10.1016/j.schres.2017.01.024

Chawla, N., Deep, R., Khandelwal, S. K., and Garg, A. (2019). Reduced integrity of superior longitudinal fasciculus and arcuate fasciculus as a marker for auditory hallucinations in schizophrenia: a DTI tractography study. *Asian J. Psychiatr.* 44, 179–186. doi: 10.1016/j.ajp.2019.07.043

Cheah, S. Y., Lawford, B. R., Young, R. M., Morris, C. P., and Voisey, J. (2015). Dysbindin (DTNBP1) variants are associated with hallucinations in schizophrenia. *Eur. Psychiatry* 30, 486–491. doi: 10.1016/j.eurpsy.2015.01.008

Chen, X., Liang, S., Pu, W., Song, Y., Mwansisya, T. E., Yang, Q., et al. (2015). Reduced cortical thickness in right Heschl's gyrus associated with auditory verbal hallucinations severity in first-episode schizophrenia. *BMC Psychiatry* 15:152. doi: 10.1186/s12888-015-0546-2

Chiang, Y. H., Beckstead, J. W., Lo, S. C., and Yang, C. Y. (2018). Association of auditory hallucination and anxiety symptoms with depressive symptoms in patients with schizophrenia: a three-month follow-up. *Arch. Psychiatr. Nurs.* 32, 585–590.

Cierpka, M., Wolf, N. D., Kubera, K. M., Schmitgen, M. M., Vasic, N., Frasch, K., et al. (2017). Cerebellar contributions to persistent auditory verbal hallucinations in patients with schizophrenia. *Cerebellum* 16, 964–972. doi: 10.1007/s12311-017-0874-5

Corlett, P. R., Murray, G. K., Honey, G. D., Aitken, M. R., Shanks, D. R., Robbins, T. W., et al. (2007). Disrupted prediction-error signal in psychosis: evidence for an associative account of delusions. *Brain* 130(Pt. 9), 2387–2400. doi: 10.1093/brain/awm173

Cui, L. B., Chen, G., Xu, Z. L., Liu, L., Wang, H. N., Guo, L., et al. (2017a). Cerebral blood flow and its connectivity features of auditory verbal hallucinations in schizophrenia: a perfusion study. *Psychiatry Res. Neuroimaging* 260, 53–61. doi: 10.1016/j.pscychresns.2016.12.006

Cui, L. B., Liu, L., Guo, F., Chen, Y. C., Chen, G., Xi, M., et al. (2017b). Disturbed brain activity in resting-state networks of patients with first-episode schizophrenia with auditory verbal hallucinations: a cross-sectional functional MR imaging study. *Radiology* 283, 810–819. doi: 10.1148/radiol.2016160938

Cui, Y., Liu, B., Song, M., Lipnicki, D. M., Li, J., Xie, S., et al. (2018). Auditory verbal hallucinations are related to cortical thinning in the left middle temporal Gyrus of patients with schizophrenia. *Psychol. Med.* 48, 115–122. doi: 10.1017/s0033291717001520

Curcic-Blake, B., Bais, L., Sibeijn-Kuiper, A., Pijnenborg, H. M., Knegtering, H., Liemburg, E., et al. (2017). Glutamate in dorsolateral prefrontal cortex and auditory verbal hallucinations in patients with schizophrenia: a (1)H MRS study. *Prog. Neuropsychopharmacol. Biol. Psychiatry* 78, 132–139. doi: 10.1016/j.pnpbp.2017.05.020

Curcic-Blake, B., Nanetti, L., van der Meer, L., Cerliani, L., Renken, R., Pijnenborg, G. H., et al. (2015). Not on speaking terms: hallucinations and structural network disconnectivity in schizophrenia. *Brain Struct. Funct.* 220, 407–418. doi: 10.1007/s00429-013-0663-y

Duncan, C. E., Webster, M. J., Rothmond, D. A., Bahn, S., Elashoff, M., and Shannon Weickert, C. (2010). Prefrontal GABA(A) receptor alpha-subunit expression in normal postnatal human development and schizophrenia. *J. Psychiatr Res.* 44, 673–681. doi: 10.1016/j.jpsychires.2009.12.007

Eliades, S. J., and Wang, X. (2003). Sensory-motor interaction in the primate auditory cortex during self-initiated vocalizations. *J. Neurophysiol.* 89, 2194–2207. doi: 10.1152/jn.00627.2002

Enwright, J. F., and Lewis, D. A. (2021). Similarities in cortical transcriptome alterations between schizophrenia and bipolar disorder are related to the presence of psychosis. *Schizophr. Bull.* 47, 1442–1451. doi: 10.1093/schbul/sbaa195

Faugere, M., Micoulaud-Franchi, J. A., Boyer, L., Cermolacce, M., Richieri, R., Faget, C., et al. (2016). Does sensory gating have a protective effect against hallucinatory behavior in schizophrenia? *Clin. Neurophysiol.* 127, 1746–1748. doi: 10.1016/j.clinph.2015.10.031

Fisher, D. J., Grant, B., Smith, D. M., Borracci, G., Labelle, A., and Knott, V. J. (2011). Effects of auditory hallucinations on the mismatch negativity (MMN) in schizophrenia as measured by a modified 'optimal' multi-feature paradigm. *Int. J. Psychophysiol.* 81, 245–251. doi: 10.1016/j.ijpsycho.2011.06.018

Fisher, D. J., Labelle, A., and Knott, V. J. (2008). The right profile: mismatch negativity in schizophrenia with and without auditory hallucinations as measured by a multi-feature paradigm. *Clin. Neurophysiol.* 119, 909–921. doi: 10.1016/j.clinph.2007.12.005

Fisher, D. J., Labelle, A., and Knott, V. J. (2012). Alterations of mismatch negativity (MMN) in schizophrenia patients with auditory hallucinations experiencing acute exacerbation of illness. *Schizophr. Res.* 139, 237–245. doi: 10.1016/j.schres.2012.06.004

Fisher, D. J., Smith, D. M., Labelle, A., and Knott, V. J. (2014). Attenuation of mismatch negativity (MMN) and novelty P300 in schizophrenia patients with auditory hallucinations experiencing acute exacerbation of illness. *Biol. Psychol.* 100, 43–49. doi: 10.1016/j.biopsycho.2014.05.005

Fletcher, P. C., and Frith, C. D. (2009). Perceiving is believing: a Bayesian approach to explaining the positive symptoms of schizophrenia. *Nat. Rev. Neurosci.* 10, 48–58. doi: 10.1038/nrn2536

Ford, J. M., Roach, B. J., Faustman, W. O., and Mathalon, D. H. (2007). Synch before you speak: auditory hallucinations in schizophrenia. *Am. J. Psychiatry* 164, 458–466. doi: 10.1176/ajp.2007.164.3.458

Fox, M. D., and Raichle, M. E. (2007). Spontaneous fluctuations in brain activity observed with functional magnetic resonance imaging. *Nat. Rev. Neurosci.* 8, 700–711. doi: 10.1038/nrn2201

Freedman, R., Adler, L. E., Gerhardt, G. A., Waldo, M., Baker, N., Rose, G. M., et al. (1987). Neurobiological studies of sensory gating in schizophrenia. *Schizophr. Bull.* 13, 669–678. doi: 10.1093/schbul/13.4.669

Frith, C. D., and Done, D. J. (1988). Towards a neuropsychology of schizophrenia. *Br. J. Psychiatry* 153, 437–443. doi: 10.1192/bjp.153.4.437

Garcia-Marti, G., Aguilar, E. J., Lull, J. J., Marti-Bonmati, L., Escarti, M. J., Manjon, J. V., et al. (2008). Schizophrenia with auditory hallucinations: a voxel-based morphometry study. *Prog. Neuropsychopharmacol. Biol. Psychiatry* 32, 72–80. doi: 10.1016/j.pnpbp.2007.07.014

Gaser, C., Nenadic, I., Volz, H. P., Buchel, C., and Sauer, H. (2004). Neuroanatomy of "hearing voices": a frontotemporal brain structural abnormality associated with auditory hallucinations in schizophrenia. *Cereb. Cortex* 14, 91–96. doi: 10.1093/cercor/bhg107

Gavrilescu, M., Rossell, S., Stuart, G. W., Shea, T. L., Innes-Brown, H., Henshall, K., et al. (2010). Reduced connectivity of the auditory cortex in patients with auditory hallucinations: a resting state functional magnetic resonance imaging study. *Psychol. Med.* 40, 1149–1158. doi: 10.1017/s0033291709991632

Gibbons, A. S., Bell, L. M., Udawela, M., and Dean, B. (2020). mRNA expression of the P5 ATPase ATP13A4 is increased in Broca's area from subjects with schizophrenia. *World J. Biol. Psychiatry* 21, 402–408. doi: 10.1080/15622975.2018.1548781

Gilabert-Juan, J., Sáez, A. R., Lopez-Campos, G., Sebastiá-Ortega, N., González-Martínez, R., Costa, J., et al. (2015). Semaphorin and plexin gene expression is altered in the prefrontal cortex of schizophrenia patients with and without auditory hallucinations. *Psychiatry Res.* 229, 850–857. doi: 10.1016/j.psychres.2015.07.074

Griskova-Bulanova, I., Hubl, D., van Swam, C., Dierks, T., and Koenig, T. (2016). Early- and late-latency gamma auditory steady-state response in schizophrenia during closed eyes: does hallucination status matter? *Clin. Neurophysiol.* 127, 2214–2221. doi: 10.1016/j.clinph.2016.02.009

Guo, Q., Hu, Y., Zeng, B., Tang, Y., Li, G., Zhang, T., et al. (2020). Parietal memory network and default mode network in first-episode drug-naive schizophrenia: associations with auditory hallucination. *Hum. Brain Mapp.* 41, 1973–1984. doi: 10.1002/hbm.24923

Heckers, S. (2001). Neuroimaging studies of the hippocampus in schizophrenia. *Hippocampus* 11, 520–528. doi: 10.1002/hipo.1068

Heils, A., Teufel, A., Petri, S., Stober, G., Riederer, P., Bengel, D., et al. (1996). Allelic variation of human serotonin transporter gene expression. *J. Neurochem.* 66, 2621–2624. doi: 10.1046/j.1471-4159.1996.66062621.x

Heinks-Maldonado, T. H., Mathalon, D. H., Houde, J. F., Gray, M., Faustman, W. O., and Ford, J. M. (2007). Relationship of imprecise corollary discharge in schizophrenia to auditory hallucinations. *Arch. Gen. Psychiatry* 64, 286–296. doi: 10.1001/archpsyc.64.3.286

Hirano, Y., Hirano, S., Maekawa, T., Obayashi, C., Oribe, N., Monji, A., et al. (2010). Auditory gating deficit to human voices in schizophrenia: a MEG study. *Schizophr. Res.* 117, 61–67. doi: 10.1016/j.schres.2009.09.003

Hirano, Y., Oribe, N., Kanba, S., Onitsuka, T., Nestor, P. G., and Spencer, K. M. (2015). Spontaneous gamma activity in schizophrenia. *JAMA Psychiatry* 72, 813–821. doi: 10.1001/jamapsychiatry.2014.2642

Hjelmervik, H., Craven, A. R., Sinceviciute, I., Johnsen, E., Kompus, K., Bless, J. J., et al. (2019). Intra-Regional Glu-GABA vs inter-regional glu-glu imbalance: a 1H-MRS study of the neurochemistry of auditory verbal hallucinations in schizophrenia. *Schizophr. Bull.* 46, 633–642. doi: 10.1093/schbul/sbz099

Hoffman, R. E., Fernandez, T., Pittman, B., and Hampson, M. (2011). Elevated functional connectivity along a corticostriatal loop and the mechanism of auditory/verbal hallucinations in patients with schizophrenia. *Biol. Psychiatry* 69, 407–414. doi: 10.1016/j.biopsych.2010.09.050

Huang, J., Liu, F., Wang, B., Tang, H., Teng, Z., Li, L., et al. (2019). Central and peripheral changes in FOS expression in schizophrenia based on genome-wide gene expression. *Front. Genet.* 10:232. doi: 10.3389/fgene.2019.00232

Hubl, D., Dougoud-Chauvin, V., Zeller, M., Federspiel, A., Boesch, C., Strik, W., et al. (2010). Structural analysis of Heschl's gyrus in schizophrenia patients with auditory hallucinations. *Neuropsychobiology* 61, 1–9. doi: 10.1159/000258637

Hubl, D., Koenig, T., Strik, W., Federspiel, A., Kreis, R., Boesch, C., et al. (2004). Pathways that make voices: white matter changes in auditory hallucinations. *Arch. Gen. Psychiatry* 61, 658–668. doi: 10.1001/archpsyc.61.7.658

Hugdahl, K., and Sommer, I. E. (2018). Auditory verbal hallucinations in schizophrenia from a levels of explanation perspective. *Schizophr. Bull.* 44, 234–241. doi: 10.1093/schbul/sbx142

Hugdahl, K., Craven, A. R., Nygard, M., Loberg, E. M., Berle, J. O., Johnsen, E., et al. (2015). Glutamate as a mediating transmitter for auditory hallucinations in schizophrenia: a (1)H MRS study. *Schizophr. Res.* 161, 252–260. doi: 10.1016/j.schres.2014.11.015

Jack, B. N., Le Pelley, M. E., Han, N., Harris, A. W. F., Spencer, K. M., and Whitford, T. J. (2019). Inner speech is accompanied by a temporally-precise and content-specific corollary discharge. *Neuroimage* 198, 170–180. doi: 10.1016/j.neuroimage.2019.04.038

Jardri, R., Pouchet, A., Pins, D., and Thomas, P. (2011). Cortical activations during auditory verbal hallucinations in schizophrenia: a coordinate-based meta-analysis. *Am. J. Psychiatry* 168, 73–81. doi: 10.1176/appi.ajp.2010.09101522

Javitt, D. C., and Freedman, R. (2015). Sensory processing dysfunction in the personal experience and neuronal machinery of schizophrenia. *Am. J. Psychiatry* 172, 17–31. doi: 10.1176/appi.ajp.2014.13121691

Kim, J. W., Kang, W. S., Lee, S. M., Kim, S. K., Park, H. J., Gwak, G. H., et al. (2012). Association between a synonymous SNP (rs470558, Ala216Ala) of MMP1 and schizophrenia with auditory hallucinations in Korean population. *Mol. Cell. Toxicol.* 8, 297–302. doi: 10.1007/s13273-012-0036-2

Kim, J. W., Lee, Y. S., Cho, E. Y., Jang, Y. L., Park, D. Y., Choi, K. S., et al. (2006). Linkage and association of schizophrenia with genetic variations in the locus of neuregulin 1 in Korean population. *Am. J. Med. Genet. B Neuropsychiatr. Genet.* 141b, 281–286. doi: 10.1002/ajmg.b.30209

Knochel, C., Oertel-Knochel, V., Schonmeyer, R., Rotarska-Jagiela, A., van de Ven, V., Prvulovic, D., et al. (2012). Interhemispheric hypoconnectivity in schizophrenia: fiber integrity and volume differences of the corpus callosum in patients and unaffected relatives. *Neuroimage* 59, 926–934. doi: 10.1016/j.neuroimage.2011.07.088

Koenig, T., van Swam, C., Dierks, T., and Hubl, D. (2012). Is gamma band EEG synchronization reduced during auditory driving in schizophrenia patients with auditory verbal hallucinations? *Schizophr. Res.* 141, 266–270. doi: 10.1016/j.schres.2012.07.016

Kompus, K., Westerhausen, R., and Hugdahl, K. (2011). The "paradoxical" engagement of the primary auditory cortex in patients with auditory verbal hallucinations: a meta-analysis of functional neuroimaging studies. *Neuropsychologia* 49, 3361–3369. doi: 10.1016/j.neuropsychologia.2011.08.010

Koutsoukos, E., Angelopoulos, E., Maillis, A., Papadimitriou, G. N., and Stefanis, C. (2013). Indication of increased phase coupling between theta and gamma EEG rhythms associated with the experience of auditory verbal hallucinations. *Neurosci. Lett.* 534, 242–245. doi: 10.1016/j.neulet.2012.12.005

Koyanagi, A., Stickley, A., and Haro, J. M. (2015). Subclinical psychosis and suicidal behavior in England: findings from the 2007 Adult Psychiatric Morbidity Survey. *Schizophr. Res.* 168, 62–67. doi: 10.1016/j.schres.2015.07.041

Kubera, K. M., Sambataro, F., Vasic, N., Wolf, N. D., Frasch, K., Hirjak, D., et al. (2014). Source-based morphometry of gray matter volume in patients with schizophrenia who have persistent auditory verbal hallucinations. *Prog. Neuropsychopharmacol. Biol. Psychiatry* 50, 102–109. doi: 10.1016/j.pnpbp.2013.11.015

Kuga, H., Onitsuka, T., Hirano, Y., Nakamura, I., Oribe, N., Mizuhara, H., et al. (2016). Increased BOLD signals elicited by high gamma auditory stimulation of the left auditory cortex in acute state schizophrenia. *EBioMedicine* 12, 143–149. doi: 10.1016/j.ebiom.2016.09.008

Kühn, S., and Gallinat, J. (2012). Quantitative meta-analysis on state and trait aspects of auditory verbal hallucinations in schizophrenia. *Schizophr. Bull.* 38, 779–786. doi: 10.1093/schbul/sbq152

Kurian, S. M., Le-Niculescu, H., Patel, S. D., Bertram, D., Davis, J., Dike, C., et al. (2011). Identification of blood biomarkers for psychosis using convergent functional genomics. *Mol. Psychiatry* 16, 37–58. doi: 10.1038/mp.2009.117

Laroi, F., Sommer, I. E., Blom, J. D., Fernyhough, C., Ffytche, D. H., Hugdahl, K., et al. (2012). The characteristic features of auditory verbal hallucinations in clinical and nonclinical groups: state-of-the-art overview and future directions. *Schizophr. Bull.* 38, 724–733.

Lavigne, K. M., and Woodward, T. S. (2018). Hallucination- and speech-specific hypercoupling in frontotemporal auditory and language networks in schizophrenia using combined task-based fMRI data: an fBIRN study. *Hum. Brain Mapp.* 39, 1582–1595. doi: 10.1002/hbm.23934

Lavigne, K. M., Rapin, L. A., Metzak, P. D., Whitman, J. C., Jung, K., Dohen, M., et al. (2015). Left-dominant temporal-frontal hypercoupling in schizophrenia patients with hallucinations during speech perception. *Schizophr. Bull.* 41, 259–267. doi: 10.1093/schbul/sbu004

Lee, K., Yoshida, T., Kubicki, M., Bouix, S., Westin, C. F., Kindlmann, G., et al. (2009). Increased diffusivity in superior temporal gyrus in patients with schizophrenia: a Diffusion Tensor Imaging study. *Schizophr. Res.* 108, 33–40. doi: 10.1016/j.schres.2008.11.024

Lee, S. H., Choo, J. S., Im, W. Y., and Chae, J. H. (2008). Nonlinear analysis of electroencephalogram in schizophrenia patients with persistent auditory hallucination. *Psychiatry Investig.* 5, 115–120. doi: 10.4306/pi.2008.5.2.115

Lee, S. H., Wynn, J. K., Green, M. F., Kim, H., Lee, K. J., Nam, M., et al. (2006). Quantitative EEG and low resolution electromagnetic tomography (LORETA) imaging of patients with persistent auditory hallucinations. *Schizophr. Res.* 83, 111–119. doi: 10.1016/j.schres.2005.11.025

Lefebvre, S., Demeulemeester, M., Leroy, A., Delmaire, C., Lopes, R., Pins, D., et al. (2016). Network dynamics during the different stages of hallucinations in schizophrenia. *Hum. Brain Mapp.* 37, 2571–2586. doi: 10.1002/hbm.23197

Leroux, E., Delcroix, N., and Dollfus, S. (2017). Abnormalities of language pathways in schizophrenia patients with and without a lifetime history of auditory verbal hallucinations: a DTI-based tractography study. *World J. Biol. Psychiatry* 18, 528–538. doi: 10.1080/15622975.2016.1274053

Levitan, C., Ward, P. B., and Catts, S. V. (1999). Superior temporal gyral volumes and laterality correlates of auditory hallucinations in schizophrenia. *Biol. Psychiatry* 46, 955–962. doi: 10.1016/s0006-3223(98)00373-4

Li, B., Cui, L. B., Xi, Y. B., Friston, K. J., Guo, F., Wang, H. N., et al. (2017). Abnormal effective connectivity in the brain is involved in auditory verbal hallucinations in schizophrenia. *Neurosci. Bull.* 33, 281–291. doi: 10.1007/s12264-017-0101-x

Liegeois, F., Baldeweg, T., Connelly, A., Gadian, D. G., Mishkin, M., and Vargha-Khadem, F. (2003). Language fMRI abnormalities associated with FOXP2 gene mutation. *Nat. Neurosci.* 6, 1230–1237. doi: 10.1038/nn1138

Lim, A., Hoek, H. W., Deen, M. L., and Blom, J. D. (2016). Prevalence and classification of hallucinations in multiple sensory modalities in schizophrenia spectrum disorders. *Schizophr. Res.* 176, 493–499.

Liu, L., Cui, L. B., Xi, Y. B., Wang, X. R., Liu, Y. C., Xu, Z. L., et al. (2019). Association between connectivity of hippocampal sub-regions and auditory verbal hallucinations in schizophrenia. *Front. Neurosci.* 13:424. doi: 10.3389/fnins.2019.00424

Maijer, K., Begemann, M. J. H., Palmen, S., Leucht, S., and Sommer, I. E. C. (2018). Auditory hallucinations across the lifespan: a systematic review and meta-analysis. *Psychol. Med.* 48, 879–888. doi: 10.1017/s0033291717002367

Malhotra, A. K., Goldman, D., Mazzanti, C., Clifton, A., Breier, A., and Pickar, D. (1998). A functional serotonin transporter (5-HTT) polymorphism is associated with psychosis in neuroleptic-free schizophrenics. *Mol. Psychiatry* 3, 328–332. doi: 10.1038/sj.mp.4000412

Marques, T. R., Ashok, A. H., Angelescu, I., Borgan, F., Myers, J., Lingford-Hughes, A., et al. (2020). GABA-A receptor differences in schizophrenia: a

positron emission tomography study using [(11)C]Ro154513. *Mol. Psychiatry* 26, 2616–2625. doi: 10.1038/s41380-020-0711-y

Martinez-Granados, B., Brotons, O., Martinez-Bisbal, M. C., Celda, B., Marti-Bonmati, L., Aguilar, E. J., et al. (2008). Spectroscopic metabolomic abnormalities in the thalamus related to auditory hallucinations in patients with schizophrenia. *Schizophr. Res.* 104, 13–22. doi: 10.1016/j.schres.2008.05.025

McCarthy-Jones, S., Green, M. J., Scott, R. J., Tooney, P. A., Cairns, M. J., Wu, J. Q., et al. (2014a). Preliminary evidence of an interaction between the FOXP2 gene and childhood emotional abuse predicting likelihood of auditory verbal hallucinations in schizophrenia. *J. Psychiatr Res.* 50, 66–72. doi: 10.1016/j.jpsychires.2013.11.012

McCarthy-Jones, S., Oestreich, L. K., and Whitford, T. J. (2015). Reduced integrity of the left arcuate fasciculus is specifically associated with auditory verbal hallucinations in schizophrenia. *Schizophr. Res.* 162, 1–6. doi: 10.1016/j.schres.2014.12.041

McCarthy-Jones, S., Trauer, T., Mackinnon, A., Sims, E., Thomas, N., and Copolov, D. (2014b). A new phenomenological survey of auditory hallucinations: evidence for subtypes and implications for theory and practice. *Schizophr. Bull.* 40, 231–235. doi: 10.1093/schbul/sbs156

McGuire, P. K., Shah, G. M., and Murray, R. M. (1993). Increased blood flow in Broca's area during auditory hallucinations in schizophrenia. *Lancet* 342, 703–706. doi: 10.1016/0140-6736(93)91707-s

McGuire, P. K., Silbersweig, D. A., Wright, I., Murray, R. M., David, A. S., Frackowiak, R. S., et al. (1995). Abnormal monitoring of inner speech: a physiological basis for auditory hallucinations. *Lancet* 346, 596–600. doi: 10.1016/s0140-6736(95)91435-8

Melbourne, J. K., Rosen, C., Feiner, B., and Sharma, R. P. (2018). C4A mRNA expression in PBMCs predicts the presence and severity of delusions in schizophrenia and bipolar disorder with psychosis. *Schizophr. Res.* 197, 321–327. doi: 10.1016/j.schres.2018.01.018

Modinos, G., Costafreda, S. G., van Tol, M. J., McGuire, P. K., Aleman, A., and Allen, P. (2013). Neuroanatomy of auditory verbal hallucinations in schizophrenia: a quantitative meta-analysis of voxel-based morphometry studies. *Cortex* 49, 1046–1055. doi: 10.1016/j.cortex.2012.01.009

Modinos, G., Vercammen, A., Mechelli, A., Knegtering, H., McGuire, P. K., and Aleman, A. (2009). Structural covariance in the hallucinating brain: a voxel-based morphometry study. *J. Psychiatry Neurosci.* 34, 465–469.

Morch-Johnsen, L., Nesvag, R., Jorgensen, K. N., Lange, E. H., Hartberg, C. B., Haukvik, U. K., et al. (2017). Auditory cortex characteristics in schizophrenia: associations with auditory hallucinations. *Schizophr. Bull.* 43, 75–83. doi: 10.1093/schbul/sbw130

Mou, X., Bai, F., Xie, C., Shi, J., Yao, Z., Hao, G., et al. (2013). Voice recognition and altered connectivity in schizophrenic patients with auditory hallucinations. *Prog. Neuropsychopharmacol. Biol. Psychiatry* 44, 265–270. doi: 10.1016/j.pnpbp.2013.03.006

Mulert, C., Kirsch, V., Pascual-Marqui, R., McCarley, R. W., and Spencer, K. M. (2011). Long-range synchrony of gamma oscillations and auditory hallucination symptoms in schizophrenia. *Int. J. Psychophysiol.* 79, 55–63. doi: 10.1016/j.ijpsycho.2010.08.004

Mulert, C., Kirsch, V., Whitford, T. J., Alvarado, J., Pelavin, P., McCarley, R. W., et al. (2012). Hearing voices: a role of interhemispheric auditory connectivity? *World J. Biol. Psychiatry* 13, 153–158. doi: 10.3109/15622975.2011.570789

Naatanen, R., Paavilainen, P., Rinne, T., and Alho, K. (2007). The mismatch negativity (MMN) in basic research of central auditory processing: a review. *Clin. Neurophysiol.* 118, 2544–2590. doi: 10.1016/j.clinph.2007.04.026

Nazimek, J. M., Hunter, M. D., and Woodruff, P. W. (2012). Auditory hallucinations: expectation-perception model. *Med. Hypotheses* 78, 802–810. doi: 10.1016/j.mehy.2012.03.014

Nenadic, I., Dietzek, M., Langbein, K., Rzanny, R., Gussew, A., Reichenbach, J. R., et al. (2014). Superior temporal metabolic changes related to auditory hallucinations: a (31)P-MR spectroscopy study in antipsychotic-free schizophrenia patients. *Brain Struct. Funct.* 219, 1869–1872. doi: 10.1007/s00429-013-0604-9

Nenadic, I., Smesny, S., Schlosser, R. G., Sauer, H., and Gaser, C. (2010). Auditory hallucinations and brain structure in schizophrenia: voxel-based morphometric study. *Br. J. Psychiatry* 196, 412–413. doi: 10.1192/bjp.bp.109.070441

Northoff, G., and Qin, P. (2011). How can the brain's resting state activity generate hallucinations? A 'resting state hypothesis' of auditory verbal hallucinations. *Schizophr. Res.* 127, 202–214. doi: 10.1016/j.schres.2010.11.009

O'Daly, O. G., Frangou, S., Chitnis, X., and Shergill, S. S. (2007). Brain structural changes in schizophrenia patients with persistent hallucinations. *Psychiatry Res.* 156, 15–21. doi: 10.1016/j.pscychresns.2007.03.001

O'Donnell, B. F., Vohs, J. L., Krishnan, G. P., Rass, O., Hetrick, W. P., and Morzorati, S. L. (2013). The auditory steady-state response (ASSR): a translational biomarker for schizophrenia. *Suppl. Clin. Neurophysiol.* 62, 101–112. doi: 10.1016/b978-0-7020-5307-8.00006-5

Oestreich, L. K., McCarthy-Jones, S., and Whitford, T. J. (2016). Decreased integrity of the fronto-temporal fibers of the left inferior occipito-frontal fasciculus associated with auditory verbal hallucinations in schizophrenia. *Brain Imaging Behav.* 10, 445–454. doi: 10.1007/s11682-015-9421-5

Ohayon, S., Yitzhaky, A., and Hertzberg, L. (2020). Gene expression meta-analysis reveals the up-regulation of CREB1 and CREBBP in Brodmann Area 10 of patients with schizophrenia. *Psychiatry Res.* 292:113311. doi: 10.1016/j.psychres.2020.113311

Palaniyappan, L., Balain, V., Radua, J., and Liddle, P. F. (2012). Structural correlates of auditory hallucinations in schizophrenia: a meta-analysis. *Schizophr. Res.* 137, 169–173. doi: 10.1016/j.schres.2012.01.038

Pergola, G., Di Carlo, P., Jaffe, A. E., Papalino, M., Chen, Q., Hyde, T. M., et al. (2019). Prefrontal coexpression of schizophrenia risk genes is associated with treatment response in patients. *Biol. Psychiatry* 86, 45–55. doi: 10.1016/j.biopsych.2019.03.981

Perrin, M. A., Kantrowitz, J. T., Silipo, G., Dias, E., Jabado, O., and Javitt, D. C. (2018). Mismatch negativity (MMN) to spatial deviants and behavioral spatial discrimination ability in the etiology of auditory verbal hallucinations and thought disorder in schizophrenia. *Schizophr. Res.* 191, 140–147. doi: 10.1016/j.schres.2017.05.012

Petralia, M. C., Ciurleo, R., Saraceno, A., Pennisi, M., Basile, M. S., Fagone, P., et al. (2020). Meta-Analysis of transcriptomic data of dorsolateral prefrontal cortex and of peripheral blood mononuclear cells identifies altered pathways in schizophrenia. *Genes (Basel)* 11:390. doi: 10.3390/genes11040390

Pinheiro, A. P., Farinha-Fernandes, A., Roberto, M. S., and Kotz, S. A. (2019). Self-voice perception and its relationship with hallucination predisposition. *Cogn. Neuropsychiatry* 24, 237–255. doi: 10.1080/13546805.2019.1621159

Potter, D., Summerfelt, A., Gold, J., and Buchanan, R. W. (2006). Review of clinical correlates of P50 sensory gating abnormalities in patients with schizophrenia. *Schizophr. Bull.* 32, 692–700. doi: 10.1093/schbul/sbj050

Powers, A. R., Mathys, C., and Corlett, P. R. (2017). Pavlovian conditioning-induced hallucinations result from overweighting of perceptual priors. *Science* 357, 596–600. doi: 10.1126/science.aan3458

Psomiades, M., Fonteneau, C., Mondino, M., Luck, D., Haesebaert, F., Suaud-Chagny, M. F., et al. (2016). Integrity of the arcuate fasciculus in patients with schizophrenia with auditory verbal hallucinations: a DTI-tractography study. *Neuroimage Clin.* 12, 970–975. doi: 10.1016/j.nicl.2016.04.013

Rajasekaran, A., Shivakumar, V., Kalmady, S. V., Narayanaswamy, J. C., Subbana, M., Venugopal, D., et al. (2016). The impact of HLA-G 3' UTR variants and sHLA-G on risk and clinical correlates of schizophrenia. *Hum. Immunol.* 77, 1166–1171. doi: 10.1016/j.humimm.2016.08.013

Rivero, O., Sanjuan, J., Aguilar, E. J., Gonzalez, J. C., Molto, M. D., de Frutos, R., et al. (2010). Serotonin transporter gene polymorphisms and auditory hallucinations in psychosis. *Rev. Neurol.* 50, 325–332. doi: 10.33588/rn.5006.2009387

Rolland, B., Amad, A., Poulet, E., Bordet, R., Vignaud, A., Bation, R., et al. (2015). Resting-state functional connectivity of the nucleus accumbens in auditory and visual hallucinations in schizophrenia. *Schizophr. Bull.* 41, 291–299. doi: 10.1093/schbul/sbu097

Rotarska-Jagiela, A., Oertel-Knoechel, V., DeMartino, F., van de Ven, V., Formisano, E., Roebroeck, A., et al. (2009). Anatomical brain connectivity and positive symptoms of schizophrenia: a diffusion tensor imaging study. *Psychiatry Res.* 174, 9–16. doi: 10.1016/j.pscychresns.2009.03.002

Rudolph, E. D., Ells, E. M., Campbell, D. J., Abriel, S. C., Tibbo, P. G., Salisbury, D. F., et al. (2015). Finding the missing-stimulus mismatch negativity (MMN) in early psychosis: altered MMN to violations of an auditory gestalt. *Schizophr. Res.* 166, 158–163. doi: 10.1016/j.schres.2015.05.028

Salisbury, D. F. (2012). Finding the missing stimulus mismatch negativity (MMN): emitted MMN to violations of an auditory gestalt. *Psychophysiology* 49, 544–548. doi: 10.1111/j.1469-8986.2011.01336.x

Sanjuán, J., Castro-Martínez, X. H., García-Martí, G., González-Fernández, J., Sanz-Requena, R., Haro, J. M., et al. (2021). FOXP2 expression and gray matter density in the male brains of patients with schizophrenia. *Brain Imaging Behav.* 15, 1403–1411. doi: 10.1007/s11682-020-00339-x

Sanjuan, J., Rivero, O., Aguilar, E. J., Gonzalez, J. C., Molto, M. D., de Frutos, R., et al. (2006a). Serotonin transporter gene polymorphism (5-HTTLPR) and emotional response to auditory hallucinations in schizophrenia. *Int. J. Neuropsychopharmacol.* 9, 131–133. doi: 10.1017/s1461145705005559

Sanjuan, J., Toirac, I., Gonzalez, J. C., Leal, C., Molto, M. D., Najera, C., et al. (2004). A possible association between the CCK-AR gene and persistent auditory hallucinations in schizophrenia. *Eur. Psychiatry* 19, 349–353.

Sanjuan, J., Tolosa, A., Gonzalez, J. C., Aguilar, E. J., Perez-Tur, J., Najera, C., et al. (2006b). Association between FOXP2 polymorphisms and schizophrenia with auditory hallucinations. *Psychiatr. Genet.* 16, 67–72. doi: 10.1097/01.ypg.0000185029.35558.bb

Scheinost, D., Tokoglu, F., Hampson, M., Hoffman, R., and Constable, R. T. (2019). Data-Driven analysis of functional connectivity reveals a potential auditory verbal hallucination network. *Schizophr. Bull.* 45, 415–424. doi: 10.1093/schbul/sby039

Seok, J. H., Park, H. J., Chun, J. W., Lee, S. K., Cho, H. S., Kwon, J. S., et al. (2007). White matter abnormalities associated with auditory hallucinations in schizophrenia: a combined study of voxel-based analyses of diffusion tensor imaging and structural magnetic resonance imaging. *Psychiatry Res.* 156, 93–104. doi: 10.1016/j.pscychresns.2007.02.002

Shapleske, J., Rossell, S. L., Chitnis, X. A., Suckling, J., Simmons, A., Bullmore, E. T., et al. (2002). A computational morphometric MRI study of schizophrenia: effects of hallucinations. *Cereb. Cortex* 12, 1331–1341. doi: 10.1093/cercor/12.12.1331

Shergill, S. S., Brammer, M. J., Williams, S. C., Murray, R. M., and McGuire, P. K. (2000). Mapping auditory hallucinations in schizophrenia using functional magnetic resonance imaging. *Arch. Gen. Psychiatry* 57, 1033–1038. doi: 10.1001/archpsyc.57.11.1033

Shergill, S. S., Kanaan, R. A., Chitnis, X. A., O'Daly, O., Jones, D. K., Frangou, S., et al. (2007). A diffusion tensor imaging study of fasciculi in schizophrenia. *Am. J. Psychiatry* 164, 467–473. doi: 10.1176/ajp.2007.164.3.467

Shin, S. E., Lee, J. S., Kang, M. H., Kim, C. E., Bae, J. N., and Jung, G. (2005). Segmented volumes of cerebrum and cerebellum in first episode schizophrenia with auditory hallucinations. *Psychiatry Res.* 138, 33–42. doi: 10.1016/j.pscychresns.2004.11.005

Shinn, A. K., Baker, J. T., Cohen, B. M., and Ongur, D. (2013). Functional connectivity of left Heschl's gyrus in vulnerability to auditory hallucinations in schizophrenia. *Schizophr. Res.* 143, 260–268. doi: 10.1016/j.schres.2012.11.037

Smith, D. M., Grant, B., Fisher, D. J., Borracci, G., Labelle, A., and Knott, V. J. (2013). Auditory verbal hallucinations in schizophrenia correlate with P50 gating. *Clin. Neurophysiol.* 124, 1329–1335. doi: 10.1016/j.clinph.2013.02.004

Spalletta, G., Piras, F., Gravina, P., Bello, M. L., Bernardini, S., and Caltagirone, C. (2012). Glutathione S-transferase alpha 1 risk polymorphism and increased bilateral thalamus mean diffusivity in schizophrenia. *Psychiatry Res.* 203, 180–183. doi: 10.1016/j.pscychresns.2011.12.016

Spencer, K. M., Niznikiewicz, M. A., Nestor, P. G., Shenton, M. E., and McCarley, R. W. (2009). Left auditory cortex gamma synchronization and auditory hallucination symptoms in schizophrenia. *BMC Neurosci.* 10:85. doi: 10.1186/1471-2202-10-85

Sritharan, A., Line, P., Sergejew, A., Silberstein, R., Egan, G., and Copolov, D. (2005). EEG coherence measures during auditory hallucinations in schizophrenia. *Psychiatry Res.* 136, 189–200. doi: 10.1016/j.psychres.2005.05.010

Stephan, K. E., Friston, K. J., and Frith, C. D. (2009). Dysconnection in schizophrenia: from abnormal synaptic plasticity to failures of self-monitoring. *Schizophr. Bull.* 35, 509–527. doi: 10.1093/schbul/sbn176

Tachikawa, H., Harada, S., Kawanishi, Y., Okubo, T., and Suzuki, T. (2001). Linked polymorphisms (-333G>T and -286A>G) in the promoter region of the CCK-A receptor gene may be associated with schizophrenia. *Psychiatry Res.* 103, 147–155.

Talbot, K., Eidem, W. L., Tinsley, C. L., Benson, M. A., Thompson, E. W., Smith, R. J., et al. (2004). Dysbindin-1 is reduced in intrinsic, glutamatergic terminals of the hippocampal formation in schizophrenia. *J. Clin. Invest.* 113, 1353–1363. doi: 10.1172/jci20425

Tang, J., LeGros, R. P., Louneva, N., Yeh, L., Cohen, J. W., Hahn, C.-G., et al. (2009). Dysbindin-1 in dorsolateral prefrontal cortex of schizophrenia cases is reduced in an isoform-specific manner unrelated to dysbindin-1 mRNA expression. *Hum. Mol. Genet.* 18, 3851–3863. doi: 10.1093/hmg/ddp329

Tang, T. T.-T., Yang, F., Chen, B.-S., Lu, Y., Ji, Y., Roche, K. W., et al. (2009). Dysbindin regulates hippocampal LTP by controlling NMDA receptor surface expression. *Proc. Natl. Acad. Sci. U.S.A.* 106, 21395–21400. doi: 10.1073/pnas.0910499106

Tao, R., Li, C., Jaffe, A. E., Shin, J. H., Deep-Soboslay, A., Yamin, R., et al. (2020). Cannabinoid receptor CNR1 expression and DNA methylation in human prefrontal cortex, hippocampus and caudate in brain development and schizophrenia. *Transl. Psychiatry* 10:158. doi: 10.1038/s41398-020-0832-8

Theberge, J., Al-Semaan, Y., Williamson, P. C., Menon, R. S., Neufeld, R. W., Rajakumar, N., et al. (2003). Glutamate and glutamine in the anterior cingulate and thalamus of medicated patients with chronic schizophrenia and healthy comparison subjects measured with 4.0-T proton MRS. *Am. J. Psychiatry* 160, 2231–2233. doi: 10.1176/appi.ajp.160.12.2231

Thoma, R. J., Chaze, C., Lewine, J. D., Calhoun, V. D., Clark, V. P., Bustillo, J., et al. (2016). Functional MRI evaluation of multiple neural networks underlying auditory verbal hallucinations in schizophrenia spectrum disorders. *Front. Psychiatry* 7:39. doi: 10.3389/fpsyt.2016.00039

Thoma, R. J., Meier, A., Houck, J., Clark, V. P., Lewine, J. D., Turner, J., et al. (2017). Diminished auditory sensory gating during active auditory verbal hallucinations. *Schizophr. Res.* 188, 125–131. doi: 10.1016/j.schres.2017.01.023

Toirac, I., Sanjuan, J., Aguilar, E. J., Gonzalez, J. C., Artigas, F., Rivero, O., et al. (2007). Association between CCK-AR gene and schizophrenia with auditory hallucinations. *Psychiatr. Genet.* 17, 47–53.

Tolosa, A., Sanjuan, J., Dagnall, A. M., Molto, M. D., Herrero, N., and de Frutos, R. (2010). FOXP2 gene and language impairment in schizophrenia: association and epigenetic studies. *BMC Med. Genet.* 11:114. doi: 10.1186/1471-2350-11-114

Tracy, D. K., and Shergill, S. S. (2013). Mechanisms underlying auditory hallucinations-understanding perception without stimulus. *Brain Sci.* 3, 642–669. doi: 10.3390/brainsci3020642

Uhlhaas, P. J., Haenschel, C., Nikoliæ, D., and Singer, W. (2008). The role of oscillations and synchrony in cortical networks and their putative relevance for the pathophysiology of schizophrenia. *Schizophr. Bull.* 34, 927–943. doi: 10.1093/schbul/sbn062

Uhrig, S., Hirth, N., Broccoli, L., von Wilmsdorff, M., Bauer, M., Sommer, C., et al. (2016). Reduced oxytocin receptor gene expression and binding sites in different brain regions in schizophrenia: a post-mortem study. *Schizophr. Res.* 177, 59–66. doi: 10.1016/j.schres.2016.04.019

van Lutterveld, R., Diederen, K. M., Koops, S., Begemann, M. J., and Sommer, I. E. (2013). The influence of stimulus detection on activation patterns during auditory hallucinations. *Schizophr. Res.* 145, 27–32. doi: 10.1016/j.schres.2013.01.004

van Swam, C., Federspiel, A., Hubl, D., Wiest, R., Boesch, C., Vermathen, P., et al. (2012). Possible dysregulation of cortical plasticity in auditory verbal hallucinations-A cortical thickness study in schizophrenia. *J. Psychiatr Res.* 46, 1015–1023. doi: 10.1016/j.jpsychires.2012.03.016

Vawter, M. P., Hamzeh, A. R., Muradyan, E., Civelli, O., Abbott, G. W., and Alachkar, A. (2019). Association of myoinositol transporters with schizophrenia and bipolar disorder: evidence from human and animal studies. *Mol. Neuropsychiatry* 5, 200–211. doi: 10.1159/000501125

Vercammen, A., Knegtering, H., Bruggeman, R., and Aleman, A. (2011). Subjective loudness and reality of auditory verbal hallucinations and activation of the inner speech processing network. *Schizophr. Bull.* 37, 1009–1016. doi: 10.1093/schbul/sbq007

Vercammen, A., Knegtering, H., den Boer, J. A., Liemburg, E. J., and Aleman, A. (2010). Auditory hallucinations in schizophrenia are associated with reduced functional connectivity of the temporo-parietal area. *Biol. Psychiatry* 67, 912–918. doi: 10.1016/j.biopsych.2009.11.017

Waters, F., Collerton, D., Ffytche, D. H., Jardri, R., Pins, D., Dudley, R., et al. (2014). Visual hallucinations in the psychosis spectrum and comparative information

from neurodegenerative disorders and eye disease. *Schizophr. Bull.* 40(Suppl. 4), S233–S245. doi: 10.1093/schbul/sbu036

Wei, J., and Hemmings, G. P. (1999). The CCK-A receptor gene possibly associated with auditory hallucinations in schizophrenia. *Eur. Psychiatry* 14, 67–70.

Weickert, C. S., Straub, R. E., McClintock, B. W., Matsumoto, M., Hashimoto, R., Hyde, T. M., et al. (2004). Human dysbindin (DTNBP1) gene expression in normal brain and in schizophrenic prefrontal cortex and midbrain. *Arch. Gen. Psychiatry* 61, 544–555. doi: 10.1001/archpsyc.61.6.544

Wigand, M., Kubicki, M., Clemm von Hohenberg, C., Leicht, G., Karch, S., Eckbo, R., et al. (2015). Auditory verbal hallucinations and the interhemispheric auditory pathway in chronic schizophrenia. *World J. Biol. Psychiatry* 16, 31–44. doi: 10.3109/15622975.2014.948063

Wolf, N. D., Gron, G., Sambataro, F., Vasic, N., Frasch, K., Schmid, M., et al. (2012). Magnetic resonance perfusion imaging of auditory verbal hallucinations in patients with schizophrenia. *Schizophr. Res.* 134, 285–287. doi: 10.1016/j.schres.2011.11.018

Wolf, N. D., Sambataro, F., Vasic, N., Frasch, K., Schmid, M., Schonfeldt-Lecuona, C., et al. (2011). Dysconnectivity of multiple resting-state networks in patients with schizophrenia who have persistent auditory verbal hallucinations. *J. Psychiatry Neurosci.* 36, 366–374. doi: 10.1503/jpn.110008

Wolpert, D. M., and Miall, R. C. (1996). Forward models for physiological motor control. *Neural Netw.* 9, 1265–1279. doi: 10.1016/s0893-6080(96)00035-4

Xi, Y. B., Guo, F., Li, H., Chang, X., Sun, J. B., Zhu, Y. Q., et al. (2016). The structural connectivity pathology of first-episode schizophrenia based on the cardinal symptom of auditory verbal hallucinations. *Psychiatry Res. Neuroimaging* 257, 25–30. doi: 10.1016/j.pscychresns.2016.09.011

Xie, S., Liu, B., Wang, J., Zhou, Y., Cui, Y., Song, M., et al. (2019). Hyperconnectivity in perisylvian language pathways in schizophrenia with auditory verbal hallucinations: a multi-site diffusion MRI study. *Schizophr. Res.* 210, 262–269. doi: 10.1016/j.schres.2018.12.024

Xu, J., Wang, J., Fan, L., Li, H., Zhang, W., Hu, Q., et al. (2015). Tractography-based parcellation of the human middle temporal gyrus. *Sci. Rep.* 5:18883. doi: 10.1038/srep18883

Youn, T., Park, H. J., Kim, J. J., Kim, M. S., and Kwon, J. S. (2003). Altered hemispheric asymmetry and positive symptoms in schizophrenia: equivalent current dipole of auditory mismatch negativity. *Schizophr. Res.* 59, 253–260. doi: 10.1016/s0920-9964(02)00154-8

Yu, H., Ying, W., Li, G., Lin, X., Jiang, D., Chen, G., et al. (2020). Exploring concomitant neuroimaging and genetic alterations in patients with and patients without auditory verbal hallucinations: a pilot study and mini review. *J. Int. Med. Res.* 48:300060519884856. doi: 10.1177/0300060519884856

Zhang, L., Li, B., Wang, H., Li, L., Liao, Q., Liu, Y., et al. (2017). Decreased middle temporal gyrus connectivity in the language network in schizophrenia patients with auditory verbal hallucinations. *Neurosci. Lett.* 653, 177–182. doi: 10.1016/j.neulet.2017.05.042

Zhao, Z., Li, X., Feng, G., Shen, Z., Li, S., Xu, Y., et al. (2018). Altered effective connectivity in the default network of the brains of first-episode, drug-naive schizophrenia patients with auditory verbal hallucinations. *Front. Hum. Neurosci.* 12:456. doi: 10.3389/fnhum.2018.00456

Zhu, J., Liu, C., Xiaodong Lin, M., Wang, L., Tian, H., and Chen, Q. (2019). Association of a novel long non-coding RNA-mRNAs network with default mode network hyper-connectivity in hallucinative schizophrenia. *Ann. Clin. Case Rep.* 2019:1657.

Zhuo, C., Li, G., Ji, F., Chen, C., Jiang, D., Lin, X., et al. (2020). Differences in functional connectivity density among subtypes of schizophrenic auditory hallucination. *Brain Imaging Behav.* 14, 2587–2593. doi: 10.1007/s11682-019-00210-8

Zhuo, C., Zhu, J., Qin, W., Qu, H., Ma, X., and Yu, C. (2017). Cerebral blood flow alterations specific to auditory verbal hallucinations in schizophrenia. *Br. J. Psychiatry* 210, 209–215. doi: 10.1192/bjp.bp.115.174961

Zmigrod, L., Garrison, J. R., Carr, J., and Simons, J. S. (2016). The neural mechanisms of hallucinations: a quantitative meta-analysis of neuroimaging studies. *Neurosci. Biobehav. Rev.* 69, 113–123. doi: 10.1016/j.neubiorev.2016.05.037

Conflict of Interest: The authors declare that the research was conducted in the absence of any commercial or financial relationships that could be construed as a potential conflict of interest.

Publisher's Note: All claims expressed in this article are solely those of the authors and do not necessarily represent those of their affiliated organizations, or those of the publisher, the editors and the reviewers. Any product that may be evaluated in this article, or claim that may be made by its manufacturer, is not guaranteed or endorsed by the publisher.

frontiers in Neuroscience

ORIGINAL RESEARCH
published: 09 December 2021
doi: 10.3389/fnins.2021.797849

Dissect Relationships Between Gene Co-expression and Functional Connectivity in Human Brain

*Xue Zhang[1†], Yingying Xie[1†], Jie Tang[1†], Wen Qin[1], Feng Liu[1], Hao Ding[1], Yuan Ji[1], Bingbing Yang[1], Peng Zhang[2], Wei Li[2], Zhaoxiang Ye[2] and Chunshui Yu[1,3]**

[1] Tianjin Key Laboratory of Functional Imaging, Department of Radiology, Tianjin Medical University General Hospital, Tianjin, China, [2] Key Laboratory of Cancer Prevention and Therapy, Department of Radiology, National Clinical Research Center for Cancer, Tianjin's Clinical Research Center for Cancer, Tianjin Medical University Cancer Institute and Hospital, Tianjin, China, [3] CAS Center for Excellence in Brain Science and Intelligence Technology, Chinese Academy of Sciences, Shanghai, China

Although recent evidence indicates an association between gene co-expression and functional connectivity in human brain, specific association patterns remain largely unknown. Here, using neuroimaging-based functional connectivity data of living brains and brain-wide gene expression data of postmortem brains, we performed comprehensive analyses to dissect relationships between gene co-expression and functional connectivity. We identified 125 connectivity-related genes (20 novel genes) enriched for dendrite extension, signaling pathway and schizophrenia, and 179 gene-related functional connections mainly connecting intra-network regions, especially homologous cortical regions. In addition, 51 genes were associated with connectivity in all brain functional networks and enriched for action potential and schizophrenia; in contrast, 51 genes showed network-specific modulatory effects and enriched for ion transportation. These results indicate that functional connectivity is unequally affected by gene expression, and connectivity-related genes with different biological functions are involved in connectivity modulation of different networks.

Keywords: functional connectivity, gene co-expression, coupling, network, tensor decomposition algorithm, schizophrenia

OPEN ACCESS

Edited by:
Jiajia Zhu,
First Affiliated Hospital of Anhui Medical University, China

Reviewed by:
Cun Zhang,
First Affiliated Hospital of Anhui Medical University, China
Ning Mao,
Peking University People's Hospital, China

****Correspondence:***
Chunshui Yu
chunshuiyu@tmu.edu.cn;
chunshuiyu@tjmu.edu.cn

† These authors have contributed equally to this work

Specialty section:
This article was submitted to Brain Imaging Methods, a section of the journal Frontiers in Neuroscience

Received: *19 October 2021*
Accepted: *17 November 2021*
Published: *09 December 2021*

Citation:
Zhang X, Xie Y, Tang J, Qin W, Liu F, Ding H, Ji Y, Yang B, Zhang P, Li W, Ye Z and Yu C (2021) Dissect Relationships Between Gene Co-expression and Functional Connectivity in Human Brain. Front. Neurosci. 15:797849. doi: 10.3389/fnins.2021.797849

INTRODUCTION

Functional connectivity calculated from functional magnetic resonance imaging (fMRI) has been widely used to characterize intrinsic low-frequency synchronization of brain activity at rest between anatomically distinct brain regions (Ogawa et al., 1992). Regions and connections are organized into brain functional networks responsible for such distinct functions as vision, audition, motion, attention, memory, and emotion. Different combinations of connectivity impairments are indicative of different neuropsychiatric disorders, which are useful for diagnosing diseases, monitoring clinical courses, and predicting outcomes (Seeley et al., 2009; Vertes and Bullmore, 2015). Despite functional connectivity is found to be heritable (Jansen et al., 2015), the molecular mechanisms supporting functional connectivity remain largely unknown.

Genome-wide association study (GWAS) is a putative method to identify genetic substrates of neuroimaging phenotypes, such as functional connectivity. Using a discovery dataset of 8428 subjects, a GWAS study has identified several genetic loci that are associated with a few functional

connectivity phenotypes (Elliott et al., 2018). However, rather large sample size is needed to identify reliable genetic loci in GWAS studies, and most GWAS-identified loci are located in non-coding regions of the genome. Instead, a bulk of studies have used brain-wide gene expression data from the Allen Human Brain Atlas (AHBA) to identify genes associated with functional connectivity by interrogating spatial correlations between gene co-expression and functional connectivity across brain regions.

A pioneer study reveals that brain regions within a functional network showing strong correlations of brain activity at rest also demonstrate highly correlated gene expression (CGE) and that genes with significant association with functional connectivity are enriched for ion channel and synaptic function (Richiardi et al., 2015). Thereafter, several specific associations between gene expression and functional connectivity have been reported. The long-range cortico-cortical functional connectivity is found to be associated with the co-expression of genes uniquely enriched for the supra-granular layers of the cerebral cortex in humans (Krienen et al., 2016). In human brain functional networks, high inter-modular degree and long connection distance are associated with genes enriched for oxidative metabolism and mitochondria, whereas high intra-modular degree and short connection distance are associated with genes enriched for RNA translation and nuclear components (Vertes et al., 2016). The parallel limbic and somato/motor cortico-striatal functional networks are associated with different sets of genes (Anderson et al., 2018), which is also true for the functional connectivity of different visual subregions (Zhang et al., 2021).

Although these studies have advanced our knowledge on the association between functional connectivity and gene expression in the human brain, there are at least three questions need to be further answered. Prior studies have identified genes associated with the averaged functional connectivity phenotypes derived from a group of subjects. It is still unknown that which expression-connectivity associations are consistently present in most individuals. Heritability analysis indicates that genetic and environmental factors influence functional connectivity architecture with different weights (Ge et al., 2017; Teeuw et al., 2019). It is an open question that which kinds of functional connectivity are prone to be affected by genetic factors (e.g., gene expression). Inter-regional gene expression similarity within brain functional networks is much higher than those between networks (Richiardi et al., 2015), suggesting that the distributed brain functional networks may possess dissociable genetic signatures (Richiardi et al., 2015; Anderson et al., 2018; Zhu et al., 2021). However, we barely know which genes contribute generally to functional connectivity architecture of all functional networks, and which genes contribute specifically to a certain functional network. Answering these questions will largely improve our understanding on the molecular mechanisms of functional connectivity.

In this study, we calculated correlations between gene co-expression and functional connectivity across 4005 pairs of brain regions for each of the 800 healthy subjects and identified 1291 genes with significant correlations in most of the 800 subjects (>80%). Then we used multiple comprehensive methods to identify genes associated functional connectivity and functional connectivity more likely affected by gene expression. By assigning 4005 connections into eight functional networks, a series of methods were used to differentiate genes contributing generally to all functional networks and genes contributing specifically to a certain network. The pipeline of this study is shown in **Figure 1**.

MATERIALS AND METHODS

Calculating Functional Connectivity and Networks

Subjects

According to the inclusion criteria of Chinese Han, aged 18–30 years and right handedness and the exclusion criteria of a history of alcohol or drug abuse, a history of neuropsychiatric disorders, and MRI contraindications, we recruited 800 healthy young adults (330 males, 470 females; mean age = 23.8 ± 2.4 years, range: 18–30 years) from the Tianjin Medical University General Hospital (n = 400) and Cancer Hospital (n = 400). This study was approved by the ethics committee of Tianjin Medical University and all volunteers signed written informed consent before the experiment.

MRI Data Acquisition

MRI data from the two hospitals were acquired using the same type of 3.0-Tesla MR scanners (Discovery MR750, General Electric, Milwaukee, WI, United States) with the same scan parameters. The high-resolution structural T1-weighted images were acquired using a brain volume sequence with the following parameters: repetition time (TR) = 8.14 ms; echo time (TE) = 3.17 ms; inversion time (TI) = 450 ms; field of view (FOV) = 256 mm × 256 mm; matrix = 256 × 256; flip angle (FA) = 12°; slice thickness = 1 mm; and 188 sagittal slices. The resting-state fMRI data were obtained using single shot gradient-echo echo-planar imaging (SS-GRE-EPI): TR = 2000 ms; TE = 30 ms; FOV = 220 mm × 220 mm; matrix = 64 × 64; FA = 90°; slice thickness = 3 mm; gap = 1 mm; 40 axial slices; and 180 volumes. During fMRI scans, all subjects were instructed to keep still with their eyes closed, to think of nothing in particular, to stay as motionless as possible, and to not fall asleep.

Functional Magnetic Resonance Imaging Data Preprocessing

The resting-state fMRI data were preprocessed using the Statistical Parametric Mapping (SPM12[1]). The first five volumes from each subject were discarded to allow signal to reach equilibrium and ensure the subject to adapt to scanning noise. The acquisition time delay between slices was corrected using sinc-interpolation to make the acquisition time of all voxels consistent within a TR. Head motion of each subject was assessed and corrected using rigid-body transformation. All 800 subjects had acceptable head motion (translational or rotational parameters less than 2 mm or 2°). A unified normalization-segmentation method was used to normalize fMRI images to

[1]http://www.fil.ion.ucl.ac.uk/spm

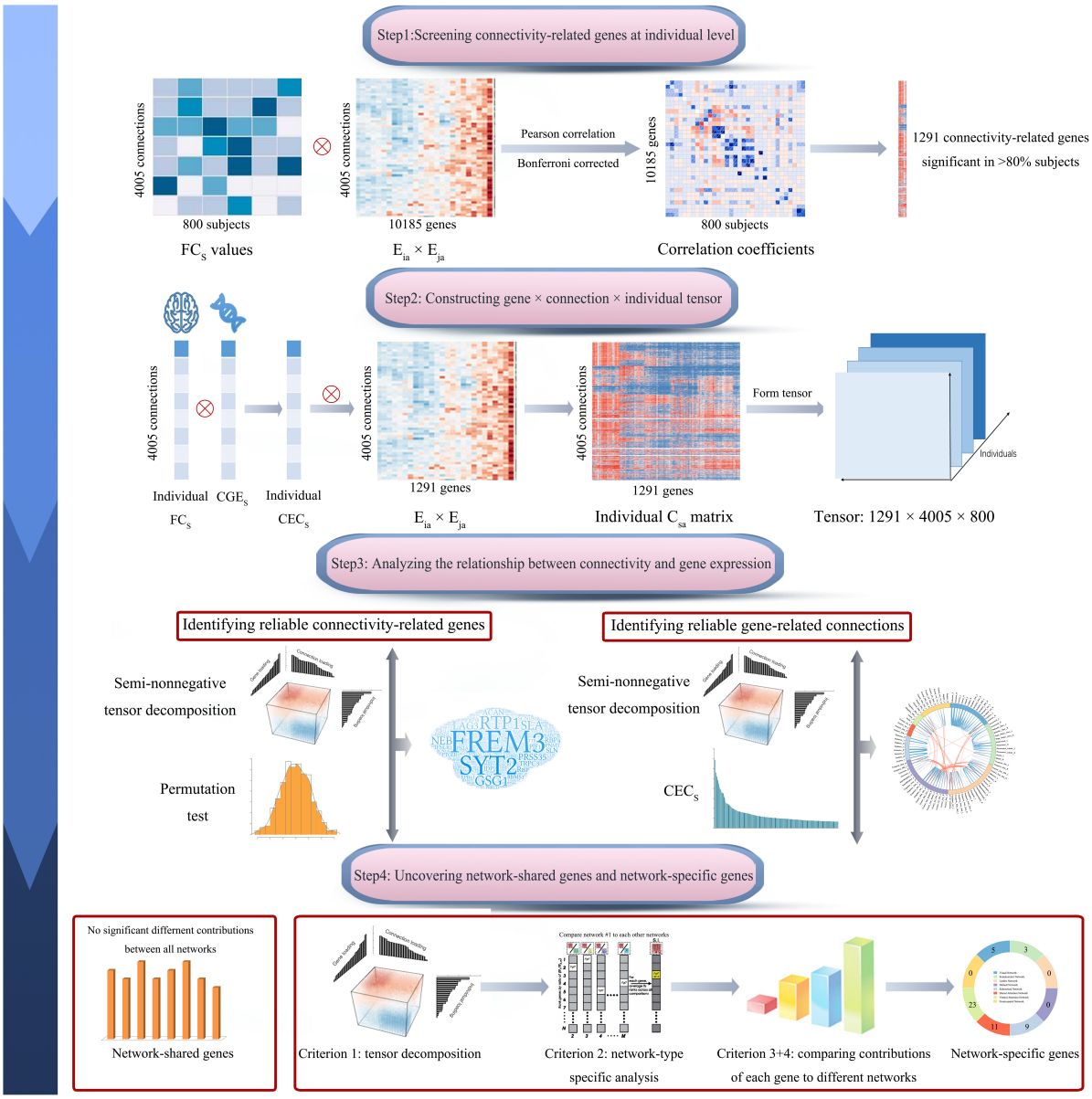

FIGURE 1 | Pipeline of data analysis. In brief, this study includes four steps: screening connectivity-related genes at individual level; constructing gene × connection × individual tensor; identifying connectivity-related genes and gene-related connections; and uncovering network-shared and network-specific connectivity-related genes. The s represents a connection between region i and region j. CEC_S, connectivity-expression coupling at connection s; CGE_S, correlated gene expression at connection s; C_{sa}, the contribution of gene a to CEC_S; $E_{ia} \times E_{ja}$, the contribution of gene a to the CGE between region i and region j; and FC_S, normalized functional connectivity strength of connection s.

the Montreal Neurological Institute (MNI) space. fMRI images were coregistered to structural images, and then structural images were segmented and coregistered to the MNI space. The transformation parameters were used to normalize fMRI images to the MNI space. The normalized fMRI images were resampled into 3-mm cubic voxels and smoothed with a Gaussian kernel of 8-mm full-width at half-maximum (FWHM). The frame-wise displacement (FD) was also calculated and time points with FD >0.3 mm were deleted and imputed using cubic spline interpolation. The linear drift, 24 head motion parameters and averaging blood oxygenation level dependent (BOLD) signals of white matter and cerebral spinal fluid were regressed out from the fMRI data. Finally, the fMRI images were filtered with a frequency range of 0.01–0.08 Hz.

Constructing Functional Connectivity Matrix and Functional Networks

For each subject, we constructed a functional connectivity matrix (90 × 90) based on the 90 non-cerebellar regions derived from the automatic anatomical labeling (AAL)

(Tzourio-Mazoyer et al., 2002) using DPABI (Yan et al., 2016), and then the obtained functional connectivity matrix was used to form a column vector including 4005 independent connections. The final functional connectivity matrix (4005 × 800) was constructed by combining the column vectors of all subjects (n = 800). Based on a canonical cortical functional network mask (Yeo et al., 2011), cortical brain regions and their connections were assigned to seven resting-state networks, including the visual network (VN), somatomotor network (SMN), dorsal attention network (DAN), ventral attention network (VAN), fronto-parietal control network (FPN), default-mode network (DMN), and limbic network (LN). And the rest subcortical regions were defined as the subcortical network.

Gene Expression Data Processing

The normalized microarray gene expression data of two donated brains with the whole brain coverage were obtained from the Allen Institute for Brain Science (AIBS). Gene expression data were processed following a newly proposed pipeline for linking brain-wide gene expression and neuroimaging data (Arnatkevic Iute et al., 2019). Briefly, the latest information from NCBI was used to re-assign probes to genes, and then the noise from gene expression signals was removed. Based on the principle of one probe for one gene, RNA-seq information was used as the reference to select a probe for each gene with more than one probe. Consequently, 10,185 genes were finally selected for 1209 samples according to the pipeline (detailed procedures see **Supplementary Material**). According to the distance between the coordinate of each sample and the boundary of brain regions in the MNI space, each sample was assigned to a specific region.

Dissecting Associations Between Gene Expression and Functional Connectivity

Screening Connectivity-Related Genes at Individual Level

In each subject, we calculated the CGE score for each pair of brain regions across genes using the following equation:

$$CGE_{ij} = \left(\sum_{a=1}^{N} \left(E_{ia} \times E_{ja}\right)\right)/N \quad (1)$$

here, N was the total number of genes (N = 10,185); i and j represented a pair of brain regions; and E_{ia} and E_{ja} were the normalized expression values (z-scores) of gene a in region i and region j. $E_{ia} \times E_{ja}$ denoted the contribution of gene a to the global gene co-expression between these two regions. CGE_{ij} was the Pearson correlation coefficient of gene expression between these two regions across all genes, which indicates the similarity of global gene expression between any pair of regions.

In each subject, we could obtain the normalized functional connectivity strength (FC_{ij}) and ($E_{ia} \times E_{ja}$) for each pair of brain regions. For a given gene (n = 10,185) of this subject, we calculated Pearson correlation between FC_{ij} and ($E_{ia} \times E_{ja}$) across the 4005 pairs of regions. If the correlation was significant (Bonferroni corrected, $P < 4.9 \times 10^{-6} = 0.05/10{,}185$), this gene was considered to be associated with functional connectivity. These steps were independently conducted in 800 subjects, and only genes with significant correlations with functional connectivity in more than 80% subjects were regarded as connectivity-related genes. The resulting 1291 connectivity-related genes (**Supplementary Table 1**) were used for the further analyses.

Identifying Genes Highly Associated With Functional Connectivity

Two additional methods were used to further identify genes with high and reliable associations with functional connectivity from genes obtained by the individual-level analysis. Before these analyses, we defined the connectivity-expression coupling (CEC_s) of a connection s (i.e., a pair of brain regions i and j) as the product ($FC_s \times CGE_s$) of the normalized FC_s and CGE_s of this connection in each subject. The global CEC of this subject was defined as the Pearson correlation coefficient between the normalized FC_s and CGE_s across the 4005 connections (Eq. 2). S was the total number of connections (S = 4005 in this study).

$$\mathrm{CEC} = \left(\sum_{s=1}^{S} \left(FC_s \times CGE_s\right)\right)/S \quad (2)$$

We also calculated the contribution of each gene to the CEC at each connection in each subject using the following Eq. 3:

$$C_{sa} = \left(FC_s \times CGE_s\right) \times \left(E_{ia} \times E_{ja}\right) \quad (3)$$

here, s represented a pair of brain regions (i and j); FC was the normalized functional connectivity strength; CGE was the normalized correlated gene expression; C_{sa} indicated the contribution of a given gene a to CEC_s. Based on this equation, a C_{sa} matrix (1291 genes × 4005 connections) was generated for each subject. In the following parts, the population-averaged C_{sa} for each gene and each connection was computed by averaging C_{sa} values of this gene at this connection in the 800 subjects; and the population- and connection-averaged C_{sa} for each gene was computed by averaging C_{sa} values of this gene for all included connections (n = 4005 for whole brain connectivity analysis and n = the number of connections within a given network for network-level analysis) and subjects (n = 800).

A Tensor Decomposition Model

The "*MultiCluster*" method[2] is proposed to explore three-way interactions of genes, tissues, and individuals using semi-nonnegative tensor decomposition (Wang et al., 2019). This approach handles heterogeneity in each dimension and learns the clustering patterns across different dimensions of the data in an unsupervised manner. In this study, we replaced tissue by functional connectivity (n = 4005) and replaced gene expression by the C_{sa} of each gene (n = 1291). Using the "*MultiCluster*" method, we can identify genes closely associated with functional connectivity and connections more influenced by these genes.

The 400 subjects from each of the two hospitals were randomly divided into two groups, and finally creating four independent groups. The semi-nonnegative tensor decomposition model

[2]https://github.com/Miaoyanwang/MultiCluster

was used to investigate complex interactions of 1291 genes, 4005 functional connections and 200 individuals of each group (**Supplementary Figure 1**). This method decomposed tensor into 10 components that represent major data variations in the group. Only the first component was selected for further analyses because this component had much greater output score than other components (**Supplementary Table 2** and **Supplementary Figure 2**). Detail methods for component selection and consistency assessment between groups are described in **Supplementary Methods**. The component included three vectors of individual, gene and connection. From each vector, we can extract a weight score for each item to represent the relative contribution of the item to the component. We defined genes with high associations with functional connectivity as those with absolute weight scores > (mean + SD) of the absolute weight scores of the 1291 genes.

A Permutation Test

The labels of genes and connections were randomly shuffled 1000 times to generate a random distribution of the population- and connection-averaged C_{sa} values of each gene. The significance of each gene was inferred by observing if the true C_{sa} value of this gene was greater than all permutation-derived C_{sa} values of this gene ($P < 0.001$). To further reduce false positive of the identified connectivity-related genes, only genes identified by both tensor decomposition and permutation test were finally considered as genes with high and reliable associations with functional connectivity.

Identifying Functional Connectivity Highly Associated With Gene Expression

The functional connections with absolute population-averaged CEC_s values greater than the (mean + SD) of all the 4005 connections were defined as connections associated with gene expression. The identified gene-related functional connections were further validated using the tensor decomposition model. From the first component of the tensor decomposition model, we can extract a weight score for each connection from the connection vector to represent the relative contribution of this connection to the component. We defined connections with high associations with gene expression as those with absolute weight scores greater than the (mean + SD) of the 4005 connections.

Dissecting Connectivity-Related Genes at the Network Level

The whole brain was divided into eight functional networks, and then functional connections within each functional network were extracted to identify connectivity-related genes common to all functional networks or specific to a certain network.

Identifying Genes Shared by Brain Functional Networks

For each gene, one-way analysis of variance (ANOVA) was used to compare the population-averaged C_{sa} values among the eight groups of intra-network connections from different functional networks. Genes without significant difference ($P \geq 0.05$) across the eight groups were defined as connectivity-related genes common to all functional networks.

Identifying Network-Specific Genes

We used conserved criteria to identify network-specific genes. A gene was considered to be specific to a given functional network if the gene satisfied the following four criteria.

Identifying Network-Specific Genes by Tensor Decomposition Model. A prerequisite for a network-specific gene is that this gene should be highly correlated with functional connections of the network. The non-negative tensor decomposition algorithm was applied to functional connections of each functional network to identify genes with higher contribution to connections of the functional network. For each network, the connectivity-related genes were defined as those with absolute weight scores > (mean + SD) of all the 1291 genes. The resulting 764 genes were used to further network-specific analyses.

Network-Type Specific Analysis. As commonly used in cell-type specific analysis (Dougherty et al., 2010; Xu et al., 2014), the specificity index (SI) was adapted to assess the specificity of a gene to a particular functional network relative to all other networks. Here, cells were replaced by brain functional networks, and gene expression values were replaced by the population-averaged C_{sa} values of each gene for connections within a functional network. For each gene, a *P*-value for SI was calculated *via* the permutation testing (1000 permutations). This method was applied to each gene identified by the network-based tensor decomposition model, and significant genes ($n = 144$) ($P < 0.001$) were used for further network-specific analyses.

Comparing Contributions of Genes to Different Networks. For each of the identified candidate genes ($n = 144$), ANOVA was performed to compared the difference in the population-averaged C_{sa} values among the eight groups of intra-network connections from different functional networks. Genes ($n = 144$) with significant difference (Bonferroni corrected, $P < 3.47 \times 10^{-4} = 0.05/144$) among the eight groups were selected for further *post hoc* analysis. According to the population- and connection-averaged C_{sa} value of each gene of each network, we can identify the first two functional networks with the greatest contribution from this gene. Two strategies were then used to assess the specificity of this gene to the first functional network. First, the gene was considered to be specific to the first network if its population- and connection-averaged C_{sa} of the first network was at least twice greater than that of the second network. To further assess the significance, a two sample *t*-test was conducted to compare the population-averaged C_{sa} differences ($P < 0.05$) between the two networks. Only genes satisfied the two criteria (twice greater and significant) were considered as genes specific to the first functional network.

Gene Enrichment Analysis

With regards to functions of our main gene clusters, Toppogene (Chen et al., 2009) was used in gene enrichment analysis,[3] which calculates the functional similarity to training gene list to prioritize candidate genes. Moreover, associations between connectivity-related genes and common brain disorders

[3]https://toppgene.cchmc.org/

were identified by MAGMA (de Leeuw et al., 2015), which provides gene-set analysis based on GWAS data. Among the common neuropsychiatric disorders, autistic spectrum disorder (ASD), attention-deficit/hyperactivity disorder (ADHD), bipolar disorder (BP), major depression disorder (MDD), and schizophrenia (SCZ) were included in our analyses. The GWAS summary statistic results of the five neuropsychiatric disorders were collected from previous studies (Schizophrenia Working Group of the Psychiatric Genomics Consortium, 2014; Autism Spectrum Disorders Working Group of The Psychiatric Genomics Consortium, 2017; Wray et al., 2018; Demontis et al., 2019; Stahl et al., 2019; **Supplementary Table 3**). For all enrichment analyses, multiple comparisons were corrected d by the Benjamini and Hochberg method of false discovery rate (FDR-BH correction, $P < 0.05$).

RESULTS

Genes Associated With Connectivity in Most Individuals

In each subject, connectivity-related genes were identified by detecting significant correlations between FC_{ij} and ($E_{ia} \times E_{ja}$) of each gene across the 4005 pairs of brain regions (Bonferroni corrected $P < 4.9 \times 10^{-6} = 0.05/10{,}185$). Correlation maps between FC_{ij} and ($E_{ia} \times E_{ja}$) of two representative genes (*VAV3* and *MAGEL2*) in two individuals are shown in **Figures 2A,B**. By calculating the ratio of a gene present in the significant gene list in the 800 subjects, 1291 connectivity-related genes were identified in at least 80% of these subjects (**Supplementary Table 1**).

Two sample *t*-test demonstrated that the mean contributions of the 1291 genes were greater ($t = 6.57$, $P = 5.3 \times 10^{-11}$) than those of the rest 8894 genes (**Figure 2C**) and the 1291 genes had much stronger population-averaged correlations ($t = 81.08$, $P < 10^{-300}$) than the rest 8894 genes (**Figure 2D** and **Supplementary Figure 3**).

Moreover, in the 800 subjects, two sample *t*-test demonstrated that the global CEC values calculated based on the 1291 genes were greater ($t = 11.00$, $P < 10^{-300}$) than those derived from the 10,185 genes (**Figure 2E**) and the population- and connection-averaged C_{sa} values of the 1291 genes were also much stronger ($t = 20.13$; $P < 10^{-300}$) than those of the 10,185 genes (**Figure 2F**).

Genes Highly and Reliably Associated With Functional Connectivity

Selecting Connectivity-Related Genes With Tensor Decomposition Model

From the 10 components derived from the tensor decomposition of each group ($n = 200$), the first component with the largest weight was selected for further analyses (**Supplementary Table 2** and **Supplementary Figure 2**), and this component showed low mismatch rate (0.077) and high component correspondence (mean correlation = 0.998) among the four groups. For each group, we defined connectivity-related genes as those with absolute weight scores > (mean + SD) of the scores of the 1291 genes. With the criterion of the 100% repeated rate among the four groups, we selected 185 candidate connectivity-related genes. In the 1291 genes, two sample *t*-test demonstrated that the population- and connection-averaged C_{sa} values of the 185 genes were much greater ($t = 34.07$; $P < 10^{-300}$) than those of the rest 1106 genes (**Figures 3A,B**).

Selecting Connectivity-Related Genes With Permutation Test

A permutation test showed that the population- and connection-averaged C_{sa} values of 143 genes were significantly greater than all permutation-derived C_{sa} values of this gene ($P < 0.001$) (**Supplementary Table 4**). Two sample *t*-test demonstrated that the population- and connection-averaged C_{sa} values of the 143 genes were much greater ($t = 34.86$; $P < 10^{-300}$) than those of the rest 1148 genes (**Figures 3C,D**).

Genes With High and Reliable Association With Functional Connectivity

The 125 genes identified by both tensor decomposition ($n = 185$) and permutation test ($n = 143$) were considered as genes with high and reliable association with functional connectivity (**Supplementary Table 4** and **Figure 3E**). Among the 125 connectivity-related genes, 105 genes have been previously reported as connectivity-related genes (Richiardi et al., 2015; Krienen et al., 2016; Anderson et al., 2018) and 20 genes were novel (**Supplementary Table 4**). The 125 genes were mainly enriched for the regulation of dendrite extension, response to external stimulus, and G protein-coupled receptor signaling pathway, protein secretion and transport, calcium ion binding (FDR-BH corrected, $P < 0.05$) (**Supplementary Table 5** and **Figure 3F**). Moreover, these genes showed significant association with schizophrenia (FDR-BH corrected, $P = 0.017$).

Functional Connections Highly Associated With Gene Expression

Firstly, the absolute value of the population-averaged CEC_s score was used to identify functional connections associated with gene expression with a threshold of greater than the (mean + SD) of all the 4005 connections. This method generated 255 gene-related functional connections (**Supplementary Table 6** and **Supplementary Figure 4**). Then we used the tensor decomposition model to independently identify gene-related connections. From the first component of the model, gene-related connections were defined as those with absolute weight scores greater than the (mean + SD) of the 4005 connections, resulting in 180 gene-related connections. Among those connections, the 179 gene-related connections identified by tensor decomposition model were completely included in the 255 gene-related connections identified based on the mean CEC_s score. Therefore, the 179 connections were considered as functional connections highly associated with gene expression (**Figure 4A** and **Supplementary Table 6**).

In the 179 connections, 140 connections (78.2%) were intra-network connections and 39 (21.8%) were inter-network connections (**Figure 4B**). In the total of 45 homologous connections between the two hemispheres, 41 homologous connections (91.1%) were identified as gene-related connections

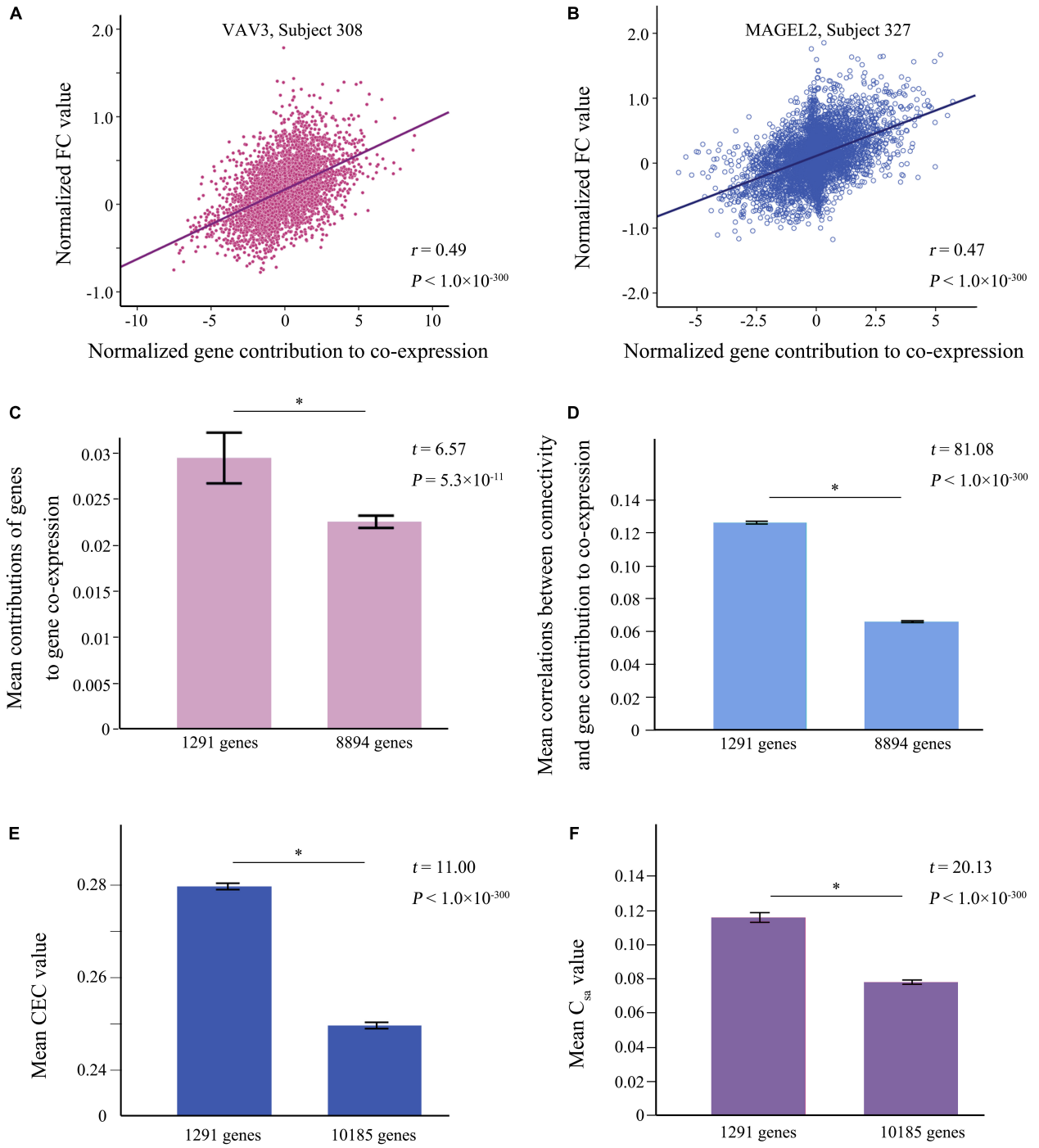

FIGURE 2 | The analysis of the connectivity-related genes. **(A,B)** Are representative correlation maps between functional connectivity and gene contribution to co-expression of *VAV3* in the 308th subject and *MAGEL2* in the 327th subject. **(C)** Shows the mean contributions of 1291 genes to gene co-expression greater (t = 6.57, P = 5.3 × 10^{-11}) than those of the rest 8894 genes. **(D)** Demonstrates the population-averaged correlations between connectivity and the contribution of 1291 genes to gene co-expression stronger (t = 81.08 and $P < 10^{-300}$) than those of the rest 8894 genes. **(E)** Shows the global CEC values calculated based on the 1291 genes greater (t = 11.00, $P < 10^{-300}$) than those derived from the 10,185 genes. **(F)** Demonstrates the population- and connection-averaged C_{sa} values of the 1291 genes stronger (t = 20.13; $P < 10^{-300}$) than those of the 10,185 genes. Mean + SEM for all graphs. The significant difference between two groups was showed as *. CEC, connectivity-expression coupling; C_{sa}, the contribution of each gene (a) to the CEC at each connection (s); FC, functional connectivity.

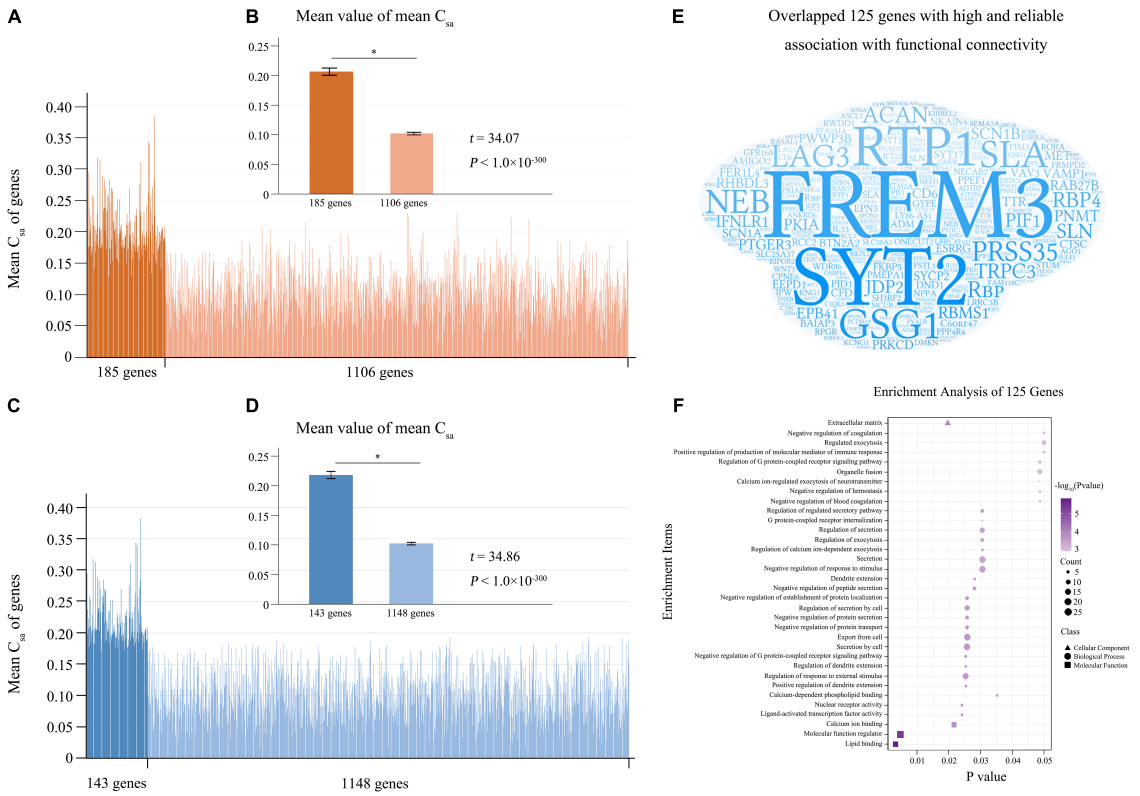

FIGURE 3 | Reliable connectivity-related genes. **(A)** Is the population- and connection-averaged C_{sa} values of the 1291 genes, and the 185 connectivity-related genes identified by tensor decomposition model are marked in dark orange. **(B)** Shows that the 185 genes demonstrate stronger population- and connection-averaged C_{sa} values ($t = 34.07$; $P < 10^{-300}$) than the rest 1106 genes. **(C)** Shows the population- and connection-averaged C_{sa} values of the 1291 genes, and the 143 connectivity-related genes identified by the permutation test are marked in dark blue. **(D)** Shows the population- and connection-averaged C_{sa} values of the 143 genes greater ($t = 34.86$; $P < 10^{-300}$) than those of the rest 1148 genes. **(E)** Is word-cloud representation of the 125 reliable connectivity-related genes identified by both methods. **(F)** Shows enrichments of the 125 reliable connectivity-related genes. Mean + SEM for all graphs. The significant difference between two groups was showed as *. C_{sa}, the contribution of each gene (a) to the connectivity-expression coupling at each connection (s).

(**Figure 4C**). The 140 intra-network connections were assigned to the eight functional networks, and the number and the percentage of gene-related connections in each network are listed in **Table 1**.

Connectivity-Related Genes Shared by Brain Functional Networks

In the 1291 genes, 51 genes without significant difference ($P \geq 0.05$) in the population-averaged C_{sa} values among the eight groups were considered as connectivity-related genes common to all functional networks (**Figure 5A**). These genes were enriched for the positive regulation of neuronal action potential (**Supplementary Table 5** and **Figure 5B**). Moreover, these network-shared connectivity-related genes were also enriched for schizophrenia (FDR-BH corrected, $P = 0.017$).

Network-Specific Genes

The tensor decomposition model was applied to each functional network to identify 764 genes with higher C_{sa} with the threshold of absolute weight scores > (mean + SD) of all the 1291 genes. The SI was then used to assess the specificity of each of the 764 genes to each network relative to other networks. We found that 144 genes were significantly enriched for a certain functional network ($P < 0.001$). All the 144 genes showed significant difference (Bonferroni corrected, $P < 3.47 \times 10^{-4} = 0.05/144$) among the eight groups by ANOVA. To further identify genes specific to each functional network, we assessed the contributions of each gene ($n = 144$) to its first two most associated functional networks with two criteria. Only 51 genes satisfied the two criteria (twice greater and significant) were considered as genes specific to the first functional network (**Table 2**, **Figure 5A**, and **Supplementary Figure 5**). These network-specific genes were mainly enriched for the regulation of ion transport and transmembrane transport, and ion homeostasis (**Supplementary Table 5** and **Figure 5B**).

DISCUSSION

In this study, we performed a comprehensive analysis on associations between functional connectivity and gene co-expression in the human brain. We identified 125 connectivity-related genes (20 novel genes), which are linked to dendrite

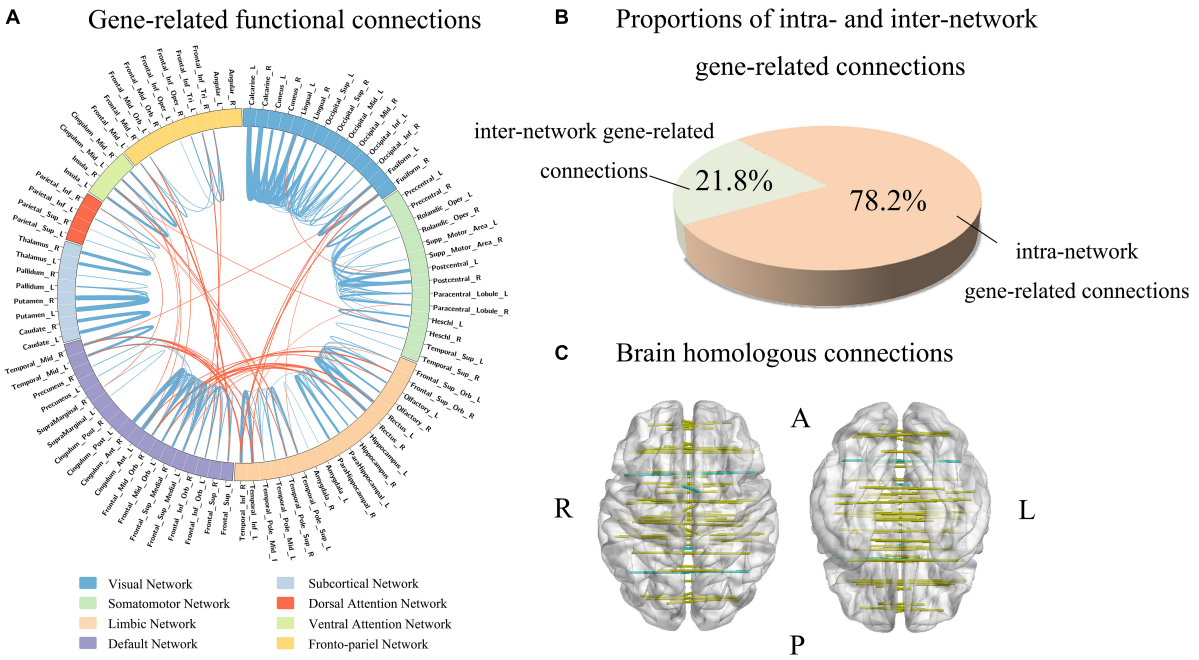

FIGURE 4 | Functional connections associated with gene expression. **(A)** Shows gene-related functional connections with a circle map. The eight functional networks are represented by different colors. The blue lines represent the intra-network functional connections, and the orange lines denote the inter-network functional connections. The thickness of a line indicates the mean strength of the connectivity-expression coupling at each connection. **(B)** Demonstrates the proportions of intra- and inter-network connections in all gene-related connections (n = 179). **(C)** Shows that 91% homologous connections are gene-related connections.

extension and signaling pathway. Moreover, we identified 179 gene-related connections that are influenced more by gene expression than other connections. Most of gene-related connections were intra-network connections, especially homologous connections. Finally, we identified 51 network-shared genes and 51 network-specific genes, which were involved in different molecular processes (action potential for the former and ion transportation for the latter). These findings may improve our understanding of the molecular mechanisms of functional connectivity in the human brain.

In previously conducted transcription-neuroimaging association studies (Fornito et al., 2011; Oh et al., 2015; Richiardi et al., 2015; Krienen et al., 2016; Vertes et al., 2016; Anderson et al., 2018; Zhang et al., 2021; Zhu et al., 2021), spatial correlations are performed between gene expression and group-averaged neuroimaging maps or inter-group difference maps, which neglect inter-individual variations in neuroimaging measures. In this study, individual variations of functional connections were considered with two strategies: (1) connectivity-expression correlations were conducted at an individual level and only genes with significant correlations in most individuals (>80%) were considered as connectivity-related genes; and (2) a tensor decomposition algorithm was used to simultaneously consider interactions among genes, connections and individuals. To further control false positive results, a permutation test was used to test the significance of each gene derived from both strategies in the connectivity-expression associations. The resulting 125 genes were defined as reliable connectivity-related genes and the correctness and reliability of this finding are supported by the fact that 105 out of 125 (84%) genes have been reported in previous connectivity-expression association studies (Richiardi et al., 2015; Krienen et al., 2016; Anderson et al., 2018). More importantly, 20 novel connectivity-related genes were identified in this study, which may provide

TABLE 1 | Intra-network functional connections associated with gene expression.

Functional networks	Numbers of intra-network connections	Numbers of gene-related connections	A (%)	B (%)
Visual network	91	44	31.4	48.4
Somatomotor network	91	23	16.4	25.3
Dorsal attention network	6	3	2.1	50.0
Ventral attention network	6	2	1.4	33.3
Limbic network	153	25	17.9	16.3
Frontoparietal network	45	8	5.7	17.8
Default mode network	153	29	20.7	19.0
Subcortical network	28	6	4.3	21.4
Sum	573	140	100	24.4

A (%) refers to the ratio of the number (44) of gene-related connections in a given network (such as the visual network) to the total number (140) of gene-related connections in all networks; B (%) refers to the ratio of the number (44) of gene-related connections in a given network (such as the visual network) to the total number (91) of connections in the network.

TABLE 2 | Numbers of network-specific connectivity-related genes identified by different combinations of criteria.

Functional networks	Criterion 1 only	Criteria 1 + 2	Criteria 1 + 2 + 3 + 4
Visual network	198	7	5
Somatomotor network	106	41	3
Dorsal attention network	150	37	11
Ventral attention network	119	28	23
Limbic network	157	2	0
Frontoparietal network	173	27	0
Default mode network	176	4	0
Subcortical network	133	13	9

Criterion 1: the gene should have higher C_{sa} in the tensor decomposition model of the functional network; Criterion 2: the gene should show significant enrichment for the functional network in network-type specific analysis; Criterion 3: the population-averaged C_{sa} values of the functional network were significantly greater than those of any other networks; and Criterion 4: the population- and connection-averaged C_{sa} value of the functional network was twice greater than those of any other networks.

new insight or evidence on the molecular mechanisms of functional connectivity.

In consistent with prior studies linking connectivity-related genes to signal transmission processes (Richiardi et al., 2015; Anderson et al., 2018), the identified 125 connectivity-related genes in this study were also enriched for various biological processes associated with signal transmission. Six connectivity-related genes are directly related to G protein-coupled receptor signaling pathway, and many other genes involve in signal transmission by regulating protein secretion and transport, and dendrite extension. Fourteen genes including two novel ones (*MCUB* and *DOC2B*) are associated with Ca^{2+} binding and Ca^{2+}-mediated biological processes. As an important second messenger, these Ca^{2+}-related biological processes are critical for signal transmission (Bando et al., 2016; Toth et al., 2016). Twenty-five genes including four novel ones (*RIPOR2*, *ADTRP*, *IFNLR1*, and *PMEPA1*) are related to the regulation of response to stimulus, including the immune response. These findings indicate that a series of complex biological processes are involved in the formation, development, and plasticity of functional connectivity.

The identified 125 reliable connectivity-related genes and the 51 network-shared connectivity-related genes were significantly enriched for schizophrenia (34/125 reliable genes and 17/51 network-shared genes) rather than other common psychiatric disorders (ASD, ADHD, BP, and MDD), which is well consistent with the notion that the functional disconnection is the most prominent neuroimaging feature in schizophrenia (van den Heuvel and Fornito, 2014; Dong et al., 2018). These findings indicate that connectivity-related genes identified in healthy subjects may be also related to functional disconnection in schizophrenia. The resulting 51 (34 + 17) connectivity- and schizophrenia-related genes are the potential candidates for investigating the molecular mechanisms underlying the functional disconnection in schizophrenia.

It is well known that functional connectivity is influenced by both genetic and environmental factors (Ge et al., 2017;

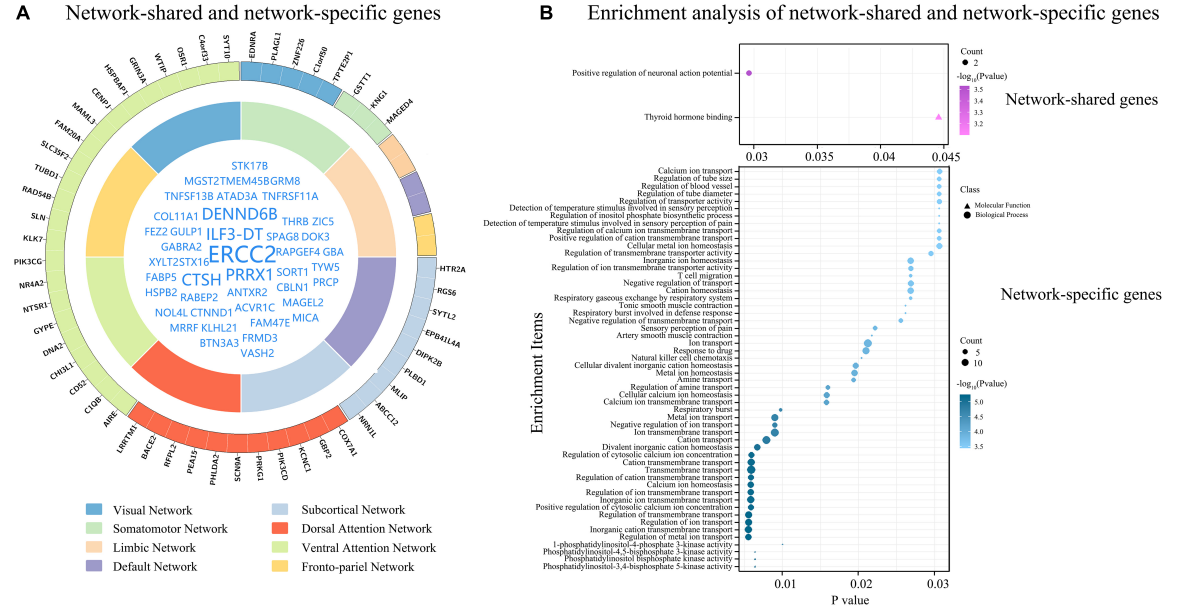

FIGURE 5 | Network-shared and network-specific genes. **(A)** Shows network-shared genes (inner circle) and network-specific genes (outer circle). The eight functional networks are represented by different colors. **(B)** Demonstrates the results of enrichment analyses of the 51 network-shared genes and the 51 network-specific genes.

Teeuw et al., 2019). However, we barely know which kinds of functional connections are prone to be regulated by gene expression. In this study, we identified 179 functional connections that were highly associated with gene expression. Most of the gene-related functional connections (78.2%) were located in the same functional network, which is consistent with the higher correlations between gene expression and functional connectivity within functional networks than between networks (Richiardi et al., 2015; Zhu et al., 2021). Notably, 41/45 (91.1%) homologous connections were identified as gene-related connections, indicating that homologous connections are prone to be regulated by gene expression. This result is also consistent with the knowledge that homologous regions between the bilateral hemispheres have both higher genetic correlations and stronger anatomical connections (Stark et al., 2008; Eyler et al., 2014; Shen et al., 2015; Elliott et al., 2018).

In this study, we identified 51 network-shared genes associated with functional connectivity, which were enriched for positive regulation of neuronal action potential, which is the core biological process in brain activity throughout the brain. Specifically, *CTNND1* is related to adhesion between cells and signal transduction, and is involved in the regulation of protein kinase and signaling receptor binding, WNT signaling pathway, and postsynaptic membrane neurotransmitter receptor levels (Tang et al., 2016). *GABRA2* plays a role in the regulation of GABA-gated chloride ion channel activity and chemical synaptic transmission (Lengeling et al., 1999).

We also identified 51 network-specific connectivity-related genes, which were mainly enriched for the regulation of ion transport and ion homeostasis. Several network-specific genes are involved in various signaling pathways, such as *EDNRA* and *KNG1* are related to the G protein-coupled receptor signaling pathway (Horstmeyer et al., 1996; Sato et al., 2008), *HTR2A* is involved in the CREB and ELK-SRF/GATA4 signaling pathways, and *NR4A2* is associated with canonical WNT signaling pathway (Zagani et al., 2009). Several network-specific genes (*COX7A1*, *SLN, GBP2, BACE2, PRKG1, SYTL2, ABCC12*, and *RGS6*) are related to energy metabolism, such as ATP synthesis and GTPase activity. Several network-specific genes (*PIK3CD, AIRE, PEA15, C1QB*, and *CHI3L1*) play a role in immune response.

Two limitations should be mentioned when one interprets the results of this study. First, brain imaging data and gene expression data were obtained from different subjects and these two groups of subjects differ in age and race. Thus, the spatial correlation analyses between gene co-expression and functional connectivity may be confounded by inter-individual conservation of brain gene expression and inter-group differences in these demographic data. Second, we still do not know if gene–gene spatial autocorrelation is a meaningful biological phenomenon or a meaningless confounding factor, and thus we did not correct for gene–gene spatial autocorrelation in this study, which may bias our findings.

In conclusion, this study provides new knowledge for the relationship between gene expression and functional connectivity in the human brain. Firstly, we confirmed that most of the previously identified connectivity-related genes can be detected in individual-level transcription-neuroimaging association analysis. Secondly, we found unequal influences of gene expression on functional connections and identified 179 functional connections linking more closely to gene expression than other connections. Thirdly, we identified network-shared genes and network-specific genes for the first time, which are involved in different molecular processes. These findings may improve our understanding of the relationship between gene expression and functional connectivity.

DATA AVAILABILITY STATEMENT

The datasets presented in this study can be found in online repositories. The names of the repository/repositories and accession number(s) can be found in the article/**Supplementary Material**.

ETHICS STATEMENT

The studies involving human participants were reviewed and approved by the Ethics Committee of Tianjin Medical University. The patients/participants provided their written informed consent to participate in this study. Written informed consent was obtained from the individual(s) for the publication of any potentially identifiable images or data included in this article.

AUTHOR CONTRIBUTIONS

WQ: methodology and conceptualization. FL: software and formal analysis. HD, YJ, and BY: visualization. PZ, WL, and ZY: resources. CY: conceptualization, methodology, writing – review and editing, and supervision. All authors contributed to the article and approved the submitted version.

FUNDING

This work was supported by the National Key Research and Development Program of China (2018YFC1314300), the National Natural Science Foundation of China (82030053 and 81425013), and the Tianjin Key Technology R&D Program (17ZXMFSY00090).

SUPPLEMENTARY MATERIAL

The Supplementary Material for this article can be found online at: https://www.frontiersin.org/articles/10.3389/fnins.2021.797849/full#supplementary-material

REFERENCES

Anderson, K. M., Krienen, F. M., Choi, E. Y., Reinen, J. M., Yeo, B. T. T., and Holmes, A. J. (2018). Gene expression links functional networks across cortex and striatum. *Nat. Commun.* 9:1428.

Arnatkevic Iute, A., Fulcher, B. D., and Fornito, A. (2019). A practical guide to linking brain-wide gene expression and neuroimaging data. *NeuroImage* 189, 353–367. doi: 10.1016/j.neuroimage.2019.01.011

Autism Spectrum Disorders Working Group of The Psychiatric Genomics Consortium (2017). Meta-analysis of GWAS of over 16,000 individuals with autism spectrum disorder highlights a novel locus at 10q24.32 and a significant overlap with schizophrenia. *Mol. Autism* 8:21. doi: 10.1186/s13229-017-0137-9

Bando, Y., Irie, K., Shimomura, T., Umeshima, H., Kushida, Y., Kengaku, M., et al. (2016). Control of spontaneous Ca2+ transients is critical for neuronal maturation in the developing neocortex. *Cereb. Cortex* 26, 106–117. doi: 10.1093/cercor/bhu180

Chen, J., Bardes, E. E., Aronow, B. J., and Jegga, A. G. (2009). ToppGene Suite for gene list enrichment analysis and candidate gene prioritization. *Nucleic Acids Res.* 37, W305–W311. doi: 10.1093/nar/gkp427

de Leeuw, C. A., Mooij, J. M., Heskes, T., and Posthuma, D. (2015). MAGMA: generalized gene-set analysis of GWAS data. *PLoS Comput. Biol.* 11:e1004219. doi: 10.1371/journal.pcbi.1004219

Demontis, D., Walters, R. K., Martin, J., Mattheisen, M., Als, T. D., Agerbo, E., et al. (2019). Discovery of the first genome-wide significant risk loci for attention deficit/hyperactivity disorder. *Nat. Genet.* 51, 63–75.

Dong, D., Wang, Y., Chang, X., Luo, C., and Yao, D. (2018). Dysfunction of large-scale brain networks in schizophrenia: a meta-analysis of resting-state functional connectivity. *Schizophr. Bull.* 44, 168–181. doi: 10.1093/schbul/sbx034

Dougherty, J. D., Schmidt, E. F., Nakajima, M., and Heintz, N. (2010). Analytical approaches to RNA profiling data for the identification of genes enriched in specific cells. *Nucleic Acids Res.* 38, 4218–4230.

Elliott, L. T., Sharp, K., Alfaro-Almagro, F., Shi, S., Miller, K. L., Douaud, G., et al. (2018). Genome-wide association studies of brain imaging phenotypes in UK Biobank. *Nature* 562, 210–216. doi: 10.1038/s41586-018-0571-7

Eyler, L. T., Vuoksimaa, E., Panizzon, M. S., Fennema-Notestine, C., Neale, M. C., Chen, C. H., et al. (2014). Conceptual and data-based investigation of genetic influences and brain asymmetry: a twin study of multiple structural phenotypes. *J. Cogn. Neurosci.* 26, 1100–1117. doi: 10.1162/jocn_a_00531

Fornito, A., Zalesky, A., Bassett, D. S., Meunier, D., Ellison-Wright, I., Yucel, M., et al. (2011). Genetic influences on cost-efficient organization of human cortical functional networks. *J. Neurosci.* 31, 3261–3270. doi: 10.1523/JNEUROSCI.4858-10.2011

Ge, T., Holmes, A. J., Buckner, R. L., Smoller, J. W., and Sabuncu, M. R. (2017). Heritability analysis with repeat measurements and its application to resting-state functional connectivity. *Proc. Natl. Acad. Sci. U.S.A.* 114, 5521–5526. doi: 10.1073/pnas.1700765114

Horstmeyer, A., Cramer, H., Sauer, T., Muller-Esterl, W., and Schroeder, C. (1996). Palmitoylation of endothelin receptor A. Differential modulation of signal transduction activity by post-translational modification. *J. Biol. Chem.* 271, 20811–20819. doi: 10.1074/jbc.271.34.20811

Jansen, A. G., Mous, S. E., White, T., Posthuma, D., and Polderman, T. J. (2015). What twin studies tell us about the heritability of brain development, morphology, and function: a review. *Neuropsychol. Rev.* 25, 27–46. doi: 10.1007/s11065-015-9278-9

Krienen, F. M., Yeo, B. T., Ge, T., Buckner, R. L., and Sherwood, C. C. (2016). Transcriptional profiles of supragranular-enriched genes associate with corticocortical network architecture in the human brain. *Proc. Natl. Acad. Sci. U.S.A.* 113, E469–E478. doi: 10.1073/pnas.1510903113

Lengeling, A., Wiltshire, T., Otmani, C., and Bucan, M. (1999). A sequence-ready BAC contig of the GABAA receptor gene cluster Gabrg1-Gabra2-Gabrb1 on mouse chromosome 5. *Genome Res.* 9, 732–738.

Ogawa, S., Tank, D. W., Menon, R., Ellermann, J. M., Kim, S. G., Merkle, H., et al. (1992). Intrinsic signal changes accompanying sensory stimulation: functional brain mapping with magnetic resonance imaging. *Proc. Natl. Acad. Sci. U.S.A.* 89, 5951–5955.

Oh, K., Hwang, T., Cha, K., and Yi, G. S. (2015). Disease association and inter-connectivity analysis of human brain specific co-expressed functional modules. *Biol. Res.* 48:67. doi: 10.1186/s40659-015-0061-4

Richiardi, J., Altmann, A., Milazzo, A. C., Chang, C., Chakravarty, M. M., Banaschewski, T., et al. (2015). BRAIN NETWORKS. Correlated gene expression supports synchronous activity in brain networks. *Science (New York, NY)* 348, 1241–1244.

Sato, T., Kawamura, Y., Asai, R., Amano, T., Uchijima, Y., Dettlaff-Swiercz, D. A., et al. (2008). Recombinase-mediated cassette exchange reveals the selective use of Gq/G11-dependent and -independent endothelin 1/endothelin type A receptor signaling in pharyngeal arch development. *Development (Cambridge England)* 135, 755–765. doi: 10.1242/dev.012708

Schizophrenia Working Group of the Psychiatric Genomics Consortium (2014). Biological insights from 108 schizophrenia-associated genetic loci. *Nature* 511, 421–427. doi: 10.1038/nature13595

Seeley, W. W., Crawford, R. K., Zhou, J., Miller, B. L., and Greicius, M. D. (2009). Neurodegenerative diseases target large-scale human brain networks. *Neuron* 62, 42–52.

Shen, K., Misic, B., Cipollini, B. N., Bezgin, G., Buschkuehl, M., Hutchison, R. M., et al. (2015). Stable long-range interhemispheric coordination is supported by direct anatomical projections. *Proc. Natl. Acad. Sci. U.S.A.* 112, 6473–6478. doi: 10.1073/pnas.1503436112

Stahl, E. A., Breen, G., Forstner, A. J., McQuillin, A., Ripke, S., Trubetskoy, V., et al. (2019). Genome-wide association study identifies 30 loci associated with bipolar disorder. *Nat. Genet.* 51, 793–803.

Stark, D. E., Margulies, D. S., Shehzad, Z. E., Reiss, P., Kelly, A. M., Uddin, L. Q., et al. (2008). Regional variation in interhemispheric coordination of intrinsic hemodynamic fluctuations. *J. Neurosci.* 28, 13754–13764. doi: 10.1523/JNEUROSCI.4544-08.2008

Tang, B., Tang, F., Wang, Z., Qi, G., Liang, X., Li, B., et al. (2016). Overexpression of CTNND1 in hepatocellular carcinoma promotes carcinous characters through activation of Wnt/beta-catenin signaling. *J. Exp. Clin. Cancer Res. CR* 35:82. doi: 10.1186/s13046-016-0344-9

Teeuw, J., Brouwer, R. M., Guimaraes, J., Brandner, P., Koenis, M. M. G., Swagerman, S. C., et al. (2019). Genetic and environmental influences on functional connectivity within and between canonical cortical resting-state networks throughout adolescent development in boys and girls. *Neuroimage* 202:116073. doi: 10.1016/j.neuroimage.2019.116073

Toth, A. B., Shum, A. K., and Prakriya, M. (2016). Regulation of neurogenesis by calcium signaling. *Cell Calcium* 59, 124–134. doi: 10.1016/j.ceca.2016.02.011

Tzourio-Mazoyer, N., Landeau, B., Papathanassiou, D., Crivello, F., Etard, O., Delcroix, N., et al. (2002). Automated anatomical labeling of activations in SPM using a macroscopic anatomical parcellation of the MNI MRI single-subject brain. *Neuroimage* 15, 273–289. doi: 10.1006/nimg.2001.0978

van den Heuvel, M. P., and Fornito, A. (2014). Brain networks in schizophrenia. *Neuropsychol. Rev.* 24, 32–48.

Vertes, P. E., and Bullmore, E. T. (2015). Annual research review: growth connectomics–the organization and reorganization of brain networks during normal and abnormal development. *J. Child Psychol. Psychiatry Allied Disciplines* 56, 299–320. doi: 10.1111/jcpp.12365

Vertes, P. E., Rittman, T., Whitaker, K. J., Romero-Garcia, R., Vasa, F., Kitzbichler, M. G., et al. (2016). Gene transcription profiles associated with inter-modular hubs and connection distance in human functional magnetic resonance imaging networks. *Philos. Trans. R. Soc. Lond. B Biol. Sci.* 371:20150362. doi: 10.1098/rstb.2015.0362

Wang, M., Fischer, J., and Song, Y. S. (2019). Three-way clustering of multi-tissue multi-individual gene expression data using semi-nonnegative tensor decomposition. *Ann. Appl. Stat.* 13, 1103–1127. doi: 10.1214/18-aoas1228

Wray, N. R., Ripke, S., Mattheisen, M., Trzaskowski, M., Byrne, E. M., Abdellaoui, A., et al. (2018). Genome-wide association analyses identify 44 risk variants and refine the genetic architecture of major depression. *Nat. Genet.* 50, 668–681. doi: 10.1038/s41588-018-0090-3

Xu, X., Wells, A. B., O'Brien, D. R., Nehorai, A., and Dougherty, J. D. (2014). Cell type-specific expression analysis to identify putative cellular mechanisms for neurogenetic disorders. *J. Neurosci.* 34, 1420–1431. doi: 10.1523/JNEUROSCI.4488-13.2014

Yan, C. G., Wang, X. D., Zuo, X. N., and Zang, Y. F. (2016). DPABI: data processing & analysis for (resting-state) brain imaging. *Neuroinformatics* 14, 339–351.

Yeo, B. T., Krienen, F. M., Sepulcre, J., Sabuncu, M. R., Lashkari, D., Hollinshead, M., et al. (2011). The organization of the human cerebral cortex estimated by intrinsic functional connectivity. *J. Neurophysiol.* 106, 1125–1165. doi: 10.1152/jn.00338.2011

Zagani, R., Hamzaoui, N., Cacheux, W., de Reynies, A., Terris, B., Chaussade, S., et al. (2009). Cyclooxygenase-2 inhibitors down-regulate osteopontin and Nr4A2-new therapeutic targets for colorectal cancers. *Gastroenterology* 137, 1358–1366.e1-3. doi: 10.1053/j.gastro.2009.06.039

Zhang, C., Cai, H. H., Xu, X. T., Li, Q., Li, X. Y., Zhao, W. M., et al. (2021). Genetic architecture underlying differential resting-state functional connectivity of subregions within the human visual cortex. *Cereb. Cortex*. doi: 10.1093/cercor/bhab335 [Epub ahead of print].

Zhu, D., Yuan, T. F., Gao, J. F., Xu, Q., Xue, K. Z., Zhu, W. S., et al. (2021). Correlation between cortical gene expression and resting-state functional network centrality in healthy young adults. *Hum. Brain Mapp.* 42, 2236–2249. doi: 10.1002/hbm.25362

Conflict of Interest: The authors declare that the research was conducted in the absence of any commercial or financial relationships that could be construed as a potential conflict of interest.

Publisher's Note: All claims expressed in this article are solely those of the authors and do not necessarily represent those of their affiliated organizations, or those of the publisher, the editors and the reviewers. Any product that may be evaluated in this article, or claim that may be made by its manufacturer, is not guaranteed or endorsed by the publisher.

frontiers in Neuroscience

ORIGINAL RESEARCH
published: 05 January 2022
doi: 10.3389/fnins.2021.791831

Transcriptomic Signatures Associated With Gray Matter Volume Changes in Patients With Functional Constipation

Wangli Cai[1†], Yujing Zhou[2†], Lidi Wan[1], Ruiling Zhang[1], Ting Hua[1], Jian Gong[1], Bo Yang[3] and Guangyu Tang[1]*

[1] Department of Radiology, Shanghai Tenth People's Hospital, School of Clinical Medicine of Nanjing Medical University, Shanghai, China, [2] Department of Radiology, The First Affiliated Hospital of Dalian Medical University, Dalian, China, [3] Department of Colorectal and Anal Surgery, Shanghai Tenth People's Hospital, School of Clinical Medicine of Nanjing Medical University, Shanghai, China

OPEN ACCESS

Edited by:
Jiajia Zhu,
First Affiliated Hospital of Anhui Medical University, China

Reviewed by:
Huaigui Liu,
Tianjin Medical University General Hospital, China
Huawang Wu,
The Affiliated Brain Hospital of Guangzhou Medical University, China

***Correspondence:**
Guangyu Tang
tgy17@126.com

† These authors have contributed equally to this work

Specialty section:
This article was submitted to Brain Imaging Methods, a section of the journal Frontiers in Neuroscience

Received: *09 October 2021*
Accepted: *23 November 2021*
Published: *05 January 2022*

Citation:
Cai W, Zhou Y, Wan L, Zhang R, Hua T, Gong J, Yang B and Tang G (2022) Transcriptomic Signatures Associated With Gray Matter Volume Changes in Patients With Functional Constipation. Front. Neurosci. 15:791831. doi: 10.3389/fnins.2021.791831

Functional constipation, which belongs to the functional gastrointestinal disorder (FGID), is a common disease and significantly impacts daily life. FGID patients have been progressively proven with functional and structural alterations in various brain regions, but whether and how functional constipation affects the brain gray matter volume (GMV) remains unclear; besides, which genes are associated with the GMV changes in functional constipation is largely unknown. On account of the structural MRI image from the 30 functional constipation patients and 30 healthy controls (HCs), GMV analysis showed that functional constipation patients had significantly decreased GMV in the right orbital prefrontal cortex (OFC), left precentral gyrus (PreG), and bilateral thalamus (THA). Correlation analysis showed that the self-rating depressive scale, patient assessment of constipation quality of life (PAC-QOL), and Wexner constipation scores were negatively correlated with GMV of the OFC and negative correlations between PAC-QOL score and GMV of the bilateral THA. Based on the Allen Human Brain Atlas, a cross-sample spatial correlation was conducted and found that 18 genes' expression values showed robust correlations with GMV changes in functional constipation patients. These outcomes highlight our recognition of the transcriptional features related to GMV changes in functional constipation and could be regarded as candidates to detect biological mechanisms of abnormality in functional constipation patients.

Keywords: functional constipation, Allen Human Brain Atlas, gene expression analysis, gray matter volume, imaging-genetics

INTRODUCTION

Functional constipation, as one type of the functional gastrointestinal disorder (FGID), is portrayed by rare bowel movements, painful defecation, uncomfortable feeling of incomplete evacuation, hard/big stools, and frequently joined with abdominal distension and/or abdominal pain (Alame and Bahna, 2012). The incidence rate of functional constipation is relatively high in the entire

community, about 0.7–79% (Mugie et al., 2011). Besides, an impressive proportion of functional constipation patients would accompany anxiety and varying severity of depression (Hosseinzadeh et al., 2011). These symptoms severely sway the quality of their daily life and emotional status (Glia and Lindberg, 1997; Bongers et al., 2009).

At present, robust evidence demonstrated that FGID results from physiological changes of the gastrointestinal system because of the bidirectional brain–gut axis, which may influence brain functional/structural alterations, and subsequently arising from anxiety and depression symptoms (Mayer et al., 2006; Mazur et al., 2012). Accordingly, neuroimaging methods have been progressively applied to investigate brain structural and functional anomalies of FGID patients (Blankstein et al., 2010; Zhu et al., 2016; Jin et al., 2019; Hu et al., 2020; Duan et al., 2021; Liu et al., 2021). They found the functional abnormalities in brain regions enrolled in emotion modulating, including the orbitofrontal cortex (OFC), anterior insula, dorsal anterior cingulate cortex, and hippocampus, and motor control, including the precentral gyrus and supplementary motor area. Besides, several pieces of research in FGID patients demonstrated functional impairments in the thalamus, assuming a fundamental part in sensory and motor signal processing (Tillisch et al., 2011; Liu et al., 2021). Moreover, a new structural MRI research had shown that functional constipation patients demonstrated significant diminished cortical thickness of different brain regions, including the left orbitofrontal cortex, left middle frontal gyrus, left medial prefrontal gyrus, left supplementary motor area, right dorsal anterior cingulate cortex, right middle temporal gyrus, and bilateral posterior cingulate cortex/precuneus; decreased cortical volume in the left middle temporal gyrus and bilateral posterior cingulate cortex/precuneus; and induced cortical surface area in the right precentral gyrus additionally (Hu et al., 2020). The above-mentioned brain regions are primarily associated with somatic movement controlling and emotion modulating (Zhu et al., 2016; Hu et al., 2020), and these alterations were implicated in the symptoms of functional constipation patients containing disorder of defecation and unhealthy mood (Ringel, 2002; Alame and Bahna, 2012; Al Omran and Aziz, 2014). Notwithstanding, there has been no study of transcriptional neuroimaging analysis to identify genes related to GMV alterations in functional constipation patients.

Currently, based on the Allen Human Brain Atlas (AHBA)[1], we acquired the gene expression data and conducted the transcriptional neuroimaging analysis to find the genes related to GMV changes in functional constipation patients. We extracted gene expression data from each sample and calculated GMV changes depending on the high-resolution structural MRI image of functional constipation and controls, in sequence, cross-sample spatial association analysis between GMV changes and gene expression values. An illustration of the handling flow chart is displayed in **Figure 1**.

[1]http://human.brain-map.org

MATERIALS AND METHODS

Subjects

The experiment was approved by the Ethical Committee of Shanghai Tenth People's Hospital, and each subject gave written informed consent before the study. Utilizing Rome IV criteria (Drossman, 2016), patients diagnosed by a gastroenterologist expert as having functional constipation with history over 1 year were enrolled in our study. Subjects were barred from the study if they had the following diseases, namely, congenital giant colon, excess sigmoid colon, and mental disease, or who were drug abusers. Besides, subjects with other brain disorders or abnormalities (such as severe white matter hyperintensity, lacunes, microbleeds, and tumors), as determined using T2 fluid-attenuated inversion recovery (FLAIR) sequence, were excluded. Finally, there were 30 right-handed patients with functional constipation (10 men, right-handed, 46.00 $\pm$ 18.03 years) who finished the MRI scans. The healthy control group comprised 30 subjects who were right-handed and age and gender matched (9 men, right-handed, 45.77 $\pm$ 14.63 years). Self-directed surveys, including the patient assessment of constipation quality of life (PAC-QOL) and Wexner constipation score, were displayed to all members to comprehensively assess the burden of constipation on patients' regular working and life (Marquis et al., 2005). Patients were additionally approached to finish the Zung (1965) self-rating depressive scale (SDS) and Zung (1971) self-rating anxiety scale (SAS) to survey their seriousness of depression and anxiety.

Data Acquisition and Gray Matter Volume Calculation

Sagittal 3D high-resolution T1-weighted data were collected by a turbo field echo (TFE) sequence. The parameters are as followed: repetition time (TR)/echo time (TE) = 7.0 ms/3.2 ms; field of view = 256 mm $\times$ 256 mm; matrix = 256 $\times$ 256. The thickness slice is 1.0 mm, and there were 192 slices with no gap (Ingenia 3.0, Philips).

All the structural MRI data were preprocessed utilizing CAT12 software (version r1364) with the accompanying methodology: bias correction, segmentation, the creation of population-specific tissue templates, spatial normalization using the DARTEL technique, and smoothing with an 8 mm $\times$ 8 mm $\times$ 8 mm full-width. After these preprocessing steps, we acquired the normalized, modulated, and smoothed GMV images, and each voxel represented volume information.

Case–Control Gray Matter Volume Changes

We conducted the voxel-based comparisons to distinguish the brain regions that showed group differences in GMV by utilizing the two-sample *t*-test, controlling the impacts of gender, age, and whole intracranial volume. The multiple comparisons were adjusted by the false discovery rate method ($p < 0.05$) and a cluster size > 200 voxels using the SPM12 software. Then, a region of interest (ROI)-based association analysis was applied to test relationships between the GMVs of the brain areas, which showed

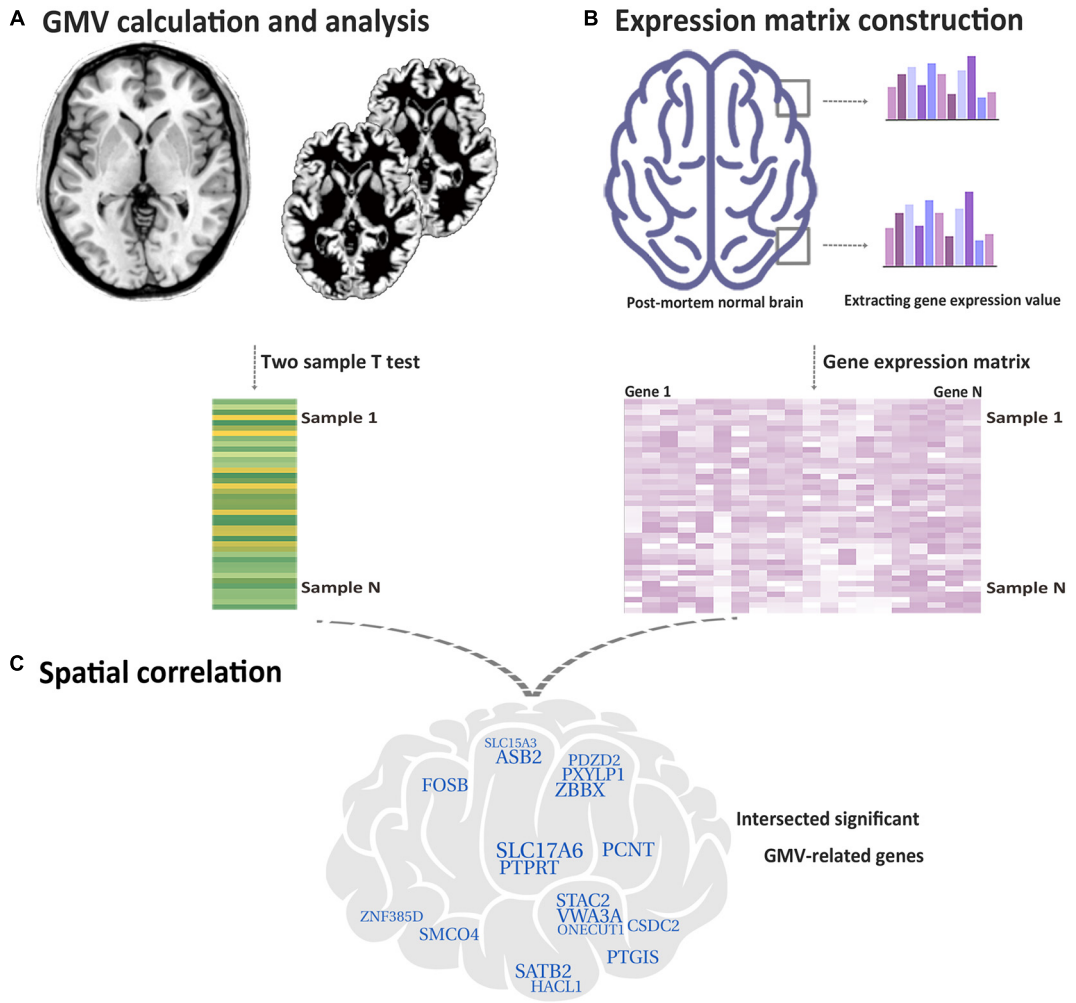

FIGURE 1 | Flow chart of the study design. **(A)** Based on functional constipation and HC, utilizing the two-sample *t*-test to make voxel-wise GMV changes for each tissue sample. **(B)** Acquired gene expression values in each tissue sample. **(C)** Identifying genes related with GMV changes in functional constipation. The crossed specific genes are characterized as genes related with GMV changes in functional constipation.

significant group differences with the SDS, SAS, PAC-QOL, and Wexner constipation scores.

Gene Expression Data Preprocessing

Freely accessible gene expression data of six postmortem human brains were obtained from the AHBA dataset (Hawrylycz et al., 2012), and they were handled utilizing a new flow chart to combine gene expression data with neuroimage data (Arnatkeviciute et al., 2019). We divided the AHBA dataset into two datasets: the first dataset consisted of two donors with the whole brain gene expression data, which have 820 samples, and the second dataset consisted of six donors only with the left-brain gene expression data, which have 1,782 samples. The short processing work was as follows: first, we reassigned probes to genes by using the most recent sequencing databases; second, we barred probes with lower expression signal intensity compared to background noise; third, the probes showing high consistency with the RNA-sequence data were picked; lastly, the expression data were normalized. After such handling process, we obtained 10,185 genes with a normalized expression value of each sample.

Genes Associated With Gray Matter Volume Changes in Functional Constipation Patients

After extracting gene expression data from each sample (820/1,782 samples) and calculating GMV changes (t-statistic values) in these samples derived from the two-sample *t*-test based on the high-resolution structural MRI image of functional constipation patients and HC, we performed a gene-wise cross-sample Spearman correlation analysis to decide the relationships between GMV changes and gene expression values independently (n = 10,185). Considering the multiple comparisons at the gene level (n = 10,185), we adjusted the Bonferroni correction method and set a $p < 4.91 \times 10^{-7} = 0.05/10{,}185$ to identify the significant genes. At last, the genes related to GMV changes

TABLE 1 | The general clinical characteristics of functional constipation and HC.

	FCon (*N* = 30) (Mean ± SE)	HC (*N* = 30) (Mean ± SE)	FCon vs. HC *p*-value
Age (years)	46.00 ± 18.03	45.77 ± 14.63	0.123
Gender	10M/20F	9M/21F	0.781
BMI (kg/m^2)	22.62 ± 3.17	21.53 ± 2.87	0.594
Depression (SDS)	53.47 ± 10.74	30.93 ± 7.01	0.008
Anxiety (SAS)	50.60 ± 9.76	33.27 ± 7.34	0.213
PAC-QOL	57.27 ± 20.18	N/A	N/A
Wexner constipation score	13.47 ± 3.35	N/A	N/A

FCon, patients with functional constipation; HC, healthy controls; SE, standard error; BMI, body mass index; SDS, Zung Self-rating Depressive Scale; SAS, Zung Self-Rating Anxiety Scale; PAC-QOL, patient assessment of constipation quality of life.

in functional constipation patients were characterized as those whose expression values derived from two expression datasets were prominently associated with GMV changes.

RESULTS

Demographic and Clinical Characteristics

The general clinical characteristics of functional constipation patients and HC are summed up in **Table 1**. The two groups have not shown significant differences in gender ($\chi^2 = 0.077$, df = 1, $p = 0.781$), age ($F = 2.451$, df = 58, $p = 0.123$), body mass index (BMI) ($F = 0.287$, df = 58, $p = 0.594$), and anxiety ($F = 1.582$, df = 58, $p = 0.213$) between the two groups. There was significant group difference on depression ($F = 7.474$, df = 58, $p = 0.008$).

Gray Matter Volume Changes of Functional Constipation Patients

After analyzing voxel-wise GMV alterations ($P < 0.05$, FDR corrected) between the patients with functional constipation and HC, compared to HC groups, we found that functional constipation patients primarily demonstrated decreased GMV in the right orbital prefrontal cortex (OFC, peak MNI coordinates: $x = 15$, $y = 37.5$, $z = -22.5$; cluster size = 230 voxels), left precentral gyrus (PreG, peak MNI coordinates: $x = -42$, $y = 24$, $z = 52.5$; cluster size = 230 voxels), and bilateral thalamus (THA, peak MNI coordinates: $x = 4.5$, $y = -19.5$, $z = -1.5$; cluster size = 338 voxels) (**Figure 2**). In addition, there were no regions demonstrating a significant increased GMV in functional constipation patients.

Correlation analysis showed that the PAC-QOL, Wexner constipation score, and SDS score were negatively correlated with GMV of the OFC ($r = -0.638$, $p < 0.001$; $r = -0.466$, $p = 0.009$; and $r = -0.412$, $p = 0.024$, respectively) in functional constipation patients (**Figure 3**). There was negative correlation between PAC-QOL score and GMV of the bilateral THA ($r = -0.415$, $p = 0.023$) in functional constipation patients (**Figure 3**). However, the data showed expected heterogeneity due to the small sample size; we should restrict the wide application of such conclusions, as there exist correlated tendencies, which need further verification in the future.

Genes Related to Gray Matter Volume Changes in Functional Constipation Patients

After the gene expression data processing, we ultimately achieved 10,185 genes with normalized expression values for every 820 and 1,782 samples from the two AHBA datasets. A cross-sample spatial correlation was conducted between GMV changes in functional constipation patients and gene expression value. There were 345 genes that revealed a significant correlation with GMV changes in functional constipation in the first dataset and 208 genes in the second ($p < 0.05$, Bonferroni corrected). The crossed 18 genes of the two AHBA expression datasets were chosen. Detailed descriptions and correlation coefficients of these genes are exhibited in **Table 2**. Hence, the positive correlation that implies higher gene expression in brain samples manifested a more prominent GMV decrease in functional constipation patients. The negative correlation that implies lower gene expression in brain samples manifested a more noteworthy GMV decrease in functional constipation patients (**Figure 4**).

DISCUSSION

In this study, we mainly identified genes preferentially correlated to GMV changes in functional constipation patients by linking gene expression patterns to GMV difference patterns in humans. We found 18 genes' expression values showing robust correlations with GMV changes in functional constipation, including the orbitofrontal cortex, precentral gyrus, and thalamus. These outcomes could highlight our recognition of the transcriptional features correlated with GMV changes in functional constipation patients.

Here, we found the decreased GMV in the right OFC and its association with constipation scores and depression. As one of the least understood regions, OFC assumes a vital part in emotional regulation, visceral information integration (including sensory and motor information), and decision-making (Kringelbach and Rolls, 2004; Price, 2007; Rolls and Grabenhorst, 2008; Bongers et al., 2009; Rolls, 2019). Additionally, the OFC shows anatomical connection with the cingulate gyrus, amygdala, hypothalamus, and midbrain (Price, 2007), which subsequently portrays its contribution to emotional modulation and visceral coordination. Previous functional MRI (fMRI) studies have reported that the distension of the lower gastrointestinal tract will activate OFC (Derbyshire, 2003), followed by another study that showed that the painful and non-painful gastric stimulation will also activate the right OFC (Guleria et al., 2017). Thereby, these studies further support the vital role of OFC in regulating visceral function. Meanwhile, increased baseline activity in OFC was found in patients with functional constipation and showed a correlation with the sensation of incomplete evacuation (Zhu et al., 2016). Functional constipation is often accompanied by mental issues; the most common are anxiety and depression (Emmanuel et al., 2001; Waters et al., 2013). In this study, we found that the

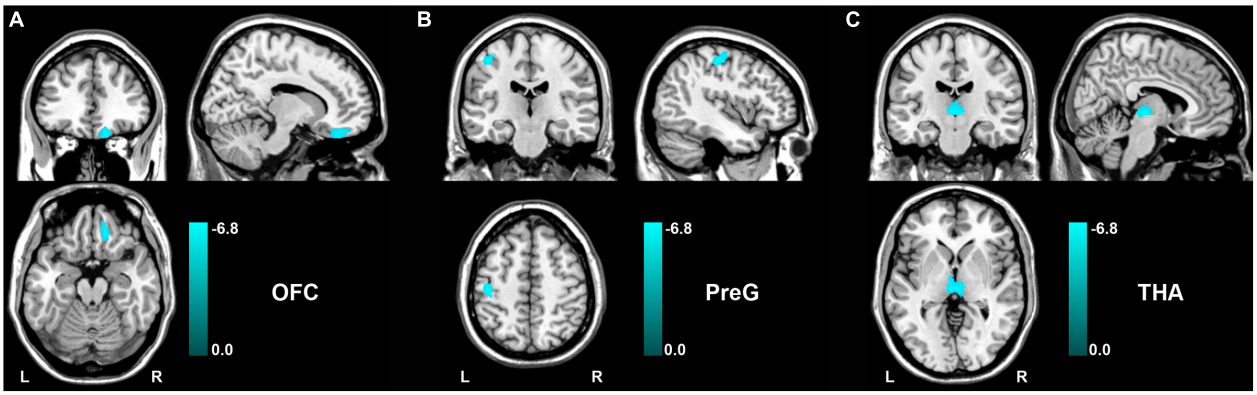

FIGURE 2 | GMV changes between functional constipation and healthy controls ($p < 0.05$, FDR correction). The color bar showed the range of t-value. There was significantly decreased GMV in the right OFC **(A)**, left PreG **(B)**, and bilateral THA **(C)**. GMV, gray matter volume; L, left; OFC, orbital prefrontal cortex; PreG, precentral gyrus; R, right; THA, thalamus.

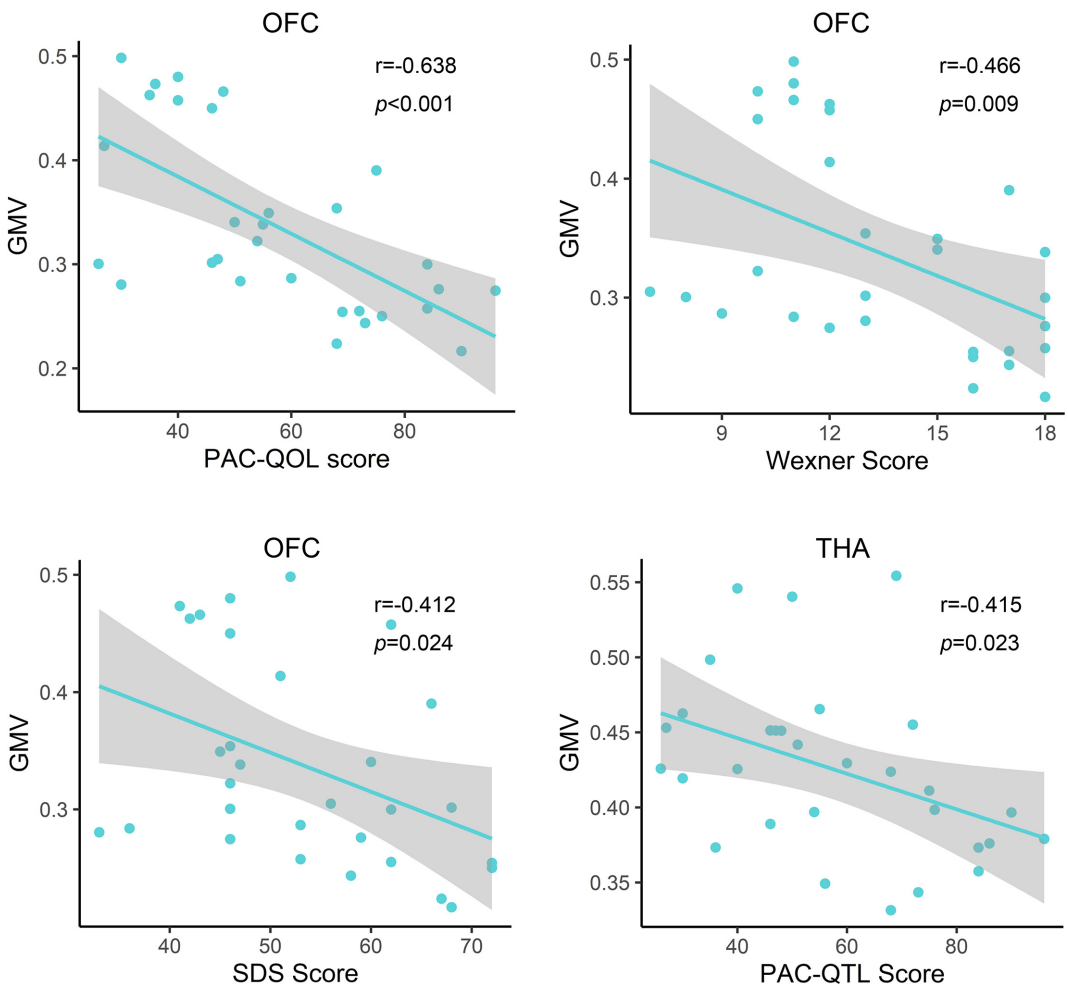

FIGURE 3 | Relationship between clinical information and gray matter volume of the impaired brain region in functional constipation patients. In the functional constipation patients, the PAC-QOL, Wexner constipation score, and SDS score were negatively correlated with GMV of the right OFC. There was negative correlation between PAC-QOL score and GMV of the bilateral THA. GMV, gray matter volume; L, left; OFC, orbital prefrontal cortex; PAC-QOL, patient assessment of constipation quality of life; PreG, precentral gyrus; R, right; SDS, self-rating depressive scale; THA, thalamus.

TABLE 2 | The candidate 18 genes manifesting prominent relationships between gene expression and GMV alterations in functional constipation.

Gene symbol	Correlation coefficients	Entrez ID	Gene name
VWA3A	0.233	ENSG00000175267	Von Willebrand factor A domain-containing protein 3A
ZBBX	0.226	ENSG00000169064	Zinc Finger B-Box domain containing
PTPRT	0.208	ENSG00000196090	Protein tyrosine phosphatase receptor type T
ASB2	0.201	ENSG00000100628	Ankyrin repeat and SOCS box containing 2
PXYLP1	0.192	ENSG00000155893	2-Phosphoxylose phosphatase 1
STAC2	0.185	ENSG00000141750	SH3 and cysteine rich domain 2
ZNF385D	0.180	ENSG00000151789	Zinc finger protein 385D
SMCO4	0.166	ENSG00000166002	Single-pass membrane protein with coiled-coil domains 4
PTGIS	0.159	ENSG00000124212	Prostaglandin I2 synthase
SATB2	0.156	ENSG00000119042	SATB homeobox 2
HACL1	0.153	ENSG00000131373	2-Hydroxyacyl-CoA lyase 1
CSDC2	0.147	ENSG00000172346	Cold shock domain containing C2
PCNT	0.143	ENSG00000160299	Pericentrin
FOSB	0.140	ENSG00000125740	FosB proto-oncogene, AP-1 transcription factor subunit
PDZD2	−0.137	ENSG00000133401	PDZ domain containing 2
SLC15A3	−0.151	ENSG00000110446	Solute carrier family 15 member 3
ONECUT1	−0.174	ENSG00000169856	One cut homeobox 1
SLC17A6	−0.185	ENSG00000091664	Solute carrier family 17 member 6

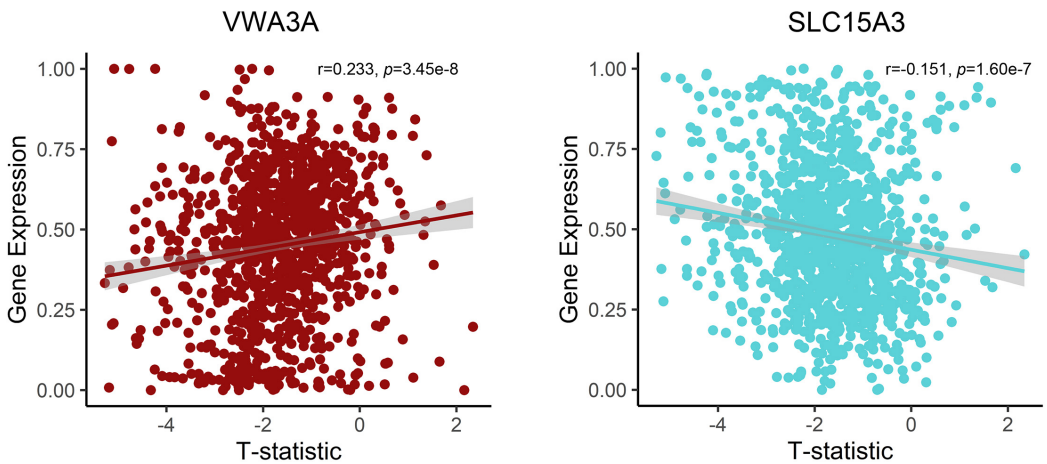

FIGURE 4 | Correlations between expression of two representative genes and GMV changes in patients with functional constipation. The *x*-axis shows the T-statistic of GMV difference between functional constipation patients and healthy controls, and the *y*-axis is the gene expression value.

decreased GMV in the right OFC showed association with constipation scores and depression, indicating that the structural injury in OFC might cause the functional abnormality in visceral sensory and motor integration and emotional processing.

In addition, we noticed reduced GMV in the left precentral gyrus and the bilateral thalamus, and the GMV of the bilateral thalamus in patients with functional constipation showed association with PAC-QOL score. The precentral gyrus contributes to controlling the movement execution (Zhu et al., 2016). The structural abnormality of PreG in patients with functional constipation indicated the altered ability to control bowel movement (Hu et al., 2020). Thalamus, as an integrative hub, prominently participates in relaying/integrating/transmitting numerous inputs and connections with various cortical brain areas (Rouiller et al., 1999; Sherman, 2017). Some studies focusing on irritable bowel syndrome revealed the vital role of the thalamus in controlling sensory information (Keszthelyi et al., 2012; Labus et al., 2014) and displayed the activation when distending the rectum (Mayer et al., 2009). Neuroimaging studies depicted numerous functional abnormalities in the thalamus of the functional constipation patients, including the lower amplitude of low-frequency fluctuation in the female functional constipation patients and the decreased nodal degree based on the resting-state fMRI (Jin et al., 2019; Liu et al., 2021). Recently, a study that employed diffusion tensor imaging showed a decreased fractional anisotropy in the fibers communicating with the precentral gyrus, postcentral gyrus, amygdala, and hippocampus in patients with functional constipation, which may imply that the function of integrating the visceral sensory or motor inputs and connecting with other

brain regions was impaired in functional constipation patients (Al Omran and Aziz, 2014; Liu et al., 2021).

Currently, we identified that the expression of genes (*VWA3A*, *ZBBX*, *PTPRT*, *ASB2*, *PXYLP1*, *STAC2*, *ZNF385D*, *SMCO4*, *PTGIS*, *SATB2*, *HACL1*, *CSDC2*, *PCNT*, and *FOSB*) showed positive correlations with GMV difference, and the expression of genes (*ONECUT1*, *PDZD2*, *SLC15A3*, and *SLC17A6*) showed negative correlations. For example, there was a positive correlation for *SATB2*, encoding the special AT-rich sequence-binding protein 2, which is a known member of the AT-rich matrix attachment region-binding transcription factor family with a role in the central nervous system and craniofacial development (FitzPatrick et al., 2003; Britanova et al., 2005), also highly expressed and specific for colorectal origins (Magnusson et al., 2011). The more prominent expression of *SATB2* in brain samples with significant GMV decrease in functional constipation may be due to its aberrant expression influence on the brain–gut axis. In contrast, *SLC17A6* acted a negative correlation, i.e., the lower gene expression in brain samples manifested a more notable GMV decrease in functional constipation. *SLC17A6* is a protein-coding gene, also known as VGluT2, highly expressed in glutamatergic neurons. As a primary afferent neurotransmitter, glutamate transfers information from the mucosa to the enteric plexuses and brain. Changes in *SLC17A6* expression could indicate glutamatergic dysfunction in bowel disease (Tong et al., 2001). Even though the genes related to GMV changes in functional constipation is a backhanded technique, we accept that the strategy can suggest valuable discovery on account of such firsthand datasets lacking (Richiardi et al., 2015).

LIMITATIONS

Some limitations should be considered when interpreting our findings. First, we have not collected a larger sample of patients with functional constipation and healthy controls, which restricted the wide application and weakened the statistical robustness. Second, all the functional constipation patients that we enrolled had a history over 1 year, and their medications are different. Some patients only took healthcare products, while some took laxatives occasionally. In this study, we did not take into account the effect of medicines on the results. Third, genes with undetectable expression variation across individuals were omitted in such analysis, since the gene expression data and neuroimage data were acquired from different individuals. Finally, our study is experimental, and further, we should explore whether the identified genes have a causal influence on the altered GMV in functional constipation patients.

CONCLUSION

In brief, we performed transcriptional neuroimaging association to define the genes that appear to have correlation with GMV changes in functional constipation. The identified 18 genes, accordantly manifesting prominent relationships between GMV alterations in functional constipation and gene expression value, could be regarded as candidates to detect biological mechanisms of abnormality in functional constipation patients.

DATA AVAILABILITY STATEMENT

The original contributions presented in the study are included in the article/supplementary material, further inquiries can be directed to the corresponding author/s.

ETHICS STATEMENT

The studies involving human participants were reviewed and approved by the Ethical Committee of Shanghai Tenth People's Hospital. The patients/participants provided their written informed consent to participate in this study.

AUTHOR CONTRIBUTIONS

WC and YZ designed the research, analyzed the data, and wrote the manuscript. WC, LW, and RZ performed the research. WC, LW, RZ, and BY were involved in the clinical assessment. WC, YZ, TH, and JG processed part of the data. GT provided guidance and advice. All authors contributed to the article and approved the submitted version.

FUNDING

This study was funded by the National Natural Science Foundation of China (No. 81871325), Project of STCSM (20Y11911800 and 19411965300), and SCDSTC (CKY2021-41).

REFERENCES

Al Omran, Y., and Aziz, Q. (2014). Functional brain imaging in gastroenterology: to new beginnings. *Nat. Rev. Gastroenterol. Hepatol.* 11, 565–576. doi: 10.1038/nrgastro.2014.89

Alame, A. M., and Bahna, H. (2012). Evaluation of constipation. *Clin. Colon Rectal Surg.* 25, 5–11.

Arnatkeviciute, A., Fulcher, B. D., and Fornito, A. (2019). A practical guide to linking brain-wide gene expression and neuroimaging data. *Neuroimage* 189, 353–367. doi: 10.1016/j.neuroimage.2019.01.011

Blankstein, U., Chen, J., Diamant, N. E., and Davis, K. D. (2010). Altered brain structure in irritable bowel syndrome: potential contributions of pre-existing and disease-driven factors. *Gastroenterology* 138, 1783–1789. doi: 10.1053/j.gastro.2009.12.043

Bongers, M. E., van Dijk, M., Benninga, M. A., and Grootenhuis, M. A. (2009). Health related quality of life in children with constipation-associated fecal incontinence. *J. Pediatr.* 154, 749–753. doi: 10.1016/j.jpeds.2008.11.029

Britanova, O., Akopov, S., Lukyanov, S., Gruss, P., and Tarabykin, V. (2005). Novel transcription factor Satb2 interacts with matrix attachment region DNA elements in a tissue-specific manner and demonstrates cell-type-dependent

expression in the developing mouse CNS. *Eur. J. Neurosci.* 21, 658–668. doi: 10.1111/j.1460-9568.2005.03897.x

Derbyshire, S. W. (2003). A systematic review of neuroimaging data during visceral stimulation. *Am. J. Gastroenterol.* 98, 12–20. doi: 10.1111/j.1572-0241.2003.07168.x

Drossman, D. A. (2016). Functional gastrointestinal disorders: history, pathophysiology, clinical features and Rome IV. *Gastroenterology* 150, 1262–1279E2. doi: 10.1053/j.gastro.2016.02.032

Duan, S., Liu, L., Li, G., Wang, J., Hu, Y., Zhang, W., et al. (2021). Altered functional connectivity within and between salience and sensorimotor networks in patients with functional constipation. *Front. Neurosci.* 15:628880. doi: 10.3389/fnins.2021.628880

Emmanuel, A. V., Mason, H. J., and Kamm, M. A. (2001). Relationship between psychological state and level of activity of extrinsic gut innervation in patients with a functional gut disorder. *Gut* 49, 209–213. doi: 10.1136/gut.49.2.209

FitzPatrick, D. R., Carr, I. M., McLaren, L., Leek, J. P., Wightman, P., Williamson, K., et al. (2003). Identification of SATB2 as the cleft palate gene on 2q32-q33. *Hum. Mol. Genet.* 12, 2491–2501. doi: 10.1093/hmg/ddg248

Glia, A., and Lindberg, G. (1997). Quality of life in patients with different types of functional constipation. *Scand. J. Gastroenterol.* 32, 1083–1089. doi: 10.3109/00365529709002985

Guleria, A., Karyampudi, A., Singh, R., Khetrapal, C. L., Verma, A., Ghoshal, U. C., et al. (2017). Mapping of brain activations to rectal balloon distension stimuli in male patients with irritable bowel syndrome using functional magnetic resonance imaging. *J. Neurogastroenterol. Motil.* 23, 415–427. doi: 10.5056/jnm16148

Hawrylycz, M. J., Lein, E. S., Guillozet-Bongaarts, A. L., Shen, E. H., Ng, L., Miller, J. A., et al. (2012). An anatomically comprehensive atlas of the adult human brain transcriptome. *Nature* 489, 391–399. doi: 10.1038/nature11405

Hosseinzadeh, S. T., Poorsaadati, S., Radkani, B., and Forootan, M. (2011). Psychological disorders in patients with chronic constipation. *Gastroenterol. Hepatol. Bed Bench* 4, 159–163.

Hu, C., Liu, L., Liu, L., Zhang, J., Hu, Y., Zhang, W., et al. (2020). Cortical morphometry alterations in brain regions involved in emotional, motor-control and self-referential processing in patients with functional constipation. *Brain Imaging Behav.* 14, 1899–1907. doi: 10.1007/s11682-019-00133-4

Jin, Q., Duan, S., Li, G., Sun, L., Hu, Y., Hu, C., et al. (2019). Sex-related differences in resting-state brain activity and connectivity in the orbital frontal cortex and insula in patients with functional constipation. *Neurogastroenterol. Motil.* 31:e13566. doi: 10.1111/nmo.13566

Keszthelyi, D., Troost, F. J., and Masclee, A. A. (2012). Irritable bowel syndrome: methods, mechanisms, and pathophysiology. Methods to assess visceral hypersensitivity in irritable bowel syndrome. *Am. J. Physiol. Gastrointest. Liver Physiol.* 303, G141–G154. doi: 10.1152/ajpgi.00060.2012

Kringelbach, M. L., and Rolls, E. T. (2004). The functional neuroanatomy of the human orbitofrontal cortex: evidence from neuroimaging and neuropsychology. *Prog. Neurobiol.* 72, 341–372. doi: 10.1016/j.pneurobio.2004.03.006

Labus, J. S., Dinov, I. D., Jiang, Z., Ashe-McNalley, C., Zamanyan, A., Shi, Y., et al. (2014). Irritable bowel syndrome in female patients is associated with alterations in structural brain networks. *Pain* 155, 137–149. doi: 10.1016/j.pain.2013.09.020

Liu, L., Hu, C., Hu, Y., Zhang, W., Zhang, Z., Ding, Y., et al. (2021). Abnormalities in the thalamo-cortical network in patients with functional constipation. *Brain Imaging Behav.* 15, 630–642. doi: 10.1007/s11682-020-00273-y

Magnusson, K., de Wit, M., Brennan, D. J., Johnson, L. B., McGee, S. F., Lundberg, E., et al. (2011). SATB2 in combination with cytokeratin 20 identifies over 95% of all colorectal carcinomas. *Am. J. Surg. Pathol.* 35, 937–948. doi: 10.1097/PAS.0b013e31821c3dae

Marquis, P., De La Loge, C., Dubois, D., McDermott, A., and Chassany, O. (2005). Development and validation of the patient assessment of constipation quality of life questionnaire. *Scand. J. Gastroenterol.* 40, 540–551. doi: 10.1080/00365520510012208

Mayer, E. A., Aziz, Q., Coen, S., Kern, M., Labus, J. S., Lane, R., et al. (2009). Brain imaging approaches to the study of functional GI disorders: a Rome working team report. *Neurogastroenterol. Motil.* 21, 579–596. doi: 10.1111/j.1365-2982.2009.01304.x

Mayer, E. A., Naliboff, B. D., and Craig, A. D. (2006). Neuroimaging of the brain-gut axis: from basic understanding to treatment of functional GI disorders. *Gastroenterology* 131, 1925–1942. doi: 10.1053/j.gastro.2006.10.026

Mazur, M., Furgala, A., Jablonski, K., Mach, T., and Thor, P. (2012). Autonomic nervous system activity in constipation-predominant irritable bowel syndrome patients. *Med. Sci. Monit.* 18, CR493–CR499. doi: 10.12659/msm.883269

Mugie, S. M., Benninga, M. A., and Di Lorenzo, C. (2011). Epidemiology of constipation in children and adults: a systematic review. *Best Pract. Res. Clin. Gastroenterol.* 25, 3–18. doi: 10.1016/j.bpg.2010.12.010

Price, J. L. (2007). Definition of the orbital cortex in relation to specific connections with limbic and visceral structures and other cortical regions. *Ann. N. Y. Acad. Sci.* 1121, 54–71. doi: 10.1196/annals.1401.008

Richiardi, J., Altmann, A., Milazzo, A. C., Chang, C., Chakravarty, M. M., Banaschewski, T., et al. (2015). BRAIN NETWORKS. Correlated gene expression supports synchronous activity in brain networks. *Science* 348, 1241–1244.

Ringel, Y. (2002). Brain research in functional gastrointestinal disorders. *J. Clin. Gastroenterol.* 35(1 Suppl), S23–S25.

Rolls, E. T. (2019). The orbitofrontal cortex and emotion in health and disease, including depression. *Neuropsychologia* 128, 14–43. doi: 10.1016/j.neuropsychologia.2017.09.021

Rolls, E. T., and Grabenhorst, F. (2008). The orbitofrontal cortex and beyond: from affect to decision-making. *Prog. Neurobiol.* 86, 216–244. doi: 10.1016/j.pneurobio.2008.09.001

Rouiller, E. M., Tanne, J., Moret, V., and Boussaoud, D. (1999). Origin of thalamic inputs to the primary, premotor, and supplementary motor cortical areas and to area 46 in macaque monkeys: a multiple retrograde tracing study. *J. Comp. Neurol.* 409, 131–152. doi: 10.1002/(sici)1096-9861(19990621)409:1<131::aid-cne10>3.0.co;2-a

Sherman, S. M. (2017). Functioning of circuits connecting thalamus and cortex. *Compr. Physiol.* 7, 713–739. doi: 10.1002/cphy.c160032

Tillisch, K., Mayer, E. A., and Labus, J. S. (2011). Quantitative meta-analysis identifies brain regions activated during rectal distension in irritable bowel syndrome. *Gastroenterology* 140, 91–100. doi: 10.1053/j.gastro.2010.07.053

Tong, Q., Ma, J., and Kirchgessner, A. L. (2001). Vesicular glutamate transporter 2 in the brain-gut axis. *Neuroreport* 12, 3929–3934. doi: 10.1097/00001756-200112210-00015

Waters, A. M., Schilpzand, E., Bell, C., Walker, L. S., and Baber, K. (2013). Functional gastrointestinal symptoms in children with anxiety disorders. *J. Abnorm. Child Psychol.* 41, 151–163.

Zhu, Q., Cai, W., Zheng, J., Li, G., Meng, Q., Liu, Q., et al. (2016). Distinct resting-state brain activity in patients with functional constipation. *Neurosci. Lett.* 632, 141–146. doi: 10.1016/j.neulet.2016.08.042

Zung, W. W. (1965). A self-rating depression scale. *Arch. Gen. Psychiatry* 12, 63–70.

Zung, W. W. (1971). A rating instrument for anxiety disorders. *Psychosomatics* 12, 371–379. doi: 10.1016/S0033-3182(71)71479-0

Conflict of Interest: The authors declare that the research was conducted in the absence of any commercial or financial relationships that could be construed as a potential conflict of interest.

Publisher's Note: All claims expressed in this article are solely those of the authors and do not necessarily represent those of their affiliated organizations, or those of the publisher, the editors and the reviewers. Any product that may be evaluated in this article, or claim that may be made by its manufacturer, is not guaranteed or endorsed by the publisher.

frontiers in Neuroscience

CORRECTION
published: 15 March 2022
doi: 10.3389/fnins.2022.878535

Corrigendum: Transcriptomic Signatures Associated With Gray Matter Volume Changes in Patients With Functional Constipation

Wangli Cai[1†], Yujing Zhou[2†], Lidi Wan[1], Ruiling Zhang[1], Ting Hua[1], Jian Gong[1], Bo Yang[3] and Guangyu Tang[1]*

[1] Department of Radiology, Shanghai Tenth People's Hospital, School of Clinical Medicine of Nanjing Medical University, Shanghai, China, [2] Department of Radiology, The First Affiliated Hospital of Dalian Medical University, Dalian, China, [3] Department of Colorectal and Anal Surgery, Shanghai Tenth People's Hospital, School of Clinical Medicine of Nanjing Medical University, Shanghai, China

Keywords: functional constipation, Allen Human Brain Atlas, gene expression analysis, gray matter volume, imaging-genetics

OPEN ACCESS

Approved by:
Frontiers Editorial Office, Frontiers Media SA, Switzerland

***Correspondence:**
Guangyu Tang
tgy17@126.com

[†]These authors have contributed equally to this work

Specialty section:
This article was submitted to Brain Imaging Methods, a section of the journal Frontiers in Neuroscience

Received: *18 February 2022*
Accepted: *21 February 2022*
Published: *15 March 2022*

Citation:
Cai W, Zhou Y, Wan L, Zhang R, Hua T, Gong J, Yang B and Tang G (2022) Corrigendum: Transcriptomic Signatures Associated With Gray Matter Volume Changes in Patients With Functional Constipation. Front. Neurosci. 16:878535. doi: 10.3389/fnins.2022.878535

A Corrigendum on

Transcriptomic Signatures Associated With Gray Matter Volume Changes in Patients With Functional Constipation

by Cai, W., Zhou, Y., Wan, L., Zhang, R., Hua, T., Gong, J., Yang, B., and Tang, G. (2022). Front. Neurosci. 15:791831. doi: 10.3389/fnins.2021.791831

In the published article, there was an error in affiliations 1 and 3. For affiliation 1, instead of "Department of Radiology, School of Clinical Medicine, Shanghai Tenth People's Hospital, Nanjing Medical University, Shanghai, China," it should be "Department of Radiology, Shanghai Tenth People's Hospital, School of Clinical Medicine of Nanjing Medical University, Shanghai, China." For affiliation 3, instead of "Department of Colorectal and Anal Surgery, School of Clinical Medicine, Shanghai Tenth People's Hospital, Nanjing Medical University, Shanghai, China," it should be "Department of Colorectal and Anal Surgery, Shanghai Tenth People's Hospital, School of Clinical Medicine of Nanjing Medical University, Shanghai, China."

The authors apologize for this error and state that this does not change the scientific conclusions of the article in any way. The original article has been updated.

frontiers in Neuroscience

ORIGINAL RESEARCH
published: 10 January 2022
doi: 10.3389/fnins.2021.794151

Dynamic Functional Connectivity Alterations and Their Associated Gene Expression Pattern in Autism Spectrum Disorders

Lin Ma[1†], Tengfei Yuan[1†], Wei Li[2†], Lining Guo[1], Dan Zhu[1,3], Zirui Wang[1], Zhixuan Liu[1], Kaizhong Xue[1], Yaoyi Wang[1], Jiawei Liu[1], Weiqi Man[1], Zhaoxiang Ye[2], Feng Liu[1*] and Junping Wang[1*]*

[1] *Department of Radiology and Tianjin Key Laboratory of Functional Imaging, Tianjin Medical University General Hospital, Tianjin, China,* [2] *Department of Radiology, Tianjin Medical University Cancer Institute and Hospital, National Clinical Research Center for Cancer, Key Laboratory of Cancer Prevention and Therapy, Tianjin's Clinical Research Center for Cancer, Tianjin, China,* [3] *Department of Radiology, Tianjin Medical University General Hospital Airport Hospital, Tianjin, China*

OPEN ACCESS

Edited by:
Javier Gonzalez-Castillo, National Institute of Mental Health, National Institutes of Health (NIH), United States

Reviewed by:
Lauren Kupis, University of California, Los Angeles, United States
Nataliia Kozhemiako, Brigham and Women's Hospital and Harvard Medical School, United States

***Correspondence:**
Zhaoxiang Ye
yezhaoxiang@163.com
Feng Liu
fengliu@tmu.edu.cn
Junping Wang
wangjunping_tj@163.com

[†] These authors have contributed equally to this work

Specialty section:
This article was submitted to Brain Imaging Methods, a section of the journal Frontiers in Neuroscience

Received: *13 October 2021*
Accepted: *16 December 2021*
Published: *10 January 2022*

Citation:
Ma L, Yuan T, Li W, Guo L, Zhu D, Wang Z, Liu Z, Xue K, Wang Y, Liu J, Man W, Ye Z, Liu F and Wang J (2022) Dynamic Functional Connectivity Alterations and Their Associated Gene Expression Pattern in Autism Spectrum Disorders. Front. Neurosci. 15:794151. doi: 10.3389/fnins.2021.794151

Autism spectrum disorders (ASDs) are a group of heterogeneous neurodevelopmental disorders that are highly heritable and are associated with impaired dynamic functional connectivity (DFC). However, the molecular mechanisms behind DFC alterations remain largely unknown. Eighty-eight patients with ASDs and 87 demographically matched typical controls (TCs) from the Autism Brain Imaging Data Exchange II database were included in this study. A seed-based sliding window approach was then performed to investigate the DFC changes in each of the 29 seeds in 10 classic resting-state functional networks and the whole brain. Subsequently, the relationships between DFC alterations in patients with ASDs and their symptom severity were assessed. Finally, transcription-neuroimaging association analyses were conducted to explore the molecular mechanisms of DFC disruptions in patients with ASDs. Compared with TCs, patients with ASDs showed significantly increased DFC between the right dorsolateral prefrontal cortex (DLPFC) and left fusiform/lingual gyrus, between the DLPFC and the superior temporal gyrus, between the right frontal eye field (FEF) and left middle frontal gyrus, between the FEF and the right angular gyrus, and between the left intraparietal sulcus and the right middle temporal gyrus. Moreover, significant relationships between DFC alterations and symptom severity were observed. Furthermore, the genes associated with DFC changes in ASDs were identified by performing gene-wise across-sample spatial correlation analysis between gene expression extracted from six donors' brain of the Allen Human Brain Atlas and case-control DFC difference. In enrichment analysis, these genes were enriched for processes associated with synaptic signaling and voltage-gated ion channels and calcium pathways; also, these genes were highly expressed in autistic disorder, chronic alcoholic intoxication and several disorders related to depression. These results not only demonstrated higher DFC in patients with ASDs but also provided novel insight into the molecular mechanisms underlying these alterations.

Keywords: Allen Human Brain Atlas, transcriptome, autism spectrum disorders, neuroimaging, dynamic functional connectivity

INTRODUCTION

Autism spectrum disorders (ASDs) are a group of heterogeneous neurodevelopmental disorders characterized by social communication defects, stereotyped behaviors and restricted interests or activities (Lai et al., 2014). The increasing global prevalence of ASDs in recent years is consistent across different data sources (Morales-Hidalgo et al., 2018). Neuroimaging techniques have been used to characterize the complex biomarkers of these disorders and a great deal of evidence supports the aberrant functional connectivity (FC) of various cortical networks. However, most previous studies used traditional "static" approaches based on resting-state functional magnetic resonance imaging (rs-fMRI) to describe the abnormal FC in individuals with ASDs (Kennedy and Courchesne, 2008; Assaf et al., 2010; Rudie et al., 2012; Di Martino et al., 2014). An increasing body of evidence suggests that rs-fMRI data are dynamic in essence (Hutchison et al., 2013; Allen et al., 2014), and static functional connectivity (SFC) does not clearly show the changes that occur over a short period of time during the scan (Chang and Glover, 2010). It has been proposed that quantifying changes in FC metrics over time may provide greater insight into fundamental properties of brain networks. Recently, researchers have conducted more dynamic functional connectivity (DFC) studies (Liu et al., 2017; Preti et al., 2017; Du et al., 2018). Briefly, the BOLD signals in rs-fMRI time series were divided into some overlapping intervals, and a functional correlation matrix was derived for each of these intervals. It was possible to track the ongoing changes in FC between brain regions over time (Betzel et al., 2016; Shakil et al., 2016).

There are a few studies investigating DFC in individuals with ASDs. For example, Li et al. (2020) revealed higher DFC between the posterior cingulate cortex (PCC) and middle temporal pole in patients with ASDs than in typical controls (TCs). Chen et al. (2017) demonstrated increased DFC in the medial superior frontal gyrus and temporal pole in patients with ASDs. Harlalka et al. (2019) also observed significantly higher DFC between the attention network (AN) and the default mode network (DMN) in patients with ASDs than in TCs. However, these previous studies only performed within or between network DFC analysis, which does not provide comprehensive information on DFC changes in ASDs. Specifically, DFC analysis within a given network only provides a series of relationships between a given region and all other voxels within its network, instead of the full pattern of whole-brain dynamic connections. Likewise, DFC analysis between network only reveals patterns of connectivity between these networks without taking into account internal FC.

Recently, several studies found correlations between DFC and symptom severity, but in the opposite direction. He et al. (2018) found that decreased DFC between the PCC and right precentral gyrus was negatively associated with social motivation scores. However, Chen et al. (2017) found that greater DFC was positively related to Autism Diagnostic Observation Schedule (ADOS) total score in patients with ASDs. Li et al. (2020) also found that the increased DFC between the PCC and pars opercularis of the inferior frontal gyrus was positively associated with Social Responsiveness Scale (SRS) total raw scores, social awareness and cognition scores. Further exploration of the relationship between DFC and symptom severity may provide more insights into the pathophysiological mechanisms of ASDs.

Although the recent studies have found atypical DFC in patients with ASDs, questions remain about the genetic mechanisms of higher DFC. Barber et al. (2021) examined the heritability of rs-fMRI data of healthy young adults from the Human Connectome Project and found that heritability was moderate and tended to be higher for DFC than for SFC. Epidemiological studies have shown that patients with ASDs have high heritability, twin studies evaluating the heritability of ASDs showed high concordance rates (up to 90%) in monozygotic twins (Freitag, 2007), and common genetic variations account for approximately 50% of the genetic risk for ASDs (Gaugler et al., 2014). In the past few years, transcription-neuroimaging association analyses have emerged as a popular and powerful strategy for investigating the molecular basis of brain imaging phenotypes (Fornito et al., 2019). To the best of our knowledge, there have been no studies using such approach to identify genes related to alterations of brain DFC patterns in patients with ASDs.

In the current study, rs-fMRI data from Autism Brain Imaging Data Exchange II (ABIDE II) were used, and 29 core seeds of 10 classic functional networks were selected to perform sliding-window seed-to-whole-brain DFC analyses in a comprehensive manner. Moreover, the relationships between significant DFC changes and symptom severity were further explored in patients with ASDs. Furthermore, transcription-neuroimaging association analyses were conducted to explore the molecular mechanisms of the DFC alterations in patients with ASDs by leveraging the Allen Human Brain Atlas (AHBA) database. On the basis of the findings of the previous studies, we hypothesized that: (1) patients with ASDs have significantly increased DFC; (2) there are positive relationship between DFC alterations and severity of symptoms; and (3) there are correlations between DFC alterations and gene expression. An organized workflow diagram of our study is summarized in **Figure 1**.

MATERIALS AND METHODS

Participants

The ASDs patient and TCs data used in this study were downloaded from the ABIDE II project (Di Martino et al., 2014, 2017), and all experimental procedures were approved by the local Institutional Review Board. The subject inclusion criteria were as follows: (1) male only, as the prevalence of ASDs has a strong male bias (Pisula and Porebowicz-Dorsmann, 2017); (2) strong right-handedness; (3) TR = 2 s, for consistency in the temporal scale (Li et al., 2020); (4) younger 18 years old, due to the greater effects of intervention on brain plasticity in children and adolescents (Dawson, 2008; Van Hecke et al., 2015); (5) subjects with Full Scale Intelligence Quotient (FIQ) within 2 standard deviation (SD) of overall ABIDE sample mean;

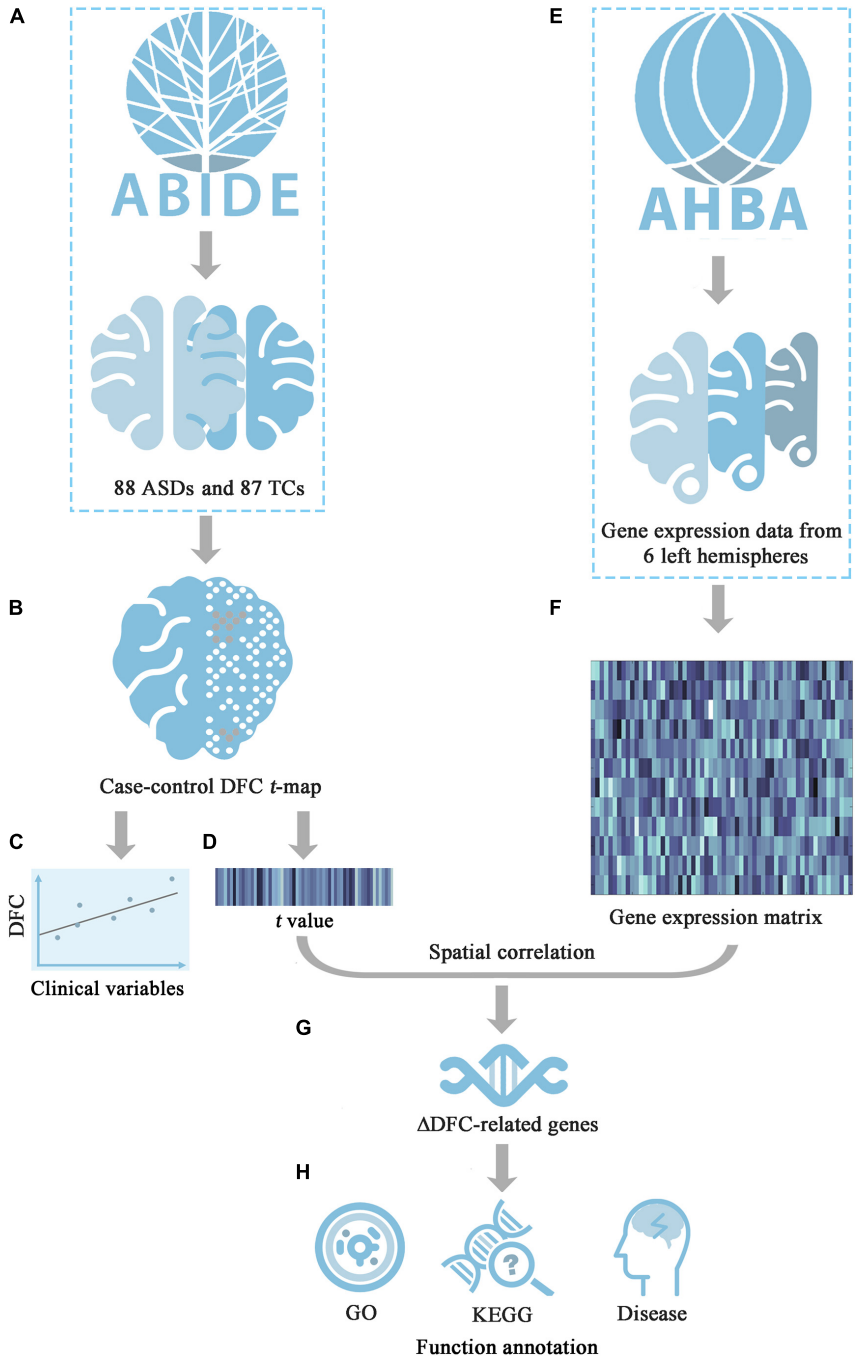

FIGURE 1 | The workflow diagram of this study. **(A)** Download rs-fMRI data of ASDs and TCs groups from ABIDE II; **(B)** Calculate case-control DFC *t*-map; **(C)** Investigate the relationship between the DFC values in areas with significant group differences and symptom severity; **(D)** Extract the mean *t* value of each tissue sample; **(E)** Obtain the whole-genomic transcriptomic profiles in tissue samples from AHBA; **(F)** Generate the sample-wise gene expression matrix of six donors; **(G)** Identify ΔDFC-related genes by calculating cross-sample spatial correlation between gene expression and ΔDFC; **(H)** Functional annotations for ΔDFC-related genes, including GO, KEGG and disease enrichment analysis. ABIDE, Autism Brain Imaging Data Exchange; AHBA, Allen Human Brain Atlas; DFC, dynamic functional connectivity; GO, gene ontology; KEGG, Kyoto encyclopedia of genes and genomes; *t*, *t*-statistic.

(6) subjects with mean framewise displacement (FD) (Power et al., 2012) not exceeding 2 SD above the sample mean; (7) availability of both structural and functional images that provide complete whole-brain coverage with successful segmentation, good registration and good image quality; and (8) sites with at least 10 subjects in each group after meeting the above criteria (Di Martino et al., 2014). Finally, 88 patients with ASDs and 87 TCs were included in our study; the number of the subjects

excluded due to each of the exclusion criteria is shown in **Supplementary Figure 1**. The detailed demographic information of each site (**Supplementary Table 1**) and MRI acquisition parameters are summarized in the **Supplementary Materials**. For more information, see http://fcon_1000.projects.nitrc.org/indi/abide/.

The ADOS is a tool that can be used by clinical doctor to perform a standardized clinical observation of a child (Lord et al., 2012), and comprises two behavioral domains: restricted and repetitive behaviors and social affect. The SRS is a parent-report quantitative assessment scale (Bruni, 2014), and designed to evaluate children's social deficits. SRS provides a total score and separate scores for five subdomains, including social awareness, social cognition, social communication, social motivation, and autistic mannerisms. Separate scores of each domain would provide a clearer picture of ASDs dimensions. These tools offer distinct information from different sources and perspectives (Duvekot et al., 2015), and the complementary information contributed to acquire a comprehensive view of the characteristics of ASDs. The ADOS and SRS scores can be used to assess the severity of symptoms related to ASDs, and higher scores indicate more severe ASD symptoms (Plitt et al., 2015; Chen et al., 2019; Li et al., 2020).

Magnetic Resonance Imaging Data Pre-processing

Both structural and functional images of all the subjects were examined independently by two researchers, and all images were reoriented to the anterior–posterior commissure line. Functional images were pre-processed using the Data Processing and Analysis for Brain Imaging (DPABI)[1] toolbox (Yan et al., 2016). Specifically, the first five volumes of each subject were removed to allow the signal to reach equilibrium. Slice timing and realignment were then performed to correct the temporal differences between slices and head motion. The mean FD was calculated based on head motion parameters (Van Dijk et al., 2012), and subjects with mean FD > 0.5 were excluded (no subjects were excluded in this step). Next, individual structural images were co-registered to the mean motion-corrected functional images, the transformed structural images were segmented into gray matter (GM), white matter (WM), and cerebrospinal fluid (CSF), and the motion-corrected functional images were normalized spatially to the standard Montreal Neurological Institute (MNI) space using the normalization parameters estimated by the Diffeomorphic Anatomical Registration Through Exponentiated Lie algebra (DARTEL) (Ashburner, 2007) tool and resampled to 3 mm cubic voxels. Subsequently, nuisance covariates [including linear trend, Friston-24 head motion parameters (Friston et al., 1996) and mean signals from WM and CSF] were regressed out, and temporal bandpass filtering (0.01–0.08 Hz) was applied. Finally, the functional images were spatially smoothed with an 8 mm full-width at half-maximum Gaussian kernel.

Resting State Network Selection and Dynamic Functional Connectivity Calculation

Based on prior studies (Damoiseaux et al., 2006; Mantini et al., 2007; Power et al., 2010; van den Heuvel and Hulshoff Pol, 2010; Zuo et al., 2010; Allen et al., 2011), 29 core seeds within 10 classic brain networks were selected as regions of interest (ROIs) in this study. Specifically, spherical regions with radius of 6 mm centered at the MNI coordinates served as the ROIs. These regions were as follows: (1) the AN: bilateral superior temporal gyrus (STG) (Albouy et al., 2013); (2) the central executive network (CEN): bilateral dorsolateral prefrontal cortex (DLPFC) and bilateral posterior parietal cortex (Denkova et al., 2019); (3) the dorsal attention network (DAN): bilateral frontal eye field (FEF) and bilateral intraparietal sulcus (IPS) (McCarthy et al., 2013); (4) the DMN: medial prefrontal cortex and PCC (Fox et al., 2005); (5) the dorsal visual network: bilateral superior occipital gyrus (Shen et al., 2019); (6) the primary visual network: calcarine fissure (Shen et al., 2019); (7) the sensorimotor network: bilateral precentral gyrus, bilateral postcentral gyrus and bilateral supplementary motor area (Behroozmand et al., 2015); (8) the salience network: dorsal anterior cingulate cortex and bilateral frontoinsular cortex (Denkova et al., 2019); (9) the ventral attention network: bilateral orbitofrontal cortex and bilateral temporoparietal junction (Majerus et al., 2012); and (10) the ventral visual network (VVN): calcarine gyri (Shen et al., 2019). The detailed MNI coordinates and the spatial distribution of these ROIs are shown in **Supplementary Table 2** and **Supplementary Figure 2**, respectively.

To calculate the whole-brain resting-state DFC map of each ROI, a widely used sliding-window approach was adopted. First, as suggested by previous studies (Li et al., 2019; Christiaen et al., 2020), a window length of 50 TRs (100 s) and a step size of 1 TR (2 s) were employed to obtain windowed time series. Second, in each window, the whole-brain DFC map for each ROI was created for each subject by calculating Pearson's correlation coefficient between the mean time series of all voxels in the ROI and the time series from all other brain voxels in the GM. Third, Fisher's r-to-z transformation was applied for all DFC maps to improve the normality of the correlation distribution. Finally, the SD map across time windows was calculated in each subject to characterize the changes in individual ROI-to-whole-brain DFC, which is a commonly used metric in previous DFC studies (Falahpour et al., 2016; Kaiser et al., 2016; Harlalka et al., 2019; Xue et al., 2020).

A ComBat approach[2], which can remove intersite variation, preserve biological variability, and is robust to small sample size data, was utilized to harmonize individual DFC maps from the five independent datasets (Fortin et al., 2017). Subsequently, a voxel-wise general linear model was used to compare the DFC maps of each ROI between the ASDs and TCs groups while controlling for age, FIQ and mean FD. The Gaussian random-field (GRF) method was used to correct for multiple comparisons of the resulting statistical map with significant thresholds of voxel

[1] http://rfmri.org/dpabi

[2] https://github.com/Jfortin1/ComBatHarmonization

level $p < 0.001$ and cluster level $p < 0.0017$ (0.05/29 ROIs). Furthermore, linear regression analyses were conducted to assess the relationship between the DFC from significant clusters of between-group comparison and symptom severity in patients with ASDs with age, FIQ, and mean FD as nuisance covariates.

Gene Expression Data Processing

Gene expression data were obtained from the AHBA. The AHBA comprises the normalized expression data of 20737 genes represented by 58692 probes taken from 3702 brain tissue samples from six donors (one female and five males, aged 24–57 years) (Hawrylycz et al., 2012). According to the pipeline (Arnatkeviciute et al., 2019), the gene expression data preprocessing steps included (1) gene information reannotation, (2) data filtering, (3) probe selection, (4) sample assignment, (5) gene filtering, and (6) accounting for spatial effects. Given that all donors provided tissue samples from the left hemisphere but only two donors provided samples from the right hemisphere, tissue samples from the left hemisphere were used in the following analyses. In addition, consistent with previous studies (Kang et al., 2011; Fan et al., 2016), we restricted our analyses to the cerebral cortex due to the substantial differences in the gene expression patterns of the cerebral cortex, subcortex, and cerebellum. Finally, we obtained a normalized gene expression matrix of 1285 × 10185 (sample × gene). The detailed preprocessing steps are described in **Supplementary Material**, and the process of brain tissue samples selection is presented in **Supplementary Figure 3**.

Transcription-Neuroimaging Association Analysis

For each of the *t*-maps that survived from multiple comparisons, the mean *t* value of the spherical region with a 6 mm radius centered at the MNI coordinate of each tissue sample was extracted based on the uncorrected case-control DFC *t*-maps, and the mean *t* value was defined as the ΔDFC of the sample. Then, a gene-wise across-sample spatial correlation was performed to explore the correlation between gene expression and ΔDFC in patients with ASDs. Multiple comparison correction was performed using the Benjamini-Hochberg false discovery rate (BH-FDR) method ($q < 0.05$), and the surviving genes were defined as ΔDFC-related genes.

Functional annotations of the identified ΔDFC-related genes of each ROI were created with the WEB-based WebGestalt Toolkit (Zhang et al., 2005)[3], which includes Gene Ontology (GO) (enriching genes for specific biological processes, cellular components and molecular functions) (Ashburner et al., 2000) and Kyoto Encyclopedia of Genes and Genomes (KEGG) (identifying genes associated with specific biological pathways) databases (Kanehisa et al., 2004). In addition, DisGeNET, which contains one of the largest publicly available datasets of genes and variants associated with human diseases (Pinero et al., 2017), was used to enrich the ΔDFC-related genes for specific neurodegenerative and neuropsychiatric diseases. The intersection of enriched pathways that the identified ΔDFC-related genes of each ROI for were considered to be stably related to the genetic mechanisms of abnormal DFC patterns in patients with ASDs.

[3]http://www.webgestalt.org/

Validation Analyses

To verify the robustness of our main findings, we performed the following three experiments.

First, we performed validation analyses for different window sizes (30 TRs and 70 TRs). We investigated whether the results (including those of between-group DFC comparisons, DFC-symptom severity associations and ΔDFC-related gene identification) of 50 TRs could be reproducible in other window sizes.

Second, we calculated the whole-brain resting-state SFC map of each ROI to compare with the DFC results. For each subject, the whole-brain SFC map for each ROI was created by calculating Pearson's correlation coefficient between the mean time series of all voxels in the ROI and the time series from all other brain voxels in the GM. Then, Fisher's *r*-to-*z* transformation was applied for all SFC maps to improve the normality of the correlation distribution. The subsequent procedures were the same as those mentioned above in the DFC analysis.

Third, although the mean FD was regressed out using general linear model when examining the DFC changes, we could only control the linear effect of the head motion. To further investigate whether the increased DFC is linked to the higher head motion in ASDs, a median split based on FD in both ASD and TC groups was performed and DFC were compared in the subgroups of ASD and TC.

RESULTS

Demographic Information and Clinical Characteristics

In this study, 88 patients with ASDs and 87 TCs from 5 research sites met the inclusion criteria. In the ASDs group, 61 subjects had ADOS-2 scores and 69 subjects had SRS scores; In the TCs group, no subject had ADOS-2 scores and 71 subjects had SRS scores. The two groups were matched for age and FIQ. There were significant differences in mean FD, ADOS, and SRS total score and all subscale scores. The detailed demographic and clinical information of the participants is displayed in **Table 1**.

Case-Control Dynamic Functional Connectivity Differences

We found that patients with ASDs exhibited significantly increased DFC between the right DLPFC of the CEN and the left fusiform gyrus (FFG)/lingual gyrus (LG), and between the right DLPFC of the CEN and the left STG; significantly increased DFC between the right FEF of the DAN and the left middle frontal gyrus (MFG), and between the right FEF of the DAN and the right angular gyrus (AG); and significantly increased DFC between the left IPS of the DAN and the right middle temporal gyrus (MTG) compared with the TCs [GRF corrected, voxel level

TABLE 1 | Demographic and clinical information of the participants.

Variables	ASDs ($n = 88$) (Mean ± SD)	TCs ($n = 87$) (Mean ± SD)	p value
Age (years)	(5.43–17.93) 11.30 ± 2.68	(5.90–17.60) 11.30 ± 2.65	0.987
FIQ	112.43 ± 13.85	114.69 ± 12.50	0.259
Mean FD	0.115 ± 0.073	0.090 ± 0.054	0.012
ADOS-2 calibrated severity total score	6.87 ± 2.15 ($n = 61$)	–	–
SRS total score	89.00 ± 29.51 ($n = 69$)	19.80 ± 13.55 ($n = 71$)	<0.001
SRS subscale score (raw)			
Awareness	11.71 ± 3.94	4.30 ± 2.72	<0.001
Cognition	15.90 ± 5.9	2.66 ± 2.56	<0.001
Communication	30.23 ± 11.01	6.37 ± 5.32	<0.001
Motivation	14.61 ± 5.77	4.14 ± 3.26	<0.001
Mannerisms	16.55 ± 7.39	2.34 ± 3.00	<0.001

ADOS, Autism Diagnostic Observation Schedule; ASDs, autism spectrum disorders; FD, framewise displacement; FIQ, Full-scale Intelligence Quotient; SCQ, Social Communication Questionnaire; SD, standard deviation; SRS, Social Responsiveness Scale; TCs, typical controls.
p values were obtained by two-sample t-tests; –, not available.

$p < 0.001$ and cluster level $p < 0.0017$ (0.05/29 ROIs)] (**Figure 2**). There was no significantly decreased DFC in the patients with ASDs compared with the TCs. Detailed information on the brain regions with significant ΔDFC in the patients with ASDs is presented in **Table 2**. The uncorrected case-control *t*-maps for the 29 core seeds in 10 classic resting state networks shown in **Supplementary Figures 4–13**.

Correlations Between ΔDFC and Symptom Severity

As illustrated in **Figure 3**, the DFC of the right DLPFC with left STG were positively correlated with ADOS-2 calibrated severity total score in the patients with ASDs. In addition, the DFC of the right DLPFC with the left STG was positively correlated with the SRS social awareness score, social communication score, autism mannerisms score and total scores in the patients with ASDs. The DFC of the right FEF with the left MFG was positively correlated with the SRS social awareness score, social communication score and total scores in the patients with ASDs.

Transcription-Neuroimaging Association Analysis

Gene-wise across-sample spatial correlation analysis was performed between ΔDFC [three significant *t*-maps, with the three seeds (the right DLPFC, right FEF and left IPS)] and gene expression. After multiple comparison correction (BH-FDR $q < 0.05$), 6803, 2722, and 1217 genes survived, respectively. Subsequently, gene functional annotation analysis was performed on the ΔDFC-related genes in the three groups.

Gene Ontology enrichment analysis showed that the ΔDFC-related genes were significantly enriched for the biological process of neurotransmitter secretion, neurotransmitter transport, the cellular component of ion channel complexes and synaptic membranes, and molecular function of voltage-gated ion channel activity. KEGG enrichment analysis revealed that the ΔDFC-related genes were significantly enriched in the calcium signaling pathway. In the disease-related enrichment analyses, the ΔDFC-related genes were significantly enriched for autistic disorder, chronic alcoholic intoxication, several disorders related to depression and non-organic psychosis. Please see the detailed results of enrichment analysis in **Figures 4–6**.

Validation Results

Our results showed high reproducibility across the different window sizes. We found that the brain regions with significant group differences (50 TRs) in DFC remained significantly different between the ASDs and TCs groups for both 30 TR and 70 TR windows. Moreover, we observed highly similar results in the correlation analyses of the DFC values in areas with significant group differences and symptom severity across the three window sizes. Moreover, the significantly enriched pathways (50 TRs) were largely reproducible for 30 TR and 70 TR windows. Please see the detailed results in **Supplementary Figures 14–17**. We found no significant difference in SFC in the patients with ASDs compared with the TCs. In addition, the direction of effect (higher DFC in ASDs) in these comparisons of subgroups with a median split based on FD was consistent with our main results (**Supplementary Table 3** and **Supplementary Figure 18**).

DISCUSSION

In this study, we assessed the DFC alterations among the 29 core seeds of 10 classic resting-state networks and the whole brain in patients with ASDs compared with TCs and calculated the correlation between the DFC values in areas with significant group differences and symptom severity in patients with ASDs. In patients with ASDs, we observed significantly increased DFC between the right DLPFC (the core seed of the CEN) and the left FFG/LG, between the right DLPFC and the left STG; between the right FEF (the core seed of the DAN) and the left MFG, between the right FEF and the right AG, and between the left IPS (the core seed of the DAN) and the right MTG.

High DFC could lead to the instability of information transfer within and between networks (Kung et al., 2019). The DLPFC is a core region in the CEN and is responsible for subjective

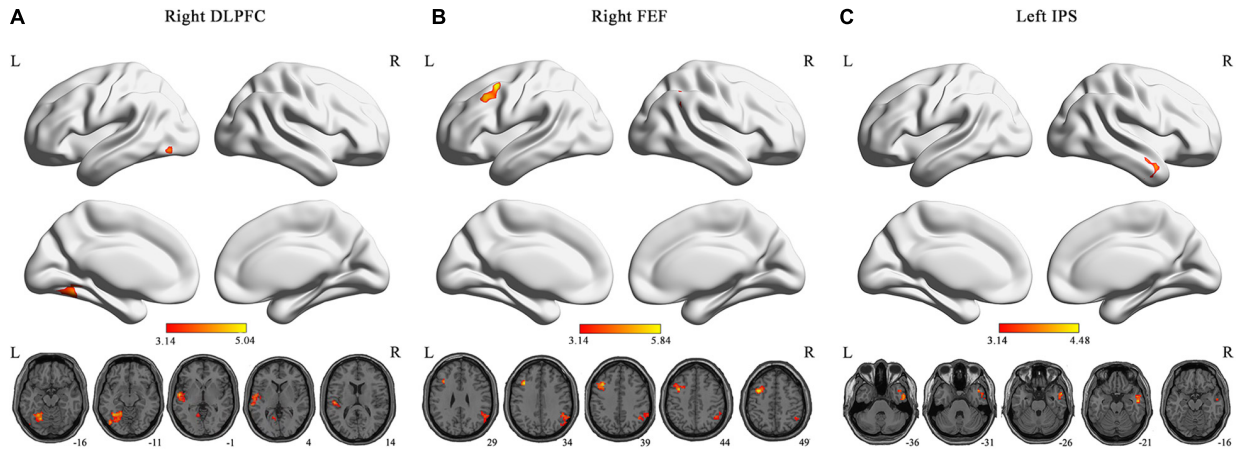

FIGURE 2 | Brain regions with significant DFC alterations. The brain regions exhibited significant DFC alterations (GRF-corrected $p < 0.0017$) with the right DLPFC **(A)** of CEN, and the right FEF **(B)** and left IPS **(C)** of DAN in the patients with ASDs, respectively. The color bar represents *t*-statistic. DLPFC, dorsolateral prefrontal cortex; FEF, frontal eye field; IPS, intraparietal sulcus; L, left; R, right.

feelings, self-awareness, emotion regulation, working memory, executive functions and the judgment and decision making under goal-directed behavior (Bunge et al., 2001; Craig, 2002; Bressler and Menon, 2010). The FFG and LG are key regions in the VVN that are associated with visual item identification, such as face recognition, memory for visual item identity and planning a response to potentially threatening stimuli (Slotnick and Schacter, 2006; Jonas et al., 2015; Li et al., 2016). The increased DFC between the CEN and VVN may be related to the loss of emotional regulation and social interaction impairment in patients with ASDs (Li et al., 2016; Bi et al., 2018). The MFG is also a core region in the CEN and is mainly responsible for integrating and processing information (Richeson et al., 2003; Bi et al., 2018). Previous studies have suggested that individuals with ASDs are unable to integrate and process information; therefore, they cannot communicate normally with others (Bi et al., 2018). We speculated that the increased DFC between the CEN and DAN may be associated with communication defects in patients with ASDs.

Frontal eye field and IPS are core regions in the DAN that are involved in mediating many higher-order cognitive tasks and supporting top-down attention to visual, auditory and somatosensory inputs (Braga et al., 2013; McCarthy et al., 2013; Xia et al., 2015; Rohr et al., 2017). The AG is an important part of the DMN, which is implicated in social cognition and affective regulation associated with empathic responses (Li et al., 2013, 2016; Vatansever et al., 2017). The increased DFC between the DAN and DMN might lead to deficits in attention switching and cognitive function in patients with ASDs (Jia et al., 2020; Meeker et al., 2021). The STG and MTG are crucial regions in the AN that are associated with auditory language, visual language and emotion (Li et al., 2013; Orlov et al., 2018; Luan et al., 2019). The increased DFC between the CEN/DAN and AN may be related to social interaction impairment in patients with ASDs. Similar to our findings, some studies observed no significant difference in SFC between the ASDs and TCs groups (Chen et al., 2015; Li et al., 2020). No significant difference has been observed in the SFC analyses, which is partially because DFC can capture the time-varying properties and seems to be more sensitive than SFC (Li et al., 2020).

In the correlation analyses between the DFC and symptom severity in patients with ASDs, we observed positive correlations between the DFC of the right DLPFC (core seed of the CEN) and the left STG (core seed of the AN) and ADOS-2 calibrated severity total score. ASDs is characterized by socio-communicational deficits and restricted and repetitive behaviors. Higher severity total score indicates more severe ASDs symptoms. Functional alterations of CEN have previously been reported in ASDs (Perez Velazquez et al., 2009). Alterations of the AN in ASDs are associated with the severity of autistic core symptom (Watanabe and Rees, 2016). The AN is mainly involved with lower-level perception (Power et al., 2011). The CEN controls attention, integrates the information processed in the other networks and plays a central role in various cognitive functions (Chadick and Gazzaley, 2011; Zanto and Gazzaley, 2013). The higher DFC between the DLPFC and STG could cause unstable transmission and impaired coupling between these

TABLE 2 | Detailed information on the brain regions with significant ΔDFC in the patients with ASDs (GRF-corrected $p < 0.0017$).

ROIs	Region	MNI coordinates (x, y, z)	Cluster size	Peak *T*
R DLPFC	L FFG/LG	−36, −57, −12	286	4.604
	L STG	−63, −27, 6	235	5.041
R FEF	R AG	60, −57, 27	168	4.166
	L MFG	−36, 21, 36	178	5.839
L IPS	R MTG	54, −6, −21	146	4.476

AG, angular gyrus; DLPFC, dorsolateral prefrontal cortex; FEF, frontal eye field; FFG, fusiform gyrus; IPS, intraparietal sulcus; L, left; LG, lingual gyrus; MFG, middle frontal gyrus; MNI, Montreal Neurological Institute; MTG, middle temporal gyrus; R, right; ROIs, regions of interest; STG, superior temporal gyrus; T, t-statistic.

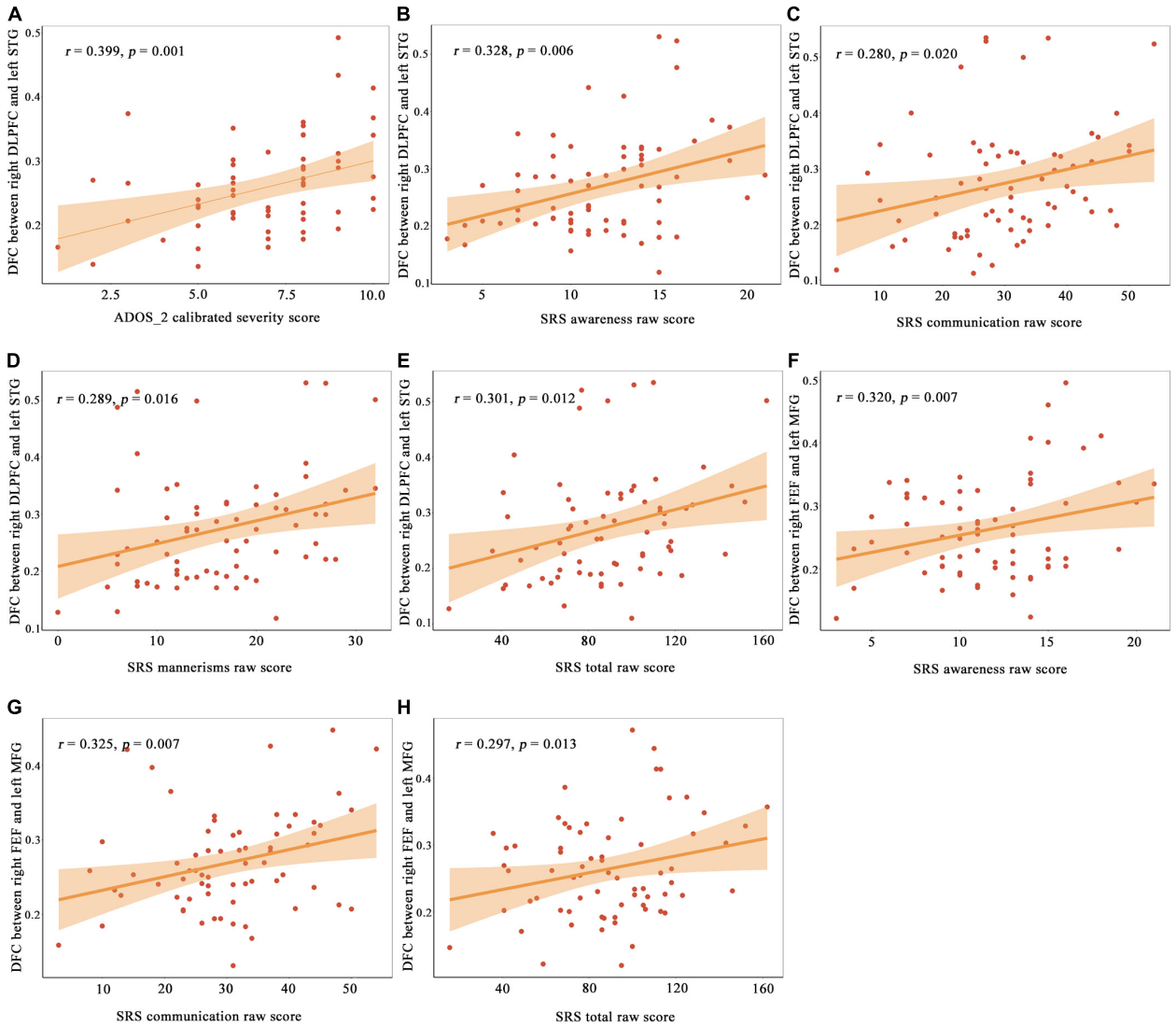

FIGURE 3 | The correlation between the DFC of the right DLPFC with the left STG and with ADOS_2 calibrated severity score **(A)**, SRS awareness raw score **(B)**, SRS communication raw score **(C)**, SRS mannerisms raw score **(D)** and SRS total raw score **(E)**. The correlation between the DFC of the right FEF with the left MFG and with SRS awareness raw score **(F)**, SRS communication raw score **(G)** and SRS total raw score **(H)**. Shades represent the 95% confidence intervals. ADOS, Autism Diagnostic Observation Schedule; DLPFC, dorsolateral prefrontal cortex; FEF, frontal eye field; FFG, fusiform gyrus; LG, lingual gyrus; MFG, middle frontal gyrus; SRS, Social Responsiveness Scale; STG, superior temporal gyrus; *p*, uncorrected *p* value.

brain regions. In addition, underconnectivity theory proposes that both the two core symptoms of ASDs are associated with impairment of integration of global information (Kana et al., 2011; Just et al., 2012). Therefore, the higher DFC between the DLPFC and STG observed in our study might cause the more severe ASDs symptoms.

Additionally, we observed a positive correlation between the DFC of the right DLPFC with the left STG and with the patients' SRS social awareness score, social communication score, autism mannerisms score and total score. We also revealed a positive correlation between the DFC of the right FEF with the left MFG and with the patients' SRS social awareness score, social communication score and total score. Social awareness contributes to one's ability to recognize and understand the thinking or feeling of others (Li et al., 2020), social communication is one's capability to respond appropriately to what others interpret (He et al., 2018), and autism mannerisms describe a collection of stereotypical behaviors or restricted interests (Plitt et al., 2015). The higher DFC between the DLPFC (core seed of the CEN) and STG (core seed of the AN) indicated unstable information transmission (Chen et al., 2017) and might influence auditory attention, semantic fluency,

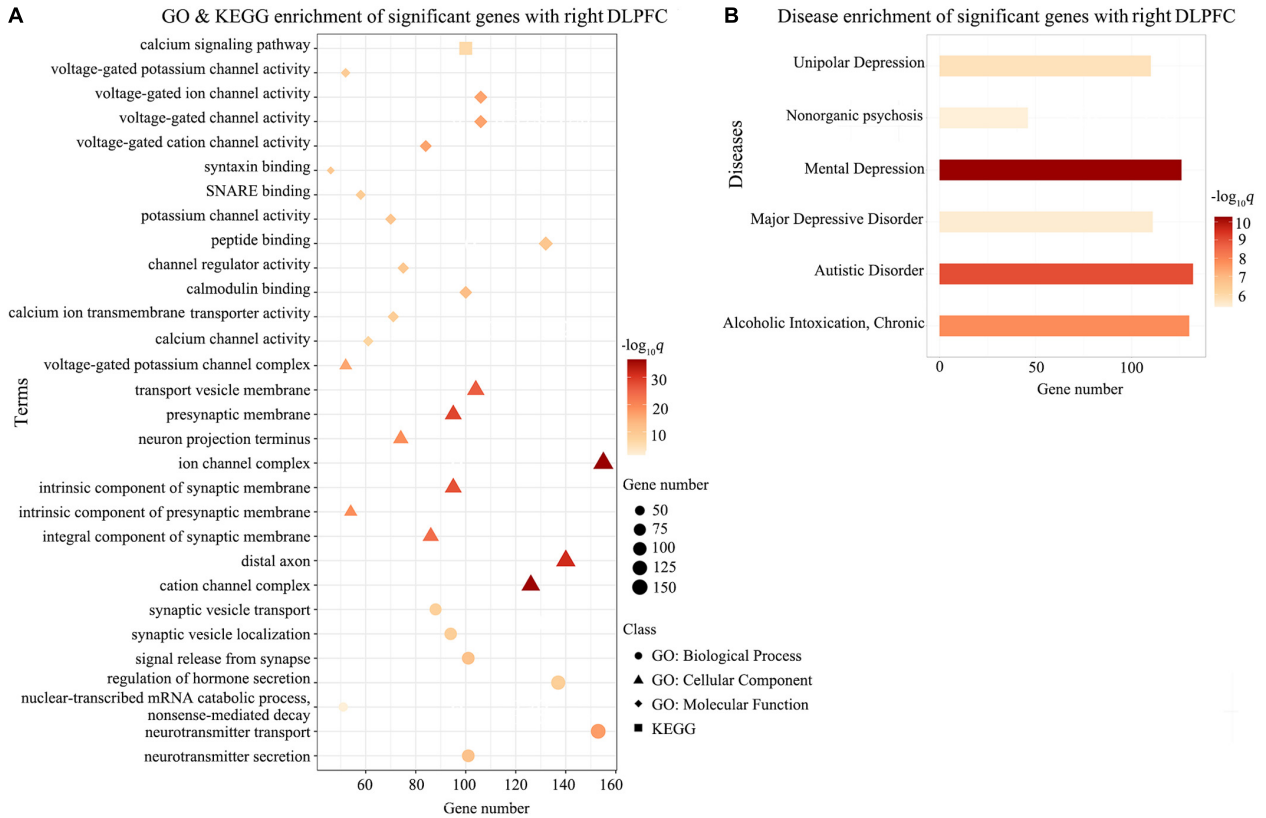

FIGURE 4 | Enrichment analysis for ΔDFC-related genes with the right DLPFC in CEN. The GO and KEGG enrichment analysis **(A)** and the disease enrichment analysis **(B)** for ΔDFC-related genes with the right DLPFC in CEN in the patients with ASDs. The color bars represent $-\log_{10}q$ with BH-FDR correction, and the size of circles (GO: biological processes), triangles (GO: cellular component), rhombus (GO: molecular functions), and squares (KEGG terms) represents the overlapping gene number. DLPFC, dorsolateral prefrontal cortex; GO, Gene Ontology; KEGG, Kyoto Encyclopedia of Genes and Genomes.

the learning of social cues and the integration of appropriate social responses. Furthermore, we found that the DFC between the right FEF (core seed of the DAN) and the left MFG (key region of the CEN) was positively correlated with the SRS social awareness score, social communication score and total score. Both the CEN and DAN are involved in cognitive regulation and may be related to social awareness. Individuals with ASDs cannot communicate normally with others due to deficits in integrating and processing information, and the MFG is mainly responsible for integrating and processing information (Richeson et al., 2003; Bi et al., 2018). This important detail may explain the positive correlation among the DFC of the right FEF-left MFG, the patient's SRS social awareness score, and the patient's communication score.

Overall, the ΔDFC-related genes were mainly enriched for voltage-gated ion channels, especially calcium and potassium channels, synaptic membranes and the related processes involved in the release and transmission of neurotransmitters. Voltage-gated ion channels are important mediators of physiological functions in the central nervous system. Activation of these channels influences neurotransmitter release, neuronal excitability, gene transcription, and plasticity. Ion channels, especially polymorphisms in calcium and potassium channels, are related to the pathogenesis of ASDs (Imbrici et al., 2013). Moreover, calcium signaling is ubiquitously involved in the process of neuronal excitability, neurotransmitter release and cell secretion (Schmunk et al., 2017). Genetic mutations related to the calcium signaling pathway can elevate the risk of developing ASDs (Cross-Disorder Group of the Psychiatric Genomics Consortium, 2013). Membrane proteins are significant components of the proteins in cells and play a key role in synaptic transmission; also, disruption of synaptic membrane components may influence synaptic signaling transmission (Wang et al., 2021). Abnormalities in synapse formation, which contribute to functional and cognitive impairments, play a vital role in the pathological mechanism of ASDs (Bourgeron, 2007). Neurotransmitters can transmit nerve impulses from neurons to other cells. Neurotransmitter transport dysfunction can affect the transmission and absorption of neurotransmitters (Bhat et al., 2021), and abnormalities in the balance between excitatory and inhibitory neurotransmission may be connected with the etiology of ASDs (Horder et al., 2018).

In the disease-related enrichment analyses, the ΔDFC-related genes were enriched for autistic disorder, chronic alcoholic intoxication, several disorders related to depression and non-organic psychosis. Upon initiation of alcohol use, individuals

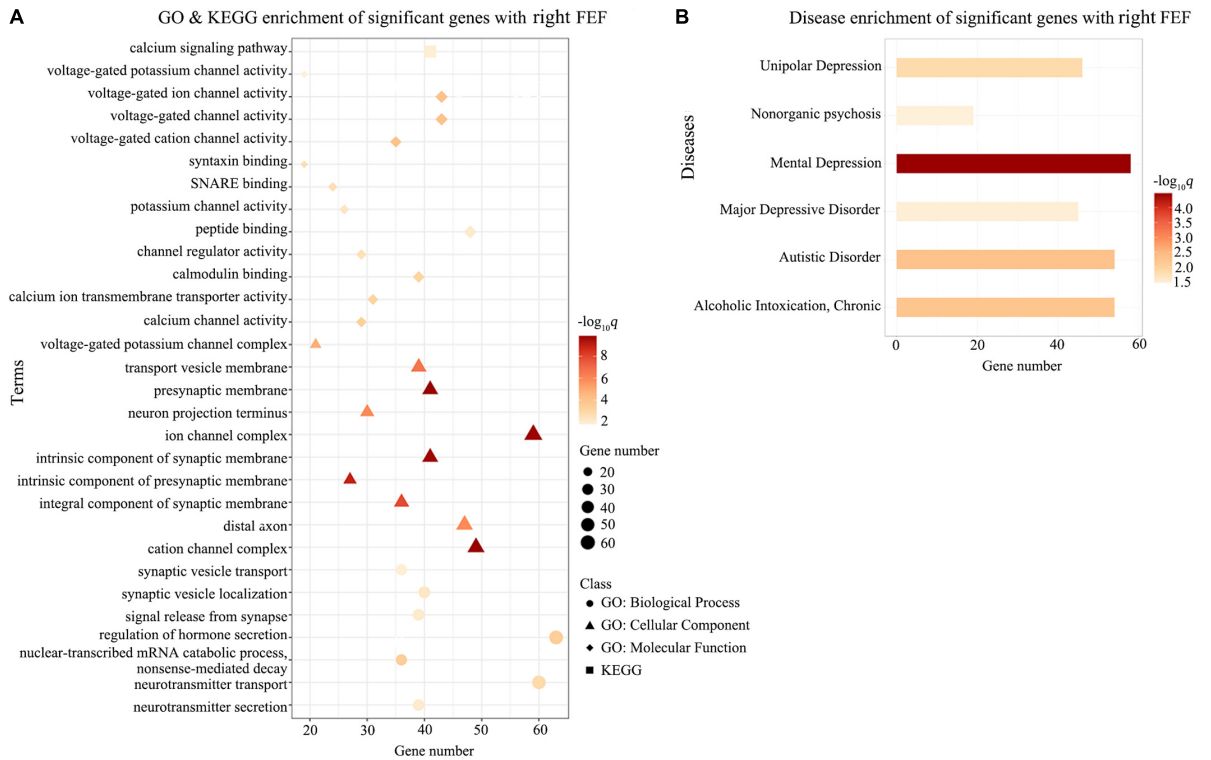

FIGURE 5 | Enrichment analysis for ΔDFC-related genes with the right FEF in DAN. The GO and KEGG enrichment analysis **(A)** and the disease enrichment analysis **(B)** for ΔDFC-related genes with the right FEF in DAN in the patients with ASDs. The color bars represent $-\log_{10}q$ with BH-FDR correction, and the size of circles (GO: biological processes), triangles (GO: cellular component), rhombus (GO: molecular functions), and squares (KEGG terms) represents the overlapping gene number. FEF, frontal eye field; GO, Gene Ontology; KEGG, Kyoto Encyclopedia of Genes and Genomes.

with ASDs were at higher risk for developing alcohol dependence (Sizoo et al., 2010). Studies have shown an increased risk for depression symptoms in children and adolescents with ASDs who had various IQs (Strang et al., 2012). Individuals with ASDs are associated with a substantially increased risk for non-affective psychotic disorder (NAPD) and bipolar disorder; notably, non-organic psychosis was the most commonly diagnosed subtype of NAPD among individuals with ASDs (Selten et al., 2015). Deficits in social interactions and emotion regulation in individuals with ASDs may be associated with elevated rates of psychiatric comorbidity (Pouw et al., 2013; Charlton et al., 2020).

Several limitations should be considered in this study. First, compared with single-site studies, the use of multicenter public imaging data in this study may have involved some issues associated with scanner differences and inconsistency assessments. Second, head motion was a confounding factor in DFC analyses. To reduce this effect, we carried out a series of procedures, including regressing 24 head motion parameters in the data pre-processing, and controlling for mean FD in group-comparisons (Yan et al., 2013). However, the effect of motion cannot be completely ruled out. In the future, it would be better to recruit subjects with matched head motion to replicate the findings. Third, although many dynamic metrics could be used to investigate DFC, we employed SD of FC values across time windows to characterize DFC because it was difficult to calculate other dynamic metrics due to the highly computational burden. Further study is needed to calculate other dynamic metrics of seed-based voxel-level DFC by using high-performance computing systems. Fourth, the results about the genes expressed in autistic disorder, chronic alcoholic intoxication and disorders related to depression were obtained from the disease enrichment analysis, the detailed information about these conditions of the autism patients included in our study was not provided by ABIDE database. Fifth, we did not include female subjects or investigate the sex-related effects in this study due to the highly male-biased sex ratios in ABIDE. Sixth, the weaker associations between DFC and symptom severity in patients with ASDs may be related to the relatively small sample size. Seventh, the average *t*-statistics were extracted around the location of AHBA tissue samples; however, the uneven spatial distribution of tissue samples in the AHBA may influence our results. Finally, in our study, the imaging and gene expression data were not derived from the same subjects. However, many studies have confirmed that genes involved in the regulation of transcription and development across human populations are highly conserved (Bejerano et al., 2004; Woolfe et al., 2005); therefore, our results of transcription-neuroimaging association studies should be reliable.

In conclusion, the patients with ASDs showed increased DFC in brain areas related to attentional and cognitive regulation,

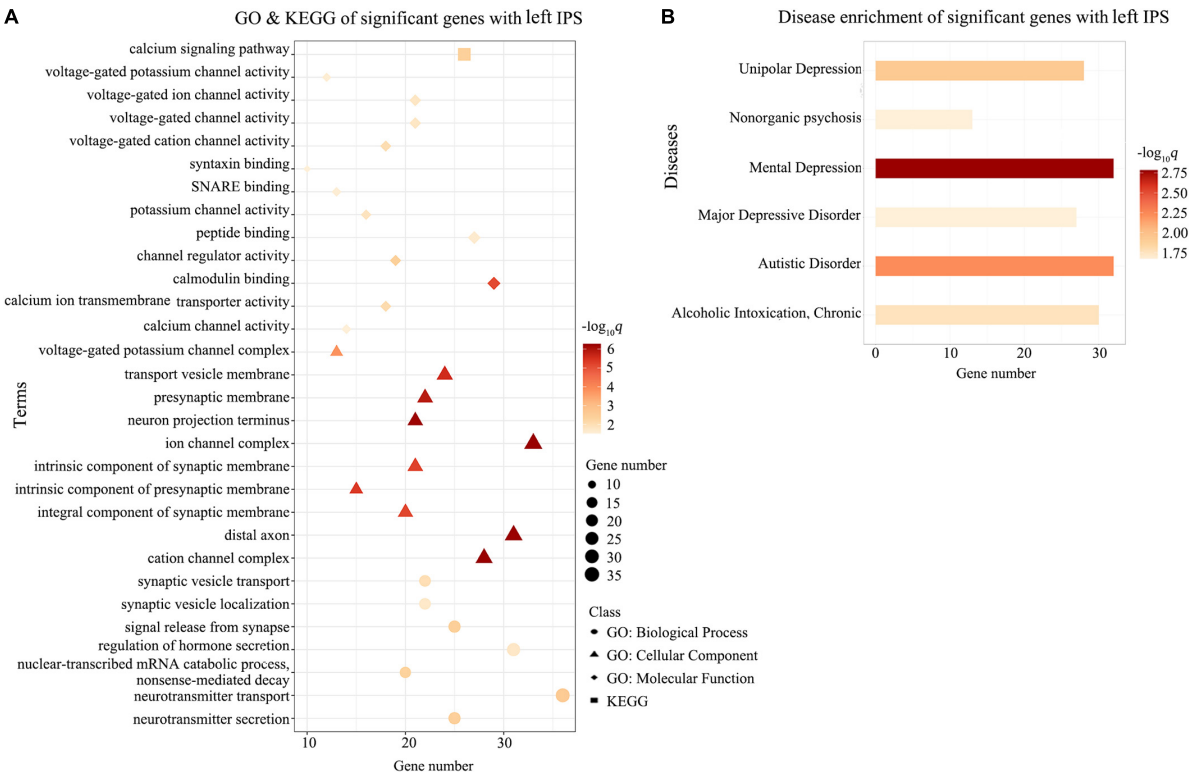

FIGURE 6 | Enrichment analysis for ΔDFC-related genes with the left IPS in DAN. The GO and KEGG enrichment analysis **(A)** and the disease enrichment analysis **(B)** for ΔDFC-related genes with the left IPS in DAN in the patients with ASDs. The color bars represent $-\log_{10}q$ with BH-FDR correction, and the size of circles (GO: biological processes), triangles (GO: cellular component), rhombus (GO: molecular functions), and squares (KEGG terms) represents the overlapping gene number. GO, Gene Ontology; IPS, intraparietal sulcus; KEGG, Kyoto Encyclopedia of Genes and Genomes.

which were associated with symptom severity. Transcription-neuroimaging association analyses identified ΔDFC-related genes, especially those involved in processes associated with synaptic signaling, voltage-gated ion channels, neurotransmitter secretion and transport. These findings provide more insight into the polygenetic and multipathway molecular mechanisms of functional impairments in patients with ASDs.

DATA AVAILABILITY STATEMENT

The original contributions presented in the study are included in the article/**Supplementary Material**, further inquiries can be directed to the corresponding author/s.

ETHICS STATEMENT

Ethical review and approval were not required for the current study in accordance with the local legislation and institutional requirements. All research procedures and ethical guidelines pertaining to the existing datasets were approved by the local Institutional Review Board of each participating institution (Di Martino et al., 2014, 2017). Written informed consent to participate in these previous studies was provided by the participants' legal guardian/next of kin.

AUTHOR CONTRIBUTIONS

JW, FL, and ZY designed the research and provided the guidance for the study. LM, TY, and WL processed the images and analyzed the data. LG, DZ, and ZW visualized the results. ZL, KX, and YW checked the data quality. JL and WM modified the language. LM wrote the initial draft. All authors read and approved the final manuscript.

FUNDING

This work was supported by National Natural Science Foundation of China (grant numbers: 81871431, 82171905, and 82072001) and Natural Science Foundation of Tianjin Municipal Science and Technology Commission (grant number: 18JCYBJC26300).

SUPPLEMENTARY MATERIAL

The Supplementary Material for this article can be found online at: https://www.frontiersin.org/articles/10.3389/fnins.2021.794151/full#supplementary-material

REFERENCES

Albouy, P., Mattout, J., Bouet, R., Maby, E., Sanchez, G., Aguera, P. E., et al. (2013). Impaired pitch perception and memory in congenital amusia: the deficit starts in the auditory cortex. *Brain* 136(Pt 5), 1639–1661. doi: 10.1093/brain/awt082

Allen, E. A., Damaraju, E., Plis, S. M., Erhardt, E. B., Eichele, T., and Calhoun, V. D. (2014). Tracking whole-brain connectivity dynamics in the resting state. *Cereb Cortex* 24, 663–676. doi: 10.1093/cercor/bhs352

Allen, E. A., Erhardt, E. B., Damaraju, E., Gruner, W., Segall, J. M., Silva, R. F., et al. (2011). A baseline for the multivariate comparison of resting-state networks. *Front. Syst. Neurosci.* 5:2. doi: 10.3389/fnsys.2011.00002

Arnatkeviciute, A., Fulcher, B. D., and Fornito, A. (2019). A practical guide to linking brain-wide gene expression and neuroimaging data. *Neuroimage* 189, 353–367. doi: 10.1016/j.neuroimage.2019.01.011

Ashburner, J. (2007). A fast diffeomorphic image registration algorithm. *Neuroimage* 38, 95–113. doi: 10.1016/j.neuroimage.2007.07.007

Ashburner, M., Ball, C. A., Blake, J. A., Botstein, D., Butler, H., Cherry, J. M., et al. (2000). Gene ontology: tool for the unification of biology. The gene ontology consortium. *Nat. Genet.* 25, 25–29. doi: 10.1038/75556

Assaf, M., Jagannathan, K., Calhoun, V. D., Miller, L., Stevens, M. C., Sahl, R., et al. (2010). Abnormal functional connectivity of default mode sub-networks in autism spectrum disorder patients. *Neuroimage* 53, 247–256. doi: 10.1016/j.neuroimage.2010.05.067

Barber, A. D., Hegarty, C. E., Lindquist, M., and Karlsgodt, K. H. (2021). Heritability of functional connectivity in resting state: assessment of the dynamic mean, dynamic variance, and static connectivity across networks. *Cereb Cortex* 31, 2834–2844. doi: 10.1093/cercor/bhaa391

Behroozmand, R., Shebek, R., Hansen, D. R., Oya, H., Robin, D. A., Howard, M. A. III, et al. (2015). Sensory-motor networks involved in speech production and motor control: an fMRI study. *Neuroimage* 109, 418–428. doi: 10.1016/j.neuroimage.2015.01.040

Bejerano, G., Pheasant, M., Makunin, I., Stephen, S., Kent, W. J., Mattick, J. S., et al. (2004). Ultraconserved elements in the human genome. *Science* 304, 1321–1325. doi: 10.1126/science.1098119

Betzel, R. F., Fukushima, M., He, Y., Zuo, X. N., and Sporns, O. (2016). Dynamic fluctuations coincide with periods of high and low modularity in resting-state functional brain networks. *Neuroimage* 127, 287–297. doi: 10.1016/j.neuroimage.2015.12.001

Bhat, S., El-Kasaby, A., Freissmuth, M., and Sucic, S. (2021). Functional and biochemical consequences of disease variants in neurotransmitter transporters: a special emphasis on folding and trafficking deficits. *Pharmacol. Ther.* 222:107785. doi: 10.1016/j.pharmthera.2020.107785

Bi, X. A., Zhao, J., Xu, Q., Sun, Q., and Wang, Z. (2018). Abnormal functional connectivity of resting state network detection based on linear ICA analysis in autism spectrum disorder. *Front. Physiol.* 9:475. doi: 10.3389/fphys.2018.00475

Bourgeron, T. (2007). The possible interplay of synaptic and clock genes in autism spectrum disorders. *Cold Spring Harb. Symp. Quant. Biol.* 72, 645–654. doi: 10.1101/sqb.2007.72.020

Braga, R. M., Wilson, L. R., Sharp, D. J., Wise, R. J., and Leech, R. (2013). Separable networks for top-down attention to auditory non-spatial and visuospatial modalities. *Neuroimage* 74, 77–86. doi: 10.1016/j.neuroimage.2013.02.023

Bressler, S. L., and Menon, V. (2010). Large-scale brain networks in cognition: emerging methods and principles. *Trends Cogn. Sci.* 14, 277–290. doi: 10.1016/j.tics.2010.04.004

Bruni, T. P. (2014). Test review: social responsiveness scale–Second edition (SRS-2). *J. Psychoeducat. Assess.* 32, 365–369.

Bunge, S. A., Ochsner, K. N., Desmond, J. E., Glover, G. H., and Gabrieli, J. D. (2001). Prefrontal regions involved in keeping information in and out of mind. *Brain* 124(Pt 10), 2074–2086. doi: 10.1093/brain/124.10.2074

Chadick, J. Z., and Gazzaley, A. (2011). Differential coupling of visual cortex with default or frontal-parietal network based on goals. *Nat. Neurosci.* 14, 830–832. doi: 10.1038/nn.2823

Chang, C., and Glover, G. H. (2010). Time-frequency dynamics of resting-state brain connectivity measured with fMRI. *Neuroimage* 50, 81–98. doi: 10.1016/j.neuroimage.2009.12.011

Charlton, A. S., Smith, I. C., Mazefsky, C. A., and White, S. W. (2020). The role of emotion regulation on co-occurring psychopathology in emerging adults with ASD. *J. Autism. Dev. Disord.* 50, 2585–2592. doi: 10.1007/s10803-019-03983-5

Chen, C. M., Yang, P., Wu, M. T., Chuang, T. C., and Huang, T. Y. (2019). Deriving and validating biomarkers associated with autism spectrum disorders from a large-scale resting-state database. *Sci. Rep.* 9:9043. doi: 10.1038/s41598-019-45465-9

Chen, H., Nomi, J. S., Uddin, L. Q., Duan, X., and Chen, H. (2017). Intrinsic functional connectivity variance and state-specific under-connectivity in autism. *Hum. Brain Mapp.* 38, 5740–5755. doi: 10.1002/hbm.23764

Chen, S., Kang, J., and Wang, G. (2015). An empirical Bayes normalization method for connectivity metrics in resting state fMRI. *Front. Neurosci.* 9:316. doi: 10.3389/fnins.2015.00316

Christiaen, E., Goossens, M. G., Descamps, B., Larsen, L. E., Boon, P., Raedt, R., et al. (2020). Dynamic functional connectivity and graph theory metrics in a rat model of temporal lobe epilepsy reveal a preference for brain states with a lower functional connectivity, segregation and integration. *Neurobiol. Dis.* 139:104808. doi: 10.1016/j.nbd.2020.104808

Craig, A. D. (2002). How do you feel? Interoception: the sense of the physiological condition of the body. *Nat. Rev. Neurosci.* 3, 655–666. doi: 10.1038/nrn894

Cross-Disorder Group of the Psychiatric Genomics Consortium (2013). Identification of risk loci with shared effects on five major psychiatric disorders: a genome-wide analysis. *Lancet* 381, 1371–1379. doi: 10.1016/S0140-6736(12)62129-1

Damoiseaux, J. S., Rombouts, S. A., Barkhof, F., Scheltens, P., Stam, C. J., Smith, S. M., et al. (2006). Consistent resting-state networks across healthy subjects. *Proc. Natl. Acad. Sci. U.S.A.* 103, 13848–13853. doi: 10.1073/pnas.0601417103

Dawson, G. (2008). Early behavioral intervention, brain plasticity, and the prevention of autism spectrum disorder. *Dev. Psychopathol.* 20, 775–803. doi: 10.1017/S0954579408000370

Denkova, E., Nomi, J. S., Uddin, L. Q., and Jha, A. P. (2019). Dynamic brain network configurations during rest and an attention task with frequent occurrence of mind wandering. *Hum. Brain Mapp.* 40, 4564–4576. doi: 10.1002/hbm.24721

Di Martino, A., O'Connor, D., Chen, B., Alaerts, K., Anderson, J. S., Assaf, M., et al. (2017). Enhancing studies of the connectome in autism using the autism brain imaging data exchange II. *Sci. Data* 4:170010. doi: 10.1038/sdata.2017.10

Di Martino, A., Yan, C. G., Li, Q., Denio, E., Castellanos, F. X., Alaerts, K., et al. (2014). The autism brain imaging data exchange: towards a large-scale evaluation of the intrinsic brain architecture in autism. *Mol. Psychiatry* 19, 659–667. doi: 10.1038/mp.2013.78

Du, Y., Fu, Z., and Calhoun, V. D. (2018). Classification and prediction of brain disorders using functional connectivity: promising but challenging. *Front. Neurosci.* 12:525. doi: 10.3389/fnins.2018.00525

Duvekot, J., van der Ende, J., Verhulst, F. C., and Greaves-Lord, K. (2015). The screening accuracy of the parent and teacher-reported social responsiveness scale (SRS): comparison with the 3Di and ADOS. *J. Autism. Dev. Disord.* 45, 1658–1672. doi: 10.1007/s10803-014-2323-3

Falahpour, M., Thompson, W. K., Abbott, A. E., Jahedi, A., Mulvey, M. E., Datko, M., et al. (2016). Underconnected, but not broken? dynamic functional connectivity MRI shows underconnectivity in autism is linked to increased intra-individual variability across time. *Brain Connect* 6, 403–414. doi: 10.1089/brain.2015.0389

Fan, L., Li, H., Zhuo, J., Zhang, Y., Wang, J., Chen, L., et al. (2016). The human brainnetome atlas: a new brain atlas based on connectional architecture. *Cereb. Cortex* 26, 3508–3526. doi: 10.1093/cercor/bhw157

Fornito, A., Arnatkeviciute, A., and Fulcher, B. D. (2019). Bridging the gap between connectome and transcriptome. *Trends Cogn. Sci.* 23, 34–50. doi: 10.1016/j.tics.2018.10.005

Fortin, J. P., Parker, D., Tunc, B., Watanabe, T., Elliott, M. A., Ruparel, K., et al. (2017). Harmonization of multi-site diffusion tensor imaging data. *Neuroimage* 161, 149–170. doi: 10.1016/j.neuroimage.2017.08.047

Fox, M. D., Snyder, A. Z., Vincent, J. L., Corbetta, M., Van Essen, D. C., and Raichle, M. E. (2005). The human brain is intrinsically organized into dynamic, anticorrelated functional networks. *Proc. Natl. Acad. Sci. U.S.A.* 102, 9673–9678. doi: 10.1073/pnas.0504136102

Freitag, C. M. (2007). The genetics of autistic disorders and its clinical relevance: a review of the literature. *Mol. Psychiatry* 12, 2–22. doi: 10.1038/sj.mp.4001896

Friston, K. J., Williams, S., Howard, R., Frackowiak, R. S., and Turner, R. (1996). Movement-related effects in fMRI time-series. *Magn. Reson. Med.* 35, 346–355. doi: 10.1002/mrm.1910350312

Gaugler, T., Klei, L., Sanders, S. J., Bodea, C. A., Goldberg, A. P., Lee, A. B., et al. (2014). Most genetic risk for autism resides with common variation. *Nat. Genet.* 46, 881–885. doi: 10.1038/ng.3039

Harlalka, V., Bapi, R. S., Vinod, P. K., and Roy, D. (2019). Atypical flexibility in dynamic functional connectivity quantifies the severity in autism spectrum disorder. *Front. Hum. Neurosci.* 13:6. doi: 10.3389/fnhum.2019.00006

Hawrylycz, M. J., Lein, E. S., Guillozet-Bongaarts, A. L., Shen, E. H., Ng, L., Miller, J. A., et al. (2012). An anatomically comprehensive atlas of the adult human brain transcriptome. *Nature* 489, 391–399. doi: 10.1038/nature11405

He, C., Chen, Y., Jian, T., Chen, H., Guo, X., Wang, J., et al. (2018). Dynamic functional connectivity analysis reveals decreased variability of the default-mode network in developing autistic brain. *Autism. Res.* 11, 1479–1493. doi: 10.1002/aur.2020

Horder, J., Petrinovic, M. M., Mendez, M. A., Bruns, A., Takumi, T., Spooren, W., et al. (2018). Glutamate and GABA in autism spectrum disorder-a translational magnetic resonance spectroscopy study in man and rodent models. *Transl. Psychiatry* 8:106. doi: 10.1038/s41398-018-0155-1

Hutchison, R. M., Womelsdorf, T., Allen, E. A., Bandettini, P. A., Calhoun, V. D., Corbetta, M., et al. (2013). Dynamic functional connectivity: promise, issues, and interpretations. *Neuroimage* 80, 360–378. doi: 10.1016/j.neuroimage.2013.05.079

Imbrici, P., Camerino, D. C., and Tricarico, D. (2013). Major channels involved in neuropsychiatric disorders and therapeutic perspectives. *Front. Genet* 4:76. doi: 10.3389/fgene.2013.00076

Jia, X., Xie, Y., Dong, D., Pei, H., Jiang, S., Ma, S., et al. (2020). Reconfiguration of dynamic large-scale brain network functional connectivity in generalized tonic-clonic seizures. *Hum. Brain Mapp.* 41, 67–79. doi: 10.1002/hbm.24787

Jonas, J., Rossion, B., Brissart, H., Frismand, S., Jacques, C., Hossu, G., et al. (2015). Beyond the core face-processing network: Intracerebral stimulation of a face-selective area in the right anterior fusiform gyrus elicits transient prosopagnosia. *Cortex* 72, 140–155. doi: 10.1016/j.cortex.2015.05.026

Just, M. A., Keller, T. A., Malave, V. L., Kana, R. K., and Varma, S. (2012). Autism as a neural systems disorder: a theory of frontal-posterior underconnectivity. *Neurosci. Biobehav. Rev.* 36, 1292–1313. doi: 10.1016/j.neubiorev.2012.02.007

Kaiser, R. H., Whitfield-Gabrieli, S., Dillon, D. G., Goer, F., Beltzer, M., Minkel, J., et al. (2016). Dynamic resting-state functional connectivity in major depression. *Neuropsychopharmacology* 41, 1822–1830. doi: 10.1038/npp.2015.352

Kana, R. K., Libero, L. E., and Moore, M. S. (2011). Disrupted cortical connectivity theory as an explanatory model for autism spectrum disorders. *Phys. Life Rev.* 8, 410–437. doi: 10.1016/j.plrev.2011.10.001

Kanehisa, M., Goto, S., Kawashima, S., Okuno, Y., and Hattori, M. (2004). The KEGG resource for deciphering the genome. *Nucleic Acids Res.* 32, D277–D280. doi: 10.1093/nar/gkh063

Kang, H. J., Kawasawa, Y. I., Cheng, F., Zhu, Y., Xu, X., Li, M., et al. (2011). Spatio-temporal transcriptome of the human brain. *Nature* 478, 483–489. doi: 10.1038/nature10523

Kennedy, D. P., and Courchesne, E. (2008). The intrinsic functional organization of the brain is altered in autism. *Neuroimage* 39, 1877–1885. doi: 10.1016/j.neuroimage.2007.10.052

Kung, Y. C., Li, C. W., Chen, S., Chen, S. C., Lo, C. Z., Lane, T. J., et al. (2019). Instability of brain connectivity during nonrapid eye movement sleep reflects altered properties of information integration. *Hum. Brain Mapp.* 40, 3192–3202. doi: 10.1002/hbm.24590

Lai, M.-C., Lombardo, M. V., and Baron-Cohen, S. (2014). Autism. *Lancet* 383, 896–910. doi: 10.1016/s0140-6736(13)61539-1

Li, J., Duan, X., Cui, Q., Chen, H., and Liao, W. (2019). More than just statics: temporal dynamics of intrinsic brain activity predicts the suicidal ideation in depressed patients. *Psychol. Med.* 49, 852–860. doi: 10.1017/S0033291718001502

Li, R., Wang, S., Zhu, L., Guo, J., Zeng, L., Gong, Q., et al. (2013). Aberrant functional connectivity of resting state networks in transient ischemic attack. *PLoS One* 8:e71009. doi: 10.1371/journal.pone.0071009

Li, W., Cui, H., Zhu, Z., Kong, L., Guo, Q., Zhu, Y., et al. (2016). Aberrant functional connectivity between the amygdala and the temporal pole in drug-free generalized anxiety disorder. *Front. Hum. Neurosci.* 10:549. doi: 10.3389/fnhum.2016.00549

Li, Y., Zhu, Y., Nguchu, B. A., Wang, Y., Wang, H., Qiu, B., et al. (2020). Dynamic functional connectivity reveals abnormal variability and hyper-connected pattern in autism spectrum disorder. *Autism. Res.* 13, 230–243. doi: 10.1002/aur.2212

Liu, F., Wang, Y., Li, M., Wang, W., Li, R., Zhang, Z., et al. (2017). Dynamic functional network connectivity in idiopathic generalized epilepsy with generalized tonic-clonic seizure. *Hum. Brain Mapp.* 38, 957–973. doi: 10.1002/hbm.23430

Lord, C., Rutter, M., DiLavore, P., Risi, S., Gotham, K., and Bishop, S. (2012). *Autism Diagnostic Observation Schedule, (ADOS-2)*, 2nd Edn. Los Angeles, CA: Western Psychological Corporation, 284.

Luan, Y., Wang, C., Jiao, Y., Tang, T., Zhang, J., and Teng, G. J. (2019). Dysconnectivity of multiple resting-state networks associated with higher-order functions in sensorineural hearing loss. *Front. Neurosci.* 13:55. doi: 10.3389/fnins.2019.00055

Majerus, S., Attout, L., D'Argembeau, A., Degueldre, C., Fias, W., Maquet, P., et al. (2012). Attention supports verbal short-term memory via competition between dorsal and ventral attention networks. *Cereb. Cortex* 22, 1086–1097. doi: 10.1093/cercor/bhr174

Mantini, D., Perrucci, M. G., Del Gratta, C., Romani, G. L., and Corbetta, M. (2007). Electrophysiological signatures of resting state networks in the human brain. *Proc. Natl. Acad. Sci. U.S.A.* 104, 13170–13175. doi: 10.1073/pnas.0700668104

McCarthy, H., Skokauskas, N., Mulligan, A., Donohoe, G., Mullins, D., Kelly, J., et al. (2013). Attention network hypoconnectivity with default and affective network hyperconnectivity in adults diagnosed with attention-deficit/hyperactivity disorder in childhood. *JAMA Psychiatry* 70, 1329–1337. doi: 10.1001/jamapsychiatry.2013.2174

Meeker, K. L., Ances, B. M., Gordon, B. A., Rudolph, C. W., Luckett, P., Balota, D. A., et al. (2021). Cerebrospinal fluid Abeta42 moderates the relationship between brain functional network dynamics and cognitive intraindividual variability. *Neurobiol. Aging* 98, 116–123. doi: 10.1016/j.neurobiolaging.2020.10.027

Morales-Hidalgo, P., Roige-Castellvi, J., Hernandez-Martinez, C., Voltas, N., and Canals, J. (2018). Prevalence and characteristics of autism spectrum disorder among spanish school-age children. *J. Autism. Dev. Disord.* 48, 3176–3190. doi: 10.1007/s10803-018-3581-2

Orlov, N. D., Giampietro, V., O'Daly, O., Lam, S. L., Barker, G. J., Rubia, K., et al. (2018). Real-time fMRI neurofeedback to down-regulate superior temporal gyrus activity in patients with schizophrenia and auditory hallucinations: a proof-of-concept study. *Transl. Psychiatry* 8:46. doi: 10.1038/s41398-017-0067-5

Perez Velazquez, J. L., Barcelo, F., Hung, Y., Leshchenko, Y., Nenadovic, V., Belkas, J., et al. (2009). Decreased brain coordinated activity in autism spectrum disorders during executive tasks: reduced long-range synchronization in the fronto-parietal networks. *Int. J. Psychophysiol.* 73, 341–349. doi: 10.1016/j.ijpsycho.2009.05.009

Pinero, J., Bravo, A., Queralt-Rosinach, N., Gutierrez-Sacristan, A., Deu-Pons, J., Centeno, E., et al. (2017). DisGeNET: a comprehensive platform integrating information on human disease-associated genes and variants. *Nucleic Acids Res.* 45, D833–D839. doi: 10.1093/nar/gkw943

Pisula, E., and Porebowicz-Dorsmann, A. (2017). Family functioning, parenting stress and quality of life in mothers and fathers of Polish children with high functioning autism or Asperger syndrome. *PLoS One* 12:e0186536. doi: 10.1371/journal.pone.0186536

Plitt, M., Barnes, K. A., Wallace, G. L., Kenworthy, L., and Martin, A. (2015). Resting-state functional connectivity predicts longitudinal change in autistic traits and adaptive functioning in autism. *Proc. Natl. Acad. Sci. U.S.A.* 112, E6699–E6706. doi: 10.1073/pnas.1510098112

Pouw, L. B. C., Rieffe, C., Stockmann, L., and Gadow, K. D. (2013). The link between emotion regulation, social functioning, and depression in boys with ASD. *Res. Autis. Spect. Disord.* 7, 549–556. doi: 10.1016/j.rasd.2013.01.002

Power, J. D., Barnes, K. A., Snyder, A. Z., Schlaggar, B. L., and Petersen, S. E. (2012). Spurious but systematic correlations in functional connectivity MRI networks arise from subject motion. *Neuroimage* 59, 2142–2154. doi: 10.1016/j.neuroimage.2011.10.018

Power, J. D., Cohen, A. L., Nelson, S. M., Wig, G. S., Barnes, K. A., Church, J. A., et al. (2011). Functional network organization of the human brain. *Neuron* 72, 665–678. doi: 10.1016/j.neuron.2011.09.006

Power, J. D., Fair, D. A., Schlaggar, B. L., and Petersen, S. E. (2010). The development of human functional brain networks. *Neuron* 67, 735–748. doi: 10.1016/j.neuron.2010.08.017

Preti, M. G., Bolton, T. A., and Van De Ville, D. (2017). The dynamic functional connectome: State-of-the-art and perspectives. *Neuroimage* 160, 41–54. doi: 10.1016/j.neuroimage.2016.12.061

Richeson, J. A., Baird, A. A., Gordon, H. L., Heatherton, T. F., Wyland, C. L., Trawalter, S., et al. (2003). An fMRI investigation of the impact of interracial contact on executive function. *Nat. Neurosci.* 6, 1323–1328. doi: 10.1038/nn1156

Rohr, C. S., Vinette, S. A., Parsons, K. A. L., Cho, I. Y. K., Dimond, D., Benischek, A., et al. (2017). Functional connectivity of the dorsal attention network predicts selective attention in 4-7 year-old Girls. *Cereb. Cortex* 27, 4350–4360. doi: 10.1093/cercor/bhw236

Rudie, J. D., Shehzad, Z., Hernandez, L. M., Colich, N. L., Bookheimer, S. Y., Iacoboni, M., et al. (2012). Reduced functional integration and segregation of distributed neural systems underlying social and emotional information processing in autism spectrum disorders. *Cereb. Cortex* 22, 1025–1037. doi: 10.1093/cercor/bhr171

Schmunk, G., Nguyen, R. L., Ferguson, D. L., Kumar, K., Parker, I., and Gargus, J. J. (2017). High-throughput screen detects calcium signaling dysfunction in typical sporadic autism spectrum disorder. *Sci. Rep.* 7:40740. doi: 10.1038/srep40740

Selten, J. P., Lundberg, M., Rai, D., and Magnusson, C. (2015). Risks for nonaffective psychotic disorder and bipolar disorder in young people with autism spectrum disorder: a population-based study. *JAMA Psychiatry* 72, 483–489. doi: 10.1001/jamapsychiatry.2014.3059

Shakil, S., Lee, C. H., and Keilholz, S. D. (2016). Evaluation of sliding window correlation performance for characterizing dynamic functional connectivity and brain states. *Neuroimage* 133, 111–128. doi: 10.1016/j.neuroimage.2016.02.074

Shen, W., Tu, Y., Gollub, R. L., Ortiz, A., Napadow, V., Yu, S., et al. (2019). Visual network alterations in brain functional connectivity in chronic low back pain: a resting state functional connectivity and machine learning study. *Neuroimage Clin.* 22:101775. doi: 10.1016/j.nicl.2019.101775

Sizoo, B., van den Brink, W., Koeter, M., Gorissen van Eenige, M., van Wijngaarden-Cremers, P., and van der Gaag, R. J. (2010). Treatment seeking adults with autism or ADHD and co-morbid substance use disorder: prevalence, risk factors and functional disability. *Drug. Alcohol. Depend.* 107, 44–50. doi: 10.1016/j.drugalcdep.2009.09.003

Slotnick, S. D., and Schacter, D. L. (2006). The nature of memory related activity in early visual areas. *Neuropsychologia* 44, 2874–2886. doi: 10.1016/j.neuropsychologia.2006.06.021

Strang, J. F., Kenworthy, L., Daniolos, P., Case, L., Wills, M. C., Martin, A., et al. (2012). Depression and anxiety symptoms in children and adolescents with autism spectrum disorders without intellectual disability. *Res. Autism. Spectr. Disord.* 6, 406–412. doi: 10.1016/j.rasd.2011.06.015

van den Heuvel, M. P., and Hulshoff Pol, H. E. (2010). Exploring the brain network: a review on resting-state fMRI functional connectivity. *Eur. Neuropsychopharmacol.* 20, 519–534. doi: 10.1016/j.euroneuro.2010.03.008

Van Dijk, K. R., Sabuncu, M. R., and Buckner, R. L. (2012). The influence of head motion on intrinsic functional connectivity MRI. *Neuroimage* 59, 431–438. doi: 10.1016/j.neuroimage.2011.07.044

Van Hecke, A. V., Stevens, S., Carson, A. M., Karst, J. S., Dolan, B., Schohl, K., et al. (2015). Measuring the plasticity of social approach: a randomized controlled trial of the effects of the PEERS intervention on EEG asymmetry in adolescents with autism spectrum disorders. *J. Autism. Dev. Disord.* 45, 316–335. doi: 10.1007/s10803-013-1883-y

Vatansever, D., Manktelow, A. E., Sahakian, B. J., Menon, D. K., and Stamatakis, E. A. (2017). Angular default mode network connectivity across working memory load. *Hum. Brain Mapp.* 38, 41–52. doi: 10.1002/hbm.23341

Wang, X., Yang, Z., Fang, S., Zhang, Y., Guo, J., and Gou, L. (2021). Declining levels of specialized synaptic surface proteins in nNOS-expressing interneurons in mice treated prenatally with valproic acid. *Neurochem Res* 46, 1794–1800. doi: 10.1007/s11064-021-03326-w

Watanabe, T., and Rees, G. (2016). Anatomical imbalance between cortical networks in autism. *Sci. Rep.* 6:31114. doi: 10.1038/srep31114

Woolfe, A., Goodson, M., Goode, D. K., Snell, P., McEwen, G. K., Vavouri, T., et al. (2005). Highly conserved non-coding sequences are associated with vertebrate development. *PLoS Biol.* 3:e7. doi: 10.1371/journal.pbio.0030007

Xia, W., Wang, S., Rao, H., Spaeth, A. M., Wang, P., Yang, Y., et al. (2015). Disrupted resting-state attentional networks in T2DM patients. *Sci. Rep.* 5:11148. doi: 10.1038/srep11148

Xue, K., Liang, S., Yang, B., Zhu, D., Xie, Y., Qin, W., et al. (2020). Local dynamic spontaneous brain activity changes in first-episode, treatment-naive patients with major depressive disorder and their associated gene expression profiles. *Psychol. Med.* 3, 1–10. doi: 10.1017/S0033291720003876

Yan, C. G., Cheung, B., Kelly, C., Colcombe, S., Craddock, R. C., Di Martino, A., et al. (2013). A comprehensive assessment of regional variation in the impact of head micromovements on functional connectomics. *Neuroimage* 76, 183–201. doi: 10.1016/j.neuroimage.2013.03.004

Yan, C. G., Wang, X. D., Zuo, X. N., and Zang, Y. F. (2016). DPABI: Data Processing & Analysis for (Resting-State) Brain Imaging. *Neuroinformatics* 14, 339–351. doi: 10.1007/s12021-016-9299-4

Zanto, T. P., and Gazzaley, A. (2013). Fronto-parietal network: flexible hub of cognitive control. *Trends Cogn. Sci.* 17, 602–603. doi: 10.1016/j.tics.2013.10.001

Zhang, B., Kirov, S., and Snoddy, J. (2005). WebGestalt: an integrated system for exploring gene sets in various biological contexts. *Nucleic Acids Res.* 33, W741–W748. doi: 10.1093/nar/gki475

Zuo, X. N., Kelly, C., Adelstein, J. S., Klein, D. F., Castellanos, F. X., and Milham, M. P. (2010). Reliable intrinsic connectivity networks: test-retest evaluation using ICA and dual regression approach. *Neuroimage* 49, 2163–2177. doi: 10.1016/j.neuroimage.2009.10.080

Conflict of Interest: The authors declare that the research was conducted in the absence of any commercial or financial relationships that could be construed as a potential conflict of interest.

Publisher's Note: All claims expressed in this article are solely those of the authors and do not necessarily represent those of their affiliated organizations, or those of the publisher, the editors and the reviewers. Any product that may be evaluated in this article, or claim that may be made by its manufacturer, is not guaranteed or endorsed by the publisher.

frontiers in Neuroscience

ORIGINAL RESEARCH
published: 17 February 2022
doi: 10.3389/fnins.2022.826609

Integrative Functional, Molecular, and Transcriptomic Analyses of Altered Intrinsic Timescale Gradient in Depression

Shaoqiang Han[1,2,3,4,5,6,7], Ruiping Zheng[1,2,3,4,5,6,7], Shuying Li[8], Bingqian Zhou[1,2,3,4,5,6,7], Yu Jiang[1,2,3,4,5,6,7], Caihong Wang[1,2,3,4,5,6,7], Yarui Wei[1,2,3,4,5,6,7], Jianyue Pang[8], Hengfen Li[8], Yong Zhang[1,2,3,4,5,6,7], Yuan Chen[1,2,3,4,5,6,7]* and Jingliang Cheng[1,2,3,4,5,6,7]**

[1] Department of Magnetic Resonance Imaging, The First Affiliated Hospital of Zhengzhou University, Zhengzhou, China, [2] Key Laboratory for Functional Magnetic Resonance Imaging and Molecular Imaging of Henan Province, Zhengzhou, China, [3] Engineering Technology Research Center for Detection and Application of Brain Function of Henan Province, Zhengzhou, China, [4] Engineering Research Center of Medical Imaging Intelligent Diagnosis and Treatment of Henan Province, Zhengzhou, China, [5] Key Laboratory of Magnetic Resonance and Brain Function of Henan Province, Zhengzhou, China, [6] Key Laboratory of Brain Function and Cognitive Magnetic Resonance Imaging of Zhengzhou, Zhengzhou, China, [7] Key Laboratory of Imaging Intelligence Research Medicine of Henan Province, Zhengzhou, China, [8] Department of Psychiatry, The First Affiliated Hospital of Zhengzhou University, Zhengzhou, China

The pathophysiology and pharmacology of depression are hypothesized to be related to the imbalance of excitation–inhibition that gives rise to hierarchical dynamics (or intrinsic timescale gradient), further supporting a hierarchy of cortical functions. On this assumption, intrinsic timescale gradient is theoretically altered in depression. However, it remains unknown. We investigated altered intrinsic timescale gradient recently developed to measure hierarchical brain dynamics gradient and its underlying molecular architecture and brain-wide gene expression in depression. We first presented replicable intrinsic timescale gradient in two independent Chinese Han datasets and then investigated altered intrinsic timescale gradient and its possible underlying molecular and transcriptional bases in patients with depression. As a result, patients with depression showed stage-specifically shorter timescales compared with healthy controls according to illness duration. The shorter timescales were spatially correlated with monoamine receptor/transporter densities, suggesting the underlying molecular basis of timescale aberrance and providing clues to treatment. In addition, we identified that timescale aberrance-related genes ontologically enriched for synapse-related and neurotransmitter (receptor) terms, elaborating the underlying transcriptional basis of timescale aberrance. These findings revealed atypical timescale gradient in depression and built a link between neuroimaging, transcriptome, and neurotransmitter information, facilitating an integrative understanding of depression.

Keywords: first-episode depression, gene expression profiling, fMRI, intrinsic timescale gradient, neurotransmitter

OPEN ACCESS

Edited by:
Jiajia Zhu,
First Affiliated Hospital of Anhui Medical University, China

Reviewed by:
Le Gao,
Yanshan University, China
Fali Li,
University of Electronic Science and Technology of China, China
Junjie Bu,
Anhui Medical University, China

****Correspondence:***
Shaoqiang Han
shaqianghan@163.com
Yuan Chen
chenyuanshizt@163.com
Jingliang Cheng
fccchengjl@zzu.edu.cn

Specialty section:
This article was submitted to Brain Imaging Methods, a section of the journal Frontiers in Neuroscience

Received: *01 December 2021*
Accepted: *10 January 2022*
Published: *17 February 2022*

Citation:
Han S, Zheng R, Li S, Zhou B, Jiang Y, Wang C, Wei Y, Pang J, Li H, Zhang Y, Chen Y and Cheng J (2022) Integrative Functional, Molecular, and Transcriptomic Analyses of Altered Intrinsic Timescale Gradient in Depression. Front. Neurosci. 16:826609. doi: 10.3389/fnins.2022.826609

INTRODUCTION

As one of the leading disabling diseases worldwide (Murray et al., 2012), depression affects approximately 350 million people each year (Schmaal et al., 2017). Recent studies point out that imbalance of the excitation–inhibition (E/I) underlays the pathophysiology and pharmacology of the depression (Voineskos et al., 2019). Imbalance of E/I ratio hypothetically results in the aberrance of hierarchically organized intrinsic neural timescales (Kiebel et al., 2008) that support synchronizing large-scale brain networks usually measured with resting-state functional connectivity (rsFC; Buzsáki and Draguhn, 2004). Accordingly, the intrinsic timescale gradient is theoretically altered in depression that remains unknown yet.

The brain regions are hierarchically organized into increasing polyfunctional neural circuits embodied in topographic gradients of molecular, cellular, and anatomical properties (Huntenburg et al., 2018). Emerging through hierarchically organized feature (Burt et al., 2018) such as pyramidal cell dendritic spine density (Elston, 2003), long-range interactions (Wang, 2020), and gene expression gradients (Fulcher et al., 2019), intrinsic neural dynamics (or intrinsic timescale gradient) are also hierarchically organized, supporting a hierarchy of cortical functions (Kiebel et al., 2008; Hasson et al., 2015). Brain dynamics is also hierarchically organized along spatial gradients extending from sensorimotor regions to association cortex (Hasson et al., 2008) supporting functional communications between brain regions (Cocchi et al., 2016). Regions with longer "temporal receptive windows" are subsequently found to exhibit more slowly changing activity and *vice versa* (Hasson et al., 2015). In particular, regions such as prefrontal areas and parietal areas, densely interconnected central regions, have longer timescales compared to peripheral sensory areas (Chaudhuri et al., 2015) for the reason that prolonged neural timescale is needed to enable these high-order brain regions to integrate various information for robust sensory perception (Hasson et al., 2008), stable memory processing (Bernacchia et al., 2011), and decision-making (Cavanagh et al., 2016). By developing a large-scale biophysical model, Chaudhuri et al. (2015) elaborate that intrinsic timescale gradient depends crucially on recurrent network activity. Aberrance of neural timescales is supposed to the result of imbalance of the excitation–inhibition (E/I) ratio (Wengler et al., 2020). Wengler et al. (2020) find evidence for distinct hierarchical aberrance in timescale gradient as a function of hallucination and delusion, supporting glutamatergic and dopamine theories of psychosis (Corlett et al., 2011; Jardri et al., 2016). Imbalance of the E/I is also implicated in the pathophysiology and pharmacology of the depression (Covington et al., 2010; Voineskos et al., 2019) and the mechanism of fast-acting antidepressant is related to E/I rebalance (Li, 2020). Although the intrinsic timescale gradient should be altered in depression theoretically, it remains unknown yet.

Brain function such as rsFC is also modulated by genetic factors (Richiardi et al., 2015; Fornito et al., 2019; Richiardi et al., 2015) and coupled to neurotransmitters (Stagg et al., 2014; Kringelbach and Cruzat, 2020). Twin studies show that functional connectivity within the default-mode network and topological measures in the human brain are moderate to highly heritable (Glahn et al., 2010; Fornito et al., 2011; van den Heuvel et al., 2013). Recently, Allen Human Brain Atlas (AHBA) (Hawrylycz et al., 2012), a newly proposed brain-wide gene expression atlas, provides the possibility of bridging the gap between transcriptome and large-scale connectome organization (Fornito et al., 2019). Following the work of Richiardi et al. (2015) where they find that the transcriptome profile similarity within networks is higher than that between networks, a number of studies begin to explore the transcriptional basis of macroscopic neuroimaging phenotypes (Krienen et al., 2016; Vértes et al., 2016; Anderson et al., 2018; Li and Seidlitz, 2021). Recently, Zhu et al. (2021) find that spatial distribution of functional connectivity strength is modulated by genes enriched for terms such as synaptic transmission in health (Zhang et al., 2021). In depression, Li et al. (2021) identify that altered morphometric similarity network is correlated with transcriptional signatures (Li and Seidlitz, 2021). In addition, rsFC is found to be coupled to neurotransmitter transporters/receptors (Stagg et al., 2014; Kringelbach and Cruzat, 2020). Dysconnectivity in schizophrenia is linked to altered neurotransmission (Landek-Salgado et al., 2016; Limongi et al., 2020). Chen et al. (2021) find that abnormal functional topography of brain networks is associated with the dopaminergic and serotonergic systems underlying cognitive decline in schizophrenia by investigating the molecular architecture facilitating a link to treatment. The variation of timescales is hypothesized to arise from local biophysical properties of neurons across the cortical hierarchy, such as the density of glutamate receptors, calcium channels, and regulators of synaptic depression and facilitation (Zucker and Regehr, 2002; Wong and Wang, 2006). Investigating the molecular and transcriptional basis of altered intrinsic timescale gradient in depression helps to advance our understanding of how alterations at microscale architecture drive macroscale neuroimaging aberrance in depression.

In this study, we aimed to explore altered intrinsic timescale gradient and its underlying molecular and transcriptional signatures bridging the gap between molecular mechanism and macroscopic neuroimaging phenotypes in depression. First, we presented replicable landscape of intrinsic timescale gradient and its association with commonly used functional indicators including amplitude of low-frequency fluctuation (ALFF) and functional connectivity density (FCD) in two independent Chinese Han cohorts. Second, we investigated altered intrinsic timescale gradient in different stages of depression according to illness duration. Third, we inquired molecular and transcriptional basis of altered intrinsic timescale gradient in depression. Fourth, a functional enrichment analysis was performed to inquire ontological pathways of timescale aberrance-related genes in depression.

MATERIALS AND METHODS

Datasets

Two independent Chinese Han datasets were used in this study. The first dataset come from the Southwest University Adult Lifespan Dataset (SALD) study including 494 healthy participants (female: male, 308:187, 19–80 years old). The second dataset included 121 HCs and 191 patients with depression. The resting-state functional MRI data were acquired and preprocessed using Data Processing & Analysis for Brain Imaging (DPABI)[1] (Yan et al., 2016). The details about dataset description, scan acquisition, and preprocessing procedures were included in **Supplementary Methods**. The study was approved by the research ethical committee of the First Affiliated Hospital of Zhengzhou University.

Calculation of Timescales and Its Association With Functional Connectivity Density and Amplitude of Low-Frequency Fluctuation

Based on previous studies (Watanabe et al., 2019; Raut and Snyder, 2020), we calculated intrinsic neural timescales by calculating the magnitude of autocorrelation of the resting-state brain signals. There were two different definitions of timescales. First, the timescale was defined as the sum of positive autocorrelation function (ACF) values and then multiplied by the repetition time (TR) (Watanabe et al., 2019). The results reported in the next steps were based on this definition. The second was defined as the half of the full width at half maximum of the ACF (Raut and Snyder, 2020). To inquire the relationship between these two definitions, spatial correlation was obtained between the two mean timescale maps across healthy subjects in dataset 1 and healthy subjects in dataset 2, respectively. In addition, we also compared spatial correlation between the altered timescale maps of depression using these two definitions (see below).

As a newly proposed index, factors affecting landscape of timescales remained unclear. To explore these factors, we investigated whether factors such as gender (female vs. male), age, motion movement, and education level could affect intrinsic timescale gradient (**Supplementary Methods**). The timescales were calculated using custom MATLAB code publicly available at https://github.com/RaichleLab.

To intuitively elucidate the intrinsic timescale gradient measured, we inquired the association between intrinsic timescale gradient with other common functional indexes such as ALFF and FCD. For FCD maps, local, long-range, and global FCD maps were calculated (Tomasi and Volkow, 2010) where correlation threshold was determined by significance of single functional connection (p-value). A functional connection (correlation coefficient) was considered significant if its $p < 0.05$ (Bonferroni corrected). The obtained FCD maps were transformed to z-scores by subtracting the mean value and dividing by the standard deviation across gray matter voxels. The ALFF maps were calculated using resting-state functional magnetic resonance imaging data processing toolbox (REST) (Song et al., 2011), and normalized ALFF maps (dividing the mean value across gray matter voxels) were chosen for the following steps.

Dominance analysis was used to quantify the association between mean FCD (including local, long-range and global FCD), and mean ALFF maps to landscape of timescales across healthy subjects in each dataset (Budescu and David, 1993; Azen and Budescu, 2003).[2] The details are provided in **Supplementary Methods**.

All of the above analysis steps were done in the discovery cohort (dataset 1) and validated in the replication cohort (HCs of dataset 2); results reported were based on the discovery cohort, unless stated otherwise.

Altered Intrinsic Timescale Gradient in Depression

Then, we explored whether intrinsic timescale gradient was altered in depression. The altered timescale was obtained by using two-tailed two-sample t-test equipped in SPM 12 where gender, age, mean FD, SNR0, and educational level were included as covariates. To explore whether aberrance of intrinsic timescale gradient was stage-dependent for the reason that mental disorders were found to present progressive brain structural alterations (Koutsouleris et al., 2014; Treadway et al., 2015; Cao et al., 2017; Zhang et al., 2017; Yüksel et al., 2018), patients with depression were further divided into three stages according to illness duration (Stage 1: $0 \leq$ illness duration $\leq$12 months; Stage 2: 12 <illness duration $\leq$24 months; Stage 3: illness duration $\geq$24 months). Moreover, we also compared timescales in patients whose illness duration is less than 3/6 months to inquire whether timescale aberrance emerged from the beginning of the disease. Results reported in this study were corrected for multiple comparison (voxel-wise $p < 0.001$, cluster-level $p < 0.05$; GRF correction). To further explore the relationship between two definitions of timescales, the same statistical procedures were done in the second definition of timescales (half maximum of the ACF).

Spatial Correlation Between Altered Timescales of Depression With Receptor/Transporter Densities

To explore association between depression-induced changes in timescales and expression of a specific receptor/transporter, we evaluated the spatial relationship between altered timescales and the distribution of receptors/transporters. The timescale difference map was spatially correlated with PET/SPECT maps in JuSpace toolbox[3] (Dukart et al., 2021). The default neuromorphometrics atlas excluding white matter and cerebrospinal fluid regions was used. Dopamine (D1 and D2), serotonin receptors (5-HT1a, 5-HT1b, and 5-HT2a), transporters (dopamine transporter and serotonin

[1] http://rfmri.org/dpabi

[2] https://github.com/dominance-analysis/dominance-analysis

[3] https://github.com/juryxy/JuSpace

reuptake transporter 5-HTT), F-DOPA (a reflection of presynaptic dopamine synthesis capacity), the GABAergic receptor, and the noradrenaline transporter (NAT) were investigated. The correlation results were adjusted for spatial autocorrelation of local gray matter probabilities, and the significance of results was computed using permutation statistics (Dukart et al., 2021). To exclude the effect of atlas choice on our results, we used another two atlas (268 and 246 regions) (Shen et al., 2013; Fan et al., 2016) to validate these results.

What is more, to inquire whether the association with receptor/transporter densities was specific to altered timescales, we calculated spatial correlation between ALFF differences of depression with PET/SPECT maps using default neuromorphometrics atlas. The ALFF was chosen for the reason that it was widely used in resting-state fMRI studies.

Cortical Gene Expression Related to Altered Timescale of Depression

Inspired by a previous study (Reardon and Seidlitz, 2018), we ranked genes based on the spatial correlation between gene expression pattern and the voxel-wise unthresholded *t*-statistic map of timescale difference in depression. The gene expression data come from theAHBA[4] (Hawrylycz et al., 2012), obtained from six adult human brains (Hawrylycz et al., 2012). Details and preprocessing procedures of AHBA were included in **Supplementary Methods**. The preprocessed AHBA used in this study comes from the Brain Annotation Toolbox (BAT)[5] (Liu et al., 2019). Because only two right hemisphere data were included in the AHBA, we only considered the left hemisphere in our analysis (Arnatkeviciute et al., 2019). The correlation results were considered significant if $|r| > 0.2$ and $p < 0.05$ (FWE corrected). Finally, the positive and negative correlation gene lists were identified with timescale aberrance.

Enrichment Pathways Associated With Altered Timescales of Depression

We performed the gene ontology (GO) and Kyoto Encyclopedia of Genes and Genomes (KEGG) pathways with the genes presenting significant spatial correlation with altered timescales of depression using Metascape (Zhou et al., 2019). Results reported here were corrected by the FDR ($p < 0.05$). This procedure was done in positive and negative correlation genes separately.

As done in a previous study (Li and Seidlitz, 2021), we further investigated shared enrichment terms between previously reported polygenic risk for depression and the timescale-related gene list (Wray et al., 2018; Howard and Adams, 2019). A multi-gene list meta-analysis was carried out between the timescale aberrance-related gene list and the gene list provided by these two studies.

[4]http://human.brain-map.org/

[5]https://istbi.fudan.edu.cn/lnen/info/1173/1788.htm

RESULTS

Clinical Demographics

The clinical demographics of subjects in dataset 1 and dataset 2 are included in **Supplementary Tables 1**, **2**.

The Landscape of Resting-State Timescales and Its Association With Functional Connectivity Density and Amplitude of Low-Frequency Fluctuation

The mean timescale maps across healthy subjects in dataset 1 and dataset 2 are drawn in **Figure 1**. In accordance with a previous study (Watanabe et al., 2019), both dataset 1 and dataset 2 (only HCs) presented similar whole-brain patterns of timescales with longer timescales in frontal and parietal cortices and shorter timescales in other regions such as sensorimotor and visual areas (**Figure 1**). The spatial correlation between dataset 1 and dataset 2 (only HCs) was $r = 0.783$ ($p < 0.05$, permutation test). As there were two definitions of timescale, we calculated the spatial correlation between mean maps of the two definitions in dataset 1 and dataset 2 (only HCs). The landscapes of these two definitions were in good agreement (dataset 1, $r = 0.961$, $p < 0.05$ for permutation test; dataset 2, $r = 0.893$, $p < 0.05$ for permutation test) (**Supplementary Figure 2**). We observed significantly negative correlation between age and timescales only in dataset 1 (**Supplementary Figure 3**), suggesting that the timescales might be related to normal brain aging; results of HCs in dataset 2 were not significant, possibly due to the limited sample size. In addition, timescales in regions such as the left inferior temporal gyrus, sensorimotor cortex, and left middle frontal gyrus presented significantly negative correlation with educational level stating its potential role in the landscape of educational level in HCs of dataset 2 (**Supplementary Figure 4**).

Then, we assessed the association between intrinsic timescale gradient with common resting-state functional indexes including FCD and ALFF using dominance analysis. Results revealed the relative importance of each predictor (collective $R^2 = 0.4528$, long-range FCD = 29.19%, global FCD = 27.64%, local FCD = 16.05%, ALFF = 27.11%), suggesting that long-range and global FCD contributed the most to intrinsic neural timescales. These results were validated in HCs of dataset 2 (**Supplementary Table 3**).

Altered Timescales in Depression

Overall, there was no significant aberrance of timescales in patients with depression across stages according to illness duration. Whereafter, we investigated altered timescales in patients at different stages according to illness duration. Timescales in patients with depression presented stage-specific aberrance. In particular, patients presented shorter timescales in regions including right anterior insula extending to right putamen only at the first stage (<12 months). To further explore whether this aberrance occurred at disease onset, we investigated timescale aberrance in patients with shorter illness duration (<3/6 months). Regions such as ventral medial prefrontal cortex vmPFC/subgenual PFC, dorsal ACC, dorsal lateral PFC, the

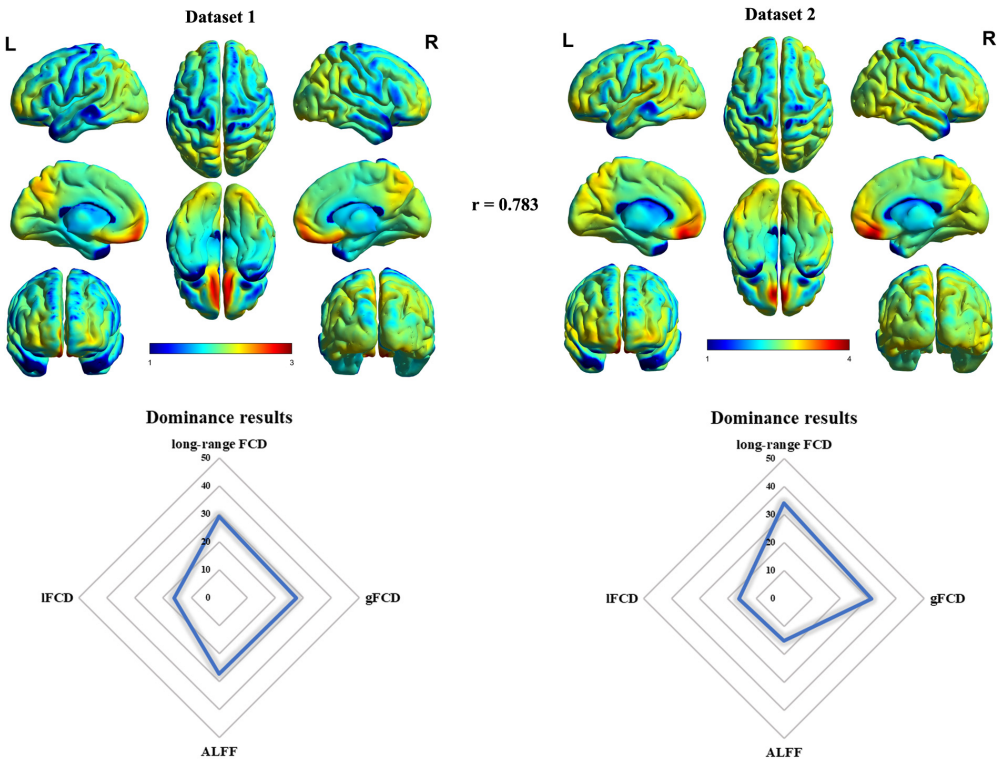

FIGURE 1 | The landscape of timescales and its association with ALFF and FCD. The "r" meant the spatial correlation between mean timescales maps in dataset 1 and dataset 2. The number in the dominance results meant the percentage of ALFF/FCD contributing to timescales where higher number meant higher association with timescales.

bilateral nucleus accumbens (NAcc), the striatum, and the bilateral insula presented decreased timescales in patients with an illness duration of less than 3/6 months. With the prolongation of the disease course, the timescale alterations gradually faded away (**Figure 2** and **Supplementary Table 4**). In addition, to further explore the relationship between two definitions of timescales, the same statistical procedures were done in the second definition of timescales (half maximum of the ACF), and the results are included in **Supplementary Figure 5**. These results confirmed good consistency of altered intrinsic timescale gradient with different definitions.

To exclude the possibility that the gradual reduction of timescales resulted from the samples used in the current study, we also inquired whether another functional index also presented stage-specific aberrance. For the reason mentioned above, ALFF was chosen. As a result, patients with depression did not present gradual ALFF aberrance in depression (**Supplementary Figure 6**).

Relationship to Receptor/Transporter Densities

Altered timescales were significantly correlated ($p < 0.05$ for permutation, FWE corrected) with seven receptor/transporter densities (**Figure 3** and **Supplementary Table 5**) including 5-HT2a (5-HT subtype 2a), D1 (dopamine D1), DAT (dopamine transporter), F-DOPA (dopamine synthesis capacity), NAT (noradrenaline transporter), and SERT (serotonin transporter). These results were validated with a different brain atlas (**Figure 3**). In addition, to explore whether the correlation results were specific to altered timescales, we also calculated spatial correlation between ALFF differences of depression with receptor/transporter densities using default neuromorphometrics atlas. As a result, there was no significant spatial correlation between ALFF aberrance and receptor/transporter densities, hinting that the association was specific to timescale aberrance in depression.

Note: 5-HT1a, 5-HT subtype 1a; 5-HT1b, 5-HT subtype 1b; 5-HTaa, 5-HT subtype aa; D1, dopamine D1; D2, dopamine D2; DAT, dopamine transporter; F-DOPA, dopamine synthesis capacity; NAT, noradrenaline transporter; SERT, serotonin transporter.

Cortical Gene Expression Related to Altered Timescales in Depression

As timescales presented stage-specific aberrance and the differences faded away as the progression of illness in depression, we calculated the spatial correlation between gene expression with timescale differences in patients with an illness duration of less than 3 months (see before). As a result, 865/264 genes presented positive/negative correlation with the unthresholded timescale differences in patients with depression

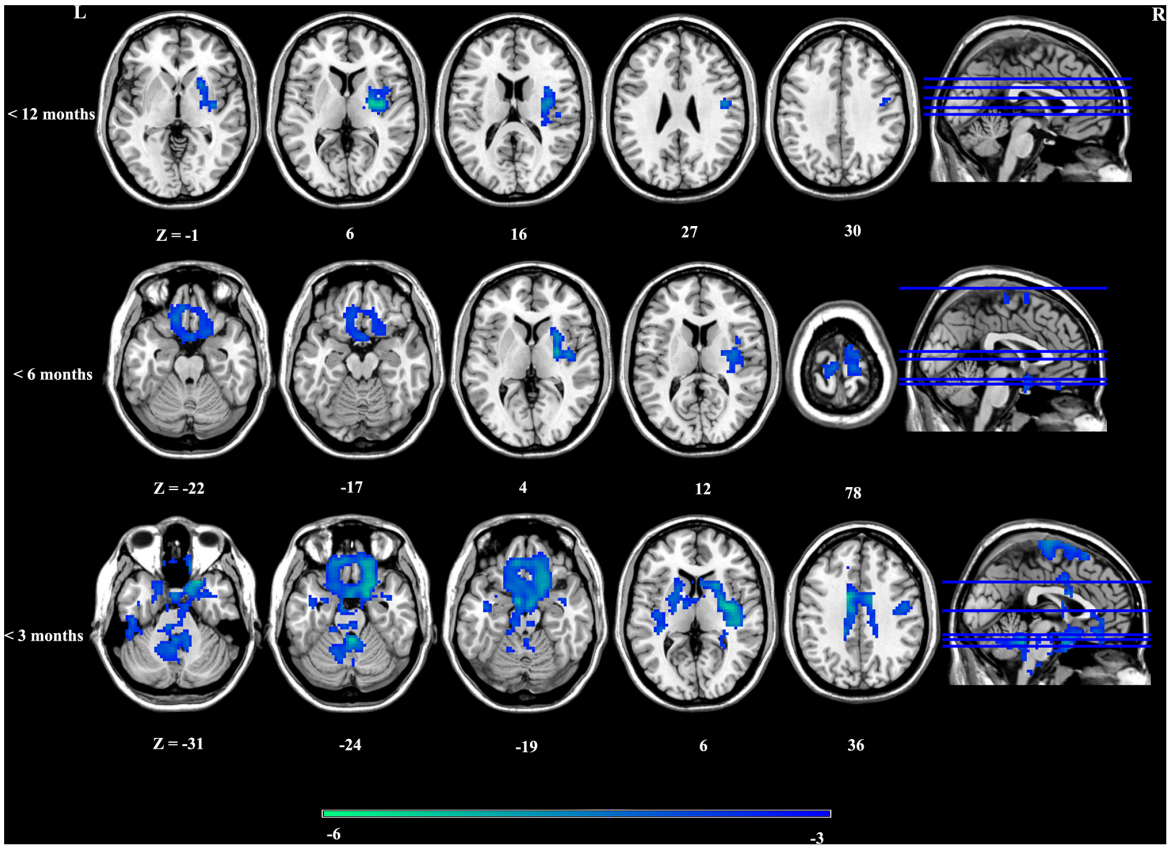

FIGURE 2 | Stage-specific aberrance of timescales in depression.

whose illness duration was less than 3 months (see section "**Supplementary Methods**").

Enrichment Pathways Associated With Altered Timescales of Depression

We performed the GO biological processes and KEGG pathways with the associated gene lists obtained in the previous step using Metascape. The top 30 significant GO biological processes, such as "*Trans*-synaptic signaling," "synapse signaling," "synapse organization," "dendrite development," and "cognition," and one KEGG pathway, "cGMP-PKG signaling pathway," were identified (**Figure 4**) for the positive correlation gene list. Regulation of neurotransmitter receptor activity such as "glutamatergic synapse," "dopaminergic synapse," "glutamate receptor signaling pathway," and "regulation of neurotransmitter secretion" was also identified (see section "**Supplementary Methods**"). These enrichment terms were clustered into clusters such as synaptic signaling, synapse organization (e.g., dendritic spine morphogenesis and dendrite development), regulation of transmembrane transport, and head development (e.g., hippocampus development and limbic system development) (**Figure 4**).

Then, we investigated shared enrichment terms between the previously reported polygenic risk for depression and the positive correlation gene list by performing a multi-gene list meta-analysis (Zhou et al., 2019). As a result, we found 11 common pathways. The enrichment pathways included "synaptic signaling," "synapse organization," "cell–cell adhesion *via* plasma membrane adhesion molecules," and "dendrite development" (**Supplementary Figure 7**).

DISCUSSION

In this study, we investigated altered intrinsic neural timescale gradient in patients with depression and its possible underlying molecular and transcriptional signatures. Timescales presented stage-specific aberrance in depression. Specifically, patients at the beginning of illness (illness duration <3 months) presented shorter timescales in regions including vmPFC, ACC, the bilateral nucleus accumbens (NAcc), the striatum, and the bilateral insula. As the illness advanced, the difference faded away (disappeared when illness duration ≥12 months). Moreover, the shorter timescales at the beginning of depression were associated with receptor/transporter densities including 5-HT2a, D1/2, DAT, F-DOPA, NAT, and SERT, suggesting the underlying molecular basis of timescale aberrance and providing clues to treatment. Then, we identified timescale aberrance-related genes ontologically enriched for synapse-related and neurotransmitter

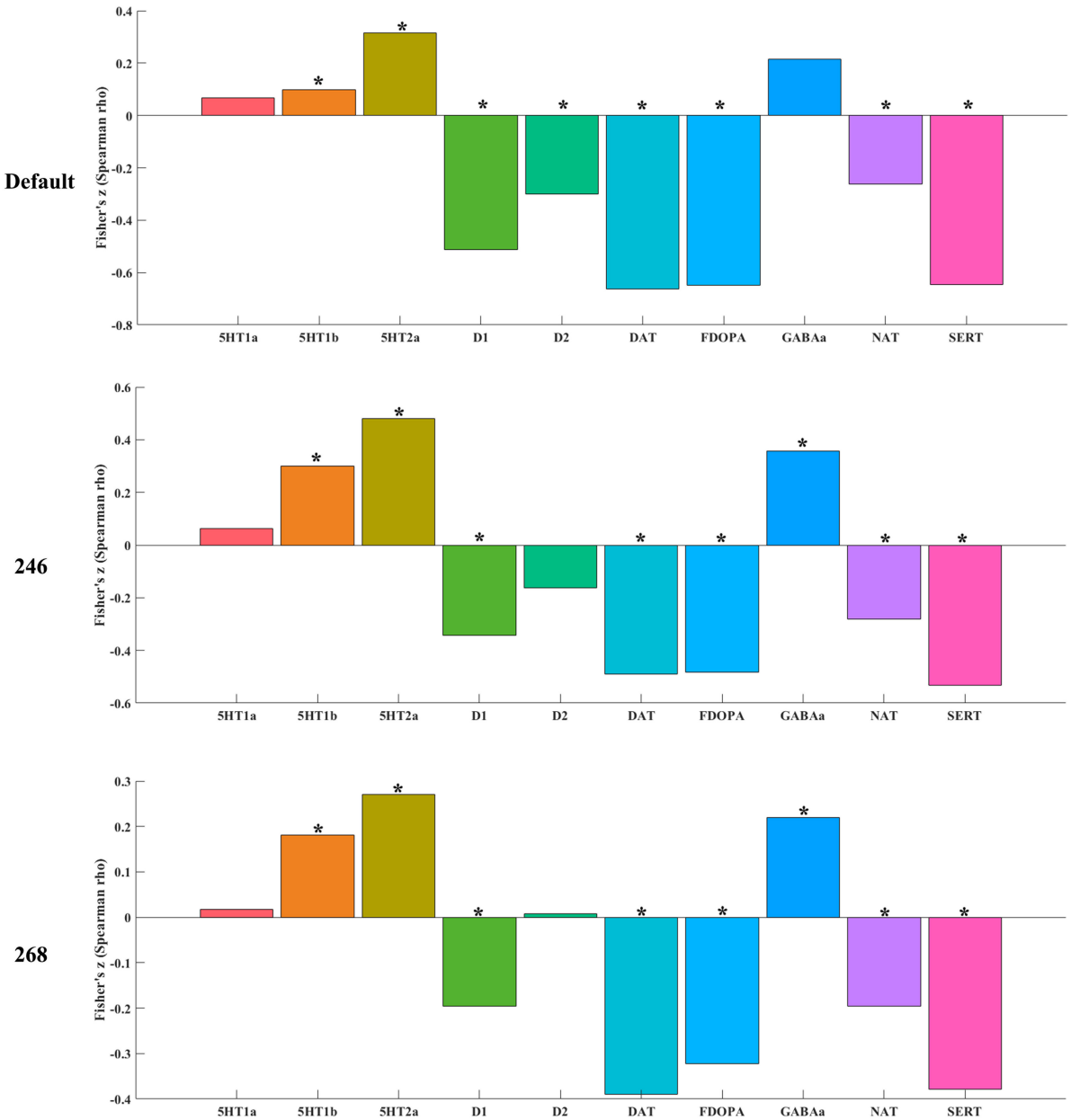

FIGURE 3 | The association between timescale aberrance with receptor/transporter densities. The "*" represented that the correlation was significant ($p < 0.05$ for permutation, FWE corrected).

(receptor) terms elaborating the underlying transcriptional basis of timescale aberrance. These findings revealed atypical intrinsic timescale gradient in depression and bridged the gap between neuroimaging, transcriptome, and neurotransmitter information facilitating an integrative understanding of depression.

Stage-Specifically Shorter Intrinsic Timescales in Depression

Patients with depression presented stage-specifically shorter timescales according to illness duration in regions including vmPFC, ACC, the bilateral NAc, the striatum, and the bilateral insula. The shorter timescales were only observed in patients with illness duration less than 12 months and then faded away as illness advanced. Converging lines of evidence confirmed that depression was a neuroprogressive illness (Kendler et al., 2001; Moylan et al., 2013); the morphometric alteration of critical brain regions was related to illness progression information (such as illness duration) (Frodl et al., 2003; McKinnon et al., 2009; van Eijndhoven et al., 2009; Alexander-Bloch et al., 2013; Chen V. C. et al., 2016). Consistent with this notion, we observed stage-specifically shorter timescales in patients with illness duration

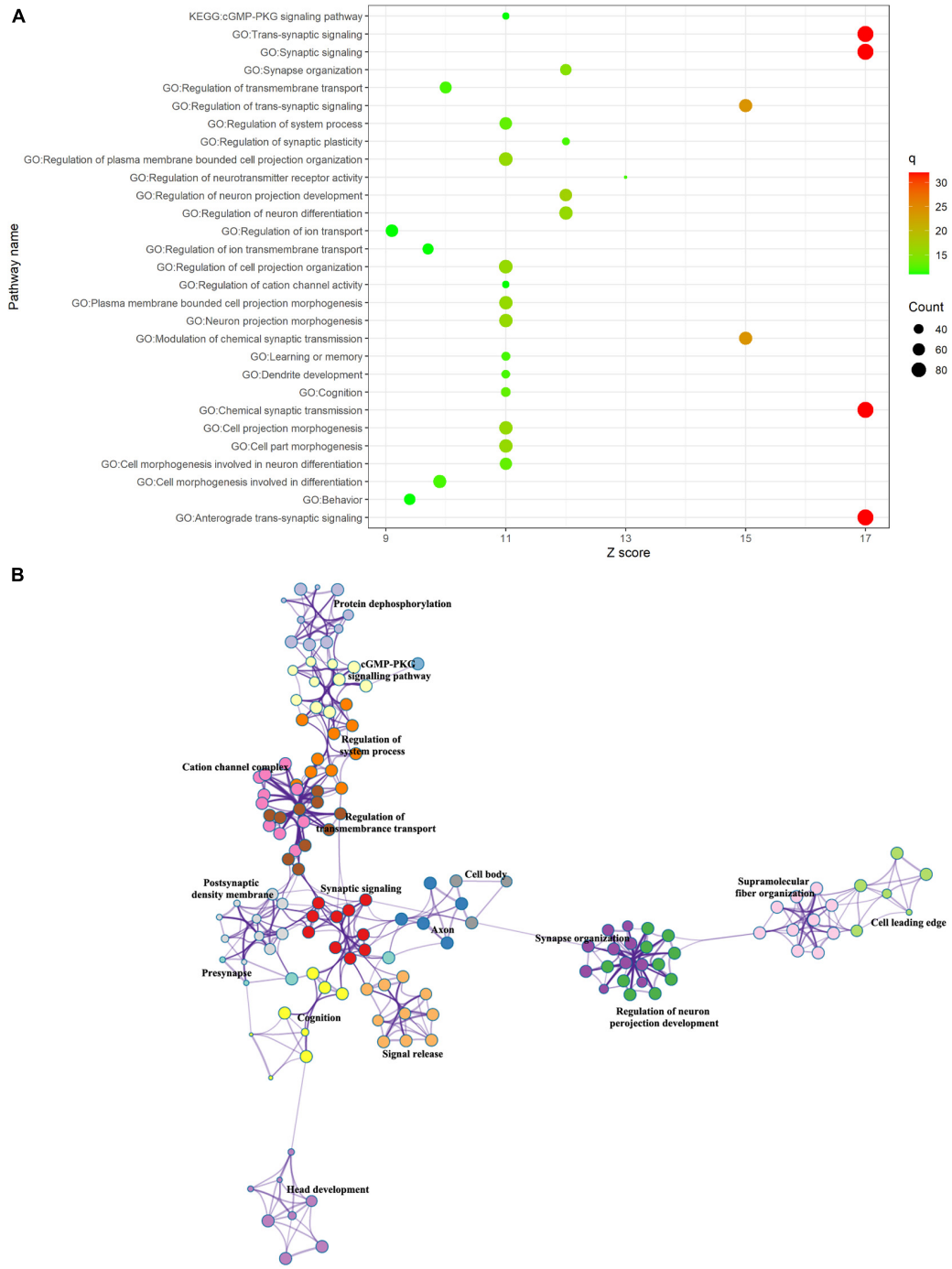

FIGURE 4 | Functional enrichment of gene transcripts. **(A)** Top 30 enrichment terms of positive correlation genes. The size of the circle represented the number of genes enriched in a given term. The color bar represented the significance of a given term. **(B)** Metascape enrichment network visualization. Each term was represented as a circle node where its size is proportional to the number of genes enriched in the term and its color represented cluster identify.

less than 12 months, and even 3 months, suggesting that shorter timescales occurred at the beginning of the disease. In our previous study, we identified that higher brain age was also stage-dependent (Han et al., 2021). This stage-specific aberrance might explain inconsistent findings in depression (Chen Z. et al., 2016). Note that the insignificant timescale aberrance in patients with longer illness duration did not necessarily mean the remission of depression for the reason that we did observe a significant difference in the total score of HAMD (p = 0.139, F = 2.00) across stages. Regions presenting shorter timescales were found

to be related to blunted processing of incentive salience, weak reward source memory, and reinforcement learning underlying the anhedonia in depression (Whitton et al., 2015; Alloy et al., 2016; Han et al., 2020). The shorter timescales of these regions might be associated with inefficient responsiveness to rewards in depression (Whitton et al., 2015; Alloy et al., 2016). On the other hand, dorsal lateral PFC, subgenual PFC, and dorsal ACC belonged to dorsal systems inhibiting amygdala activity in the unstressed state (Phillips et al., 2008). The reduced neuronal size and diminished dendritic arborization in the dorsal system were found in depression (Jaako-Movits et al., 2006; Drevets et al., 2008). The chronic stress could affect the gene expression of monoamine (serotonin)-glutamate/GABA and subsequently affected the E/I balance (Dygalo et al., 2020). Consistent with some ideas, we identified the shorter timescales in the dorsal system resulting from imbalance of the excitation–inhibition (E/I) ratio (Wengler et al., 2020), suggesting the inability of the dorsal system to regulate stress response in depression (Phillips et al., 2008).

There were two possible interpretations for the stage-dependent timescale alteration in depression. First, this phenomenon might mirror the transition from a clinically unstable period, with large variability in functioning, to a relatively stable period, when patients have reached a plateau in functioning (Davidson and McGlashan, 1997; van Haren et al., 2003). Another possible interpretation was that shorter timescales might be associated with primal brain dysfunction in depression. Here, we preferred the latter one. Multimodal lines of evidence convergently indicated that depression was a neuroprogressive illness (Kendler et al., 2001; Moylan et al., 2013). Even patients with depression suffering from only one depressive episode also displayed characteristics of a progressive illness (Moylan et al., 2013). As the disease prolonged, brain tissue damage and physiological functioning gradually changed, which underpinned symptomatology and functional decline over time (Moylan et al., 2013). Our previous results (under review) revealed that progressive morphological alteration might originate from regions like vmPFC and then expand to other regions in depression. Similar progressive morphological alterations such as advanced illness were observed in schizophrenia (Jiang et al., 2018), epilepsy (Zhang et al., 2017), and generalized anxiety disorder (Chen et al., 2020). The original dysfunction might be of great significance to the pathogeny and the treatment of depression. Actually, early treatment of patients with depression is usually accompanied with better outcome of antidepressant treatment and remission, and the reverse was also true. For example, a longer duration of untreated illness was reported to have an unfavorable effect on the subsequent course of the illness (e.g., higher number of recurrences) (Altamura et al., 2007, 2008; Li et al., 2021). A shorter duration of untreated illness was related to better remission of depression and somatic symptoms (Bukh et al., 2013). On the other hand, a longer duration of untreated illness was found to be associated with a greater severity and a lower improvement percentage (Hung et al., 2015; Kraus and Kadriu, 2019). What is more, we found that the stage-specific aberrance might be specific to an intrinsic timescale and did not result from the sample used in the current study. In summary, the shorter timescales at the beginning of disease might reflect initial functional aberrance and mean a lot to subsequent treatment.

Molecular Architecture of the Shorter Timescales

To explore the potential neurophysiological mechanism underlying the shorter timescales observed in depression helping to facilitate a link to treatment (Chen et al., 2021), we calculated spatial correlation between maps of a variety of neurotransmitter systems with that of timescale aberrance (Dukart et al., 2021). In line with the monoamine hypothesis (Liu et al., 2018), shorter timescales were associated with monoamine neurotransmitters including serotonin, noradrenaline, and dopamine at the same time. It was not unexpected that the timescale differences were associated with serotonin and noradrenaline neurotransmissions because of their fatal roles in pathogenesis (Hamon and Blier, 2013) and the first-line treatment of depression by inhibiting the action of the serotonin/noradrenaline transporter to reduce reuptake of serotonin/noradrenaline (Pirker et al., 1995). Consistent with studies showing that 5-HT2a and SERT were decreased in patients with depression (Kambeitz and Howes, 2015; Steinberg et al., 2019), we observed that the substrate of timescale differences might be related to 5-HT2a and SERT. The reason might be that the 5-HT2A receptors have both excitatory and inhibitory roles underlying the potential biological mechanism of timescale hierarchies (Chaudhuri et al., 2015). The association between SERT binding and rsFC (Beliveau et al., 2015) and dysfunction of SERT binding could result in altered functional connectivity in depression (Han et al., 2019) followed by altered timescales in depression. In addition, we found that the timescale aberrance might be also related to dopaminergic neurotransmission. Dopaminergic neurotransmission playing an essential role by rewarding prediction error (Hollerman and Schultz, 1998; Bayer and Glimcher, 2005) and mediating motivational drive by the attribution of incentive salience to reward-related stimuli (Berridge, 2007) was also related to anhedonia and amotivation in depression (Mayberg et al., 2005). Reduced DAT density in the central and basal nuclei of the amygdala was found in a post-mortem study (Klimek et al., 2002). The association between timescale differences with dopaminergic neurotransmission suggested that shorter timescales of these regions might result in inefficient responsiveness to rewards (Whitton et al., 2015; Alloy et al., 2016). Engaging additional targets (e.g., DA) could help patients with residual symptoms and treatment-resistant depression (Blier, 2016). Combining with these findings, our results revealed the role of dopaminergic neurotransmission in timescale aberrance. What is more, the validation results confirmed the robustness (selection of different atlas) and specificity (Compared with ALFF) of association between timescale aberrance and neurotransmitter information. These results suggested a potential neurophysiological mechanism underlying the shorter timescales observed in depression, providing clues to treatment.

Altered Timescale-Related Gene Expressions Enriched for Functional Annotations

We identified genes whose expression pattern presented significantly spatial (positive/negative) correlation with timescale aberrance and their ontology terms elaborated the underlying transcriptional basis of timescale aberrance. Consistent with the monoamine hypothesis in depression (Liu et al., 2018), positive correlation genes related to timescale difference were significantly enriched in monoamine neurotransmitter-related GO biological processes/KEGG pathways including neurotransmitter secretion, transport, and receptor activity/complex. These results corresponded with the aforesaid findings about monoamine aberrance, suggesting transcriptional mechanisms of association between timescale difference and monoamine neurotransmitters. In recent years, the synaptic dysfunction hypothesis that depression was caused by disruption of homeostatic mechanisms controlling synaptic plasticity (Duman and Aghajanian, 2012) has been proposed in consideration of the moderate and delayed effectiveness of the widely prescribed serotonin selective reuptake inhibitors (SSRIs) (Trivedi et al., 2006) and rapid antidepressant actions of ketamine in treatment-resistant depressed patients (Berman et al., 2000; Zarate et al., 2006). Deficits of excitatory glutamate neurons and inhibitory GABA interneurons resulted in the vulnerability of these major neurotransmitter systems followed by dendritic atrophy and spine loss in neurons of the hippocampus and prefrontal cortex (Qiao et al., 2016; Duman et al., 2019). Dendrite complexity and synaptic density can also be increased after treatment with antidepressants (Li et al., 2010; Li et al., 2011; MacQueen and Frodl, 2011). In our study, the timescale difference-related genes were enriched in terms of the charge of the balance of excitation and inhibition including glutamatergic synapse, transmission, receptor signaling pathway, GABAergic synapse, regulation of NMDA receptor activity, and G protein-coupled receptor signaling pathway. In fact, the spatial correlation ($p = 0.024$ uncorrected) between timescale aberrance and GABAa (gamma-aminobutyric acid) was also observed in the current study. These results elaborated possible transcriptional basis underlying the altered intrinsic timescale gradient in depression and provided new lines of evidence supporting the synaptic dysfunction hypothesis. In addition to the overlapping ontology terms with that in GWAS in depression, the multi-gene list results stated that timescale difference-related genes were reliable and sensitive, providing additional function-related enrichment information for depression.

There were several limitations to be considered. First, the timescale differences were obtained on a single dataset. However, the stage-specific aberrance was also observed in accelerated brain aging GMV in our previous study and might not result from sample selection (Han et al., 2021). Second, there was a substantial variation across subjects reflecting the individual susceptibility of specific receptor systems (Dukart et al., 2021); future studies should use simultaneous PET and MRI to provide more direct evidence. Third, patients enrolled in our study were under a depressive state. Whether the timescale difference was differently altered in various mood states, such as remitted state (Rive et al., 2015), could be tested in further studies. Fourth, only cross-sectional data were included in this study, and future studies could explore whether altered intrinsic timescale gradient returned to normal with antidepressant treatment especially for fast-acting antidepressants (Li, 2020).

CONCLUSION

This study revealed atypical intrinsic timescale gradient for the first time. In virtue of brain-wide gene expression and molecular imaging atlases, we investigated possible underlying molecular and transcriptional basis of timescale aberrance linking transcriptome, neurotransmitter information, and neuroimaging findings in depression. These results consistently supported the synaptic dysfunction hypothesis and promoted an integrative understanding of hierarchical dynamics aberrance in depression.

DATA AVAILABILITY STATEMENT

The raw data supporting the conclusions of this article will be made available by the authors, without undue reservation.

ETHICS STATEMENT

The studies involving human participants were reviewed and approved by the Research Ethical Committee of The First Affiliated Hospital of Zhengzhou University. The patients/participants provided their written informed consent to participate in this study.

AUTHOR CONTRIBUTIONS

SH and JC designed the study. RZ, SL, BZ, and YJ collected the data. SH and YC analyzed the data. SH and YZ drafted the work. YW, CW, JP, and HL revised the draft. All authors contributed to the article and approved the submitted version.

FUNDING

This research study was supported by the Natural Science Foundation of China (81601467, 81871327, and 62106229) and the Medical Science and Technology Research Project of Henan province (201701011, SBGJ202101013, and SBGJ202102103).

ACKNOWLEDGMENTS

We thank all subjects who participated in this study.

SUPPLEMENTARY MATERIAL

The Supplementary Material for this article can be found online at: https://www.frontiersin.org/articles/10.3389/fnins.2022.826609/full#supplementary-material

REFERENCES

Alexander-Bloch, A., Giedd, J. N., and Bullmore, E. (2013). Imaging structural co-variance between human brain regions. *Nat. Rev. Neurosci.* 14, 322–336. doi: 10.1038/nrn3465

Alloy, L. B., Olino, T., Freed, R. D., and Nusslock, R. (2016). Role of reward sensitivity and processing in major depressive and bipolar spectrum disorders. *Behav. Ther.* 47, 600–621. doi: 10.1016/j.beth.2016.02.014

Altamura, A. C., Dell'Osso, B., Mundo, E., and Dell'Osso, L. (2007). Duration of untreated illness in major depressive disorder: a naturalistic study. *Int. J. Clin. Pract.* 61, 1697–1700. doi: 10.1111/j.1742-1241.2007.01450.x

Altamura, A. C., Dell'osso, B., Vismara, S., and Mundo, E. (2008). May duration of untreated illness influence the long-term course of major depressive disorder? *Eur. Psychiatry* 23, 92–96. doi: 10.1016/j.eurpsy.2007.11.004

Anderson, K. M., Krienen, F. M., Choi, E. Y., Reinen, J. M., Yeo, B. T. T., and Holmes, A. J. (2018). Gene expression links functional networks across cortex and striatum. *Nat. Commun.* 9:1428. doi: 10.1038/s41467-018-03811-x

Arnatkeviciute, A., Fulcher, B. D., and Fornito, A. (2019). A practical guide to linking brain-wide gene expression and neuroimaging data. *Neuroimage* 189, 353–367. doi: 10.1016/j.neuroimage.2019.01.011

Azen, R., and Budescu, D. V. (2003). The dominance analysis approach for comparing predictors in multiple regression. *Psychol. Methods* 8, 129–148. doi: 10.1037/1082-989x.8.2.129

Bayer, H. M., and Glimcher, P. W. (2005). Midbrain dopamine neurons encode a quantitative reward prediction error signal. *Neuron* 47, 129–141. doi: 10.1016/j.neuron.2005.05.020

Beliveau, V., Svarer, C., Frokjaer, V. G., Knudsen, G. M., Greve, D. N., and Fisher, P. M. (2015). Functional connectivity of the dorsal and median raphe nuclei at rest. *Neuroimage* 116, 187–195. doi: 10.1016/j.neuroimage.2015.04.065

Berman, R. M., Cappiello, A., Anand, A., Oren, D. A., Heninger, G. R., Charney, D. S., et al. (2000). Antidepressant effects of ketamine in depressed patients. *Biol. Psychiatry* 47, 351–354. doi: 10.1016/s0006-3223(99)00230-9

Bernacchia, A., Seo, H., Lee, D., and Wang, X. J. (2011). A reservoir of time constants for memory traces in cortical neurons. *Nat. Neurosci.* 14, 366–372. doi: 10.1038/nn.2752

Berridge, K. C. (2007). The debate over dopamine's role in reward: the case for incentive salience. *Psychopharmacology* 191, 391–431. doi: 10.1007/s00213-006-0578-x

Blier, P. (2016). Neurobiology of depression and mechanism of action of depression treatments. *J. Clin. Psychiatry* 77:e319. doi: 10.4088/JCP.13097tx3c

Budescu, and David, V. (1993). Dominance analysis : a new approach to the problem of relative importance of predictors in multiple regression. *Psychol. Bull.* 114, 542–551.

Bukh, J. D., Bock, C., Vinberg, M., and Kessing, L. V. (2013). The effect of prolonged duration of untreated depression on antidepressant treatment outcome. *J. Affect. Dis.* 145, 42–48. doi: 10.1016/j.jad.2012.07.008

Burt, J. B., Demirtaş, M., Eckner, W. J., and Navejar, N. M. (2018). Hierarchy of transcriptomic specialization across human cortex captured by structural neuroimaging topography. *Nat. Neurosci.* 21, 1251–1259. doi: 10.1038/s41593-018-0195-0

Buzsáki, G., and Draguhn, A. (2004). Neuronal oscillations in cortical networks. *Science* 304, 1926–1929. doi: 10.1126/science.1099745

Cao, B., Passos, I. C., Mwangi, B., Amaral-Silva, H., and Tannous, J. (2017). Hippocampal subfield volumes in mood disorders. *Mol. Psychiatry* 22, 1352–1358. doi: 10.1038/mp.2016.262

Cavanagh, S. E., Wallis, J. D., Kennerley, S. W., and Hunt, L. T. (2016). Autocorrelation structure at rest predicts value correlates of single neurons during reward-guided choice. *Elife* 5:e18937. doi: 10.7554/eLife.18937

Chaudhuri, R., Knoblauch, K., Gariel, M. A., Kennedy, H., and Wang, X. J. (2015). A large-scale circuit mechanism for hierarchical dynamical processing in the primate cortex. *Neuron* 88, 419–431. doi: 10.1016/j.neuron.2015.09.008

Chen, J., Müller, V. I., Dukart, J., Hoffstaedter, F., Baker, J. T., Holmes, A. J., et al. (2021). Intrinsic connectivity patterns of task-defined brain networks allow individual prediction of cognitive symptom dimension of schizophrenia and are linked to molecular architecture. *Biol. Psychiatry* 89, 308–319. doi: 10.1016/j.biopsych.2020.09.024

Chen, V. C., Shen, C. Y., Liang, S. H., Li, Z. H., Tyan, Y. S., Liao, Y. T., et al. (2016). Assessment of abnormal brain structures and networks in major depressive disorder using morphometric and connectome analyses. *J. Affect. Dis.* 205, 103–111. doi: 10.1016/j.jad.2016.06.066

Chen, Y., Cui, Q., Fan, Y. S., Guo, X., Tang, Q., Sheng, W., et al. (2020). Progressive brain structural alterations assessed via causal analysis in patients with generalized anxiety disorder. *Neuropsychopharmacology* 45, 1689–1697. doi: 10.1038/s41386-020-0704-1

Chen, Z., Peng, W., Sun, H., Kuang, W., Li, W., Jia, Z., et al. (2016). High-field magnetic resonance imaging of structural alterations in first-episode, drug-naive patients with major depressive disorder. *Trans. Psychiatry* 6:e942. doi: 10.1038/tp.2016.209

Cocchi, L., Sale, M. V., Bell, P. T., Nguyen, V. T., Zalesky, A., and Mattingley, J. B. (2016). A hierarchy of timescales explains distinct effects of local inhibition of primary visual cortex and frontal eye fields. *Elife* 5:e15252. doi: 10.7554/eLife.15252

Corlett, P. R., Honey, G. D., Krystal, J. H., and Fletcher, P. C. (2011). Glutamatergic model psychoses: prediction error, learning, and inference. *Neuropsychopharmacology* 36, 294–315. doi: 10.1038/npp.2010.163

Covington, H. E. III, Lobo, M. K., Maze, I., Vialou, V., Hyman, J. M., Zaman, S., et al. (2010). Antidepressant effect of optogenetic stimulation of the medial prefrontal cortex. *J. Neurosci.* 30, 16082–16090. doi: 10.1523/jneurosci.1731-10.2010

Davidson, L., and McGlashan, T. H. (1997). The varied outcomes of schizophrenia. *Can. J. Psychiatry* 42, 34–43. doi: 10.1177/070674379704200105

Drevets, W. C., Price, J. L., and Furey, M. L. (2008). Brain structural and functional abnormalities in mood disorders: implications for neurocircuitry models of depression. *Brain Struct. Funct.* 213, 93–118. doi: 10.1007/s00429-008-0189-x

Dukart, J., Holiga, S., Rullmann, M., and Lanzenberger, R. (2021). JuSpace: a tool for spatial correlation analyses of magnetic resonance imaging data with nuclear imaging derived neurotransmitter maps. *Hum. Brain Mapp.* 42, 555–566. doi: 10.1002/hbm.25244

Duman, R. S., and Aghajanian, G. K. (2012). Synaptic dysfunction in depression: potential therapeutic targets. *Science* 338, 68–72. doi: 10.1126/science.1222939

Duman, R. S., Sanacora, G., and Krystal, J. H. (2019). Altered connectivity in depression: GABA and glutamate neurotransmitter deficits and reversal by novel treatments. *Neuron* 102, 75–90. doi: 10.1016/j.neuron.2019.03.013

Dygalo, N. N., Kalinina, T. S., and Shishkina, G. T. (2020). Stress-induced expression pattern of glutamate signaling genes associated with anhedonia. *Stress* 23, 700–707. doi: 10.1080/10253890.2020.1812574

Elston, G. N. (2003). Cortex, cognition and the cell: new insights into the pyramidal neuron and prefrontal function. *Cereb Cortex* 13, 1124–1138. doi: 10.1093/cercor/bhg093

Fan, L., Li, H., Zhuo, J., Zhang, Y., Wang, J., Chen, L., et al. (2016). The human brainnetome atlas: a new brain atlas based on connectional architecture. *Cerebral Cortex* 26, 3508–3526. doi: 10.1093/cercor/bhw157

Fornito, A., Arnatkevièiûtë, A., and Fulcher, B. D. (2019). Bridging the gap between connectome and transcriptome. *Trends Cogn. Sci.* 23, 34–50. doi: 10.1016/j.tics.2018.10.005

Fornito, A., Zalesky, A., Bassett, D. S., Meunier, D., Ellison-Wright, I., Yücel, M., et al. (2011). Genetic influences on cost-efficient organization of human cortical functional networks. *J. Neurosci.* 31, 3261–3270. doi: 10.1523/jneurosci.4858-10.2011

Frodl, T., Meisenzahl, E. M., Zetzsche, T., Born, C., Jäger, M., Groll, C., et al. (2003). Larger amygdala volumes in first depressive episode as compared to recurrent major depression and healthy control subjects. *Biol. Psychiatry* 53, 338–344. doi: 10.1016/s0006-3223(02)01474-9

Fulcher, B. D., Murray, J. D., Zerbi, V., and Wang, X. J. (2019). Multimodal gradients across mouse cortex. *Proc. Natl. Acad. Sci. U.S.A.* 116, 4689–4695. doi: 10.1073/pnas.1814144116

Glahn, D. C., Winkler, A. M., Kochunov, P., Almasy, L., Duggirala, R., Carless, M. A., et al. (2010). Genetic control over the resting brain. *Proc. Natl. Acad. Sci. U.S.A.* 107, 1223–1228. doi: 10.1073/pnas.0909969107

Hamon, M., and Blier, P. (2013). Monoamine neurocircuitry in depression and strategies for new treatments. *Prog. Neuropsychopharmacol. Biol. Psychiatry* 45, 54–63. doi: 10.1016/j.pnpbp.2013.04.009

Han, S., Chen, Y., Zheng, R., Li, S., Jiang, Y., Wang, C., et al. (2021). The stage-specifically accelerated brain aging in never-treated first-episode patients with depression. *Hum. Brain Mapp.* 42, 3656–3666. doi: 10.1002/hbm.25460

Han, S., Cui, Q., Wang, X., Chen, Y., Li, D., Li, L., et al. (2020). The anhedonia is differently modulated by structural covariance network of NAc in bipolar disorder and major depressive disorder. *Prog. Neuropsychopharmacol. Biol. Psychiatry* 99:109865. doi: 10.1016/j.pnpbp.2020.109865

Han, S., He, Z., Duan, X., Tang, Q., Chen, Y., Yang, Y., et al. (2019). Dysfunctional connectivity between raphe nucleus and subcortical regions presented opposite differences in bipolar disorder and major depressive disorder. *Prog. Neuropsychopharmacol. Biol. Psychiatry* 92, 76–82. doi: 10.1016/j.pnpbp.2018.12.017

Hasson, U., Chen, J., and Honey, C. J. (2015). Hierarchical process memory: memory as an integral component of information processing. *Trends Cogn. Sci.* 19, 304–313. doi: 10.1016/j.tics.2015.04.006

Hasson, U., Yang, E., Vallines, I., Heeger, D. J., and Rubin, N. (2008). A hierarchy of temporal receptive windows in human cortex. *J. Neurosci.* 28, 2539–2550. doi: 10.1523/jneurosci.5487-07.2008

Hawrylycz, M. J., Lein, E. S., Guillozet-Bongaarts, A. L., Shen, E. H., Ng, L., Miller, J. A., et al. (2012). An anatomically comprehensive atlas of the adult human brain transcriptome. *Nature* 489, 391–399. doi: 10.1038/nature11405

Hollerman, J. R., and Schultz, W. (1998). Dopamine neurons report an error in the temporal prediction of reward during learning. *Nat. Neurosci.* 1, 304–309. doi: 10.1038/1124

Howard, D. M., and Adams, M. J. (2019). Genome-wide meta-analysis of depression identifies 102 independent variants and highlights the importance of the prefrontal brain regions. *Nat. Neurosci.* 22, 343–352. doi: 10.1038/s41593-018-0326-7

Hung, C. I., Yu, N. W., Liu, C. Y., Wu, K. Y., and Yang, C. H. (2015). The impact of the duration of an untreated episode on improvement of depression and somatic symptoms. *Neuropsychiatr. Dis. Treat.* 11, 2245–2252. doi: 10.2147/ndt.s89498

Huntenburg, J. M., Bazin, P. L., and Margulies, D. S. (2018). Large-scale gradients in human cortical organization. *Trends Cogn. Sci.* 22, 21–31. doi: 10.1016/j.tics.2017.11.002

Jaako-Movits, K., Zharkovsky, T., Pedersen, M., and Zharkovsky, A. (2006). Decreased hippocampal neurogenesis following olfactory bulbectomy is reversed by repeated citalopram administration. *Cell Mol. Neurobiol.* 26, 1559–1570. doi: 10.1007/s10571-006-9090-4

Jardri, R., Hugdahl, K., Hughes, M., Brunelin, J., Waters, F., Alderson-Day, B., et al. (2016). Are hallucinations due to an imbalance between excitatory and inhibitory influences on the brain? *Schizophr. Bull.* 42, 1124–1134. doi: 10.1093/schbul/sbw075

Jiang, Y., Luo, C., Li, X., Duan, M., He, H., Chen, X., et al. (2018). Progressive reduction in gray matter in patients with schizophrenia assessed with MR imaging by using causal network analysis. *Radiology* 287, 633–642. doi: 10.1148/radiol.2017171832

Kambeitz, J. P., and Howes, O. D. (2015). The serotonin transporter in depression: meta-analysis of in vivo and post mortem findings and implications for understanding and treating depression. *J. Affect. Dis.* 186, 358–366. doi: 10.1016/j.jad.2015.07.034

Kendler, K. S., Thornton, L. M., and Gardner, C. O. (2001). Genetic risk, number of previous depressive episodes, and stressful life events in predicting onset of major depression. *Am. J. Psychiatry* 158, 582–586. doi: 10.1176/appi.ajp.158.4.582

Kiebel, S. J., Daunizeau, J., and Friston, K. J. (2008). A hierarchy of time-scales and the brain. *PLoS Comput. Biol.* 4:e1000209. doi: 10.1371/journal.pcbi.1000209

Klimek, V., Schenck, J. E., Han, H., Stockmeier, C. A., and Ordway, G. A. (2002). Dopaminergic abnormalities in amygdaloid nuclei in major depression: a postmortem study. *Biol. Psychiatry* 52, 740–748. doi: 10.1016/s0006-3223(02)01383-5

Koutsouleris, N., Davatzikos, C., Borgwardt, S., Gaser, C., Bottlender, R., Frodl, T., et al. (2014). Accelerated brain aging in schizophrenia and beyond: a neuroanatomical marker of psychiatric disorders. *Schizophr. Bull.* 40, 1140–1153. doi: 10.1093/schbul/sbt142

Kraus, C., and Kadriu, B. (2019). Prognosis and improved outcomes in major depression: a review. *Trans. Psychiatry* 9:127. doi: 10.1038/s41398-019-0460-3

Krienen, F. M., Yeo, B. T., Ge, T., Buckner, R. L., and Sherwood, C. C. (2016). Transcriptional profiles of supragranular-enriched genes associate with corticocortical network architecture in the human brain. *Proc. Natl. Acad. Sci. U.S.A.* 113, E469–E478. doi: 10.1073/pnas.1510903113

Kringelbach, M. L., and Cruzat, J. (2020). Dynamic coupling of whole-brain neuronal and neurotransmitter systems. *Proc. Natl. Acad. Sci. U.S.A.* 117, 9566–9576. doi: 10.1073/pnas.1921475117

Landek-Salgado, M. A., Faust, T. E., and Sawa, A. (2016). Molecular substrates of schizophrenia: homeostatic signaling to connectivity. *Mol. Psychiatry* 21, 10–28. doi: 10.1038/mp.2015.141

Li, J., and Seidlitz, J. (2021). Cortical structural differences in major depressive disorder correlate with cell type-specific transcriptional signatures. *Nat. Commun.* 12:1647. doi: 10.1038/s41467-021-21943-5

Li, N., Lee, B., Liu, R. J., Banasr, M., Dwyer, J. M., Iwata, M., et al. (2010). mTOR-dependent synapse formation underlies the rapid antidepressant effects of NMDA antagonists. *Science* 329, 959–964. doi: 10.1126/science.1190287

Li, N., Liu, R. J., Dwyer, J. M., Banasr, M., Lee, B., Son, H., et al. (2011). Glutamate N-methyl-D-aspartate receptor antagonists rapidly reverse behavioral and synaptic deficits caused by chronic stress exposure. *Biol. Psychiatry* 69, 754–761. doi: 10.1016/j.biopsych.2010.12.015

Li, X., Zhang, Y., Meng, C., Zhang, C., Zhao, W., Zhu, D. M., et al. (2021). Functional stability predicts depressive and cognitive improvement in major depressive disorder: a longitudinal functional MRI study. *Prog. Neuropsychopharmacol. Biol. Psychiatry* 111:110396. doi: 10.1016/j.pnpbp.2021.110396

Li, Y. F. (2020). A hypothesis of monoamine (5-HT) - glutamate/GABA long neural circuit: aiming for fast-onset antidepressant discovery. *Pharmacol. Ther.* 208:107494. doi: 10.1016/j.pharmthera.2020.107494

Limongi, R., Jeon, P., Mackinley, M., Das, T., Dempster, K., Théberge, J., et al. (2020). Glutamate and dysconnection in the salience network: neurochemical, effective connectivity, and computational evidence in schizophrenia. *Biol. Psychiatry* 88, 273–281. doi: 10.1016/j.biopsych.2020.01.021

Liu, J. J., Hezghia, A., Shaikh, S. R., and Cenido, J. F. (2018). Regulation of monoamine transporters and receptors by lipid microdomains: implications for depression. *Neuropsychopharmacology* 43, 2165–2179. doi: 10.1038/s41386-018-0133-6

Liu, Z., Rolls, E. T., Liu, Z., Zhang, K., Yang, M., Du, J., et al. (2019). Brain annotation toolbox: exploring the functional and genetic associations of neuroimaging results. *Bioinformatics* 35, 3771–3778. doi: 10.1093/bioinformatics/btz128

MacQueen, G., and Frodl, T. (2011). The hippocampus in major depression: evidence for the convergence of the bench and bedside in psychiatric research? *Mol. Psychiatry* 16, 252–264. doi: 10.1038/mp.2010.80

Mayberg, H. S., Lozano, A. M., Voon, V., McNeely, H. E., Seminowicz, D., Hamani, C., et al. (2005). Deep brain stimulation for treatment-resistant depression. *Neuron* 45, 651–660. doi: 10.1016/j.neuron.2005.02.014

McKinnon, M. C., Yucel, K., Nazarov, A., and MacQueen, G. M. (2009). A meta-analysis examining clinical predictors of hippocampal volume in patients with major depressive disorder. *J. Psychiatry Neurosci.* 34, 41–54.

Moylan, S., Maes, M., Wray, N. R., and Berk, M. (2013). The neuroprogressive nature of major depressive disorder: pathways to disease evolution and resistance, and therapeutic implications. *Mol. Psychiatry* 18, 595–606. doi: 10.1038/mp.2012.33

Murray, C. J., Vos, T., Lozano, R., Naghavi, M., Flaxman, A. D., Michaud, C., et al. (2012). Disability-adjusted life years (DALYs) for 291 diseases and injuries in 21 regions, 1990-2010: a systematic analysis for the global burden of disease study 2010. *Lancet* 380, 2197–2223. doi: 10.1016/s0140-6736(12)61689-4

Phillips, M. L., Ladouceur, C. D., and Drevets, W. C. (2008). A neural model of voluntary and automatic emotion regulation: implications for understanding the pathophysiology and neurodevelopment of bipolar disorder. *Mol. Psychiatry* 829, 833–857. doi: 10.1038/mp.2008.65

Pirker, W., Asenbaum, S., Kasper, S., Walter, H., Angelberger, P., Koch, G., et al. (1995). beta-CIT SPECT demonstrates blockade of 5HT-uptake sites by citalopram in the human brain in vivo. *J. Neural. Trans. Gen. Sect.* 100, 247–256. doi: 10.1007/bf01276462

Qiao, H., Li, M. X., Xu, C., Chen, H. B., An, S. C., and Ma, X. M. (2016). Dendritic spines in depression: what we learned from animal models. *Neural. Plast* 2016:8056370. doi: 10.1155/2016/8056370

Raut, R. V., and Snyder, A. Z. (2020). Hierarchical dynamics as a macroscopic organizing principle of the human brain. *Proc. Natl. Acad. Sci. U.S.A.* 117, 20890–20897. doi: 10.1073/pnas.2003383117

Reardon, P. K., and Seidlitz, J. (2018). Normative brain size variation and brain shape diversity in humans. *Science* 360, 1222–1227. doi: 10.1126/science.aar2578

Richiardi, J., Altmann, A., Milazzo, A. C., Chang, C., Chakravarty, M. M., Banaschewski, T., et al. (2015). Brain networks. correlated gene expression supports synchronous activity in brain networks. *Science* 348, 1241–1244. doi: 10.1126/science.1255905

Rive, M. M., Mocking, R. J. T., Koeter, M. W. J., Wingen, G. V., Wit, S. J. D., Heuvel, O. A. V. D., et al. (2015). State-dependent differences in emotion regulation between unmedicated bipolar disorder and major depressive disorder. *JAMA Psychiatry* 72:687. doi: 10.1001/jamapsychiatry.2015.0161

Schmaal, L., Hibar, D. P., Sämann, P. G., Hall, G. B., Baune, B. T., Jahanshad, N., et al. (2017). Cortical abnormalities in adults and adolescents with major depression based on brain scans from 20 cohorts worldwide in the ENIGMA major depressive disorder working group. *Mol. Psychiatry* 22, 900–909. doi: 10.1038/mp.2016.60

Shen, X., Tokoglu, F., Papademetris, X., and Constable, R. T. (2013). Groupwise whole-brain parcellation from resting-state fMRI data for network node identification. *Neuroimage* 82, 403–415. doi: 10.1016/j.neuroimage.2013.05.081

Song, X. W., Dong, Z. Y., Long, X. Y., Li, S. F., Zuo, X. N., Zhu, C. Z., et al. (2011). REST: a toolkit for resting-state functional magnetic resonance imaging data processing. *PLoS One* 6:e25031. doi: 10.1371/journal.pone.0025031

Stagg, C. J., Bachtiar, V., Amadi, U., Gudberg, C. A., Ilie, A. S., Sampaio-Baptista, C., et al. (2014). Local GABA concentration is related to network-level resting functional connectivity. *Elife* 3:e01465. doi: 10.7554/eLife.01465

Steinberg, L. J., Underwood, M. D., Bakalian, M. J., Kassir, S. A., Mann, J. J., and Arango, V. (2019). 5-HT1A receptor, 5-HT2A receptor and serotonin transporter binding in the human auditory cortex in depression. *J. Psychiatry Neurosci.* 44, 294–302. doi: 10.1503/jpn.180190

Tomasi, D., and Volkow, N. D. (2010). Functional connectivity density mapping. *Proc. Natl. Acad. Sci. U.S.A.* 107, 9885–9890. doi: 10.1073/pnas.1001414107

Treadway, M. T., Waskom, M. L., Dillon, D. G., Holmes, A. J., Park, M. T. M., Chakravarty, M. M., et al. (2015). Illness progression, recent stress, and morphometry of hippocampal subfields and medial prefrontal cortex in major depression. *Biol. Psychiatry* 77, 285–294. doi: 10.1016/j.biopsych.2014.06.018

Trivedi, M. H., Rush, A. J., Wisniewski, S. R., Nierenberg, A. A., Warden, D., Ritz, L., et al. (2006). Evaluation of outcomes with citalopram for depression using measurement-based care in STAR*D: implications for clinical practice. *Am. J. Psychiatry* 163, 28–40. doi: 10.1176/appi.ajp.163.1.28

van den Heuvel, M. P., van Soelen, I. L., Stam, C. J., Kahn, R. S., Boomsma, D. I., and Hulshoff Pol, H. E. (2013). Genetic control of functional brain network efficiency in children. *Eur. Neuropsychopharmacol.* 23, 19–23. doi: 10.1016/j.euroneuro.2012.06.007

van Eijndhoven, P., van Wingen, G., van Oijen, K., Rijpkema, M., Goraj, B., Jan Verkes, R., et al. (2009). Amygdala volume marks the acute state in the early course of depression. *Biol. Psychiatry* 65, 812–818. doi: 10.1016/j.biopsych.2008.10.027

van Haren, N. E., Cahn, W., Hulshoff Pol, H. E., Schnack, H. G., Caspers, E., Lemstra, A., et al. (2003). Brain volumes as predictor of outcome in recent-onset schizophrenia: a multi-center MRI study. *Schizophr. Res.* 64, 41–52. doi: 10.1016/s0920-9964(03)00018-5

Vértes, P. E., Rittman, T., Whitaker, K. J., Romero-Garcia, R., Váša, F., and Kitzbichler, M. G. (2016). Gene transcription profiles associated with inter-modular hubs and connection distance in human functional magnetic resonance imaging networks. *Philos. Trans. R Soc. Lond. B Biol. Sci.* 371:362. doi: 10.1098/rstb.2015.0362

Voineskos, D., Blumberger, D. M., Zomorrodi, R., Rogasch, N. C., Farzan, F., Foussias, G., et al. (2019). Altered transcranial magnetic stimulation-electroencephalographic markers of inhibition and excitation in the dorsolateral prefrontal cortex in major depressive disorder. *Biol. Psychiatry* 85, 477–486. doi: 10.1016/j.biopsych.2018.09.032

Wang, X. J. (2020). Macroscopic gradients of synaptic excitation and inhibition in the neocortex. *Nat. Rev. Neurosci.* 21, 169–178. doi: 10.1038/s41583-020-0262-x

Watanabe, T., Rees, G., and Masuda, N. (2019). Atypical intrinsic neural timescale in autism. *Elife* 8:e42256. doi: 10.7554/eLife.42256

Wengler, K., Goldberg, A. T., Chahine, G., and Horga, G. (2020). Distinct hierarchical alterations of intrinsic neural timescales account for different manifestations of psychosis. *Elife* 9, e56151. doi: 10.7554/eLife.56151

Whitton, A. E., Treadway, M. T., and Pizzagalli, D. A. (2015). Reward processing dysfunction in major depression, bipolar disorder and schizophrenia. *Curr. Opin. Psychiatry* 28, 7–12. doi: 10.1097/YCO.0000000000000122

Wong, K. F., and Wang, X. J. (2006). A recurrent network mechanism of time integration in perceptual decisions. *J. Neurosci.* 26, 1314–1328. doi: 10.1523/jneurosci.3733-05.2006

Wray, N. R., Ripke, S., Mattheisen, M., Trzaskowski, M., Byrne, E. M., Abdellaoui, A., et al. (2018). Genome-wide association analyses identify 44 risk variants and refine the genetic architecture of major depression. *Nat. Genet.* 50, 668–681. doi: 10.1038/s41588-018-0090-3

Yan, C.-G., Wang, X.-D., Zuo, X.-N., and Zang, Y.-F. (2016). DPABI: data processing & analysis for (resting-state) brain imaging. *Neuroinformatics* 14, 339–351. doi: 10.1007/s12021-016-9299-4

Yüksel, D., Engelen, J., Schuster, V., Dietsche, B., Konrad, C., Jansen, A., et al. (2018). Longitudinal brain volume changes in major depressive disorder. *J. Neural. Trans.* 125, 1433–1447. doi: 10.1007/s00702-018-1919-8

Zarate, C. A. Jr., Singh, J. B., Carlson, P. J., Brutsche, N. E., Ameli, R., Luckenbaugh, D. A., et al. (2006). A randomized trial of an N-methyl-D-aspartate antagonist in treatment-resistant major depression. *Arch. Gen. Psychiatry* 63, 856–864. doi: 10.1001/archpsyc.63.8.856

Zhang, C., Cai, H., and Xu, X. (2021). Genetic architecture underlying differential resting-state functional connectivity of subregions within the human visual cortex. *Cerebral Cortex*. doi: 10.1093/cercor/bhab335 [Epub ahead of print].

Zhang, Z., Liao, W., Xu, Q., Wei, W., Zhou, H. J., Sun, K., et al. (2017). Hippocampus-associated causal network of structural covariance measuring structural damage progression in temporal lobe epilepsy. *Hum. Brain Mapp.* 38, 753–766. doi: 10.1002/hbm.23415

Zhou, Y., Zhou, B., Pache, L., and Chang, M. (2019). Metascape provides a biologist-oriented resource for the analysis of systems-level datasets. *Nat. Commun.* 10:1523. doi: 10.1038/s41467-019-09234-6

Zhu, D., Yuan, T., Gao, J., Xu, Q., Xue, K., Zhu, W., et al. (2021). Correlation between cortical gene expression and resting-state functional network centrality in healthy young adults. *Hum. Brain Mapp.* 42, 2236–2249. doi: 10.1002/hbm.25362

Zucker, R. S., and Regehr, W. G. (2002). Short-term synaptic plasticity. *Annu Rev. Physiol.* 64, 355–405. doi: 10.1146/annurev.physiol.64.092501.114547

Conflict of Interest: The authors declare that the research was conducted in the absence of any commercial or financial relationships that could be construed as a potential conflict of interest.

Publisher's Note: All claims expressed in this article are solely those of the authors and do not necessarily represent those of their affiliated organizations, or those of the publisher, the editors and the reviewers. Any product that may be evaluated in this article, or claim that may be made by its manufacturer, is not guaranteed or endorsed by the publisher.

frontiers | Frontiers in Neuroscience

ORIGINAL RESEARCH
published: 14 June 2022
doi: 10.3389/fnins.2022.908650

Alzheimer's Disease-Related Genes Identified by Linking Spatial Patterns of Pathology and Gene Expression

Roger Mullins and Dimitrios Kapogiannis**

Laboratory of Neurosciences, National Institute on Aging, Baltimore, MD, United States

Background: Alzheimer's Disease (AD) is an age-related neurodegenerative disease with a poorly understood etiology, shown to be partly genetic. Glucose hypometabolism, extracellular Amyloid-beta (Aβ) deposition, and intracellular Tau deposition are cardinal features of AD and display characteristic spatial patterns in the brain. We hypothesize that regional differences in underlying gene expression confer either resistance or susceptibility to AD pathogenic processes and are associated with these spatial patterns. Data-driven methods for the identification of genes involved in AD pathogenesis complement hypothesis-driven approaches that reflect current theories about the disease. Here we present a data driven method for the identification of genes involved in AD pathogenesis based on comparing spatial patterns of normal gene expression to Positron Emission Tomography (PET) images of glucose hypometabolism, Aβ deposition, and Tau deposition.

Methods: We performed correlations between the cerebral cortex microarray samples from the six cognitively normal (CN) post-mortem Allen Human Brain Atlas (AHBA) specimens and PET FDG-18, AV-45, and AV-1451 tracer images from AD and CN participants in the Alzheimer's Disease and Neuroimaging Initiative (ADNI) database. Correlation coefficients for each gene by each ADNI subject were then entered into a partial least squares discriminant analysis (PLS-DA) to determine sets that best classified the AD and CN groups. Pathway analysis *via* BioPlanet 2019 was then used to infer the function of implicated genes.

Results: We identified distinct sets of genes strongly associated with each PET modality. Pathway analyses implicated novel genes involved in mitochondrial function, and Notch signaling, as well as genes previously associated with AD.

Conclusion: Using an unbiased approach, we derived sets of genes with expression patterns spatially associated with FDG hypometabolism, Aβ deposition, and Tau deposition in AD. This methodology may complement population-based approaches for identifying the genetic underpinnings of AD.

Keywords: tau, FDG-18, PLS-DA, ADNI, allen human brain atlas, Alzheimer's disease, Alzheimer's, amyloid-β

OPEN ACCESS

Edited by:
Jiajia Zhu,
First Affiliated Hospital of Anhui Medical University, China

Reviewed by:
Kathryn Bowles,
Icahn School of Medicine at Mount Sinai, United States
Felix Carbonell,
Biospective Inc., Canada

****Correspondence:***
Roger Mullins
roger.mullins@nih.gov
Dimitrios Kapogiannis
kapogiannisd@mail.nih.gov

Specialty section:
This article was submitted to Brain Imaging Methods, a section of the journal Frontiers in Neuroscience

Received: *30 March 2022*
Accepted: *26 May 2022*
Published: *14 June 2022*

Citation:
Mullins R and Kapogiannis D (2022) Alzheimer's Disease-Related Genes Identified by Linking Spatial Patterns of Pathology and Gene Expression. Front. Neurosci. 16:908650. doi: 10.3389/fnins.2022.908650

INTRODUCTION

Alzheimer's disease (AD) is a progressive neurodegenerative disease that accounts for 60–70% of dementia cases in the aging population. The pathophysiology of the disease includes glucose hypometabolism, whereas its cardinal neuropathological features are the accumulation of aggregates of amyloid beta-peptide (Aβ) in extracellular plaques and intracellular hyperphosphorylated tau tangles. Pathologic forms of these proteins and their aggregates impair synaptic function and induce maladaptive neuroinflammation involving astrocytes and microglia. This process eventually results in synaptic and neuronal loss, macroscopically evident as brain atrophy (De Strooper and Karran, 2016; Frisoni et al., 2022). Although the proximate causes for Aβ and Tau aggregation have been largely crystalized in the "amyloid hypothesis," the ultimate causes of AD remain unknown (Frisoni et al., 2022). Specific brain regions, such as the medial temporal, precuneus/posterior cingulate, lateral temporoparietal cortices, are more prone to develop severe AD pathologies and manifest them earlier during the disease. By contrast, other regions such as the primary motor cortex, sensory cortex and cerebellum remain almost intact (Frisoni et al., 2022). Attempts to explain this selective regional vulnerability have focused on the structural and functional connectivity of the default mode network (Buckner et al., 2009; Seeley et al., 2009) and the spatial interplay of distinct processes leading to glucose hypometabolism, Aβ plaques, and Tau deposition within networks (Sepulcre et al., 2016).

The pathogenic cascade of AD extends over decades and follows a characteristic regional progression, starting in distinct brain regions for Aβ and Tau (Arnold et al., 1991; Braak and Braak, 1991; Braak and Del Tredici, 2012; Sepulcre et al., 2016). AD pathology is preceded or accompanied by changes in the expression of many genes. The brains of late-stage AD patients exhibit severe neuronal loss, which could result in an altered gene expression profile. The underlying spatial patterns of gene expression have been shown to account for both structural (Burt et al., 2018; Reardon et al., 2018) and functional (Richiardi et al., 2015; Vertes et al., 2016) features in the human brain, and similar methods have been used successfully to examine genes implicated in disease states such as Parkinson's (Keo et al., 2021) and Huntington's disease (McColgan et al., 2018).

Given that the distribution of most gene expression varies widely throughout the brain, we previously hypothesized that regional differences in normal gene expression during young to middle age may relate to or mediate regional vulnerability to Aβ and Tau pathologies (Diehl et al., 2017; Mullins et al., 2017). In prior studies, we focused on limited sets of genes associated with insulin resistance, and revealed compelling associations between the Brodmann area topography of normal expression of metabolism and insulin signaling-related genes, and those of established (Arnold et al., 1991) pathological Aβ and Tau.

In the present study we expand this hypothesis to investigate whether normal regional cortical differences in gene expression are related to the cardinal pathological features of AD, and to use this information to identify specific genes and pathways related to AD pathology. Given the striking and well-characterized regional differences in glucose hypometabolism, Aβ and Tau, we focused on these intermediate disease phenotypes. To establish reliable image maps of these pathologies, we used FDG-18 (glucose metabolism), AV-45 (Aβ), and AV-1451 (Tau) PET scans from the large ADNI cohort of AD and CN subjects. Next, we examined the spatial correlation of these maps with co-registered maps of gene expression from the Allen Human Brain Atlas (AHBA)(Hawrylycz et al., 2012). We then used the resulting correlation coefficients, one for each gene per subject, as inputs to a Partial Least Squares Discriminant Analysis (PLS-DA). Underlying this approach is PLS regression (PLS-R) (Wold et al., 2001), a flexible Principal Components Analysis-based method often used to assess commonalities between AHBA transcriptome data and 3D imaging data from other modalities. Specifically, PLS-R has been used to find the spatial correlation between AHBA gene expression and resting-state functional connectivity in healthy subjects (Vertes et al., 2016; Zhu et al., 2021), and with regional cortical thickness changes in Parkinson's (Keo et al., 2021) and Huntington's disease (McColgan et al., 2018). An assumption of PLS-R is that the system under investigation is primarily influenced by a small set of underlying "latent" variables which are maximally correlated between the datasets. PLS-DA extends this method toward classification, regressing binary group variables against a corresponding set of predictor variables (Perez-Enciso and Tenenhaus, 2003). See **Figure 1** for a flowchart of this process.

It is worth noting that this method does not intend to reveal the actual spatial distribution of gene expression in the disease condition, only that a pathology is more or less correlated spatially with a given gene expression pattern. The rationale for conducting a correlative analysis between data obtained from individuals at different age groups is provided by the natural history of AD: AD pathologies start developing in young-middle age in brain areas with different transcriptomic signatures, these pathologies evolve over time in varying degrees for different brain areas and culminate at distinct patterns of pathology in older brains. Given that gene expression was assessed in the brains of individuals who died young or in mid-life, before the typical age when AD pathologies begin accumulating, the correlations may reveal genes implicated in the mechanisms conferring regional resilience or vulnerability to the development of AD.

This study demonstrates a novel data-driven bioinformatic approach using the spatial correlation between normal gene expression and image intensity of three types of PET conducted in AD and Cognitively Normal (CN) individuals as input to a discriminant analysis. Our specific hypothesis is that the spatial patterns of emergent pathologies in the AD brain are associated with the normal spatial expression of specific genes. Our primary aim was to use this method to derive sets of genes for optimal classification of AD and CN individuals based on their PET measures of FDG-18 hypometabolism, Aβ, and Tau deposits. As a secondary aim, we sought to identify novel genes associated with distinct aspects of AD pathology and uncover biological processes that may contribute to their development.

MATERIALS AND METHODS

Participants

Alzheimer's Disease and Neuroimaging Initiative Participants

Baseline FDG-PET, AV45-PET (Aβ), and AV1451-PET (Tau) images from the ADNI Image & Data Archive site[1] were downloaded as Neuroimaging Informatics Technology Initiative (NIFTI) file format volumes in January of 2022. We analyzed each PET tracer for CN and AD ADNI participants ranging from 55 to 95 years old (**Table 1**). ADNI was launched in 2003 by the National Institute on Aging (NIA), the National Institute of Biomedical Imaging and Bioengineering (NIBIB), the Food and Drug Administration (FDA), private pharmaceutical companies and non-profit organizations, as a $60 million, 5-year public-private partnership. The primary goal of ADNI has been to test whether serial magnetic resonance imaging (MRI), PET, other biological markers, and clinical and neuropsychological assessment can be combined to measure the progression of MCI and early AD. The Principal Investigator of this initiative is Michael W. Weiner, MD, VA Medical Center and University of California San Francisco. For up-to-date information, see www.adni-info.org.

Allen Human Brain Atlas Human Brain Specimens

The Allen Human Brain Atlas (AHBA) incorporates microarray data from six postmortem brain specimens obtained from normal donors with no known prior neuropathological or neuropsychiatric history (Hawrylycz et al., 2012). Each specimen provided 501–946 distributed sample sites for the microarray set of 29,191 unique genes, with multiple probes available for 93% of these genes. Detailed donor profile information is available in **Supplementary Table 1** and the http://human.brain-map.org/ documentation section.

Allen Human Brain Atlas Microarray Data Preprocessing

Data for the probes, sample sites, and normalized expression values was imported from the files available for download at the Allen Institute for Brain Science, Allen Human Brain Atlas site: http://human.brain-map.org/static/download. Detailed information and white papers for the survey, platform selection, and normalization of the Agilent 8x60K custom microarray data is available at the http://human.brain-map.org/ documentation section. These consisted of 58,692 probes (replicates for the 29,191 genes) for each sample. Preprocessing was performed using R (v.4.1.0) and the Bioconductor package (Biobase v.2.5.2). The following steps were applied: (1) Removed AHBA microarray probes with no gene ontology (GO) annotation or entrez-id, leaving 43,714 probes. (2) Set sample values with expression values below background as missing "NA" *via* the present-absent call (PAC) files provided in the AHBA data, then removed probes missing more than 50% of the samples within any specimen, leaving 27,349 probes. (3) To further reduce missing values, improve signal, and enable gene set expression analysis, we selected the "best" probe for each gene using the WGCNA library *collapseRows* function and the "*MaxMean*" method. This selected the row with the highest mean value within a probe or the highest connectivity among the rows if three or more probes were available. This aggregation reduced the number of probes to the final 13,753 individual genes used in the rest of the analysis, with only 3.4% of the values missing. (4) Missing value imputation was performed on the microarray data for each of the six specimens individually *via* the missMDA (v. 1.18) package *imputePCA* function, which uses a principal components analysis to impute missing values (Josse and Husson, 2016). The microarray data for each of the six donors was then concatenated into one profile. Only the 2,754 samples from the cerebral cortex were included in this analysis, as the cerebellum and brain stem are largely spared by AD and could drive spurious associations due only to systematic genome-wide differences in expression levels between these regions (Kang et al., 2011; Mahfouz et al., 2015).

[1]http://ida.loni.usc.edu

TABLE 1 | Positron emission tomography (PET) pathology image demographics.

PET modality	Group	N	Age (yrs ± SD)	Age (range)	Sex (F:M)
FDG-18	AD	305	75.33 ± 7.41	55–91	123:182
	CN	351	75.26 ± 5.93	56–94	177:174
AV-45	AD	174	74.59 ± 8.42	56–90	73:101
	CN	421	74.27 ± 7.30	56–95	228:193
AV-1451	AD	65	74.35 ± 8.47	56–89	24:41
	CN	435	73.13 ± 7.90	55–94	248:187

Alzheimer's Disease and Neuroimaging Initiative Positron Emission Tomography Image Processing

All PET images were fully preprocessed by ADNI, including smoothing, coregistration, frame averaging, AC-PC orientation, and intensity normalization. Each individual pre-processed image was registered to the median image for that modality *via* FSL-flirt, which was then registered to the T1 152-subject MNI (Montreal Neurological Institute) standard template and manually inspected for accuracy of registration. All images were then co-registered to the MNI template using that transform. See **Figure 2** for aggregate images in each modality.

Spatial Correlation

The first step in this process was to obtain matching PET intensity values for the brain locations sampled by the AHBA microarray. A custom R script using RNifti (version 1.4.0) was used to load in each PET image and read the intensity values at the coordinates specified in the AHBA data. An optimized set of ANTs (Avants et al., 2011) nonlinear-registered MNI coordinates[2] was used as corresponding microarray sample locations for the AHBA and PET images. This provided tabular output with each row being an ADNI participant and each column the PET intensity in each

[2]https://github.com/chrisgorgo/alleninf

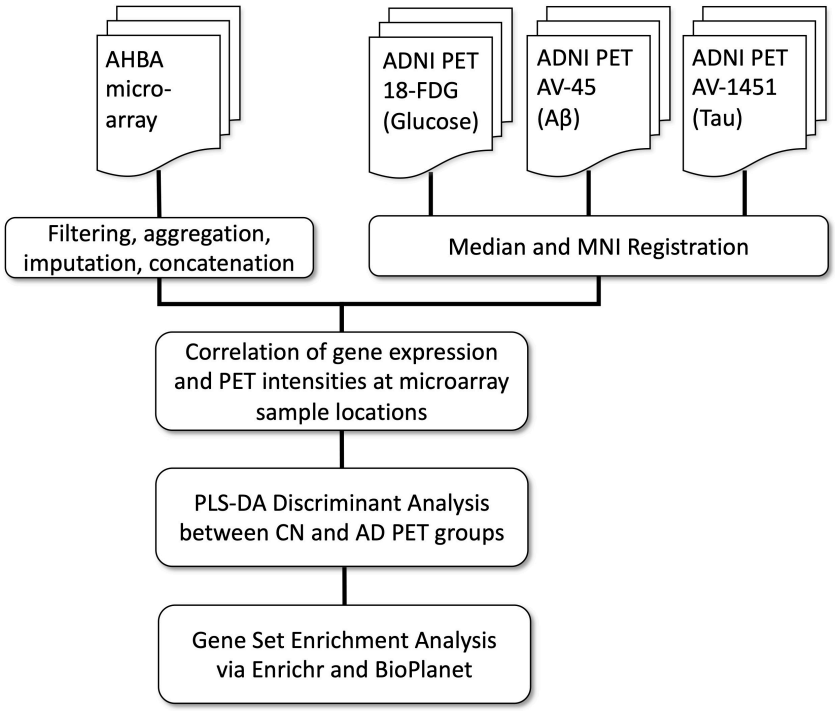

FIGURE 1 | Processing and analysis flow chart.

of the 2,754 cerebral cortex sample locations from the six AHBA specimens. This was repeated to create a separate data table for each PET modality.

Next, correlation coefficients as *r*-values were derived as pairwise distances *via* the dist2 function in MATLAB (Mathworks, Natick, MA, United States), using a Pearson correlation metric. This correlation was performed between the single concatenated set of AHBA gene expression values and the PET pathology intensities for each ADNI participant in the same AHBA sample locations. This correlation was repeated within each PET modality, resulting in a new data table with each row being an ADNI participant and each column being the respective *r*-values for each gene. These *r*-values were then converted to z-scores using the Fisher r-to-z transform and entered into the following PLS-DA model.

(Sparse)PLS-DA

Starting with a table of *z*-values reflecting the spatial correlation between gene expression and PET pathology in the cerebral cortex microarray samples, we used the sparse PLS-DA (sPLS-DA) from the mixomics (Rohart et al., 2017) R package (v.6.16.3) to perform a discriminant analysis between Alzheimer's disease (AD) and cognitively normal (CN) ADNI participants. Sparse PLS-DA classified the samples based on the best predictive or discriminative features in a one-step procedure (Le Cao et al., 2011). The table of *z*-scores was used as the input dataset and the AD or CN diagnosis as the classifier. The model was tuned using the *tune.splsda* function with leave-one-out (loo) validation and 50 repeats. The tuning function consistently revealed that the optimal number of components was two for each PET pathology. The optimal number of classification variables for components 1 and 2, respectively were 6 & 10 for FDG, 30 & 20 for AV45, and 35 & 5 for AV1451.

Gene Set Enrichment Analysis

Enrichr (Chen et al., 2013; Kuleshov et al., 2016; Xie et al., 2021) was used to query the gene sets derived from the PLS-DA analysis above, using the *enrichR* version 3.0 package in R. The gene sets derived from the first principal component of the PLS-DA step were used as inputs for the enrichment analysis individually and assessed with BioPlanet 2019 (Huang et al., 2019), which integrates pathways from curated sources including the Kyoto Encyclopedia of Genes and Genomes (KEGG), NCI-Nature, BioCarta, Science Signaling, Reactome, NetPath, and WikiPathways.

RESULTS

Sparse PLS-DA Gene Selection

Sparse PLS-DA was used to identify the optimal set of genes whose expression-intensity correlation value discriminated between CN and AD participants. Separate models were created for FDG-18, AV-45, and AV-1451 PET, as described above. The first component of the PLS-DA analysis for FDG-18 explained 21.2% of the variance, AV-45 71.6%, AV-1451 41.4%. The first component was retained for further analyses, as the variance explained by the second components for FDG-18, Aβ, and Tau

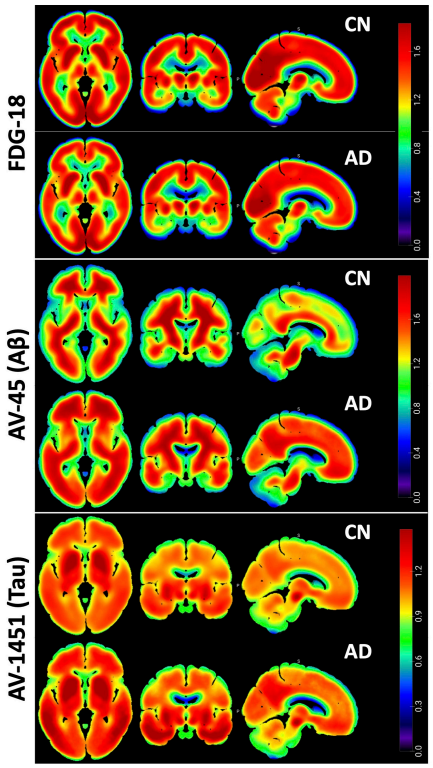

FIGURE 2 | Pet Pathology Z-maps. Multi-planar Axial, Coronal, and Sagittal views of the median of the MNI-registered ADNI AD and CN participant images. Top row is FDG-18 maps of hypometabolism, middle is AV-45 Aβ distribution, bottom is AV-1451 Tau distribution. FDG-18 images were normalized to the median of a manually drawn pons ROI. AV-45 and AV1451 were normalized to whole cerebellum. Thresholding for the figures is consistent between AD and CN groups for visual comparison. Non-brain areas are masked and the "NIH" look-up-table was used for color scale. Figure created in MRIcroGL v1.2.

distribution was marginal: 2.3, 2.6, and 2.6%, respectively. Sample plots for each PET pathology showing the distribution of the data in latent space are in **Figure 3A**.

Receiver Operator Characteristic (ROC) Area Under the Curve (AUC) plots were used to further evaluate the classification results. Results were similar between each pathology. For discrimination between AD and CN on the first component, the FDG-18-associated set had an AUC of 0.88, the AV-45-associated set an AUC of 0.87, and the AV-1451-associated set an AUC of 0.89. AUC curves presented in **Figure 3B** are for comparison only, as they are generated using specificity and sensitivity cutoff maximization rather than PLS-DA distance metrics (Rohart et al., 2017).

Genes selected by the sPLS-DA model are shown in the loading plots, which show the direction each expression-intensity correlation classifies toward (**Figure 4**). For genes that classified toward AD, their underlying average expression-intensity correlation was higher in the AD group. Likewise, genes that classified toward CN had higher expression-intensity correlations in the CN group. This signifies that the spatial pattern of the PET image intensity diverged far enough in either direction from the spatial pattern of normal gene expression that it would aid in classification. See **Supplementary Tables 2,3** for annotations and loading statistics output for these genes.

Gene Set Enrichment Analysis

Enrichr was used to examine the biological relevance of groups of genes within the selected gene sets according to the BioPlanet 2019 pathway set. Plots of the top 15 significant ($p < 0.05$) pathways for each pathology by p-value and gene count are shown in **Figure 5**. The overlap with many Bioplanet pathway gene sets is unavoidably low due to the optimal small size (6–35 genes) of the sPLS-DA derived classifier sets, so this analysis is an exploratory measure to infer function. Correcting for multiple comparisons by the Benjamini-Hochberg (BH) procedure, the adjusted p-values for FDG-18 retained all pathways, those of AV-1451 exceeded a p of.05 after the 8th listed pathway (Metabolism), and AV-45 retained no significant pathways. See **Supplementary Table 4** for a full list of pathway outputs, associated genes, and statistics.

DISCUSSION

Using an unbiased approach, we derived sets of genes with expression patterns spatially associated with FDG hypometabolism, Aβ deposition, and Tau deposition in AD. Pathway analysis of these gene sets *via* BioPlanet revealed links to mitochondrial function, Notch signaling, and other neuropathologically interesting pathways that may underlie the canonically distinct spatial patterns of FDG hypometabolism, Aβ and Tau deposition in AD.

From a broad perspective, the regional patterns of different AD pathologies implicated different sets of genes, with the exception of NDUSF4, which was implicated in regional vulnerability to both Tau and FDG hypometabolism. All sets classified between AD and CN with similar accuracy, with Aβ marginally on the low end and Tau on the highest. FDG reached optimal classification using only six genes, compared to 30 for Aβ and 35 for Tau. All revealed significant and meaningful pathway results, but only FDG and Tau survived correction for multiple comparisons. FDG and Tau also showed higher numbers of genes classifying toward CN in the discriminant analysis, which may imply regional protective effects of these genes against the development of FDG hypometabolism and Tau deposition. Such protective effects are less pronounced for Aβ, which has genes classifying toward either group. Tau and FDG are also the only gene sets that map to a pathway indicative of AD itself, which does not emerge for the Aβ-associated gene set. It is worth noting that these results reflect the current focus of AD research, which is shifting away from the amyloid hypothesis (Morris et al., 2014) and toward Tau (Josse and Husson, 2016) and brain metabolism (Neth and Craft, 2017) as primary pathogenic events of interest.

The nominal "Alzheimer's disease" pathway is the foremost one identified by BioPlanet for the discriminant gene set for FDG-18, implicated *via* the influence of BACE2 and NDUFS4. BACE2 is the focus of considerable interest in

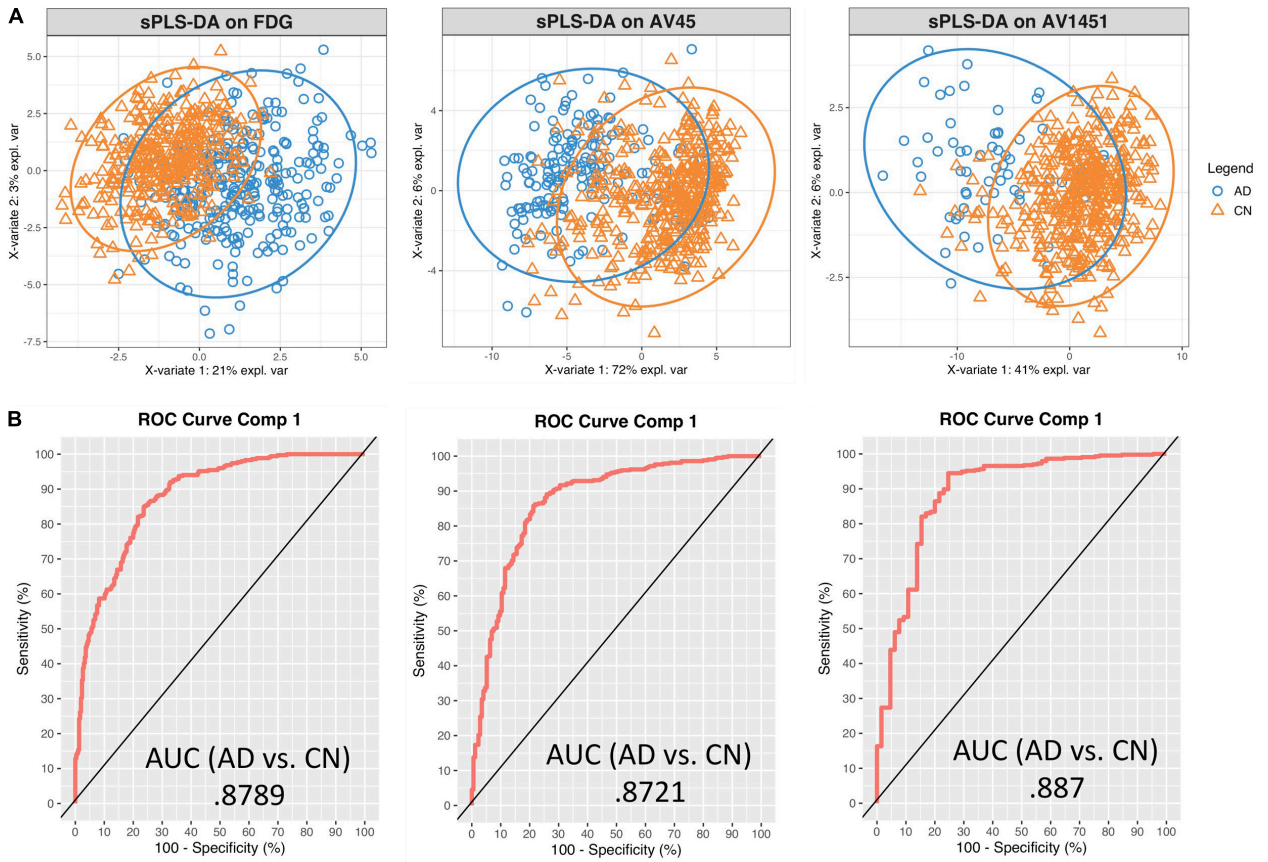

FIGURE 3 | Sparse PLS-DA plots for gene selection. **(A)** Sample plots from sPLS-DA performed on the gene expression – PET intensity correlation data including 95% confidence ellipses. The samples are projected into the space spanned by the first two components and colored by group: blue for AD and orange for CN. **(B)** Receiver Operator Characteristic (ROC) curve and AUC on the expression-intensity correlation data for component 1.

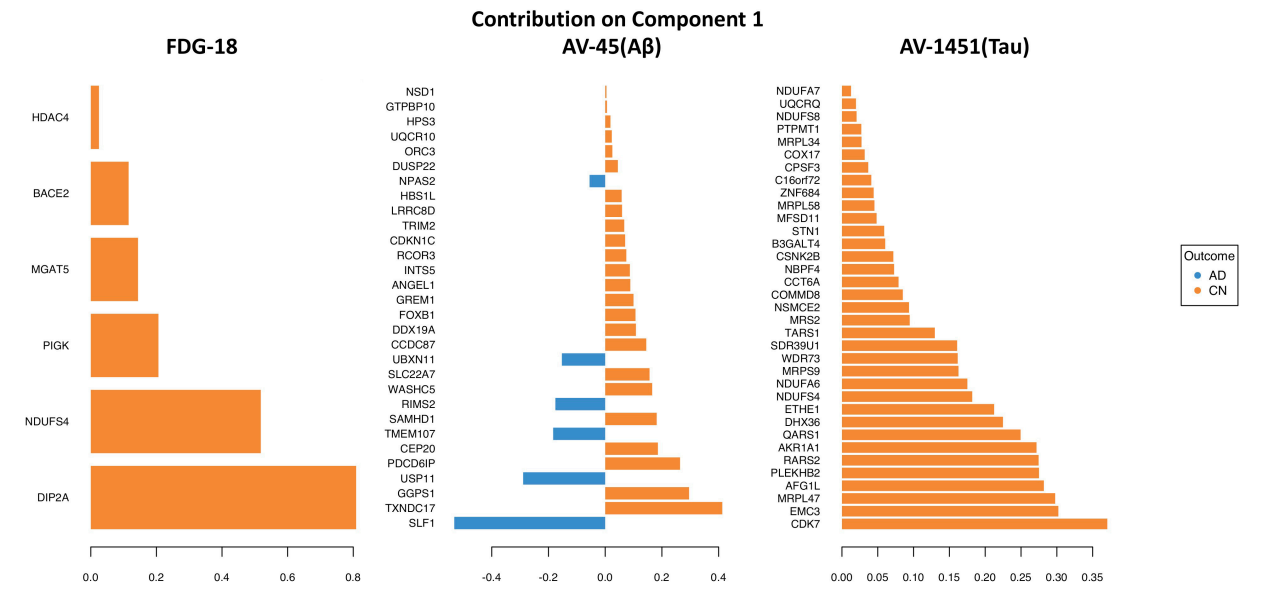

FIGURE 4 | Loading plots for the optimal classifying genes in the sPLS-DA analysis. Highest loading genes or pathologies are on the bottom (descending order), leftward (blue) deflected bars classify to AD, rightward (orange) to CN.

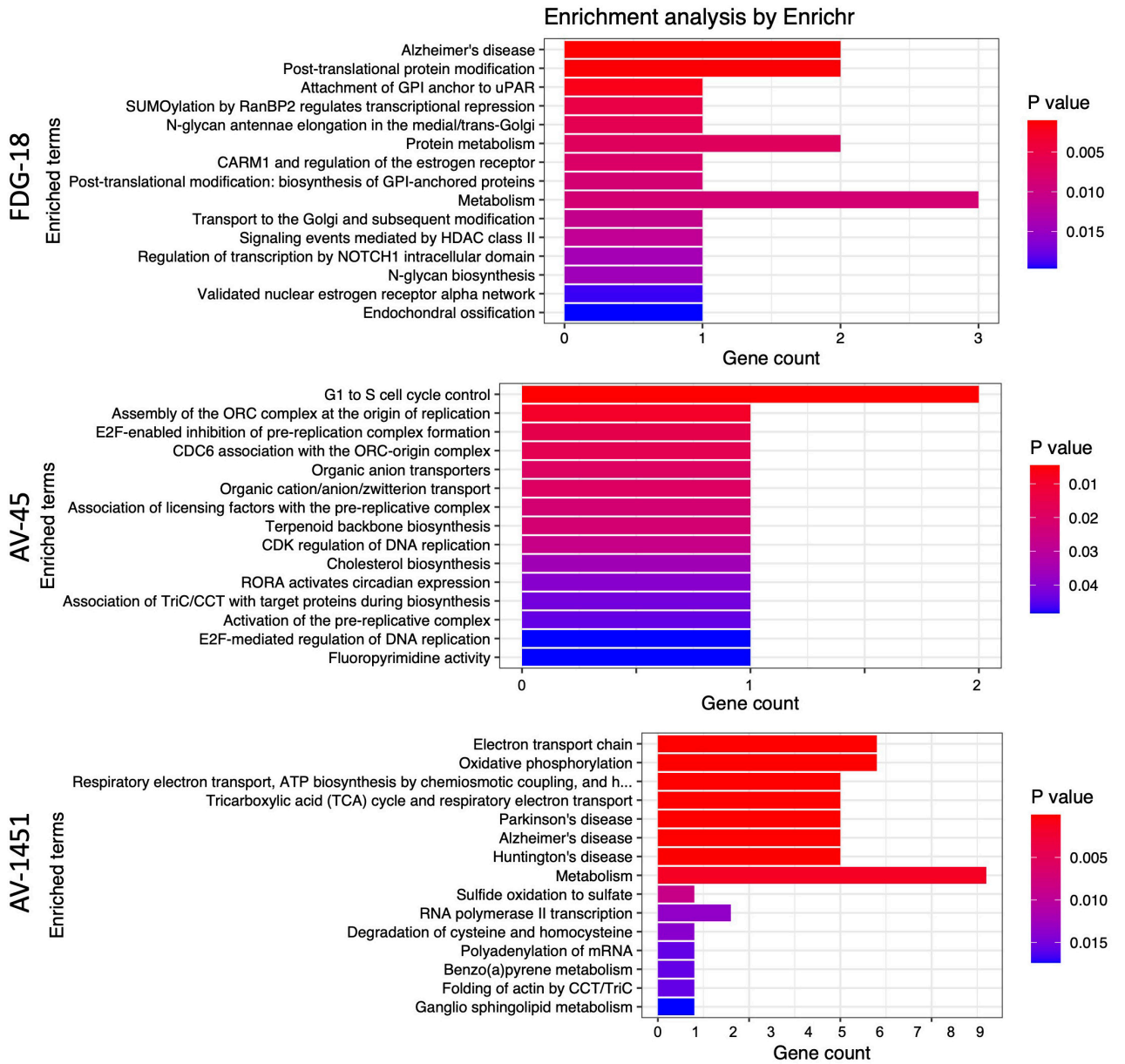

FIGURE 5 | Enrichr results as barplots for FDG-18, AV-45, and AV-1451 PET gene sets. These figures are limited to the top 15 significant pathways ($p < 0.05$), the complete set is in **Supplementary Table 3**. The *x*-axis categories are the BioPlanet pathways arranged by *p*-value from lowest (top) to highest (bottom). The *y*-axis is the gene count, or number of genes found in that pathway.

AD as a conditional β-secretase that normally suppresses the amyloidogenic processing of APP (Huentelman et al., 2019; Wang et al., 2019). NDUFS4 codes for a mitochondrial subunit known to bind oligomeric Aβ (Olah et al., 2011) and may have a role in the cognitive deficits of AD *via* oxidative stress (Harris et al., 2007). The full BioPlanet pathway list in **Supplementary Table 4** also revealed numerous several entries for NOTCH signaling *via* the influence of HDAC4, a histone deacetylase with an important role in nerve function by promoting neuronal apoptosis (Bolger and Yao, 2005) and of interest as a therapeutic target for AD due to its deregulation and accumulation in the AD brain (Xu et al., 2011; Shen et al., 2016; Wu et al., 2016). Recent evidence has suggested that aberrant Notch signaling could result in the neurodegeneration seen in AD (Woo et al., 2009; Kapoor and Nation, 2021). In addition, the failure of γ-secretase inhibitors as treatments of AD has been partly attributed to its deleterious effects on Notch signaling, which may have counteracted any benefits from reduced Aβ production (Luo and Li, 2022). MGAT5 was implicated as part of Golgi metabolic pathways and has attracted recent interest due to its human-specific differential expression in brain tissue layers as well as in AD (Jorge et al., 2021). PIGK, and DIP2A were also high

classifier loadings in the PLS-DA. Potentially a novel candidate gene, PIGK has little current implication in AD literature but is linked to the maturation or modification of APP (Del Prete et al., 2017). Similarly, the function of DIP2A is still unclear, but it was the strongest loading gene in our FDG-18-related analysis and has been associated with amyloid burden in epigenome-wide association (EWAS) studies of AD using post-mortem brain tissue (De Jager et al., 2014; Li et al., 2020).

Of the three AD pathologies probed by PET imaging, Tau deposition (by AV-1451) appears to reveal the most relevant pathways related to AD, as well as including "Alzheimer's disease" itself as the most highly significant BioPlanet-identified pathway *via* NDUFS4 & 8, NDUFA6 & 7 and UQCRQ. This "Alzheimer's disease" pathway overlaps with other AV-1451-associated pathways that relate to mitochondrial respiration, electron transport, and oxidative phosphorylation (NDUFS4 & 8, NDUFA6 &7, UQCRQ, & COX17), as well as metabolism (NDUFS4 & 8, NDUFA6 &7, UQCRQ, COX17, & ETHE1). The mitochondrial subunit NDUSF4 was also found in the FDG-18 gene set as above, through which it shares common features in terms of electron transport, oxidative phosphorylation, and metabolism. Disruptions in these pathways may contribute to both AD metabolic abnormalities and Tau pathology by impairment of mitochondrial function (Yao et al., 2009; Chakravorty et al., 2019; Lim et al., 2020).

In this setting, it is important to note that FDG hypometabolism has long been considered more closely spatially, temporally and causally linked to Tau deposition than Aβ deposition (Ossenkoppele et al., 2016). A common genetic underpinning of mitochondrial and metabolic abnormalities could help account for this relationship. Recently, we identified decreased levels and activity of mitochondrial electron transport chain components in plasma neuronal-derived Extracellular Vesicles of individuals with AD compared to Controls (Yao et al., 2021), as well as in individuals with major depressive disorder (Goetzl et al., 2021) or neuropsychiatric symptoms due to long COVID-19 compared to controls (Peluso et al., 2022). These studies indicate that mitochondrial dysfunction in AD can be studied in living individuals through biomarkers, opening the way to establishing it as a core feature of AD progression.

Many individual genes within the AV-1451 set have been implicated in AD pathogenesis in the past, supporting the validity of our approach. The strongest loading individual gene on the AV-1451 list was the cyclin-dependent kinase CDK7, which is elevated early in AD pathogenesis and may upregulate Amyloid(β) Precursor Protein (APP) and Tau (Zhu et al., 2000; Lukasik et al., 2021). EMC3 is involved in endoplasmic reticulum associated degradation, which has been implicated in neurodegeneration in a mouse AD model (Zhu et al., 2017). AKR1A1 codes for an aldehyde reductase, which is protective against neurodegeneration in AD (Picklo et al., 2001). Differentially methylated positions on B3GALT4 are linked to late onset AD and have been associated with memory performance and CSF levels of Aβ and tau (Madrid et al., 2018). CPSF3 is involved in the RNA life cycle and has been identified as part of the molecular interaction network for AD (Rosenthal et al., 2022). COX17 codes for a cytochrome C oxidase copper chaperone involved in copper homeostastis, which has been tentatively linked to AD (Ejaz et al., 2020). PTMPT1 is part of an AD-risk locus identified *via* genome-wide analyses (Efthymiou and Goate, 2017). However, STN1, AFG1L, PLEKHB2, DHX36, WDR73, SDR39U1, MRS2, NSCME2, COMMD8, CCT6A, NBPF4, SCNK2B, MFSD11, SNF684, and C16orf72, are relatively unstudied in the context of neurodegenerative diseases and AD, raising the possibility of having identified novel mechanisms.

Amyloid-β deposition *via* AV-45 PET revealed the fewest interpretable pathways and did not reveal a significant pathway for "Alzheimer's disease" ($p = 0.22$). Of the pathways identified, there were some related to the cell cycle *via* CDKN1C and ORC3. Concerning this, there are existing hypotheses that disruptions to cell cycling may be a cause for the neuronal death observed in AD (Raina et al., 1999, 2004) but little in the way of experimental research to test it or the possible role of CDKN1C and ORC3. In terms of individual genes, there were many hints about their involvement in AD pathophysiology. TXNDC17 interacts with the cellular prion protein (PrPc)(Ulbrich et al., 2018), which is the main receptor for oligomeric Aβ. GPPS1 is elevated in the AD frontal cortex and may modify Aβ production (Hooff et al., 2010). PDCD6IP (as ALIX) is decreased in the serum of AD patients and AβPP/PS1 mice (Sun et al., 2015) and directs the trafficking of APP into extracellular vesicles (Cone et al., 2020). RCOR3 is down-regulated in the hippocampus of AD brain specimens (Yan et al., 2019). The tripartite motif protein TRIM2 has high hippocampal expression that may be impacted by the presence of Aβ plaques *via* modulatory miRNA (Schonrock et al., 2012). LRRC8D may interact with Aβ as a binding protein (Virok et al., 2011). DUSP22 inhibits protein-kinase A activity and hence Tau phosphorylation and CREB signaling (Sanchez-Mut et al., 2014). SLF1, UPS11, CEP20, TMEM107, SAMHD1, RIMS2, WASHC5, SLC22A7, UBXN11, CCDC87, DDX19A, FOXB1, GREM1, ANGEL1, INTS5, TRIM2, HBS1NL, NPAS2, UQCR10, HPS3, GTPBP10, and NSD1 are relatively unstudied in this context.

While the spatial correlation was meant to identify genes implicated in the regional vulnerability to AD and not necessarily to improve AD group classification, we also performed a *post-hoc* comparison using only the mean PET intensity for each of the three modalities as the dependent variable, entering each into otherwise identical sPLS-DA models. This resulted in notably lower AUCs: 0.63 for FDG, 0.63 for AV-45, and 0.71 for AV-1451.

A limitation of this study is the fact that while the AHBA contains numerous samples, they are derived from only six brain specimens and from a younger cohort than the ADNI group. The method of spatial correlation we implemented in this study is currently unable to apply covariates for factors such as age and sex, since the spatial correlation involves data derived from two separate sets of subjects. Fortunately, the ADNI participants are consistent in terms of age and sex, and the AHBA specimens have undergone substantial normalization for array and batch-specific biases. Both sex and age interact with gene expression in the brain, particularly in terms of immune activation and metabolism (Berchtold et al., 2008). Until there are comprehensive richly sampled post-mortem studies of regional gene expression with

a variety of ages, sexes, and disease statuses, it will be difficult to predict or account for the effects of these potential confounds.

Regarding AD-related genes revealed by genome and epigenome – wide association studies that essentially create binary contrasts of diseased/non-diseased individuals in large populations, we should note that a gene product may still be important in AD without being spatially correlated with a pathology, and vice-versa. The methodology employed in the present study may complement these population-based approaches for identifying the genetic underpinnings of AD. We hope that data-driven methods like ours can identifying novel genes implicated in vulnerability to AD for further evaluation.

CONCLUSION

We present a novel method to extract information from the melding of microarray and imaging data to identify genes involved in AD pathology and its regional distribution. This method allowed us to identify both known and novel candidate genes and highlights certain pathways for further investigation, but also as potential therapeutic targets. This methodology is flexible, produces an interpretable list of only the best-classifying genes, and can be extended to provide insight into the genetic underpinnings of other brain diseases with their own characteristic spatial patterns of pathology.

AUTHOR'S NOTE

Data used in preparation of this article were obtained from the Alzheimer's disease Neuroimaging Initiative (ADNI) database (https://adni.loni.usc.edu). As such, the investigators within the ADNI contributed to the design and implementation of ADNI and/or provided data but did not participate in analysis or writing of this report. A complete listing of ADNI investigators can be found at: http://adni.loni.usc.edu/wp-content/uploads/how_to_apply/ADNI_Acknowledgments_List.pdf.

DATA AVAILABILITY STATEMENT

The datasets presented in this study can be found in online repositories. The ADNI PET images used here are available at https://adni.loni.usc.edu. AHBA microarray transcriptomic data are available at http://human.brain-map.org/static/download.

ETHICS STATEMENT

Ethical review and approval was not required for the study on human participants in accordance with the local legislation and institutional requirements. Written informed consent for participation was not required for this study in accordance with the national legislation and the institutional requirements.

AUTHOR CONTRIBUTIONS

RM and DK formulated the hypothesis, designed the study, and wrote the manuscript. RM performed the bioinformatics analysis. Both authors contributed to the article and approved the submitted version.

ACKNOWLEDGMENTS

Data collection and sharing for this project was funded by the Alzheimer's Disease Neuroimaging Initiative (ADNI, National Institutes of Health Grant U01 AG024904) and DOD ADNI (Department of Defense award number W81XWH-12-2-0012). ADNI was funded by the National Institute on Aging, the National Institute of Biomedical Imaging and Bioengineering, and through generous contributions from the following: AbbVie, Alzheimer's Association; Alzheimer's Drug Discovery Foundation; Araclon Biotech; BioClinica, Inc.; Biogen; Bristol-Myers Squibb Company; CereSpir, Inc.; Cogstate; Eisai Inc.; Elan Pharmaceuticals, Inc.; Eli Lilly and Company; EuroImmun; F. Hoffmann-La Roche Ltd. and its affiliated company Genentech, Inc.; Fujirebio; GE Healthcare; IXICO Ltd.; Janssen Alzheimer Immunotherapy Research & Development, LLC.; Johnson & Johnson Pharmaceutical Research & Development LLC.; Lumosity; Lundbeck; Merck & Co., Inc.; Meso Scale Diagnostics, LLC.; NeuroRx Research; Neurotrack Technologies; Novartis Pharmaceuticals Corporation; Pfizer Inc.; Piramal Imaging; Servier; Takeda Pharmaceutical Company; and Transition Therapeutics. The Canadian Institutes of Health Research is providing funds to support ADNI clinical sites in Canada. Private sector contributions are facilitated by the Foundation for the National Institutes of Health (www.fnih.org). The grantee organization is the Northern California Institute for Research and Education, and the study is coordinated by the Alzheimer's Therapeutic Research Institute at the University of Southern California. ADNI data are disseminated by the Laboratory for Neuro Imaging at the University of Southern California.

SUPPLEMENTARY MATERIAL

The Supplementary Material for this article can be found online at: https://www.frontiersin.org/articles/10.3389/fnins.2022.908650/full#supplementary-material

REFERENCES

Arnold, S. E., Hyman, B. T., Flory, J., Damasio, A. R., and Van Hoesen, G. W. (1991). The topographical and neuroanatomical distribution of neurofibrillary tangles and neuritic plaques in the cerebral cortex of patients with Alzheimer's disease. *Cereb. Cortex* 1, 103–116. doi: 10.1093/cercor/1.1.103

Avants, B. B., Tustison, N. J., Song, G., Cook, P. A., Klein, A., and Gee, J. C. (2011). A reproducible evaluation of ANTs similarity metric performance in brain

image registration. *Neuroimage* 54, 2033–2044. doi: 10.1016/j.neuroimage.2010.09.025

Berchtold, N. C., Cribbs, D. H., Coleman, P. D., Rogers, J., Head, E., Kim, R., et al. (2008). Gene expression changes in the course of normal brain aging are sexually dimorphic. *Proc. Natl. Acad. Sci. U.S.A.* 105, 15605–15610. doi: 10.1073/pnas.0806883105

Bolger, T. A., and Yao, T. P. (2005). Intracellular trafficking of histone deacetylase 4 regulates neuronal cell death. *J. Neurosci.* 25, 9544–9553. doi: 10.1523/JNEUROSCI.1826-05.2005

Braak, H., and Braak, E. (1991). Neuropathological stageing of Alzheimer-related changes. *Acta Neuropathol.* 82, 239–259. doi: 10.1007/BF00308809

Braak, H., and Del Tredici, K. (2012). Where, when, and in what form does sporadic Alzheimer's disease begin? *Curr. Opin. Neurol.* 25, 708–714. doi: 10.1097/WCO.0b013e32835a3432

Buckner, R. L., Sepulcre, J., Talukdar, T., Krienen, F. M., Liu, H., Hedden, T., et al. (2009). Cortical hubs revealed by intrinsic functional connectivity: mapping, assessment of stability, and relation to Alzheimer's disease. *J. Neurosci.* 29, 1860–1873. doi: 10.1523/JNEUROSCI.5062-08.2009

Burt, J. B., Demirtas, M., Eckner, W. J., Navejar, N. M., Ji, J. L., Martin, W. J., et al. (2018). Hierarchy of transcriptomic specialization across human cortex captured by structural neuroimaging topography. *Nat. Neurosci.* 21, 1251–1259. doi: 10.1038/s41593-018-0195-0

Chakravorty, A., Jetto, C. T., and Manjithaya, R. (2019). Dysfunctional mitochondria and mitophagy as drivers of alzheimer's disease pathogenesis. *Front. Aging Neurosci.* 11:311. doi: 10.3389/fnagi.2019.00311

Chen, E. Y., Tan, C. M., Kou, Y., Duan, Q., Wang, Z., Meirelles, G. V., et al. (2013). Enrichr: interactive and collaborative HTML5 gene list enrichment analysis tool. *BMC Bioinformatics* 14:128. doi: 10.1186/1471-2105-14-128

Cone, A. S., Hurwitz, S. N., Lee, G. S., Yuan, X., Zhou, Y., Li, Y., et al. (2020). Alix and Syntenin-1 direct amyloid precursor protein trafficking into extracellular vesicles. *BMC Mol. Cell Biol.* 21:58. doi: 10.1186/s12860-020-00302-0

De Jager, P. L., Srivastava, G., Lunnon, K., Burgess, J., Schalkwyk, L. C., Yu, L., et al. (2014). Alzheimer's disease: early alterations in brain DNA methylation at ANK1, BIN1, RHBDF2 and other loci. *Nat. Neurosci.* 17, 1156–1163. doi: 10.1038/nn.3786

De Strooper, B., and Karran, E. (2016). The cellular phase of Alzheimer's Disease. *Cell* 164, 603–615.

Del Prete, D., Suski, J. M., Oules, B., Debayle, D., Gay, A. S., Lacas-Gervais, S., et al. (2017). Localization and processing of the amyloid-beta protein precursor in mitochondria-associated membranes. *J. Alzheimers Dis.* 55, 1549–1570. doi: 10.3233/JAD-160953

Diehl, T., Mullins, R., and Kapogiannis, D. (2017). Insulin resistance in Alzheimer's disease. *Transl. Res.* 183, 26–40.

Efthymiou, A. G., and Goate, A. M. (2017). Late onset Alzheimer's disease genetics implicates microglial pathways in disease risk. *Mol. Neurodegener.* 12:43. doi: 10.1186/s13024-017-0184-x

Ejaz, H. W., Wang, W., and Lang, M. (2020). Copper toxicity links to pathogenesis of alzheimer's disease and therapeutics approaches. *Int. J. Mol. Sci.* 21:7660. doi: 10.3390/ijms21207660

Frisoni, G. B., Altomare, D., Thal, D. R., Ribaldi, F., van der Kant, R., Ossenkoppele, R., et al. (2022). The probabilistic model of Alzheimer disease: the amyloid hypothesis revised. *Nat. Rev.* 23, 53–66. doi: 10.1038/s41583-021-00533-w

Goetzl, E. J., Wolkowitz, O. M., Srihari, V. H., Reus, V. I., Goetzl, L., Kapogiannis, D., et al. (2021). Abnormal levels of mitochondrial proteins in plasma neuronal extracellular vesicles in major depressive disorder. *Mol. Psychiatry* 26, 7355–7362. doi: 10.1038/s41380-021-01268-x

Harris, S. E., Fox, H., Wright, A. F., Hayward, C., Starr, J. M., Whalley, L. J., et al. (2007). A genetic association analysis of cognitive ability and cognitive ageing using 325 markers for 109 genes associated with oxidative stress or cognition. *BMC Genet.* 8:43. doi: 10.1186/1471-2156-8-43

Hawrylycz, M. J., Lein, E. S., Guillozet-Bongaarts, A. L., Shen, E. H., Ng, L., Miller, J. A., et al. (2012). An anatomically comprehensive atlas of the adult human brain transcriptome. *Nature* 489, 391–399. doi: 10.1038/nature11405

Hooff, G. P., Peters, I., Wood, W. G., Muller, W. E., and Eckert, G. P. (2010). Modulation of cholesterol, farnesylpyrophosphate, and geranylgeranylpyrophosphate in neuroblastoma SH-SY5Y-APP695 cells: impact on amyloid beta-protein production. *Mol. Neurobiol.* 41, 341–350. doi: 10.1007/s12035-010-8117-5

Huang, R., Grishagin, I., Wang, Y., Zhao, T., Greene, J., Obenauer, J. C., et al. (2019). The NCATS bioplanet – an integrated platform for exploring the universe of cellular signaling pathways for toxicology, systems biology, and chemical genomics. *Front. Pharmacol.* 10:445. doi: 10.3389/fphar.2019.00445

Huentelman, M., De Both, M., Jepsen, W., Piras, I. S., Talboom, J. S., Willeman, M., et al. (2019). Common BACE2 polymorphisms are associated with altered risk for alzheimer's disease and CSF amyloid biomarkers in APOE epsilon4 non-carriers. *Sci. Rep.* 9:9640. doi: 10.1038/s41598-019-45896-4

Jorge, N. A. N., Ueberham, U., Knobloch, M., Stadler, P. F., Fallmann, J., and Arendt, T. (2021). Disturbance of phylogenetic layer-specific adaptation of human brain gene expression in Alzheimer's disease. *Sci. Rep.* 11:20200.

Josse, J., and Husson, F. (2016). missMDA: a package for handling missing values in multivariate data analysis. *J. Stat. Softw.* 70, 1–31.

Kang, H. J., Kawasawa, Y. I., Cheng, F., Zhu, Y., Xu, X., Li, M., et al. (2011). Spatio-temporal transcriptome of the human brain. *Nature* 478, 483–489.

Kapoor, A., and Nation, D. A. (2021). Role of Notch signaling in neurovascular aging and Alzheimer's disease. *Semin. Cell Dev. Biol.* 116, 90–97. doi: 10.1016/j.semcdb.2020.12.011

Keo, A., Dzyubachyk, O., van der Grond, J., van Hilten, J. J., Reinders, M. J. T., and Mahfouz, A. (2021). Transcriptomic signatures associated with regional cortical thickness changes in parkinson's disease. *Front. Neurosci.* 15:733501. doi: 10.3389/fnins.2021.733501

Kuleshov, M. V., Jones, M. R., Rouillard, A. D., Fernandez, N. F., Duan, Q., Wang, Z., et al. (2016). Enrichr: a comprehensive gene set enrichment analysis web server 2016 update. *Nucleic Acids Res.* 44, W90–W97. doi: 10.1093/nar/gkw377

Le Cao, K. A., Boitard, S., and Besse, P. (2011). Sparse PLS discriminant analysis: biologically relevant feature selection and graphical displays for multiclass problems. *BMC Bioinformatics* 12:253. doi: 10.1186/1471-2105-12-253

Li, Q. S., Sun, Y., and Wang, T. (2020). Epigenome-wide association study of Alzheimer's disease replicates 22 differentially methylated positions and 30 differentially methylated regions. *Clin. Epigenet.* 12:149. doi: 10.1186/s13148-020-00944-z

Lim, J. W., Lee, J., and Pae, A. N. (2020). Mitochondrial dysfunction and Alzheimer's disease: prospects for therapeutic intervention. *BMB Rep.* 53, 47–55. doi: 10.5483/BMBRep.2020.53.1.279

Lukasik, P., Zaluski, M., and Gutowska, I. (2021). Cyclin-dependent kinases (CDK) and their role in diseases development-review. *Int. J. Mol. Sci.* 22:2935. doi: 10.3390/ijms22062935

Luo, J. E., and Li, Y. M. (2022). Turning the tide on Alzheimer's disease: modulation of gamma-secretase. *Cell Biosci.* 12:2. doi: 10.1186/s13578-021-00738-7

Madrid, A., Hogan, K. J., Papale, L. A., Clark, L. R., Asthana, S., Johnson, S. C., et al. (2018). DNA Hypomethylation in blood links B3GALT4 and ZADH2 to Alzheimer's Disease. *J. Alzheimers Dis.* 66, 927–934. doi: 10.3233/JAD-180592

Mahfouz, A., van de Giessen, M., van der Maaten, L., Huisman, S., Reinders, M., Hawrylycz, M. J., et al. (2015). Visualizing the spatial gene expression organization in the brain through non-linear similarity embeddings. *Methods* 73, 79–89. doi: 10.1016/j.ymeth.2014.10.004

McColgan, P., Gregory, S., Seunarine, K. K., Razi, A., Papoutsi, M., Johnson, E., et al. (2018). Brain regions showing white matter loss in huntington's disease are enriched for synaptic and metabolic genes. *Biol. Psychiatry* 83, 456–465. doi: 10.1016/j.biopsych.2017.10.019

Morris, G. P., Clark, I. A., and Vissel, B. (2014). Inconsistencies and controversies surrounding the amyloid hypothesis of Alzheimer's disease. *Acta Neuropathol. Commun.* 2:135. doi: 10.1186/s40478-014-0135-5

Mullins, R. J., Diehl, T. C., Chia, C. W., and Kapogiannis, D. (2017). Insulin resistance as a link between amyloid-beta and tau pathologies in Alzheimer's Disease. *Front. Aging Neurosci.* 9:118. doi: 10.3389/fnagi.2017.00118

Neth, B. J., and Craft, S. (2017). Insulin Resistance and Alzheimer's Disease: bioenergetic linkages. *Front. Aging Neurosci.* 9:345. doi: 10.3389/fnagi.2017.00345

Olah, J., Vincze, O., Virok, D., Simon, D., Bozso, Z., Tokesi, N., et al. (2011). Interactions of pathological hallmark proteins: tubulin polymerization promoting protein/p25, beta-amyloid, and alpha-synuclein. *J. Biol. Chem.* 286, 34088–34100. doi: 10.1074/jbc.M111.243907

Ossenkoppele, R., Schonhaut, D. R., Scholl, M., Lockhart, S. N., Ayakta, N., Baker, S. L., et al. (2016). Tau PET patterns mirror clinical and neuroanatomical variability in Alzheimer's disease. *Brain* 139, 1551–1567. doi: 10.1093/brain/aww027

Peluso, M. J., Deeks, S. G., Mustapic, M., Kapogiannis, D., Henrich, T. J., Lu, S., et al. (2022). SARS-CoV-2 and mitochondrial proteins in neural-derived exosomes of COVID-19. *Ann. Neurol.* 91, 772–781. doi: 10.1002/ana.26350

Perez-Enciso, M., and Tenenhaus, M. (2003). Prediction of clinical outcome with microarray data: a partial least squares discriminant analysis (PLS-DA) approach. *Hum. Genet.* 112, 581–592. doi: 10.1007/s00439-003-0921-9

Picklo, M. J., Olson, S. J., Markesbery, W. R., and Montine, T. J. (2001). Expression and activities of aldo-keto oxidoreductases in Alzheimer disease. *J. Neuropathol. Exp. Neurol.* 60, 686–695. doi: 10.1093/jnen/60.7.686

Raina, A. K., Monteiro, M. J., McShea, A., and Smith, M. A. (1999). The role of cell cycle-mediated events in Alzheimer's disease. *Int. J. Exp. Pathol.* 80, 71–76. doi: 10.1046/j.1365-2613.1999.00106.x

Raina, A. K., Zhu, X., and Smith, M. A. (2004). Alzheimer's disease and the cell cycle. *Acta Neurobiol. Exp. (Wars)* 64, 107–112.

Reardon, P. K., Seidlitz, J., Vandekar, S., Liu, S., Patel, R., Park, M. T. M., et al. (2018). Normative brain size variation and brain shape diversity in humans. *Science* 360, 1222–1227. doi: 10.1126/science.aar2578

Richiardi, J., Altmann, A., Milazzo, A. C., Chang, C., Chakravarty, M. M., Banaschewski, T., et al. (2015). BRAIN NETWORKS. Correlated gene expression supports synchronous activity in brain networks. *Science* 348, 1241–1244.

Rohart, F., Gautier, B., Singh, A., and Le Cao, K. A. (2017). mixOmics: An R package for 'omics feature selection and multiple data integration. *PLoS Comput. Biol.* 13:e1005752. doi: 10.1371/journal.pcbi.1005752

Rosenthal, S. B., Wang, H., Shi, D., Liu, C., Abagyan, R., McEvoy, L. K., et al. (2022). Mapping the gene network landscape of Alzheimer's disease through integrating genomics and transcriptomics. *PLoS Comput. Biol.* 18:e1009903. doi: 10.1371/journal.pcbi.1009903

Sanchez-Mut, J. V., Aso, E., Heyn, H., Matsuda, T., Bock, C., Ferrer, I., et al. (2014). Promoter hypermethylation of the phosphatase DUSP22 mediates PKA-dependent TAU phosphorylation and CREB activation in Alzheimer's disease. *Hippocampus* 24, 363–368. doi: 10.1002/hipo.22245

Schonrock, N., Humphreys, D. T., Preiss, T., and Gotz, J. (2012). Target gene repression mediated by miRNAs miR-181c and miR-9 both of which are down-regulated by amyloid-beta. *J. Mol. Neurosci.* 46, 324–335. doi: 10.1007/s12031-011-9587-2

Seeley, W. W., Crawford, R. K., Zhou, J., Miller, B. L., and Greicius, M. D. (2009). Neurodegenerative diseases target large-scale human brain networks. *Neuron* 62, 42–52. doi: 10.1016/j.neuron.2009.03.024

Sepulcre, J., Schultz, A. P., Sabuncu, M., Gomez-Isla, T., Chhatwal, J., Becker, A., et al. (2016). *In vivo* tau, amyloid, and gray matter profiles in the aging brain. *J. Neurosci.* 36, 7364–7374. doi: 10.1523/JNEUROSCI.0639-16.2016

Shen, X., Chen, J., Li, J., Kofler, J., and Herrup, K. (2016). Neurons in vulnerable regions of the Alzheimer's Disease brain display reduced ATM signaling. *eNeuro* 3, 1–8. doi: 10.1523/ENEURO.0124-15.2016

Sun, Y., Rong, X., Lu, W., Peng, Y., Li, J., Xu, S., et al. (2015). Translational study of Alzheimer's disease (AD) biomarkers from brain tissues in AbetaPP/PS1 mice and serum of AD patients. *J. Alzheimers Dis.* 45, 269–282. doi: 10.3233/JAD-142805

Ulbrich, S., Janning, P., Seidel, R., Matschke, J., Gonsberg, A., Jung, S., et al. (2018). Alterations in the brain interactome of the intrinsically disordered N-terminal domain of the cellular prion protein (PrPC) in Alzheimer's disease. *PLoS One* 13:e0197659. doi: 10.1371/journal.pone.0197659

Vertes, P. E., Rittman, T., Whitaker, K. J., Romero-Garcia, R., Vasa, F., Kitzbichler, M. G., et al. (2016). Gene transcription profiles associated with inter-modular hubs and connection distance in human functional magnetic resonance imaging networks. *Philos. Trans. R. Soc. Lond. B Biol. Sci.* 371, 735–769. doi: 10.1098/rstb.2015.0362

Virok, D. P., Simon, D., Bozso, Z., Rajko, R., Datki, Z., Balint, E., et al. (2011). Protein array based interactome analysis of amyloid-beta indicates an inhibition of protein translation. *J. Proteome Res.* 10, 1538–1547. doi: 10.1021/pr1009096

Wang, Z., Xu, Q., Cai, F., Liu, X., Wu, Y., and Song, W. (2019). BACE2, a conditional beta-secretase, contributes to Alzheimer's disease pathogenesis. *JCI Insight* 4:e123431. doi: 10.1172/jci.insight.123431

Wold, S., Sjöström, M., and Eriksson, L. (2001). PLS-regression: a basic tool of chemometrics. *Chemom. Intell. Lab. Syst.* 58, 109–130.

Woo, H. N., Park, J. S., Gwon, A. R., Arumugam, T. V., and Jo, D. G. (2009). Alzheimer's disease and Notch signaling. *Biochem. Biophys. Res. Commun.* 390, 1093–1097.

Wu, Y., Hou, F., Wang, X., Kong, Q., Han, X., and Bai, B. (2016). Aberrant expression of histone deacetylases 4 in cognitive disorders: molecular mechanisms and a potential target. *Front. Mol. Neurosci.* 9:114. doi: 10.3389/fnmol.2016.00114

Xie, Z., Bailey, A., Kuleshov, M. V., Clarke, D. J. B., Evangelista, J. E., Jenkins, S. L., et al. (2021). Gene set knowledge discovery with enrichr. *Curr. Protoc.* 1:e90. doi: 10.1002/cpz1.90

Xu, K., Dai, X. L., Huang, H. C., and Jiang, Z. F. (2011). Targeting HDACs: a promising therapy for Alzheimer's disease. *Oxid. Med. Cell Longev.* 2011:143269. doi: 10.1155/2011/143269

Yan, T., Ding, F., and Zhao, Y. (2019). Integrated identification of key genes and pathways in Alzheimer's disease *via* comprehensive bioinformatical analyses. *Hereditas* 156:25. doi: 10.1186/s41065-019-0101-0

Yao, J., Irwin, R. W., Zhao, L., Nilsen, J., Hamilton, R. T., and Brinton, R. D. (2009). Mitochondrial bioenergetic deficit precedes Alzheimer's pathology in female mouse model of Alzheimer's disease. *Proc. Natl. Acad. Sci. U.S.A.* 106, 14670–14675. doi: 10.1073/pnas.0903563106

Yao, P. J., Eren, E., Goetzl, E. J., and Kapogiannis, D. (2021). Mitochondrial electron transport chain protein abnormalities detected in plasma extracellular vesicles in Alzheimer's Disease. *Biomedicines* 9:1587. doi: 10.3390/biomedicines9111587

Zhu, B., Jiang, L., Huang, T., Zhao, Y., Liu, T., Zhong, Y., et al. (2017). ER-associated degradation regulates Alzheimer's amyloid pathology and memory function by modulating gamma-secretase activity. *Nat. Commun.* 8:1472. doi: 10.1038/s41467-017-01799-4

Zhu, D., Yuan, T., Gao, J., Xu, Q., Xue, K., Zhu, W., et al. (2021). Correlation between cortical gene expression and resting-state functional network centrality in healthy young adults. *Hum. Brain Mapp.* 42, 2236–2249. doi: 10.1002/hbm.25362

Zhu, X., Rottkamp, C. A., Raina, A. K., Brewer, G. J., Ghanbari, H. A., Boux, H., et al. (2000). Neuronal CDK7 in hippocampus is related to aging and Alzheimer disease. *Neurobiol. Aging* 21, 807–813. doi: 10.1016/s0197-4580(00)00217-7

Conflict of Interest: The authors declare that the research was conducted in the absence of any commercial or financial relationships that could be construed as a potential conflict of interest.

Publisher's Note: All claims expressed in this article are solely those of the authors and do not necessarily represent those of their affiliated organizations, or those of the publisher, the editors and the reviewers. Any product that may be evaluated in this article, or claim that may be made by its manufacturer, is not guaranteed or endorsed by the publisher.

Advantages of publishing in Frontiers

OPEN ACCESS
Articles are free to read for greatest visibility and readership

FAST PUBLICATION
Around 90 days from submission to decision

HIGH QUALITY PEER-REVIEW
Rigorous, collaborative, and constructive peer-review

TRANSPARENT PEER-REVIEW
Editors and reviewers acknowledged by name on published articles

Frontiers
Avenue du Tribunal-Fédéral 34
1005 Lausanne | Switzerland

Visit us: www.frontiersin.org
Contact us: frontiersin.org/about/contact

REPRODUCIBILITY OF RESEARCH
Support open data and methods to enhance research reproducibility

DIGITAL PUBLISHING
Articles designed for optimal readership across devices

FOLLOW US
@frontiersin

IMPACT METRICS
Advanced article metrics track visibility across digital media

EXTENSIVE PROMOTION
Marketing and promotion of impactful research

LOOP RESEARCH NETWORK
Our network increases your article's readership